DISCOVERY AND CHARACTERIZATION OF RIBOSOMALLY SYNTHESIZED AND POST-TRANSLATIONALLY MODIFIED PEPTIDE NATURAL PRODUCTS

BY

PATRICIA MARIE BLAIR

DISSERTATION

Submitted in partial fulfillment of the requirements
for the degree of Doctor of Philosophy in Chemistry
in the Graduate College of the
University of Illinois at Urbana-Champaign, 2016

Urbana, Illinois

Doctoral Committee:

Associate Professor Douglas A. Mitchell, Chair
Professor Paul J. Hergenrother
Professor Satish Nair
Professor Wilfred A. van der Donk

ABSTRACT

Bacterial secondary metabolites have historically been a rich source of antibiotic compounds. The genomic era has shown that bacteria harbor the potential to produce even more natural products that could be developed into new antibiotic agents to combat the alarming rise in antibiotic-resistant pathogens. Ribosomally synthesized and post-translationally modified peptide (RiPP) natural products are genetically encoded peptide-derived secondary metabolites whose structures can be predicted based on gene sequence and identity of tailoring enzymes within the biosynthetic gene cluster. Post-translational modifications installed by the tailoring enzymes in a site-selective manner endow the compounds with structural rigidity and, in many cases, interesting biological activities. Once genome mining has been used to select RiPPs gene clusters, chemical and microbiological techniques are employed to characterize the structure, biosynthesis, antibiotic activity, and mode of action of newly discovered RiPPs.

Plantazolicin (PZN) is a RiPP natural product with a rigid, polyheterocyclic structure and a remarkably species-specific antibiotic activity, targeting the pathogen *Bacillus anthracis*. While the highly modified natural product bears the characteristic heterocycles of a linear azol(in)e-containing RiPP, N-terminal dimethylation after cleavage of the leader peptide is also essential for bioactivity. The methyltransferase responsible for this post-translational modification is highly evolved for PZN-like substrates, with very little tolerance to mutant sequences.

The underlying cause of the ultra-narrow spectrum bioactivity was investigated using a broad range of chemical and microbiological techniques. PZN was not found to have a proteinaceous target; instead, the bioactivity was found to be dependent on the diphosphatidylglycerol lipid cardiolipin. PZN is thought to localize to weakened sections of the *B. anthracis* membrane that contain aggregates of cardiolipin. These lipid aggregates create regions

of membrane instability in *B. anthracis*, and PZN is able to insert into these regions, causing membrane depolarization and eventual cell lysis. Exogenous cardiolipin synergizes with PZN to enhance antibiotic potency.

The citrulassin sub-family of lasso peptides contain a citrulline post-translational modification which inspired reactivity-based screening for additional citrullinated natural products from bacteria. While ubiquitous in eukaryotes, deamination in bacteria is poorly characterized and exceedingly rare. Surprisingly, the peptidyl arginine deiminase responsible for the modification of arginine to citrulline in bacteria is not known. Comparative genomics was employed to find a putative PAD enzyme, which was subsequently heterologously expressed and tested for arginine deiminase activity. The scope of citrulline post-translational modifications in the citrulassins was further investigated, and the utility of the probe to label citrulline-containing natural products in complex biological extracts was studied. The bacterial arginine deiminase responsible for the modification of peptidic substrates was investigated. The citrulline-specific reaction is useful for labeling of not just RiPPs, but other citrulline-containing natural products as well.

To my beloved grandparents

George and Doris Boyd

Gordon and Margaret Blair

ACKNOWLEDGEMENTS

"Have I not commanded you? Be strong and courageous. Do not be terrified, do not be discouraged, for the Lord your God will be with you wherever you go." Joshua 1:9

Above all else, I thank the Lord for the opportunity to study at the University of Illinois and for the amazing privilege of completing my PhD. I am weak, but He is strong; my wisdom and knowledge are not my own but are gifts from Him, which I freely give back to His service.

Many amazing people also helped me reach this day. My advisor, Doug Mitchell, took a very big risk when hiring a girl with no organic chemistry or chemical biology laboratory experience, and during my time in graduate school he continually encouraged me to pursue my scientific interests. My incredible labmates – in particular Dr. Joel Melby, Dr. Kyle Dunbar, Dr. Abhishek Sharma, Dr. Courtney Cox, Dr. Katie Molohon Hess, Dr. Tucker Maxson, Dr. Caitlin Deane, Dr. Jonathan Tietz, Christopher Schwalen, and Graham Hudson – made the strain of graduate school that much more tolerable. I thank them for the collaborations and scientific insight, but also for the life advice and strong friendships.

Though busy with their own careers and families, I am grateful for the continual prayers and support of my dear sisters, Anne and Emmy. Their amazing accomplishments in medicine and in architecture, respectively, motivated me to set and relentlessly pursue my own academic achievements.

My mentor, Abby Hobbs, suffered through many years of struggle but provided a bright spot every week. She will be ever reminding me that this time in graduate school has been marked by one example after another of God answering prayer. Though he came in late to the picture, Adam Luchies was a rock during the final stretch of this PhD marathon. Members of the Graduate

Christian Fellowship were vital to my maintaining a life outside of the classroom. I am particularly indebted to Beth Ann Williams, Juliana Wilhoit, Jenna Wall Beuttler, Annie Wang Robertson, Mindy Cartolano Rak, and every member of Centennial House, past and present. The community at Twin City Bible Church deserves endless thanks for their prayers and especially their excitement and joy over every small victory.

My parents deserve more than an acknowledgement, and should have a dedication all of their own. They went above and beyond to love and care for me during the good and bad seasons, and were unafraid to admonish and direct when I lost perspective. Dad and Mom, I love you endlessly, and am so grateful for the way you encouraged me over the years. Thank you for the many sacrifices you have made to help me reach this moment.

TABLE OF CONTENTS

CHAPTER 1: INTRODUCTION 1
1.1 Genomics-driven antibiotic discovery 1
1.1.1 The golden age of antibiotics and the rise of antibiotic resistance 1
1.1.2 Impact of the genomic revolution on antibiotic discovery 2
1.1.3 Reactivity-based screening for natural product discovery 3
1.2 Ribosomally synthesized and post-translationally modified peptide natural products 5
1.2.1 Thiazole-oxazole modified microcins 6
1.2.2 Lasso peptides 7
1.3 Determining antibiotic mode of action 8
1.3.1 Affinity purification 9
1.3.2 Fluorescence microscopy 10
1.3.3 Other methods to determine mode of action 11
1.4 Summary and outlook 12
1.5 Acknowledgment 15
1.6 Figures 15
1.7 References 19

CHAPTER 2: INSIGHTS INTO METHYLTRANSFERASE SPECIFICITY AND BIOACTIVITYOF DERIVATIVES OF THE ANTIBIOTIC PLANTAZOLICIN 25
2.1 Abstract 25
2.2 Introduction 26
2.3 Results 28
2.3.1 Kinetic characterization of truncated desmethylPZN substrates 28
2.3.2 Cocrystal structures of plantazolicin methyltransferases 29
2.3.3 A polymorphic capping region undergoes structural changes in response to (poly)azolic substrate 31
2.3.4 Kinetic analysis of active site variants with Arg-Az_3 as substrate 32
2.3.5 The molecular basis for substrate specificity 33
2.3.6 Antibacterial profile of truncated PZN derivatives 34
2.4 Conclusions 35
2.5 Methods 36
2.5.1 Protein expression and crystallization 36
2.5.2 Data collection, integration and structure determination 37
2.5.3 Kinetic analysis of BamL and BpumL methyltransferases 37
2.5.4 Antibacterial assays 38
2.5.5 Microscopy 38
2.6 Acknowledgments 39
2.7 Figures 40
2.8 Tables 52
2.9 References 55

CHAPTER 3: PLANTAZOLICIN IS AN ULTRA-NARROW SPECTRUM ANTIBIOTIC THAT TARGETS THE *BACILLUS ANTHRACIS* MEMBRANE 58
3.1 Abstract 58
3.2 Introduction 59
3.3 Results 61
3.3.1 Defining the species selectivity of PZN 61
3.3.2 Assessing potential macromolecules as the target of PZN 64
3.3.3 Gene expression signature of PZN 65

3.3.4 PZN depolarizes the *B. anthracis* membrane 67
3.3.5 Subcellular localization of PZN 67
3.3.6 Isolation and characterization of PZN-resistant mutants 69
3.3.7 Exogenous cardiolipin increases sensitivity to PZN 72
3.3.8 PZN Co-localizes with cardiolipin and regions of increased fluidity 72
3.4 Conclusion 76
3.5 Methods 77
3.5.1 Strain and growth conditions 77
3.5.2 PZN production 77
3.5.3 PZN purification 78
3.5.4 Bacterial endospore preparation and susceptibility screening 78
3.5.5 PZN bioactivity 79
3.5.6 Gamma (γ) phage sensitivity 80
3.5.7 RNA isolation and transcriptional profiling of PZN-treated Sterne cells 80
3.5.8 Membrane depolarization 81
3.5.9 Confocal microscopy 81
3.5.10 Super-resolution microscopy (STORM) 82
3.5.11 2D projection analysis 83
3.5.12 PZN-Cy5 cluster analysis 84
3.5.13 Selection of spontaneous PZN-resistant mutants 84
3.5.14 Whole genome sequencing and assembly 85
3.5.15 Effect of cardiolipin on fluorescence intensity 86
3.5.16 Cardiolipin quantification from total lipid extracts 86
3.5.17 *C. elegans* nematicidal assays 87
3.5.18 cDNA construction and qRT-PCR analysis 87
3.5.19 Compound preparation 88
3.5.20 Structural characterization of PZN derivatives 90
3.5.21 Affinity purification using PZN-Biotin 91
3.5.22 Photoaffinity purification using PZN-diazirine-alkyne 92
3.5.23 Macromolecular synthesis assay 92
3.5.24 Genetic deletion of *bas4114-bas4117* 93
3.6 Figures 95
3.7 Tables 114
3.8 References 131

CHAPTER 4: REACTIVITY-BASED SCREENING FOR CITRULLINE-CONTAINING NATURAL PRODUCTS REVEALS A FAMILY OF BACTERIAL PEPTIDYL ARGININE DEIMINASES 137
4.1 Abstract 137
4.2 Introduction 138
4.3 Results 141
4.3.1 Glyoxal probe validation for RBS 142
4.3.2 RBS of predicted citrulassin producers 143
4.3.3 Comparative genomics to identify peptidyl arginine deiminases 144
4.3.4 Comparison with other characterized PADs 144
4.3.5 Genetic context of the bacterial PAD 145
4.3.6 *In vitro* reconstitution of the *Streptomyces* PAD 147
4.4 Conclusion 148
4.5 Methods 149
4.5.1 General materials and methods 149
4.5.2 Bacterial growth and extraction 149

4.5.3 Citrulassin A isolation and purification 149
4.5.4 Citrulline labeling reaction 149
4.5.5 Molecular biology techniques 150
4.5.6 Expression and purification of MBP-PAD and MBP-CitA 151
4.5.7 *In vitro* PAD activity testing 152
4.5.8 Phenylglyoxal-biotin preparation 152
4.5.9 Partial phylogenetic profiling 153
4.5.10 Sequence similarity network (SSN) generation 153
4.5.11 Genome neighborhood network (GNN) generation 153
4.5.12 Analysis of GC content 153
4.5.13 Sequence logo generation 154
4.5.14 Percent identity matrix and sequence alignment 154
4.5.15 MALDI mass spectrometry 154
4.5.16 High resolution mass spectrometry 154
4.6 Acknowledgments 155
4.7 Figures 155
4.8 Tables 171
4.9 References 173

Appendix A: PDF REPRINTS OF OTHER COAUTHORED PUBLICATIONS 177
A.1 Structural and functional insight into an unexpectedly selective *N*-methyltransferase involved in plantazolicin biosynthesis 177
A.2 Synthesis of plantazolicin analogues enables dissection of ligand binding interactions of a highly selective methyltransferase 178
A.3 Structure, bioactivity, and resistance mechanism of streptomonomicin, an unusual lasso peptide from an understudied halophilic Actinomycete 179
A.4 Biological characterization of the hygrobafilomycin antibiotic JBIR-100 and bioinformatic insights into the hygrolide family of natural products 180
A.5 *In vitro* biosynthesis and substrate tolerance of the plantazolicin family of natural products 181
A.6 A new genome mining tool redefines the lasso peptide biosynthetic landscape 182

CHAPTER 1: INTRODUCTION

1.1 Genomics-driven antibiotic discovery

1.1.1 The golden age of antibiotics and the rise of antibiotic resistance

Historically, bacterial infections were portents of death. With treatment options limited to synthetic compounds of particularly harsh natures, even medical aid was not a guarantee for survival. However, the discovery of penicillin in 1928 ushered in a revolution in modern medical treatment. When penicillin began to be used as a treatment for infections in the 1940s, the drug seemed to promise the end of the fear surrounding disease.[1] Alexander Fleming's discovery of penicillin from the fungus *Penicillum notatum* inspired the hunt for additional bacterial and fungal compounds with potent antibiotic activity. During the so-called golden age of antibiotic discovery, many such compounds heralded a future free from pathogens.

Unfortunately, bacteria have rapidly acquired resistance to all clinically relevant classes of antibiotics.[2] Alarmingly, many of the more recently FDA-approved antibiotics have had less than one year of use prior to observed antibiotic resistance (Figure 1.1).[3] While human pathogens are not necessarily endogenously resistant to such antibiotics, there is enormous selective pressure to acquire means of survival. Human microbiota are known reservoirs of antibiotic resistance genes, enabling these organisms to survive even during antibiotic courses. Hence, when pathogens interact with the natively resistant microbiome under the stress of antibiotic treatment, horizontal gene transfer is hypothesized to provide a mechanism through which pathogens acquire resistance genes.[4]

To combat the continual threat of resistance, elaboration of the current arsenal of antibiotic scaffolds has elongated the utility of the currently available drugs. Throughout the 1970s and 1980s, chemical derivatization of antibiotics was targeted at overcoming the new resistance

mechanisms observed. Mechanisms by which bacteria survive in the presence of cytotoxic concentrations of antibiotics include expression of drug efflux pumps, acquisition of enzymes that degrade the antibiotics, mutation of the target of the antibiotic, or use of alternative metabolic pathways that enable survival.[5] Thus, the primary modes by which novel second-generation antibiotics were developed were derivatization of currently prescribed compounds or through the use of synergistic inhibitors, which in combination with the primary antibiotic enhanced efficacy by targeting certain metabolic pathways more effectively. However, drug scaffolds that target different pathways or have novel modes of action may provide many more years of effective antibiotics.[6] Increasing structural diversity of antibacterial compounds is an integral part of overcoming acquired resistance mechanisms.[7] Thus, novel methods of discovering antibiotic therapies to combat the rise of these nascent pathogens are necessary.

1.1.2 Impact of the genomic revolution on antibiotic discovery

Natural products have historically been a rich source of antibiotics (Figure 1.2),[8] though the traditional method for discovering new bioactive compounds from bacterial sources via bioactivity-driven screening of bacterial extracts is plagued by rediscovery.[9] Fortunately, the genetic revolution heralds a new wave of antibiotic discovery. Sequencing bacterial and fungal genomes provides surprising and hopeful insight into the vast number of untapped biosynthetic gene clusters predicted to produce secondary metabolites.[10] Genomics has been exploited as a way to identify novel bacterial targets for antibiotic development; targets that are specific to pathogens but are absent in commensals and eukaryotes could decrease the rapidity at which resistance develops.[7, 11]

With the rapidly declining cost of genomic sequencing, the number of sequenced organisms has grown exponentially. Mining the vast array of genomic data has shown the untapped

potential of bacteria to produce diverse natural products.[12-13] This reverse-genetics approach to finding natural products is revolutionizing the manner in which natural products, and in turn potential antibiotic scaffolds, are discovered.[14-15] Genomics can provide insight into the types of natural products an organism may be capable of producing, the potential of those compounds for interesting biological activities, and can even guide the isolation and structure elucidation process.[16-17]

1.1.3 Reactivity-based screening for natural product discovery

A recent advance in natural product discovery that has exploited the recent availability of the expontentially increasing collection of genomic data is reactivity-based screening (RBS). The main driving force behind RBS is the discovery of novel drug scaffolds, both from well-studied and new organisms. Additionally, there is interest in connecting genes to molecules, thereby elucidating new biosynthetic pathways and the genetic basis for chemistry taking place in a biological context.[16] This can, in turn, elucidate ways in which the natural product biosynthetic pathway can be altered to produce unnatural compounds and, in turn, libraries of compounds to be tested for interesting and potent antibiotic properties.[18]

In RBS, a chemical reaction is developed to specifically react with a natural product functional group of interest. These functional groups may endow the natural product with enhanced stability, improved structural rigidity, an altered conformation, or a specific reactivity. Examples of modifications of interest include terminal alkenes and alkynes, thioether bonds, aldehydes, and dehydrated amino acids. Reactions that are ideal for RBS are (a) able to specifically react with the functional group in a complex sample; (b) not adversely affected by the presence of water; (c) simple, one step reactions; (d) easily scalable and easily carried out in parallel; (e) compatible with mass spectrometry and (f) possibly extendable to guide purification or enrich for

the specific natural product.[19] The reaction is developed by testing reaction conditions on purified natural product substrates, followed by reactions in cell extracts known to contain natural products with the functional group of interest. For example, an aminooxy probe was recently validated by first labeling purified streptomycin, an aldehyde-containing aminoglycoside antibiotic. The reaction was then confirmed to label streptomycin in an extract from the producing organism, *Streptomyces griseus*.[20]

After a functional group has been selected, the enzyme or enzymes responsible for that modification are used as diagnostic markers to guide genome mining for suitable organisms. Prioritized strains containing the necessary enzymes are then grown, extracted, and a portion of the extract is subjected to the reaction with the probe. Using mass spectrometry, the unreacted extract is compared with the reacted sample. Mass shifts characteristic of the reaction are used to confirm the presence of a biomolecule bearing the functional group of interest. If the reactions successfully label a biomolecule, subsequent isolation and characterization can occur (Figure 1.3).

RBS has been used to guide the identification and purification of a number of natural products with antibiotic activity, demonstrating the utility of the technique in not only connecting genes to molecules but also providing potential leads in antibiotic discovery.[20-22] For example, RBS was used to guide identification and purification of a natural product from *Streptomyces rimosus* subsp. *rimosus*.[21] Bacterial extracts were screened with dithiothreitol, known to react with α,β-unsaturated amino acids, and a characteristic mass shift was observed. The isolated natural product, cyclothiazomycin C, is a novel thiopeptide with Gram-positive antibiotic activity. Cyclothiazomycin C belongs to a much larger family of natural products that are ribosomally synthesized and post-translationally modified. These natural products are genetically encoded and

have distinct classes of enzymes responsible for post-translational modifications, making them ideal candidates for RBS.

1.2 Ribosomally synthesized and post-translationally modified peptide natural products

The ribosomally synthesized and post-translationally modified peptide natural products (RiPPs) are a family of secondary metabolites that is rapidly growing. Due to the vast number of sequenced genomes, many newly designed bioinformatics programs have been designed to mine genomic databases for recognizable sequences.[23-25] Similar to nonribosomal petptide and polyketide biosynthetic machinery, there are genetic signatures that can be used to search new genomes for RiPP gene clusters and to predict natural product structures.[16-17, 26-27] The diversity of post-translational modifications, such as various cyclizations, dehydrations and oxidations, rearrangements, and methylations, create complex scaffolds that have inspired new thinking about the untapped chemical potential of bacteria (Figure 1.4).[28-30]

Recently, the similarities between biosynthetic gene clusters for the many families of RiPPs were characterized and the family was organized into distinct classes based on the posttranslational modification machinery involved in production of each RiPP.[28] As of 2013, RiPPs are organized into 20 classes,[28] mostly based on biosynthetic enzymes but in some based grouped around historical classifications such as producing organism[31] or biological activity.[32] The discrete, modular modification machinery of RiPPs makes these natural products extremely amenable to mutation and library generation. Interestingly, a number of RiPP biosynthetic gene clusters encode multiple precursor peptides, suggesting flexibility in the posttranslational machinery to accept multiple core peptide sequences.[33-34] Ease of genetic mutation has also facilitated the ease with which novel RiPP analogs can be generated.[18, 35]

The overarching logic of the biosynthesis of a RiPP is as follows: the precursor peptide is a short, 20 – 110 amino acid peptide that is synthesized in the ribosome. Tailoring enzymes have a specific RiPP recognition element (RRE)[26] that enable them to bind to the leader peptide and perform enzymatic modification of the core region of the precursor peptide (Figure 1.5).[36] In some cases, the core peptide is N-terminal to the leader peptide, which is then referred to as the follower peptide.[37-38] Proteolytic cleavage of the leader peptide, when not required for certain post-translational modifications (such as in the case of the cyclization of lasso peptides, for example) is required prior to export of the mature natural product. Some post-translational modifications also occur after leader peptide cleavage, such as the dimethylation of the nascent N-terminus of the linear azol(in)e-containing peptide plantazolicin[39-41] and the isopeptide bond macrocyclization of lasso peptides.[17, 28]

1.2.1 Thiazole-oxazole modified microcins

Linear azol(in)e-containing peptides (LAPs) are a subclass of thiazole-oxazole modified microcins (TOMMs), an overarching classification for RiPPs that contain cyclized Thr/Ser and Cys residues, including some thiopeptides, cyanobactins, and LAPs.[28, 42-43] LAPs are characterized by a lack of macrocyclization machinery but the presence of a cyclodehydratase complex that will process Thr/Ser and Cys residues into the corresponding (methyl)oxazoline or thiazoline. Occasionally, a dedicated dehydrogenase will perform a two-electron oxidation to further elaborate azolines into azoles (Figure 1.6).[44] The mechanism of cyclodehydration is an ATP-dependent backbone activation, followed by subsequent nucleophilic attack from the side chain O/S.[45-46] Heterocycle formation induces more complex secondary structure which rigidifies the backbone and protects the molecule from proteolytic degradation.

Some of the earliest-characterized TOMMs are members of the LAP family of TOMMs, including microcin B17[47] and streptolysin S.[48] Plantazolicin (PZN) is a LAP with an unusual polyheterocyclic structure discovered through a reverse genetics approach in the soil-dwelling bacterium *Bacillus velezensis* FZB42.[49-50] The two sets of five heterocyclized residues, which are all installed by a common cyclodehydratase complex, has inspired multiple total syntheses, although thus far none has successfully achieved one-pot cyclization of all ten residues.[51-53]

Not only does PZN have an intriguing structure, but its biological activity is also unique. PZN selectively targets the native producer of anthrax, *Bacillus anthracis*, in a species-specific manner.[54] Determination of the mode of action of PZN through standard microbiological assays was unsuccessful, but through a combination of chemical and microbiological strategies, it was determined that PZN specifically kills *B. anthracis* by interacting with unusual lipid aggregates in the cell membrane. Cardiolipin creates regions of increased fluidity and destabilization that enable PZN to insert in the membrane and cause cell lysis.[54-55] Like PZN, other TOMMs have antibiotic, antiviral, or anticancer activity, or act as virulence factors and signaling molecules.[43] At least 700 TOMMs have been identified bioinformatically, suggesting the family has great potential for future structural and functional analysis.[16, 29, 56]

1.2.2 Lasso peptides

Compared to the TOMMs, lasso peptides have very small biosynthetic gene clusters and only two necessary tailoring enzymes, a leader peptidase and a lasso cyclase. After leader peptide cleavage, the C-terminal tail region of the core peptide is encircled by a macrocycle formed between the nascent N-terminus and an Asp/Glu side chain, creating a locked lariat topology (Figure 1.6). High sequence variation within the bioinformatically characterized precursor peptides allows for a vast array of naturally occurring lassos in three different families, and suggests great potential for lasso

peptide library generation.[57] Interestingly, lasso peptides are particularly resistant to proteolysis due to the complex three-dimensional structure, which may also endow many lasso peptides with antimicrobial activity.[58-59]

Lasso peptides were recently subject to extensive bioinformatic investigation as a test case for developing an ORF recognition and natural product structure prediction program.[60] Rapid ORF Description and Evaluation Online (RODEO) showed the previously-unknown biodiversity of lasso producers and was used to map over 1400 lasso peptide biosynthetic gene clusters and 1300 precursor peptides. In the course of validating the core sequence and structure prediction portions of the program, six lassos were selected for isolation, structural confirmation, and bioactivity testing. Surprisingly, one lasso peptide was found to have an additional post-translational modification not predicted based on the biosynthetic gene cluster.[60] Citrulassin A contains an Arg-to-Cit modification, causing a mass increase of 1 Da and the loss of a net positive charge at neutral pH.[61] A distally arginine deiminase is hypothesized to perform the post-translational modification, and evaluation of this enzyme is revealing the biosynthetic potential of bacteria to install citrulline residues into proteins and peptide-derived natural products. Intriguingly, however, citrulassin A does not appear to have antibiotic activity, calling into question the role of this PTM in not just lasso peptides, but other bacterially produced citrulline-containing natural products.[60] RODEO uncovered many lasso peptide gene clusters containing phosphorylation and adenylation domains involved in bacterial signaling pathways, which suggests that deimination may also be important for signaling.[60]

1.3 Determining antibiotic mode of action

While knowledge of the mode of action is not required for the clinical deployment of an antibiotic, as in the case of daptomycin,[62] such information could play a critical role in determining useful

combination therapies and efficient structural elaboration for subsequent generations of drugs. For instance, if the target of an antibiotic is known, the interaction can be used to guide structure-activity relationship studies to improve binding to the target or diminish off-target interactions. Most of the commonly prescribed antibacterials kill bacteria by targeting cell wall biosynthesis, protein biosynthesis, or nucleic acid biosynthesis.[63] Therapeutic agents that can work in tandem to resensitize pathogens to commonly used antibiotics may provide the next set of useful antibiotics. However, this requires a deep understanding of not only drug interactions with targets, but how different modes of action can antagonize or synergize with one another. Alternatively, drug scaffolds that are entirely different from currently used drugs may target bacteria through other essential pathways for which bacteria have not acquired resistance mechanisms.

Chemical methods to determine the mode of action of antibiotic agents generally rely on substrate modification, such as the attachment of affinity tags for affinity purification or fluorescent molecules for microscopy-guided localization. These techniques can complement the microbiological techniques of RNA-Seq,[64] resistant mutant generation and sequencing,[65] and macromolecular synthesis assays, to name a few.

1.3.1 Affinity purification

A common first approach to determining antibiotic mode of action is affinity purification, which can provide relatively direct evidence to its binding ligands and hence, target information.[66] A position in the molecule that is amenable to modification is labeled with an affinity probe, such as biotin. The compound is dosed into cell lysate and allowed to bind to its target, and then isolated from the cell lysate. The tagged antibiotic and its target interact with a resin bearing the binding partner of the tag molecule, such as streptavidin for biotin tags or glutathione for GST tags, and the pair are specifically eluted after washing away noninteracting biomolecules.[67] Using

proteomics and mass spectrometry, the target can then be identified and subsequently validated through additional biochemical and microbiological investigation.[68]

Affinity purification is particularly designed for molecules that covalently modify their target biomolecule, as the drug-target bond cannot be broken during the washing and purification steps. However, there are significant drawbacks to affinity purification, limiting its utility, especially for compounds that interact in a noncovalent manner with the cellular target.[69] Indeed, the many strategies available for target identification suggest that no one technique is capable of elucidating all compound-target interactions, due to complexities that may be inherent in the compound-target interaction.[70] First, the target must remain stable in cell lysate and folded correctly for the interaction to occur. Second, the drug molecule must be amenable to derivatization without significantly affecting binding to the target.[71-72] Third, the drug-target interaction must be strong enough to persist through stringent washing protocols. Some of the difficulties can be alleviated with the use of photoaffinity reagents to covalently attach the biomolecule to the drug.[66, 73-74]

1.3.2 Fluorescence microscopy

Evaluation of antibiotic-treated cells by microscopy can be used to determine the mode of action of antibiotics through the observation of phenotypic changes. For example, cell lysis can indicate pore formation and subsequent membrane depolarization, leading to lytic activity, such as in the case of nisin.[75-76] Morphological changes of resistant mutants may signify that certain pathways are negatively affected by a drug. Streptomonomicin resistance induces a chaining phenotype in *B. anthracis*, which suggests that the lasso peptide interacts with cell wall biosynthesis.[77] In addition, localization of a fluorescent antibiotic can inform on its action within the bacterium. Vancomycin and ramoplanin each stain cells at sites of active peptidoglycan biosynthesis,

including the cell poles and in helical patterns across the side walls of bacilli.[78] Two-component action of haloduracin α/β was confirmed through labeling of both molecules and using fluorescence resonance energy transfer microscopy.[79] Similar to affinity purification, fluorescent tagging of antibiotics is limited by the fact that the fluorophore must not interfere with the ability of the antibiotic to bind to its target.[80]

More precise fluorescence microscopy in recent years has enable improved spatial localization of antibiotics, especially with the development of super-resolution microscopy to bypass the diffraction limit of traditional microscopy. Crucial to the technology is a photoswitchable dye such as Cyanine5, which can be sent into a dark or nonfluorescent state, enabling activation of only a very small subset of dye molecules at any one time.[81-82] Stochastic optical reconstruction microscopy (STORM), which can achieve resolution to 20 nm,[82-83] recently demonstrated that a fluorescent PZN derivative formed aggregates within the *B. anthracis* cell envelope, leading to cell lysis.[54] Due to the small size of bacterial cells (1 – 2 μm in diameter for many *Bacilli*), limitations to resolution make subcellular localization difficult without super-resolution microscopy. However, single molecule fluorescence imaging is a powerful technique to directly visualize drug-target interactions in real time.[54, 79, 84]

1.3.3 Other methods to determine mode of action

In order to validate an antibiotic mode of action, there must be additional means of implicating a connection between drug target and drug molecule. Growing susceptible species in the presence of sub-inhibitory concentrations of compound can lead to the evolution of resistant mutants. Genomic polymorphisms giving rise to resistance could support the involvement of certain genes and biological processes in overcoming antibiotic susceptibility. Daptomycin-resistant *Enterococci* mutate *liaF* and *GdpD*, genes which are involved in phospholipid cell wall

metabolism, confirming that the antibiotic induces cell envelope stress.[85-86] A complementary approach involves overexpression of the putative target, resulting in reduced potency of the drug.[87] Transcriptional profiling techniques, such as RNA-Seq, provide a global picture of bacterial response to an antibiotic and are also useful in highlighting pathways involved in antibiotic-induced stress response.[88] Similarly, macromolecular synthesis assays show bacterial response to antibiotic treatment in real time through measuring alterations in the incorporation of radiolabeled precursors into various biomolecules such as peptidoglycan, proteins, and DNA.[89] While no one assay is sufficient to confirm an antibiotic target, these and many other techniques can be used in combination to better understand antibiotic mode of action. Despite the challenges, determining mode of action can provide powerful new insight into biological processes in addition to furthering the search for new antibiotics and new targets for antibiotic development.

1.4 Summary and outlook

Natural product discovery is undergoing a revolution due to the advent of next-generation sequencing and the proliferation of programs designed to mine genomes for biosynthetic potential. Previously, natural products with interesting bioactivities were isolated based on biological activity; however, this yielded only high-abundance natural products in certain families. Now, however, bioinformatics is shedding light on the potential of organisms to produce compounds covering a much broader area of chemical space. These predicted compounds demonstrate the vast array of biochemical reactions, provide interesting new scaffolds to inspire the development of new antibiotics, and even inspire organic chemists to attempt new chemical reactions.

A burgeoning class of natural products benefiting from new genome mining efforts is the ribosomally synthesized and post-translationally modified peptide family of natural products. Many of these compounds display interesting biological activities and have unique biosynthetic

enzymes. Critically, natural product discovery efforts guided the isolation, purification, and characterization of the RiPP natural product, plantazolicin. The linear azol(in)e-containing peptide has ten nitrogen-containing heterocycles but also requires N-terminal dimethylation for potent anti-*B. anthracis* activity. In Chapter 2, we studied the enzyme responsible for this final post-translational modification in the biosynthesis of plantazolicin. We investigated the minimal substrate necessary for enzyme recognition and determined the kinetics of substrate binding. We crystalized the purified methyltransferase with the cofactor inhibitor S-adenosylhomocysteine and with PZN substrate analogs in order to better understand the exquisite selectivity of the methyltransferase for PZN-like substrates.

PZN generated interest not just for its biosynthesis but also its ultra-narrow spectrum of bioactivity. In Chapter 3, we covered the scope of PZN bioactivity and demonstrated its species selectivity. We investigated the mode of action through extensive bioactivity testing, chemical derivatization, genetic analysis of resistant mutants, and additional biochemical assays. While no specific target for PZN was definitevely determined, resistant mutants suggested cardiolipin misaggregation in the *B. anthracis* cell membrane was necessary for PZN bioactivity. We validated the role of cardiolipin by demonstrating synergy with PZN and studying the effects of exogenous cardiolipin on the ability of a fluorescent derivative to label *B. anthracis*. We finally suggested that ultra-narrow antibiotics may be useful in combating the rise of antibiotic resistance.

While predicting natural products through genome mining projects demonstrates the untapped potential of nature to synthesize complex scaffolds, isolation and purification of those compounds for characterization is often the rate-limiting step. Reactivity-based screening takes advantage of genomic information about specific enzymatic processes that install functional groups of interest onto natural products to streamline extract screening. In Chapter 4, we extended

reactivity-based screening to investigate the scope of citrulline modifications in ribosomally synthesized and post-translationally modified peptides, in particular the lasso peptides. We used the results of reactivity-based screening to inform the search for the bacterial peptidyl arginine deiminase responsible for the post-translational modification.

Currently, genomics is generating extreme interest in natural product discovery for antibiotic development. However, the isolation and subsequent characterization of these compounds is necessary to determine their utility as drug scaffolds. The biosynthetic evaluation of plantazolicin, determination of its mode of action, and the study of novel post-translational modifications onto peptide-derived scaffolds empowers the future of natural product discovery and characterization, and supports the continued efforts to prioritize natural products for antibiotic development.

1.5 Acknowledgement

I am grateful to Christopher Schwalen for his critical review of this introductory chapter.

1.6 Figures

Figure 1.1 Years of antibiotic efficacy prior to clinically observed resistance. Antibiotics are ordered by date of release, from left to right. Gradients indicate members of the antibiotic class have a range of years of efficacy. Data adapted from Clatworthy, Pierson, and Hung, *Nat. Chem. Biol.* **2007**, *3*, 541.

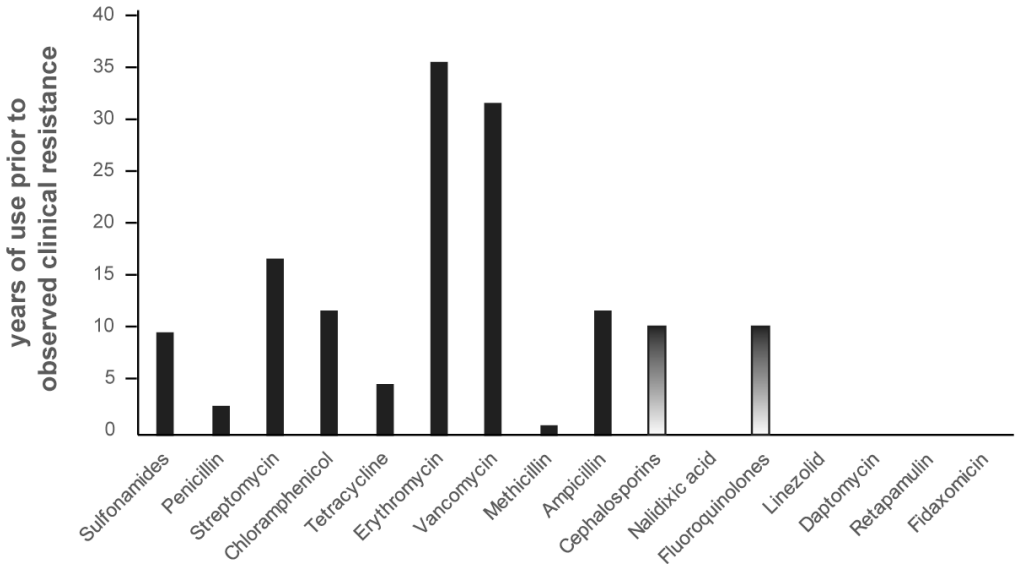

Figure 1.2 Sources of all clinically relevant antibiotic agents, demonstrating the importance of natural products as inspiration for new drug molecules. Data adapted from Newman and Cragg, *J. Nat. Prod.* **2012**, *75*, 311.

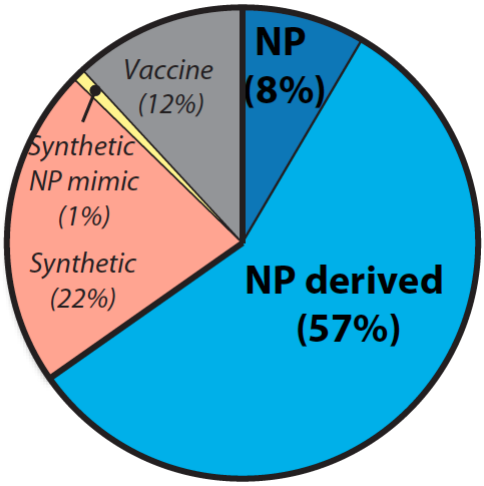

Figure 1.3 Workflow of reactivity-based screening. Genome mining for specific modification enzymes leads to prioritized strains, which can be cultured and tested with a specific labeling reaction for the production of natural products bearing the functional group of interest. If the natural product is produced under laboratory conditions, the compound can be isolated and further characterized.

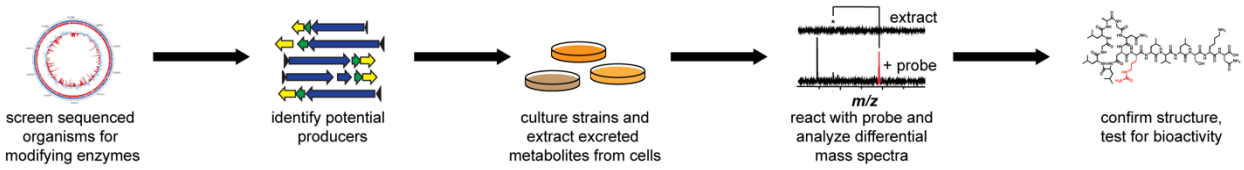

Figure 1.4 Representative structures of characterized RiPP natural products. Family-defining post-translational modifications are highlighted in red. Family names are listed in italics below the name of the natural product.

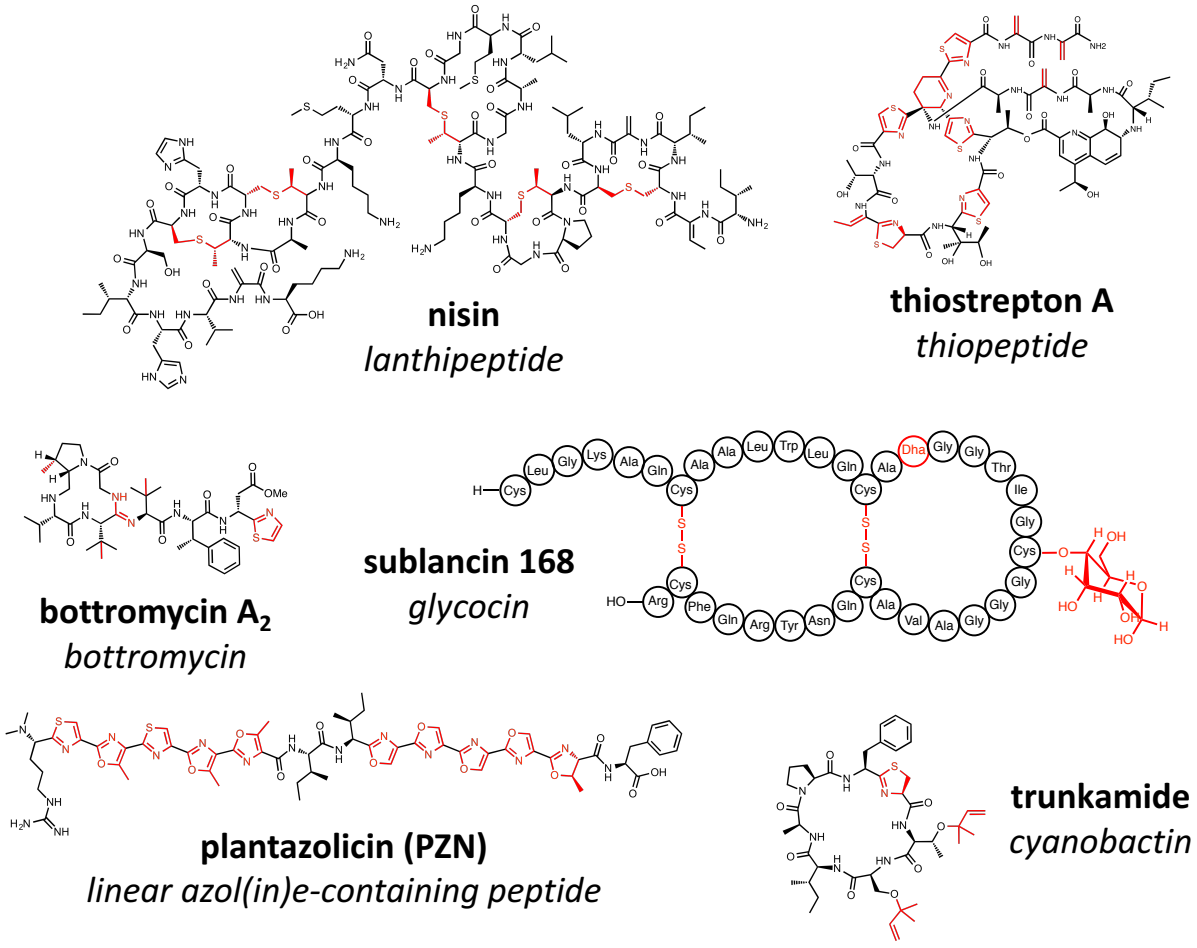

Figure 1.5 General scheme for the biosynthesis of RiPP natural products. (A) The RiPP biosynthetic gene cluster contains genes for the precursor peptide, tailoring enzymes, and additional enzymes involved in immunity, proteolysis, and export. (B) The post-translational machinery installs modifications onto the ribosomally produced precursor peptide, composed of a leader and a core peptide. After proteolytic cleavage of the leader peptide, the mature RiPP natural product is exported from the producing organism.

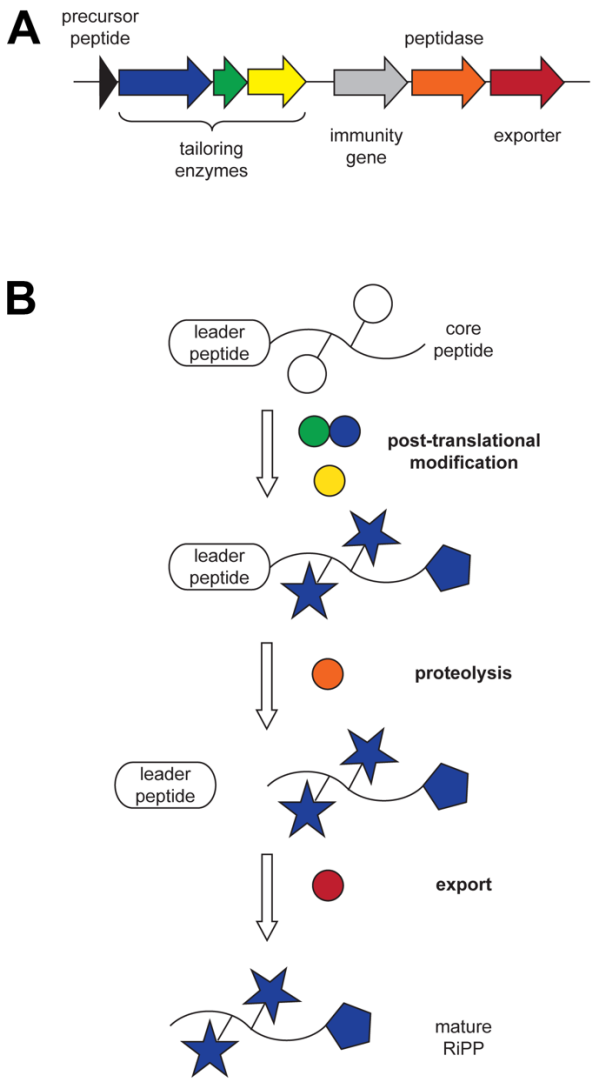

Figure 1.6 Enzymatically driven heterocycle formation in linear-azole containing peptides (LAPs) utilizes a cyclodehydratase (D protein) to guide heterocycle formation through backbone activation with an intermediate phosphorylated hemi-orthoamide. The cyclodehydratase occasionally is paired with a secondary enzyme responsible for leader peptide binding (C protein). Additional elaboration with an FMN-dependent dehydrogenase is also possible, leading to the oxidation of azolines to azoles and a total mass loss of 20 Da from the natural amino acid.

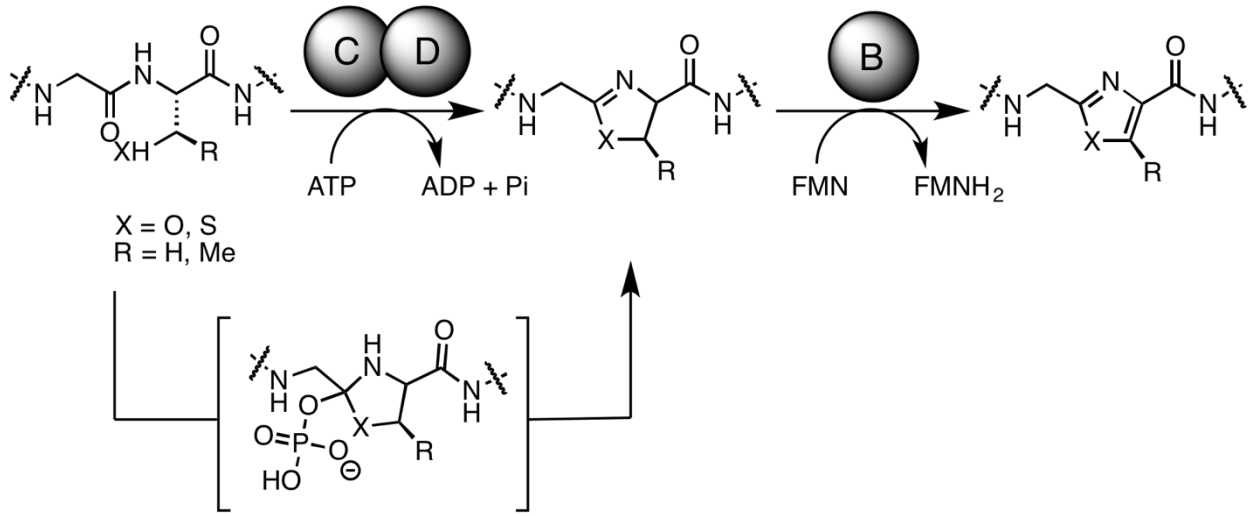

Figure 1.7 General scheme for the biosynthesis of lasso peptides. Cleavage of the leader peptide occurs prior to threading and cyclization of the core peptide, yielding the mature natural product.

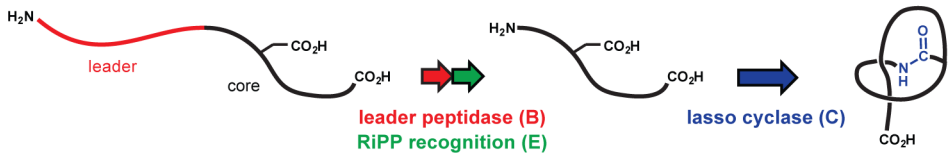

1.7 References

1. Berdy, J., Thoughts and facts about antibiotics: Where we are now and where we are heading. *J Antibiot* **2012,** *65* (8), 385-395.
2. Walsh, C. T.; Wencewicz, T. A., Prospects for new antibiotics: a molecule-centered perspective. *J Antibiot* **2014,** *67* (1), 7-22.
3. Palumbi, S. R., Humans as the world's greatest evolutionary force. *Science* **2001,** *293* (5536), 1786-1790.
4. Wright, G. D., The antibiotic resistome: The nexus of chemical and genetic diversity. *Nat Rev Micro* **2007,** *5* (3), 175-186.
5. Tenover, F. C., Mechanisms of antimicrobial resistance in bacteria. *Am J Med* **2006,** *119*, S3-10.
6. Payne, D. J., Desperately seeking new antibiotics. *Science* **2008,** *321* (5896), 1644-1645.
7. Payne, D. J.; Gwynn, M. N.; Holmes, D. J.; Pompliano, D. L., Drugs for bad bugs: confronting the challenges of antibacterial discovery. *Nat Rev Drug Discov* **2007,** *6* (1), 29-40.
8. Newman, D. J.; Cragg, G. M., Natural Products as Sources of New Drugs from 1981 to 2014. *Journal of Natural Products* **2016,** *79* (3), 629-661.
9. Baltz, R. H., Marcel Faber Roundtable: is our antibiotic pipeline unproductive because of starvation, constipation or lack of inspiration? *J Ind Microbiol Biotechnol* **2006,** *33* (7), 507-513.
10. Bode, H. B.; Muller, R., The impact of bacterial genomics on natural product research. *Angew Chem Int Ed Engl* **2005,** *44* (42), 6828-6846.
11. Brown, J. R.; Warren, P. V., Antibiotic discovery: is it all in the genes? *Drug Discov Today* **1998,** *3* (12), 564-566.
12. Bentley, S. D.; Chater, K. F.; Cerdeno-Tarraga, A. M.; Challis, G. L.; Thomson, N. R.; James, K. D.; Harris, D. E.; Quail, M. A.; Kieser, H.; Harper, D.; Bateman, A.; Brown, S.; Chandra, G.; Chen, C. W.; Collins, M.; Cronin, A.; Fraser, A.; Goble, A.; Hidalgo, J.; Hornsby, T.; Howarth, S.; Huang, C. H.; Kieser, T.; Larke, L.; Murphy, L.; Oliver, K.; O'Neil, S.; Rabbinowitsch, E.; Rajandream, M. A.; Rutherford, K.; Rutter, S.; Seeger, K.; Saunders, D.; Sharp, S.; Squares, R.; Squares, S.; Taylor, K.; Warren, T.; Wietzorrek, A.; Woodward, J.; Barrell, B. G.; Parkhill, J.; Hopwood, D. A., Complete genome sequence of the model actinomycete Streptomyces coelicolor A3(2). *Nature* **2002,** *417* (6885), 141-147.
13. Medema, M. H.; Fischbach, M. A., Computational approaches to natural product discovery. *Nat Chem Biol* **2015,** *11* (9), 639-648.
14. Doroghazi, J. R.; Metcalf, W. W., Comparative genomics of actinomycetes with a focus on natural product biosynthetic genes. *BMC Genomics* **2013,** *14*, 611.
15. Cimermancic, P.; Medema, M. H.; Claesen, J.; Kurita, K.; Wieland Brown, L. C.; Mavrommatis, K.; Pati, A.; Godfrey, P. A.; Koehrsen, M.; Clardy, J.; Birren, B. W.; Takano, E.; Sali, A.; Linington, R. G.; Fischbach, M. A., Insights into secondary metabolism from a global analysis of prokaryotic biosynthetic gene clusters. *Cell* **2014,** *158* (2), 412-421.
16. Deane, C. D.; Mitchell, D. A., Lessons learned from the transformation of natural product discovery to a genome-driven endeavor. *J Ind Microbiol Biot* **2014,** *41* (2), 315-331.
17. Tietz, J. I.; Mitchell, D. A., Using genomics for natural product structure elucidation. *Curr Top Med Chem* **2016,** *16* (15), 1645-1694.
18. Deane, C. D.; Melby, J. O.; Molohon, K. J.; Susarrey, A. R.; Mitchell, D. A., Engineering unnatural variants of plantazolicin through codon reprogramming. *ACS Chem Biol* **2013,** *8* (9), 1998-2008.

19. Odendaal, A. Y.; Trader, D. J.; Carlson, E. E., Chemoselective enrichment for natural products discovery. *Chem Sci* **2011,** *2* (4), 760-764.
20. Maxson, T. T., J.I.; Hudson, G.A.; Mitchell, D.A., Targeting aldehydes and ketones for reactivity-based natural product discovery. **2016**, In revision.
21. Cox, C. L.; Tietz, J. I.; Sokolowski, K.; Melby, J. O.; Doroghazi, J. R.; Mitchell, D. A., Nucleophilic 1,4-additions for natural product discovery. *ACS Chem Biol* **2014,** *9* (9), 2014-2022.
22. Molloy, E. M.; Tietz, J. I.; Blair, P. M.; Mitchell, D. A., Biological characterization of the hygrobafilomycin antibiotic JBIR-100 and bioinformatic insights into the hygrolide family of natural products. *Bioorg Med Chem*.
23. Weber, T.; Blin, K.; Duddela, S.; Krug, D.; Kim, H. U.; Bruccoleri, R.; Lee, S. Y.; Fischbach, M. A.; Müller, R.; Wohlleben, W.; Breitling, R.; Takano, E.; Medema, M. H., antiSMASH 3.0—a comprehensive resource for the genome mining of biosynthetic gene clusters. *Nucleic Acids Res* **2015**.
24. Mohimani, H.; Kersten, R. D.; Liu, W.-T.; Wang, M.; Purvine, S. O.; Wu, S.; Brewer, H. M.; Pasa-Tolic, L.; Bandeira, N.; Moore, B. S.; Pevzner, P. A.; Dorrestein, P. C., Automated genome mining of ribosomal peptide natural products. *ACS Chem Biol* **2014,** *9* (7), 1545-1551.
25. Lee, S. W.; Mitchell, D. A.; Markley, A. L.; Hensler, M. E.; Gonzalez, D.; Wohlrab, A.; Dorrestein, P. C.; Nizet, V.; Dixon, J. E., Discovery of a widely distributed toxin biosynthetic gene cluster. *Proc Natl Acad Sci U S A* **2008,** *105* (15), 5879-5884.
26. Burkhart, B. J.; Hudson, G. A.; Dunbar, K. L.; Mitchell, D. A., A prevalent peptide-binding domain guides ribosomal natural product biosynthesis. *Nat Chem Biol* **2015,** *11* (8), 564-570.
27. Donia, M. S.; Hathaway, B. J.; Sudek, S.; Haygood, M. G.; Rosovitz, M. J.; Ravel, J.; Schmidt, E. W., Natural combinatorial peptide libraries in cyanobacterial symbionts of marine ascidians. *Nat Chem Biol* **2006,** *2* (12), 729-735.
28. Arnison, P. G.; Bibb, M. J.; Bierbaum, G.; Bowers, A. A.; Bugni, T. S.; Bulaj, G.; Camarero, J. A.; Campopiano, D. J.; Challis, G. L.; Clardy, J.; Cotter, P. D.; Craik, D. J.; Dawson, M.; Dittmann, E.; Donadio, S.; Dorrestein, P. C.; Entian, K. D.; Fischbach, M. A.; Garavelli, J. S.; Goransson, U.; Gruber, C. W.; Haft, D. H.; Hemscheidt, T. K.; Hertweck, C.; Hill, C.; Horswill, A. R.; Jaspars, M.; Kelly, W. L.; Klinman, J. P.; Kuipers, O. P.; Link, A. J.; Liu, W.; Marahiel, M. A.; Mitchell, D. A.; Moll, G. N.; Moore, B. S.; Muller, R.; Nair, S. K.; Nes, I. F.; Norris, G. E.; Olivera, B. M.; Onaka, H.; Patchett, M. L.; Piel, J.; Reaney, M. J.; Rebuffat, S.; Ross, R. P.; Sahl, H. G.; Schmidt, E. W.; Selsted, M. E.; Severinov, K.; Shen, B.; Sivonen, K.; Smith, L.; Stein, T.; Sussmuth, R. D.; Tagg, J. R.; Tang, G. L.; Truman, A. W.; Vederas, J. C.; Walsh, C. T.; Walton, J. D.; Wenzel, S. C.; Willey, J. M.; van der Donk, W. A., Ribosomally synthesized and post-translationally modified peptide natural products: overview and recommendations for a universal nomenclature. *Nat Prod Rep* **2013,** *30* (1), 108-160.
29. Cox, C. L.; Doroghazi, J. R.; Mitchell, D. A., The genomic landscape of ribosomal peptides containing thiazole and oxazole heterocycles. *BMC Genomics* **2015,** *16* (1), 778.
30. Haft, D. H.; Basu, M. K.; Mitchell, D. A., Expansion of ribosomally produced natural products: a nitrile hydratase- and Nif11-related precursor family. *BMC Biol* **2010,** *8*, 70.
31. Duquesne, S.; Destoumieux-Garzon, D.; Peduzzi, J.; Rebuffat, S., Microcins, gene-encoded antibacterial peptides from enterobacteria. *Nat Prod Rep* **2007,** *24* (4), 708-734.
32. Klaenhammer, T. R., Genetics of bacteriocins produced by lactic acid bacteria. *FEMS Microbiol Rev* **1993,** *12* (1-3), 39-85.
33. Li, B.; Sher, D.; Kelly, L.; Shi, Y.; Huang, K.; Knerr, P. J.; Joewono, I.; Rusch, D.; Chisholm, S. W.; van der Donk, W. A., Catalytic promiscuity in the biosynthesis of cyclic peptide

secondary metabolites in planktonic marine cyanobacteria. *Proc Natl Acad Sci USA* **2010,** *107* (23), 10430-10435.
34. Schmidt, E. W.; Nelson, J. T.; Rasko, D. A.; Sudek, S.; Eisen, J. A.; Haygood, M. G.; Ravel, J., Patellamide A and C biosynthesis by a microcin-like pathway in Prochloron didemni, the cyanobacterial symbiont of Lissoclinum patella. *Proc Natl Acad Sci USA* **2005,** *102* (20), 7315-7320.
35. McIntosh, J. A.; Schmidt, E. W., Marine molecular machines: heterocyclization in cyanobactin biosynthesis. *Chembiochem* **2010,** *11* (10), 1413-1421.
36. Oman, T. J.; van der Donk, W. A., Follow the leader: The use of leader peptides to guide natural product biosynthesis. *Nat Chem Biol* **2010,** *6* (1), 9-18.
37. Huo, L.; Rachid, S.; Stadler, M.; Wenzel, S. C.; Muller, R., Synthetic biotechnology to study and engineer ribosomal bottromycin biosynthesis. *Chem Biol* **2012,** *19* (10), 1278-1287.
38. Hou, Y.; Tianero, M. D.; Kwan, J. C.; Wyche, T. P.; Michel, C. R.; Ellis, G. A.; Vazquez-Rivera, E.; Braun, D. R.; Rose, W. E.; Schmidt, E. W.; Bugni, T. S., Structure and biosynthesis of the antibiotic bottromycin D. *Org Lett* **2012,** *14* (19), 5050-5053.
39. Hao, Y.; Blair, P. M.; Sharma, A.; Mitchell, D. A.; Nair, S. K., Insights into methyltransferase specificity and bioactivity of derivatives of the antibiotic plantazolicin. *ACS Chem Biol* **2015,** *10* (5), 1209-1216.
40. Lee, J.; Hao, Y.; Blair, P. M.; Melby, J. O.; Agarwal, V.; Burkhart, B. J.; Nair, S. K.; Mitchell, D. A., Structural and functional insight into an unexpectedly selective N-methyltransferase involved in plantazolicin biosynthesis. *Proc Natl Acad Sci U S A* **2013,** *110* (32), 12954-12959.
41. Molohon, K. J.; Melby, J. O.; Lee, J.; Evans, B. S.; Dunbar, K. L.; Bumpus, S. B.; Kelleher, N. L.; Mitchell, D. A., Structure determination and interception of biosynthetic intermediates for the plantazolicin class of highly discriminating antibiotics. *ACS Chem Biol* **2011,** *6* (12), 1307-1313.
42. Metelev, M. V.; Ghilarov, D. A., Structure, function, and biosynthesis of thiazole/oxazole-modified microcins. *Molecular Biology* **2014,** *48* (1), 29-45.
43. Melby, J. O.; Nard, N. J.; Mitchell, D. A., Thiazole/oxazole-modified microcins: complex natural products from ribosomal templates. *Curr Opin Chem Biol* **2011,** *15* (3), 369-378.
44. Melby, J. O.; Li, X.; Mitchell, D. A., Orchestration of enzymatic processing by thiazole/oxazole-modified microcin dehydrogenases. *Biochemistry* **2014,** *53* (2), 413-422.
45. Dunbar, K. L.; Melby, J. O.; Mitchell, D. A., YcaO domains use ATP to activate amide backbones during peptide cyclodehydrations. *Nat Chem Biol* **2012,** *8* (6), 569-575.
46. Melby, J. O.; Dunbar, K. L.; Trinh, N. Q.; Mitchell, D. A., Selectivity, directionality, and promiscuity in peptide processing from a *Bacillus* sp. Al Hakam cyclodehydratase. *J Am Chem Soc* **2012,** *134* (11), 5309-5316.
47. Li, Y. M.; Milne, J. C.; Madison, L. L.; Kolter, R.; Walsh, C. T., From peptide precursors to oxazole and thiazole-containing peptide antibiotics: Microcin B17 synthase. *Science* **1996,** *274* (5290), 1188-1193.
48. Nizet, V.; Beall, B.; Bast, D. J.; Datta, V.; Kilburn, L.; Low, D. E.; De Azavedo, J. C., Genetic locus for streptolysin S production by group A streptococcus. *Infect Immun* **2000,** *68* (7), 4245-4254.
49. Scholz, R.; Molohon, K. J.; Nachtigall, J.; Vater, J.; Markley, A. L.; Sussmuth, R. D.; Mitchell, D. A.; Borriss, R., Plantazolicin, a novel microcin B17/streptolysin S-like natural product from *Bacillus amyloliquefaciens* FZB42. *J Bacteriol* **2011,** *193* (1), 215-224.

50. Kalyon, B.; Helaly, S. E.; Scholz, R.; Nachtigall, J.; Vater, J.; Borriss, R.; Sussmuth, R. D., Plantazolicin A and B: structure elucidation of ribosomally synthesized thiazole/oxazole peptides from *Bacillus amyloliquefaciens* FZB42. *Org Lett* **2011,** *13* (12), 2996-2999.
51. Piwowarska, N. A.; Banala, S.; Overkleeft, H. S.; Sussmuth, R. D., Arg-Thz is a minimal substrate for the N(a),N(a)-arginyl methyltransferase involved in the biosynthesis of plantazolicin. *Chem Commun* **2013,** *49* (91), 10703-10705.
52. Banala, S.; Ensle, P.; Sussmuth, R. D., Total synthesis of the ribosomally synthesized linear azole-containing peptide plantazolicin A from *Bacillus amyloliquefaciens*. *Angew Chem Int Ed Engl* **2013,** *52* (36), 9518-9523.
53. Wilson, Z. E.; Fenner, S.; Ley, S. V., Total syntheses of linear polythiazole/oxazole plantazolicin A and its biosynthetic precursor plantazolicin B. *Angew Chem Int Ed Engl* **2015,** *54* (4), 1284-1288.
54. Molohon, K. J.; Blair, P. M.; Park, S.; Doroghazi, J. R.; Maxson, T.; Hershfield, J. R.; Flatt, K. M.; Schroeder, N. E.; Ha, T.; Mitchell, D. A., Plantazolicin is an ultra-narrow spectrum antibiotic that targets the *Bacillus anthracis* membrane. *ACS Infect Dis* **2016,** *2* (3), 207-220.
55. Unsay, J. D.; Cosentino, K.; Subburaj, Y.; Garcia-Saez, A. J., Cardiolipin effects on membrane structure and dynamics. *Langmuir* **2013,** *29* (51), 15878-15887.
56. Dunbar, K. L.; Chekan, J. R.; Cox, C. L.; Burkhart, B. J.; Nair, S. K.; Mitchell, D. A., Discovery of a new ATP-binding motif involved in peptidic azoline biosynthesis. *Nat Chem Biol* **2014,** *10* (10), 823-829.
57. Maksimov, M. O.; Pan, S. J.; James Link, A., Lasso peptides: structure, function, biosynthesis, and engineering. *Nat Prod Rep* **2012,** *29* (9), 996-1006.
58. Iwatsuki, M.; Tomoda, H.; Uchida, R.; Gouda, H.; Hirono, S.; Omura, S., Lariatins, antimycobacterial peptides produced by Rhodococcus sp. K01-B0171, have a lasso structure. *J Am Chem Soc* **2006,** *128* (23), 7486-7491.
59. Rebuffat, S.; Blond, A.; Destoumieux-Garzon, D.; Goulard, C.; Peduzzi, J., Microcin J25, from the macrocyclic to the lasso structure: Implications for biosynthetic, evolutionary and biotechnological perspectives. *Curr Protein Pept Sci* **2004,** *5* (5), 383-391.
60. Tietz, J. I. S., C.J.; Patel, P.S.; Maxson, T.; Blair, P.M.; Tai, H.-C.; Zakai, U.I.; Mitchell, D.A., A new genome mining tool redefines the lasso peptide biosynthetic landscape. **2016**, In revision.
61. McGraw, W. T.; Potempa, J.; Farley, D.; Travis, J., Purification, characterization, and sequence analysis of a potential virulence factor from Porphyromonas gingivalis, peptidylarginine deiminase. *Infect Immun* **1999,** *67* (7), 3248-3256.
62. Anastasiou, D. M.; Thorne, G. M.; Luperchio, S. A.; Alder, J. D., In vitro activity of daptomycin against clinical isolates with reduced susceptibilities to linezolid and quinupristin/dalfopristin. *International Journal of Antimicrobial Agents* **2006,** *28* (5), 385-388.
63. Walsh, C., Molecular mechanisms that confer antibacterial drug resistance. *Nature* **2000,** *406* (6797), 775-781.
64. Zhang, L.; Fan, F.; Palmer, L. M.; Lonetto, M. A.; Petit, C.; Voelker, L. L.; St John, A.; Bankosky, B.; Rosenberg, M.; McDevitt, D., Regulated gene expression in *Staphylococcus aureus* for identifying conditional lethal phenotypes and antibiotic mode of action. *Gene* **2000,** *255* (2), 297-305.
65. Wacker, S. A., Using transcriptome sequencing to identify mechanisms of drug action and resistance. *Nature* **2012,** *8* (3), 235-237.

66. Leslie, B. J.; Hergenrother, P. J., Identification of the cellular targets of bioactive small organic molecules using affinity reagents. *Chem Soc Rev* **2008,** *37* (7), 1347-1360.
67. Choi-Rhee, E.; Cronan, J. E., A nucleosidase required for in vivo function of the S-adenosyl-L-methionine radical enzyme, biotin synthase. *Chem Biol* **2005,** *12* (5), 589-593.
68. Azad, M. A.; Wright, G. D., Determining the mode of action of bioactive compounds. *Bioorg Med Chem* **2012,** *20* (6), 1929-1939.
69. Burdine, L.; Kodadek, T., Target identification in chemical genetics: the (often) missing link. *Chem Biol* **2004,** *11* (5), 593-597.
70. Ziegler, S.; Pries, V.; Hedberg, C.; Waldmann, H., Target identification for small bioactive molecules: finding the needle in the haystack. *Angew Chem Int Ed Engl* **2013,** *52* (10), 2744-2792.
71. Falsey, R. R.; Marron, M. T.; Gunaherath, G. M.; Shirahatti, N.; Mahadevan, D.; Gunatilaka, A. A.; Whitesell, L., Actin microfilament aggregation induced by withaferin A is mediated by annexin II. *Nat Chem Biol* **2006,** *2* (1), 33-38.
72. Kotake, Y.; Sagane, K.; Owa, T.; Mimori-Kiyosue, Y.; Shimizu, H.; Uesugi, M.; Ishihama, Y.; Iwata, M.; Mizui, Y., Splicing factor SF3b as a target of the antitumor natural product pladienolide. *Nat Chem Biol* **2007,** *3* (9), 570-575.
73. Li, Z.; Hao, P.; Li, L.; Tan, C. Y. J.; Cheng, X.; Chen, G. Y. J.; Sze, S. K.; Shen, H.-M.; Yao, S. Q., Design and synthesis of minimalist terminal alkyne-containing diazirine photo-crosslinkers and their incorporation into kinase inhibitors for cell- and tissue-based proteome profiling. *Angew Chem Int Ed Engl* **2013,** *52* (33), 8551-8556.
74. Kotzyba-Hibert, F.; Kapfer, I.; Goeldner, M., Recent trends in photoaffinity labeling. *Angew Chem Int Ed Engl* **1995,** *34* (12), 1296-1312.
75. Ruhr, E.; Sahl, H. G., Mode of action of the peptide antibiotic nisin and influence on the membrane potential of whole cells and on cytoplasmic and artificial membrane vesicles. *Antimicrob Agents Chemother* **1985,** *27* (5), 841-845.
76. Hasper, H. E.; Kramer, N. E.; Smith, J. L.; Hillman, J. D.; Zachariah, C.; Kuipers, O. P.; de Kruijff, B.; Breukink, E., An alternative bactericidal mechanism of action for lantibiotic peptides that target lipid II. *Science* **2006,** *313* (5793), 1636-1637.
77. Metelev, M.; Tietz, J. I.; Melby, J. O.; Blair, P. M.; Zhu, L.; Livnat, I.; Severinov, K.; Mitchell, D. A., Structure, bioactivity, and resistance mechanism of streptomonomicin, an unusual lasso peptide from an understudied halophilic actinomycete. *Chem Biol* **2015,** *22* (2), 241-250.
78. Tiyanont, K.; Doan, T.; Lazarus, M. B.; Fang, X.; Rudner, D. Z.; Walker, S., Imaging peptidoglycan biosynthesis in *Bacillus subtilis* with fluorescent antibiotics. *Proc Natl Acad Sci U S A* **2006,** *103* (29), 11033-11038.
79. Bindman, N. A.; van der Donk, W. A., A general method for fluorescent labeling of the N-termini of lanthipeptides and its application to visualize their cellular localization. *J Am Chem Soc* **2013,** *135* (28), 10362-10371.
80. Vetter, M. L.; Zhang, Z.; Liu, S.; Wang, J.; Cho, H.; Zhang, J.; Zhang, W.; Gray, N. S.; Yang, P. L., Fluorescent visualization of Src by using dasatinib-BODIPY. *Chembiochem* **2014,** *15* (9), 1317-1324.
81. Dempsey, G. T.; Bates, M.; Kowtoniuk, W. E.; Liu, D. R.; Tsien, R. Y.; Zhuang, X., Photoswitching mechanism of cyanine dyes. *J Am Chem Soc* **2009,** *131* (51), 18192-18193.
82. Rust, M. J.; Bates, M.; Zhuang, X., Sub-diffraction-limit imaging by stochastic optical reconstruction microscopy (STORM). *Nat Methods* **2006,** *3* (10), 793-795.
83. Huang, B.; Wang, W.; Bates, M.; Zhuang, X., Three-dimensional super-resolution imaging by stochastic optical reconstruction microscopy. *Science* **2008,** *319* (5864), 810-813.

84. Muraih, J. K.; Pearson, A.; Silverman, J.; Palmer, M., Oligomerization of daptomycin on membranes. *Biochim Biophys Acta* **2011,** *1808* (4), 1154-1160.
85. Arias, C. A.; Panesso, D.; McGrath, D. M.; Qin, X.; Mojica, M. F.; Miller, C.; Diaz, L.; Tran, T. T.; Rincon, S.; Barbu, E. M.; Reyes, J.; Roh, J. H.; Lobos, E.; Sodergren, E.; Pasqualini, R.; Arap, W.; Quinn, J. P.; Shamoo, Y.; Murray, B. E.; Weinstock, G. M., Genetic basis for in vivo daptomycin resistance in enterococci. *N Engl J Med* **2011,** *365* (10), 892-900.
86. Palmer, K. L.; Daniel, A.; Hardy, C.; Silverman, J.; Gilmore, M. S., Genetic basis for daptomycin resistance in Enterococci. *Antimicrob Agents Chemother* **2011,** *55* (7), 3345-3356.
87. Palmer, A. C.; Kishony, R., Opposing effects of target overexpression reveal drug mechanisms. *Nat Commun* **2014,** *5*, 4296.
88. Goh, E.-B.; Yim, G.; Tsui, W.; McClure, J.; Surette, M. G.; Davies, J., Transcriptional modulation of bacterial gene expression by subinhibitory concentrations of antibiotics. *Proc Natl Acad Sci USA* **2002,** *99* (26), 17025-17030.
89. Cotsonas King, A.; Wu, L., Macromolecular synthesis and membrane perturbation assays for mechanisms of action studies of antimicrobial agents. *Curr Protoc Pharmacol* **2009,** *Chapter 13*, Unit 13A.17.

CHAPTER 2: INSIGHTS INTO METHYLTRANSFERASE SPECIFICITY AND BIOACTIVITYOF DERIVATIVES OF THE ANTIBIOTIC PLANTAZOLICIN[1]

2.1 Abstract

Peptide antibiotics represent a class of conformationally constrained natural products of growing pharmaceutical interest. Plantazolicin (PZN) is a linear, polyheterocyclic natural product with highly selective and potent activity against the anthrax-causing bacterium, *Bacillus anthracis*. The bioactivity of PZN is contingent on demethylation of its *N*-terminal Arg residue by an *S*-adenosylmethionine-dependent methyltransferase. Here, we explore the substrate tolerances of two homologous PZN methyltransferases by carrying out kinetic analyses of the enzymes against a synthetic panel of truncated PZN analogs containing the *N*-terminal Arg residue. X-ray cocrystal structures of the PZN methyltransferases with each of these heterocycle-containing substrates provide a rationale for understanding the strict substrate specificity of these enzymes. Kinetic studies of the structure-guided, site-specific variants allowed for the assignment of residues governing catalysis and substrate scope. Microbiological testing further revealed that upon demethylation of the *N*-terminal Arg, a pentaheterocyclized PZN analog retained potent anti-*B. anthracis* activity, nearly equal to that of full-length PZN. These studies may be useful in the biosynthetic engineering of natural product analogs with different bioactivity profiles, as demonstrated by our identification of a truncated plantazolicin derivative that is active against methicillin-resistant *Staphylococcus aureus* (MRSA).

[1] Reprinted with permission from Hao, Y.*.; Blair, P.M.*; Sharma, A.; Mitchell, D.A.; Nair, S.K. "Insights into methyltranferase specificity and bioactivity of derivatives of the antibiotic plantazolicin." ACS Chem. Biol., 10:1209-1216 (2015). Copyright 2015 American Chemical Society. Y.H. performed crystallization and biochemical assays. A.S. synthesized PZN analogs used in this manuscript.
*These authors contributed equally to this work.

2.2 Introduction

Ribosomally synthesized and post-translationally modified peptides (RiPPs) encompass a large and widely distributed class of bioactive secondary metabolites,[1] which include the thiazole/oxazole-modifiedmicrocins (TOMMs).[2] The natural product plantazolicin (PZN) (**1**), produced by the plant growth-promoting bacterium *Bacillus amyloliquefaciens* FZB42,[3-4] is biosynthesized from a 41-residue precursor peptide to yield a product that contains ten azol(in)es, produced through the cyclodehydration and subsequent oxidation of Cys/Ser/Thr characteristic of TOMMs.[5-6] Installation of the heterocyclic moieties is catalyzed by an ATP-dependent cyclodehydratase that converts Cys and Ser/Thr to thiazoline and (methyl)oxazoline, respectively,[7] followed by a flavin mononucleotide-dependent dehydrogenation[8] to yield the corresponding thiazole and (methyl)oxazole. Twelve out of the fourteen residues of the core region of the PZN precursor peptide are modified in the fully mature, bioactive natural product. Following the proteolytic excision of the 21-residue leader sequence from the deca-heterocyclized peptide, an *S*-adenosyl-L-methionine (SAM)-dependent methyltransferase modifies the *N*-terminus.[9] The resultant product PZN bears an N^{α},N^{α}-dimethylArg as the *N*-terminal residue, five contiguous azoles, two hydrophobic spacer residues, followed by another stretch of five contiguous heterocycles, and terminates with a *C*-terminal Phe (Figure 2.1). Genome mining has identified four other bacterial strains with the capacity to generate PZN-like molecules, with *Bacillus pumilus* being a demonstrated producer of PZN.[6]

PZN displays a narrow spectrum of activity. Using the microbroth dilution method, the only organism susceptible to the action of purified PZN to date has been *Bacillus anthracis*, the etiological agent of anthrax.[6, 10] Using the agar disk diffusion method, which allows unrealistically high concentrations of antibiotic to be impregnated into the disk, PZN displayed weak growth

inhibitory activity towards other members of the genus *Bacillus*.[4] Notably, the biological activity of PZN is contingent on the N^{α},N^{α}-methylation of the terminal Arg, as desmethylPZN activity is attenuated.[6] Reconstitution experiments demonstrated that recombinant BamL (the PZN methyltransferase from *B. amyloliquefaciens*) and BpumL (the orthologous methyltransferase from *B. pumilus*) can install both methyl groups onto desmethylPZN in an SAM-dependent manner.[9] Unlike other canonical methyltransferases involved in natural product biosynthesis,[11-13] both BamL and BpumL have highly restricted substrate tolerances, as the unmodified precursor peptide, as well as several other peptidic substrates designed to mimic the functionality of desmethylPZN, were not substrates for these enzymes.[9] BamL can also accept Arg amide (in which the α-carboxylate is replaced with an amide) as a substrate, but only so under near-single turnover conditions.[9] Another study concluded that Arg thiazole (also containing a terminal amide) is the minimal substrate for BamL, and found that residues other than Arg are not tolerated by the methyltransferase.[14] Lastly, BamL reactions with Arg-thiazole yielded mainly monomethylated product under stoichiometric (i.e. limiting) concentrations of SAM, and the BamL active site mutant Tyr182Phe also yielded monomethylated product using desmethylPZN as substrate.[14]

Our prior crystal structures of BamL (PDB Code: 4KVZ) and BpumL (PDB Code: 4KWC) in complex with *S*-adenosyl-L-homocysteine (SAH) revealed a minimalistic methyltransferase fold that lacked any additional structural decorations.[9] Due to the limited aqueous solubility of desmethylPZN, numerous attempts to solve the structures of BamL/BpumL with bound substrate were unsuccessful. Additionally, substrate solubility limitations precluded kinetic characterization of wild-type and mutant enzymes, as well as determination of binding affinities using isothermal titration calorimetry. As the methyltransferase crystal structures revealed a narrow tunnel adjacent to the bound SAH, inferred to be the substrate-binding site, whose dimensions were sufficient to

accommodate roughly the first 5 residues of desmethylPZN, we initiated the chemical synthesis of shorter desmethylPZN fragments (Figure 2.1).[15] The largest fragment consisted of the *N*-terminal Arg followed by five azoles (hereafter Arg-Az_5, **4**), and was shown to convert to the dimethylated product, Me_2-Arg-Az_5, when reacted with BamL and SAM.[15] Smaller desmethylPZN fragments, consisting of the terminal Arg followed by one (Arg-Az_1, **2**) or three (Arg-Az_3,**3**) azoles, were also accepted as BamL substrates and bound to the enzyme with low micromolar affinity (Figure 2.1). Here, we present the cocrystal structures, solved to resolutions between 1.5-1.8 Å, of BamL and BpumL in complex with each of the three azole-bearing substrates, as well as cocrystal structures of BpumL with two monomethylated products. The enhanced aqueous solubility of these analogs compared to desmethylPZN facilitated the determination of the Michaelis-Menten kinetic parameters for both the wild-type enzymes with the three truncated derivatives, as well as the kinetic characterization of several active site variants designed based on the structural data. We also show that both Me_2-Arg-Az_3 and Me_2-Arg-Az_5 display antibiotic activity with a broader-spectrum profile relative to PZN. These combined biophysical and microbiological data provide a rare example of a RiPP tailoring enzyme bound to a processed substrate, and provide the chemical framework and proof-of-concept for the engineering of PZN derivatives with improved bioactivity profiles.

2.3 Results

2.3.1 Kinetic characterization of truncated desmethylPZN substrates

In order to overcome the poor physicochemical behavior of desmethylPZN in aqueous solution, we had previously synthesized three truncated desmethylPZN analogs consisting of an *N*-terminal Arg followed by one, three, or five azoles (Figure 2.1). Each of these compounds was converted

to the corresponding dimethylated counterpart, with *N*-terminal dimethylation determined mass spectrometric analysis (Figure 2.2). The aqueous solubility of Arg-Az_1 and Arg-Az_3, and moderate solubility of Arg-Az_5, allowed for kinetic characterization of each of these substrates in a coupled assay using SAH nucleosidase to monitor SAM turnover (the pfs SAH nucleosidase has a catalytic efficiency of 11.6×10^6 $M^{-1}s^{-1}$,[16] which is greater than that of BamL and BpumL). The catalytic efficiency of BamL toward the truncated desmethylPZN substrates increases with the number of heterocycles (Arg-Az_1, 3.46×10^3 $M^{-1}s^{-1}$; Arg-Az_3, 5.75×10^3 $M^{-1}s^{-1}$; Arg-Az_5, 7.53×10^3 $M^{-1}s^{-1}$, Table 2.1). We only tested the kinetic activity of BpumL towards the Arg-Az_3 substrate, yielding a k_{cat}/K_M value of 6.38×10^3 $M^{-1}s^{-1}$ comparable to that for BamL on the same substrate (Figure 2.1 and Table 2.1). The values for k_{cat} are similar for all three substrates, with decreases in K_M values corresponding to increases in the length of the substrates. These data are consistent with the notion that the BamL active site likely accommodates the first 5 residues of desmethylPZN.

2.3.2 Cocrystal structures of plantazolicin methyltransferases

Given that several other small molecule methyltransferases demonstrate some degrees of substrate promiscuity,[11-13] it was perplexing that BamL did not accept non-heterocyclized substrates. In order to delineate the basis for the strict substrate specificity, we determined the cocrystal structures of BamL-SAH and BpumL-SAH with Arg-Az_1, and Arg-Az_3, to resolutions between 1.5 Å - 1.8 Å, and the structure of BpumL-SAH with Arg-Az_5, to 1.75 Å resolution. Crystallographic phases were determined by the molecular replacement method, and relevant data collection and refinement statistics are provided in Table 2.2. In each ternary complex structure, clear and continuous electron density for the *N*-terminal Arg and all of the azoles of Arg-Az_1 and Arg-Az_3 was observed; however, the Arg-Az_5 structures show strong density for only the first four

heterocycles, with much weaker electron density for the fifth heterocycle, which resides outside of the binding pocket (Figure 2.3).

The BamL and BpumL cocrystal structures recapitulate the core class I methyltransferase Rossmann fold consisting of six α-helices and seven β-strands.[17] The SAH byproduct is bound across the interior in a bent manner, which would dispose the electrophilic methyl group of SAM adjacent to the α-amine of Arg in each of the (poly)azolic substrates (Figure 2.4). The (poly)azolic substrates bind in an extended configuration, perpendicular to the plane of the β-strands, in a narrow tunnel formed by the helices that cap the Rossmann fold core (Figures 2.5-2.7). The *N*-terminal Arg of the substrate is nestled in this pocket and is situated orthogonally to SAH (Figure 2.4). BamL residues Leu162 and Tyr187 are along one face, and a short 3_{10} helix between Phe134 through Phe137 buttresses the opposing side. The guanidinum side chain of the substrate is held in place through hydrogen bonding interactions with the side chains of Asp161, Gln186, and Ser190, and the backbone carbonyl of Gln186 (BamL numbering). This combination of van der Waals contacts and hydrogen bond interactions establishes a planar, coaxial orientation for the substrate Arg.

The azole rings are all cradled within a hydrophobic tunnel situated along the width of BamL and are encapsulated by several residues within a large α-helix that spans the length of the enzyme (Figure 2.3). A number of hydrophobic residues surround the first two azole rings of the substrate, and these include Tyr33, Leu132, Ile141, Val160, Leu162, Tyr182, Leu183, and Tyr187 (Figures 2.5-2.7). The Thr-derived methyloxazole ring at position 3 of the peptide substrate (RC**T**CTT) makes favorable van der Waals contact with Leu132, and Leu258, but we predict that steric clashes would preclude binding of desmethylPZN analogs containing Thr at position 4 (Cys in the native substrate, RCT**C**TT). The third (and presumably) fourth, and fifth rings of Arg-

Az_3 and Arg-Az_5 (RCT**CTT**) are enclosed by a capping loop that spans BamL residues Thr244 through Ala257, and includes Met255 that makes contacts with the terminal azole in each substrate (vide infra) (Figure 2.4).

To determine structures of a product-bound ternary complex, BpumL was incubated with SAM and Arg-Az_3 and Arg-Az_5. However, the structures reveal BpumL-SAH in complex with monomethylated Me-Arg-Az_3 (1.5 Å resolution) and Me-Arg-Az_5 (1.75 Å resolution) (Figure 2.8). Subsequently, we carried out liquid chromatographic and mass spectrometric analyses demonstrating that monoalkylated intermediates are indeed observed under pseudo-single turnover conditions, which was consistent with prior experiments on truncated PZN derivatives carried out under limiting concentrations of SAM (Figure 2.9).[14] The cocrystal structures of BpumL-SAH in complex with Me-Arg-Az_3 and Me-Arg-Az_5 reveal that the monomethylated products are situated within the active site with a nearly identical orientation as the corresponding desmethyl substrates. A comparison of the pre- and post-methyl transfer structures suggest that the α-amino group of Arg is positioned in a relatively hydrophobic environment formed by Phe20, Leu130, and Leu134. Two polar residues (Asp33 and Tyr180) are in the vicinity of the α-amino group, and the contours of the pocket are sufficient to accommodate dimethylation on the Arg of the substrate (Figure 2.8).

2.3.3 A polymorphic capping region undergoes structural changes in response to (poly)azolic substrate

As noted, in BamL, the (poly)azolic substrate-binding tunnel is flanked by a region of the enzyme encompassing Thr244 through Ala257. In the absence of the substrate, this region in BamL and BpumL forms a loop that links the central Rossmann fold core to a flanking helix (Figure 2.10). The co-crystal structures of BamL with the various substrates show that this region is polymorphic and can undergo structural changes to accommodate the length of the bound ligand (Figure 2.10).

The most drastic rearrangement is seen in the BamL/SAH/Arg-Az_1 ternary complex in which Gly247 through Met255 reorganize to form an α-helix (Figure 2.10). Similarly, in the SAH/Me-Arg-Az_3 ternary structure, Ser245 through Gly248 form a one-turn helix that precedes the loop (Figure 2.10). The net result of these conformational movements is the displacement of Met255 to facilitate the packing of the terminal azole in the respective substrate. Conformational displacement of this region results in the formation of a hydrophobic pocket that is optimized for the appropriate truncated substrate. These residues are located at the *C*-terminus of the methyltransferase, and are among the least conserved amongst BamL and BpumL. Other suspected PZN methyltransferases completely lack the *C*-terminal extension that contains these residues (Figure 2.10).

2.3.4 Kinetic analysis of active site variants with Arg-Az_3 as substrate

The ternary complex structures reported here suggest potential catalytic roles for a number of residues that are in the vicinity of the bound substrate. Prior functional analysis of BamL and BpumL were limited due to issues with substrate solubility and could only be characterized using semi-quantitative mass-spectrometric analysis of product yield (9). Based on the structures of the ternary complex, several individual site-specific variants of BamL were generated and kinetic parameters were determined using Arg-Az_3 as the substrate. Thr38 is located on a helix that runs parallel to the trajectory of the (poly)azolic substrates and is in van der Waals contact with the first two heterocyclized residues (R**C****T**CTT). The T38F mutation results in a 17-fold decrease in k_{cat}/K_M (Table 2.2). Similarly, mutation of either Leu132 (in van der Waals contact with ring 2), or Leu162 (contact with ring 1) to Phe results in a decrease in k_{cat}/K_M by a factor of 16 and 48, respectively. Two other variants of BamL were of further interest and thus were kinetically characterized. In the cocrystal structures, Arg42 is involved in an ionic interaction with the SAH carboxylate, and the

R42A mutation resulted in a 12-fold decrease in k_{cat}/K_M (Table 2.3). Likewise, Tyr182 is in the vicinity of the α-amino group and the Y182F mutation results in a 17-fold decrease in k_{cat}/K_M. The effects of these mutations are consistent with roles for both residues in catalysis, as direct or indirect constituents in acid-base chemistry. Methyltransferases from the biosynthetic clusters for two other PZN-like molecules bear a Phe at this position but contain a neighboring Tyr that may similarly facilitate deprotonation of the α-amine.[9]

2.3.5 The molecular basis for substrate specificity

The PZN methyltransferases demonstrate narrow tolerance for substrates,[9] which is unexpected as natural product methyltransferases, in general, are broadly substrate-tolerant,[11-13] and the methyltransferase that catalyze similar N^{α},N^{α}-dimethylation of α-amino groups (*e.g.* during the biosynthesis of linaridins) are fairly tolerant of substrates.[18-19] An examination of the active site in the cocrystal structures of BamL and BpumL with SAM/SAH and each of the (poly)azolic truncated desmethylPZN derivatives provides a rationale for this specificity. For example, in order to accommodate unmodified peptide substrates, the residue following the Arg must be in the *cis* conformation to avoid steric clashes. In addition, steric constraints would result in energetically unfavorable Ramachandran torsion angles for the second residue, permitting only a Gly at this position. Conceding all of the steric requirements would still be unfavorable due to the placement of the charged *C*-terminal carboxylate in the hydrophobic binding tunnel. Finally, the active site contours of BamL and BpumL are constricted in a manner that could only accommodate heterocyclic substrates, and kinetic analysis of site-specific mutations at residues that line the binding site suggest that the changes in the contours of the substrate-binding tunnel are not well tolerated and that the pocket around the first azole is the least resistant to alterations in volume.

The prevalence of hydrophobic residues that line the substrate-binding tunnel provide a rationale for understanding why Arg thiazole (bearing a terminal amide) represents the minimal competent substrate for BamL.[14] Similarly, Arg amide is a poorer substrate that is turned over by BamL but only under single-turnover conditions.[9] In contrast, the amino acid Arg, which bears a charged α-carboxylate, is not accepted as a substrate, probably for the same electronic reasons noted above. Structure-activity studies demonstrate that an Arg at the amino terminus of substrate is a strict requirement, and this constraint can be understood in the context of the structural data. Both BamL and BpumL make extensive hydrogen bonding contacts with the Arg guanidino group, consistent with the observation that substrate containing either ornithine or lysine are not processed. Likewise, homoArg is a poor substrate because the steric limitations of the active site is adapted for Arg and could not accommodate the extra methylene group of this side chain.[14]

2.3.6 Antibacterial profile of truncated PZN derivatives

We have previously shown that potent antibacterial activity of PZN is dependent on the dimethylation of the *N*-terminus. As BamL and BpumL could effectively methylate the truncated PZN derivatives, we characterized the activity of these compounds. As expected, all desmethyl compounds were inactive towards the *B. anthracis* Sterne indicator strain at concentrations of up to 48 μM, underscoring the importance of *N*-terminal dimethylation for antibiotic activity (Table 2.4). Following enzymatic dimethylation and purification of each derivative, these resultant compounds were tested for bioactivity against a panel of ten diverse bacterial strains (seven Firmicutes, three Proteobacteria). As with all of the desmethyl compounds, Me_2-Arg-Az_1 did not show any appreciable bioactivity against any strain. However, both Me_2-Arg-Az_3 and Me_2-Arg-Az_5 displayed minimum inhibitory concentrations (MICs) in the low micromolar range against *B. anthracis* Sterne, with Me_2-Arg-Az_5 being nearly as potent as PZN.

Surprisingly, both Me_2-Arg-Az_3 and Me_2-Arg-Az_5 demonstrated broader-spectrum activity relative to PZN (Table 2.4). While PZN is not active up to 48 μM against other representative members of the genus *Bacillus*, both Me_2-Arg-Az_3 and Me_2-Arg-Az_5 were active against these PZN-insensitive strains. In all tested species, Me_2-Arg-Az_3 showed reduced bioactivity relative to Me_2-Arg-Az_5. Importantly, the bioactivity profile of Me_2-Arg-Az_5 was extended to include *S. aureus* ºNRS384 (a USA300 community acquired-MRSA strain), against which this derivative demonstrates an MIC comparable to that against *B. anthracis* Table 2.4). Inhibition of *B. anthracis* is similar for PZN and Me_2-Arg-Az_5 in a microbroth dilution assay, but only Me_2-Arg-Az_5 results in inhibition of *S. aureus* NRS384 (Figure 2.11). However, unlike PZN, which induces major cell lysis above the MIC, the treatment of mid-exponential *B. anthracis* with Me_2-Arg-Az_5displayed less extensive lysis Figure 2.11). A compound structurally similar to Me_2-Arg-Az_5, but instead bearing a *C*-terminal amide, has been recently shown by the Süssmuth group to be inactive towards*Bacillus megaterium* in an agar diffusion assay when 6 μg of the pure compound was spotted.[14]

2.4 Conclusions

Based to their relaxed specificity for *B. anthracis*, PZN and the truncated analogs may not share the same molecular target(s), but confirmation of this will require extensive additional study. Interestingly, Me_2-Arg-Az_5 retains nearly the same potency as full-length PZN against *B. anthracis*. Hence, it is possible that the bioactive portion of PZN is located in the *N*-terminal half of the molecule, while the *C*-terminal half may govern species specificity. An alignment of the five known PZN precursor peptides shows that the *N*-terminal portion is considerably more conserved than the *C*-terminal portion, which could support the previous conjecture.[6]

Nevertheless, some modifications to the *C*-terminus are detrimental to the anti-*B. anthracis* activity.[20] The combined biochemical, and microbiological analyses of PZN methyltransferase specificity sets the framework for future studies aimed to engineering non-natural PZN variants with expanded and/or orthogonal bioactivities.

2.5 Methods

2.5.1 Protein expression and crystallization

The gene for *E. coli* adenine deaminase was amplified using primers based on the published DNA sequence, and inserted into the pET28b vector. Details for the cloning, expression and purification of BamL and BpumL have already been reported.[9] Briefly, the coding region for BamL and BpumL were inserted into a modified pET28-MBP vector for production as a *C*-terminal fusion. Protein was purified by nickel affinity chromatography, and following removal of the affinity tag, was further purified by ion exchange and size-exclusion chromatography. Mutant proteins were generated using oligonucleotide sequences provided in Table 2.5, and the resultant proteins were purified in a similar manner. Sample purity was assessed by Coomassie-stained SDS-PAGE chromatography (Figure 2.12). The (poly)azolic substrates Arg-Az_1, Arg-Az_3, and Arg-Az_5 were synthesized as previously described. SAM was either prepared enzymatically using SAM synthase, or purchased from Sigma immediately prior to use. The integrity of SAM was routinely monitored by mass spectrometry and HPLC analysis prior to biochemical experiments. Crystals of the BpumL or BamL/SAH/Arg-Az_x complexes were grown using the hanging drop method. Briefly, a 50 μL aliquot of protein (in a buffer of 0.5 M NaCl, 20 mM Tris pH=8.0, and 10% glycerol, at a concentration of 10 mg/mL) was incubated with 2 mM SAM/SAH and 2 mM of the (poly)azolic substrate for 1 h on ice prior to crystallization. Commercially available sparse matrix screens were

used to identify initial crystallization conditions that were subsequently refined to yield samples suitable for diffraction experiments. Plate-like crystals were grown using 100 mM Bis-Tris propane, pH=5.5, 200 mM Li_2So_4, and 22-26% polyethyleneglycol 3350. Crystals were transiently submerged in the crystallization medium supplemented with 10% glycerol prior to vitrification by direct immersion in liquid nitrogen.

2.5.2 Data collection, integration and structure determination

All diffraction data were collected at the Life Sciences Collaborative Access Team (LS-CAT; Sector 21) at the Advanced Photon Source (Argonne, IL) using MAR charge coupled device detectors. The diffraction data were indexed and scaled using HKL2000[21] or XDS[22] to the appropriate limiting resolution. Initial crystallographic phases were determined by the molecular replacement method[23] as implemented in the Phenix software suite,[24] using the coordinates of unliganded BamL (PDB Code: 4KVZ) as a search probe. Rounds of manual rebuilding using COOT[25] were interspersed with crystallographic refinement using REFMAC5[26] until the free R factor dropped below 30%. All ligands and solvents were incorporated into the model at this stage, with further refinement and rebuilding of the model until convergence. Cross-validation, using 5% of the data for the calculation of the free R factor, was utilized throughout the model building process in order to monitor building bias. The validity of all models were routinely determined using PROCHECK,[27] MOLPROBITY, [28] and by using the free R factor[28] to monitor improvements during building and crystallographic refinement.

2.5.3 Kinetic analysis of BamL and BpumL methyltransferases

Kinetic analysis of BamL and BpumL utilized a coupled spectrophotometric assay. Reaction mixtures typically consisted of 50 mM Tris, pH=7.8, 200 μM $MnSO_4$, 5 μM *E. coli* pfs nucleosidase, 5 μM *B. subtilis* adenine deaminase, 80 μM SAM, and varying concentrations of the

Arg-Az_1, Arg-Az_3, and Arg-Az_5. The reaction progress was monitored at 310 K and utilized 0.5 μM of either MBP-tagged wild-type BamL or BpumL. Concentrations for the mutant enzymes are as follows: 1.4 μM R42A, 1.325 μM T38F, 1.34 μM L132F, 1.36 μM L162F, and 1.8 μM Y182F. Reaction progress was monitored as changes in absorption at a wavelength of 265 nm. Initial velocity data were calculated and fitted to the Michaelis-Menten equation using the Origin software package. Due to absorption by substrate at 265 nm, reaction rate using high concentrations (> 80 μM) of peptide substrate failed to yield reliable data.

2.5.4 Antibacterial assays

Microbroth dilution assays were performed as previously described.[6] Briefly, 10 mL stationary phase cultures (two for each bacterial species) were adjusted to OD_{600} of 0.01 in the appropriate medium and added to 96-well plates. Two-fold dilutions of each compound (stock solution at 4 mM in DMSO) were added to the cultures (0.375 μM – 48 μM). Plates were covered and incubated at 37 °C for 12 h before determination of the MIC based on culture turbidity. The cell densities after 12 h were determined for MRSA and Sterne. Vehicle (DMSO)-treated, 24 μM PZN-treated, and 24 μM Me_2-Arg-Az_5-treated wells were analyzed in duplicate on a FilterMax F5 Multi-mode Microplate Reader (Molecular Devices) using sterile LB as the plate blank and measuring cell density at 595 nm. Error bars indicate standard deviation. P-values were calculated using a two-tailed t-test between DMSO-treated and PZN- or Me_2-Arg-Az_5-treated cells of the same bacterial species.

2.5.5 Microscopy

200 μL aliquots of a stationary phase culture of *B. anthracis* Sterne was used to inoculate 5 mL fresh LB. The culture was grown to OD 0.5 and 1 mL aliquots were harvested by centrifugation (8,000 × *g*, 2 min). Bacterial pellets were resuspended in 100 μL PBS supplemented with vehicle

(DMSO), 4 μM PZN or 12 μM Me_2-Arg-Az_5. After mixing at 22 °C for 30 min, cells were washed with PBS and resuspended in 200 μL PBS. 10 μL aliquots of each cell suspension were mixed with 10 μL 2% liquefied low gelling temperature agarose (Sigma-Aldrich) on microscope slides. Differential interference contrast microscopy analyses were conducted at the Core Facility at the Institute of Genomic Biology (University of Illinois) using a Zeiss LSM 700 confocal microscope outfitted with a 405 nm laser. Linear contrast was applied when deconvoluting images in Zen 2012 software.

2.6 Acknowledgments

We are grateful to Prof. J. Cronan for the gift of the pfs expression plasmid and to Prof. W. van der Donk for the use of the Waters SYNAPT mass spectrometer. The Bruker UltrafleXtreme MALDI mass spectrometer was purchased in part with a grant from the National Center for Research Resources, NIH (S10 RR027109). Use of the Advanced Photon Source, operated for the U.S. Department of Energy (DOE) by Argonne National Laboratory, was supported by Contract No. DE-AC02-06CH11357. Y.H. is supported in part by a Lowell Hager Fellowship from the Department of Biochemistry. P.M.B. was supported in part supported by an ACS Medicinal Chemistry pre-doctoral fellowship. This work was supported in part by the institutional funds provided by the University of Illinois and the NIH Director's New Innovator Award Program (DP2 OD008463 to D.A.M.).

2.7 Figures

Figure 2.1 (A) Chemical structures of PZN and the three (poly)azolic truncated methyltransferase substrates. (B) Enzymatic conversion of Arg-Az_3 into the corresponding dimethylated compound by BamL, as analyzed by HPLC. *, internal standard. (C) Michaelis-Menten curves for the conversion of each of the (poly)azolic substrates catalyzed by BamL using a fixed SAM concentration of 5 mM. The concentration of SAM is 80 µM. The ITC data in the previous paper says the Kd is around 8 µM, so 80 µM should still be saturated.

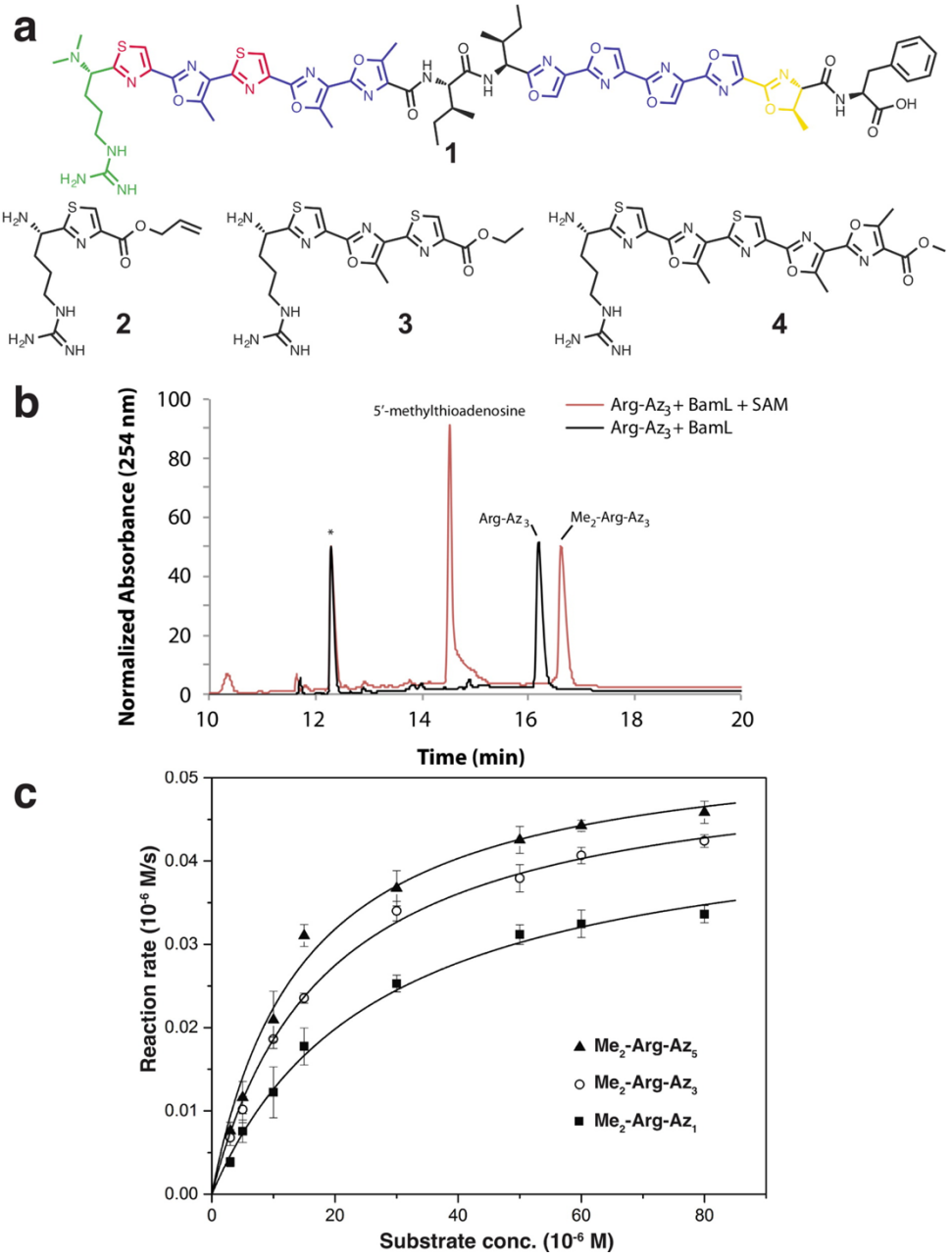

Figure 2.2 Fragmentation of the products of the enzymatic reactions confirms BamL *N*-terminally dimethylates the PZN substructures, yielding (A) Me_2-Arg-Az_1, (B) Me_2-Arg-Az_3, and (C) Me_2-Arg-Az_5.

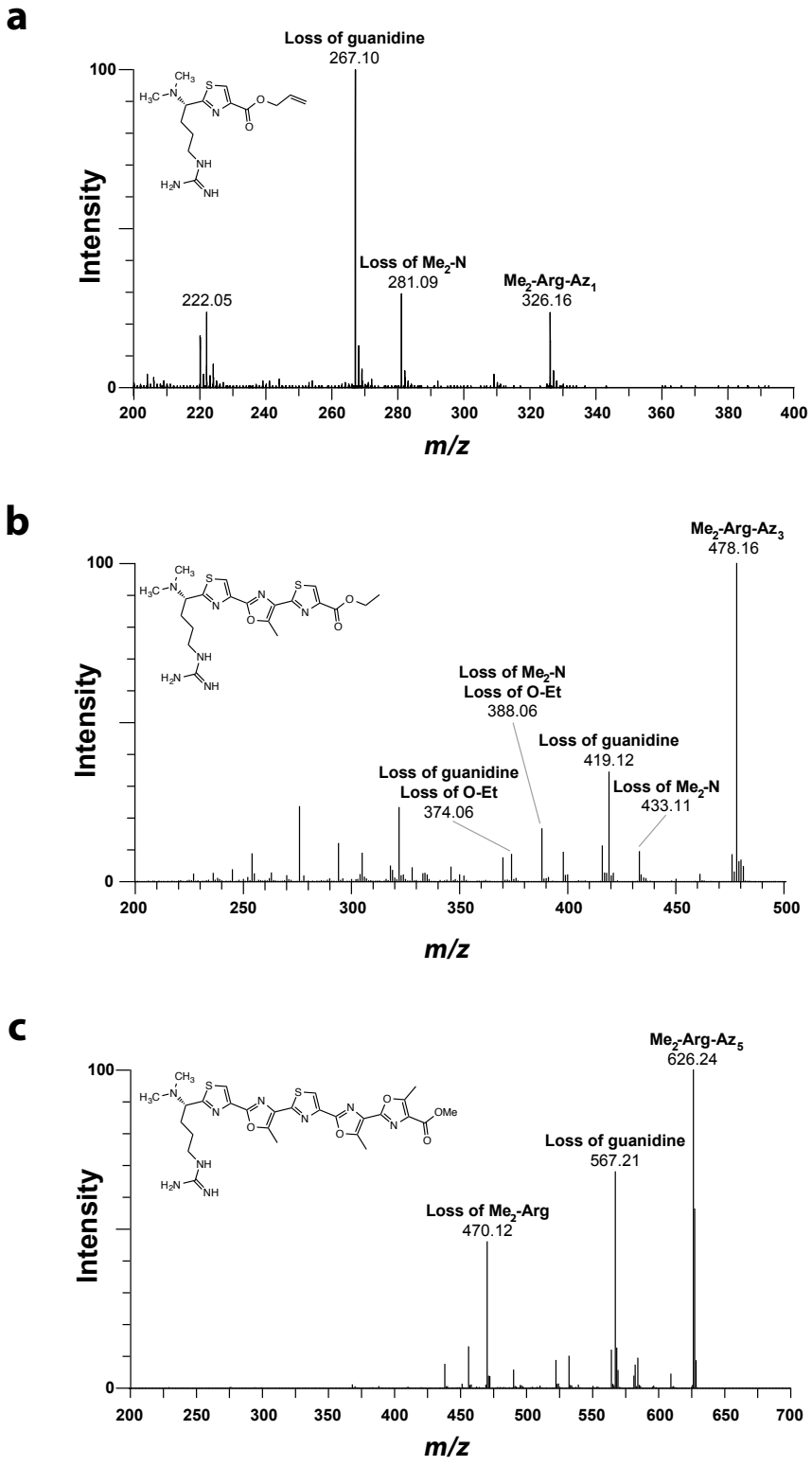

Figure 2.3 Cut-away surface view of BpumL (colored in purple) viewed parallel to the axis of the Arg-Az_5 binding site. The ligand is shown as ball and stick with carbon, nitrogen, sulfur, and oxygen atoms colored in yellow, blue, green, and red, respectively. The fourth and fifth azoles of the substrate are exposed to solvent, relative to the first three azoles. Atoms comprising the *C*-terminal ester of Arg-Az_5 are disordered.

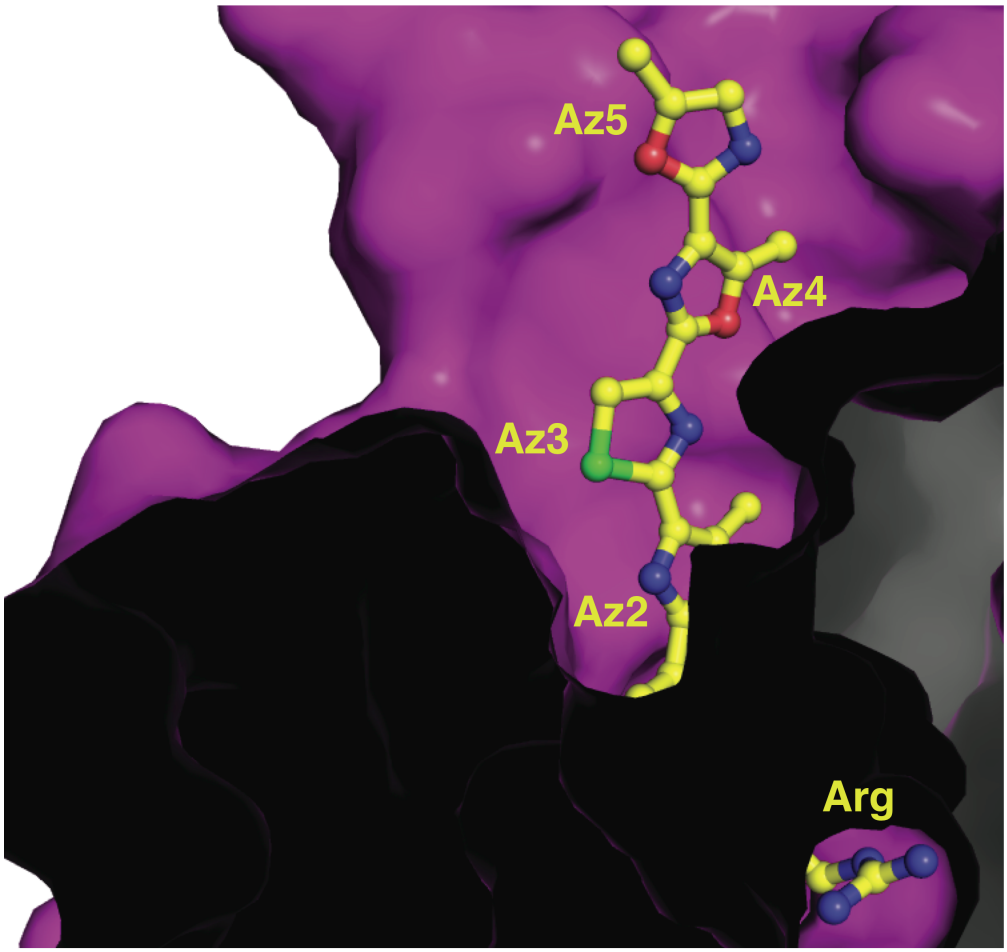

Figure 2.4 (A) Structure of the BamL (purple) in complex with SAH (gray), and Arg-Az_3 (cyan) with the capping loop colored in green. (B, C) Difference Fourier electron density maps of (B) BamL-Arg-Az_1 and (C) BamL-Arg-Az_3 contoured at 2.5σ (blue) and 8σ (red), calculated with coefficient ($F_{obs} - F_{calc}$), with phases derived from the final structure with the coordinates of the substrate removed for one round of simulated annealing refinement. The SAH is colored in gray, the substrates are colored in cyan, and important active site residues are shown as yellow ball-and-stick.

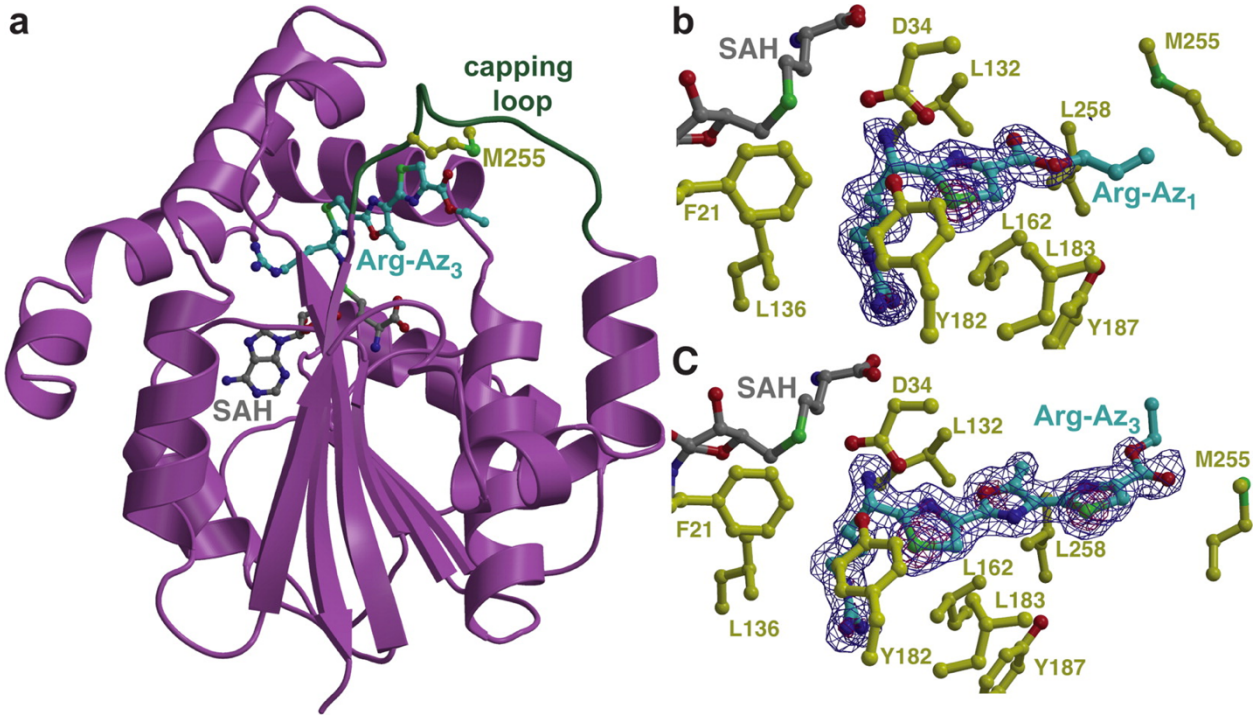

Figure 2.5 LIGPLOT diagram (1) showing the interaction between BamL and Arg-Az_1 with the bound ligand shown in purple. Carbon, nitrogen, and oxygen atoms are shown as black, blue, and red balls, respectively. Hydrogen bonds are shown as green dashed lines with indicated distances. Residues within van der Waals contact distance are represented by spiked red semicircles.

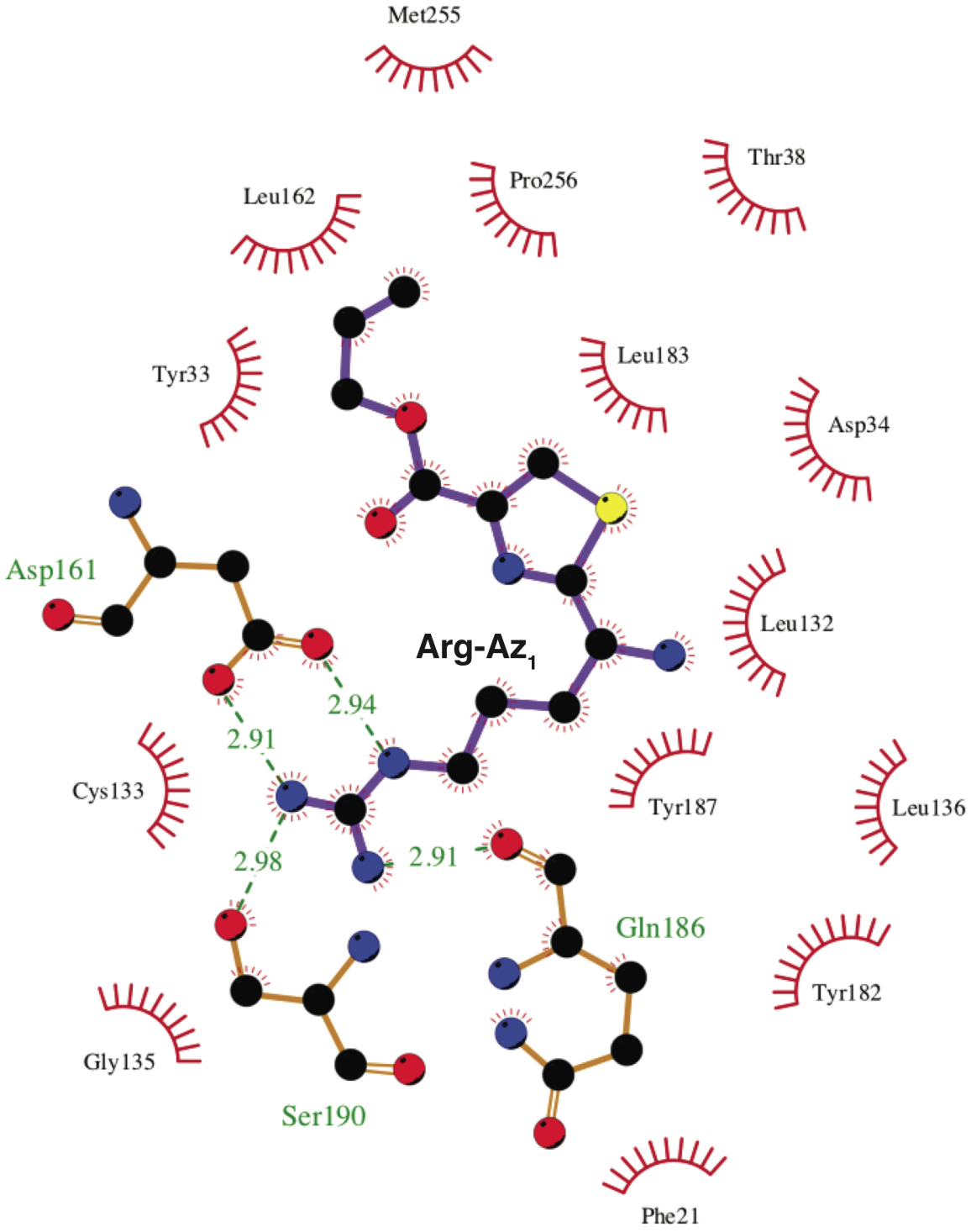

Figure 2.6 LIGPLOT diagram showing the interaction between BamL and Arg-Az_3 with the bound ligand shown in purple. Carbon, nitrogen, and oxygen atoms are shown as black, blue, and red balls, respectively. Hydrogen bonds are shown as green dashed lines with indicated distances. Residues within van der Waals contact distance are represented by spiked red semicircles.

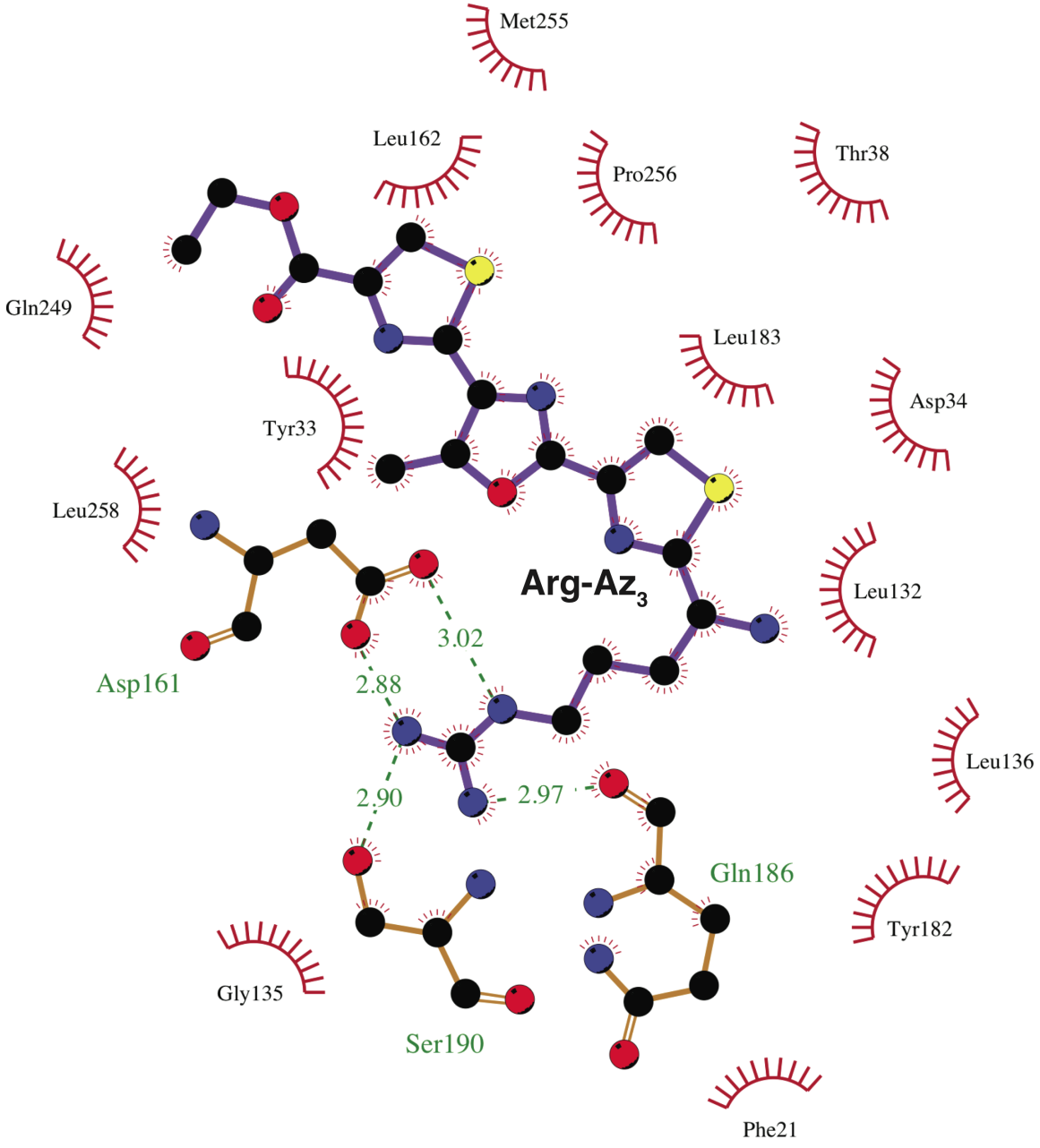

Figure 2.7 LIGPLOT diagram (1) showing the interaction between BamL and Arg-Az_3 with the bound ligand shown in purple. Carbon, nitrogen, and oxygen atoms are shown as black, blue, and red balls, respectively. Hydrogen bonds are shown as green dashed lines with indicated distances. Residues within van der Waals contact distance are represented by spiked red semicircles.

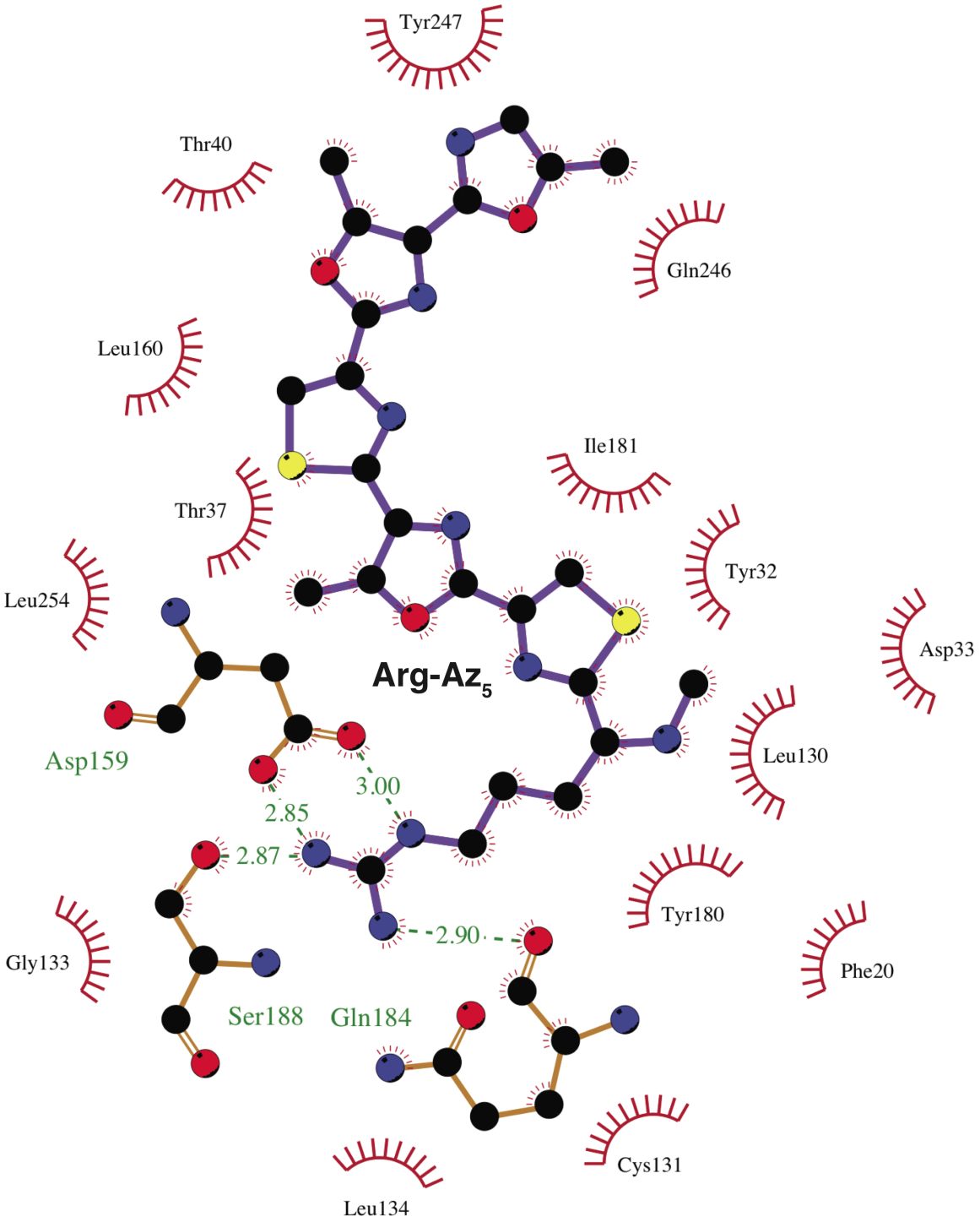

Figure 2.8 (A,B) Active site views of the structures of BpumL in complex with SAH (gray) and either (A) Me-Arg-Az_3 or (B) Me-Arg-Az_5. The substrates are colored in cyan, and important active site residues are shown as yellow ball-and-stick. The superimposed electron density maps are calculated and contoured as in Figure 2.4.

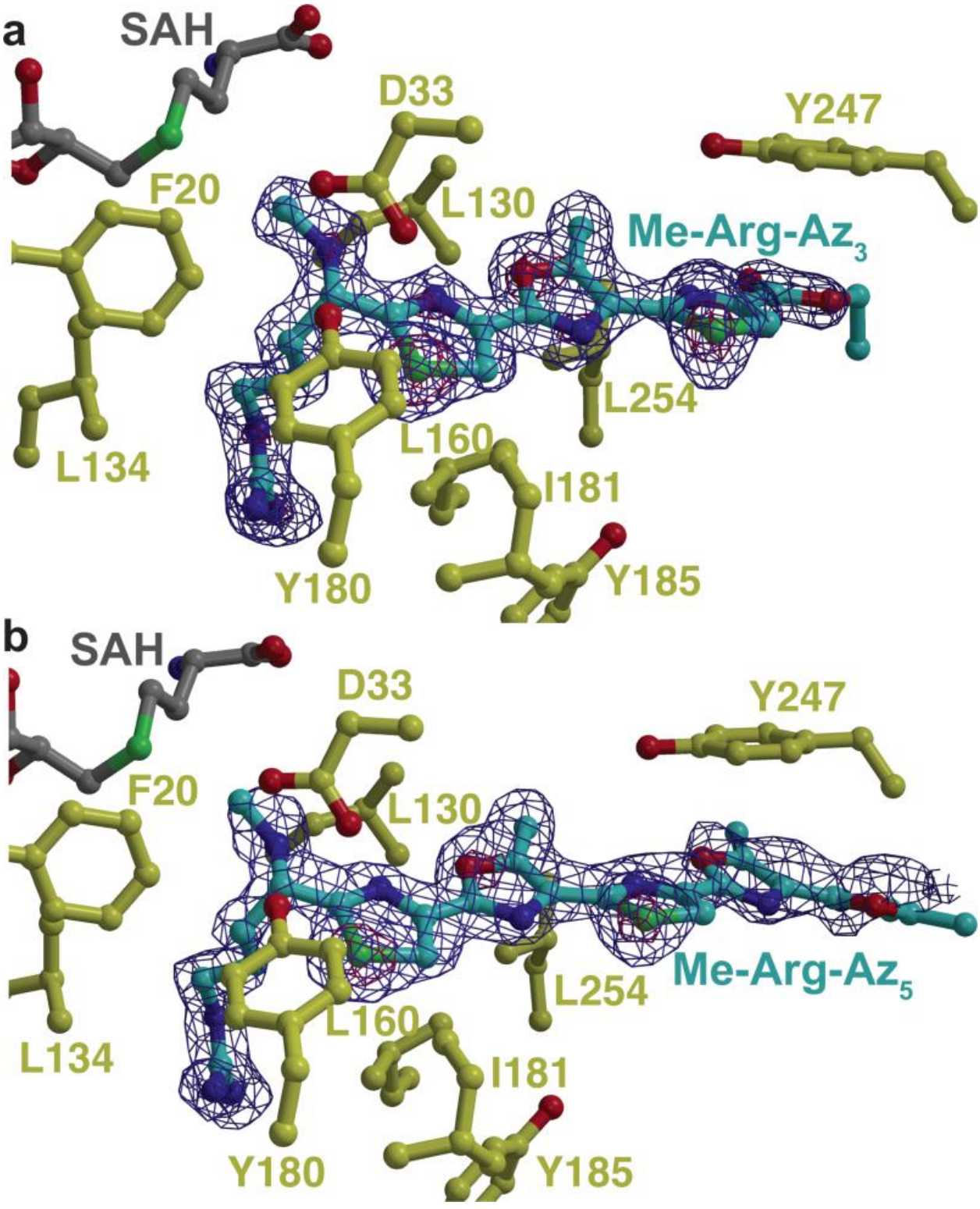

Figure 2.9 ESI-MS spectrum of a 30 min enzymatic reaction of 50 μM wild-type MBP-BamL, 10 μM Pfs, 50 μM Arg-Az_5, and 50 μM SAM in 50 mM Tris-HCl (pH 7.5) shows mono- and demethylation of Arg-Az_5.

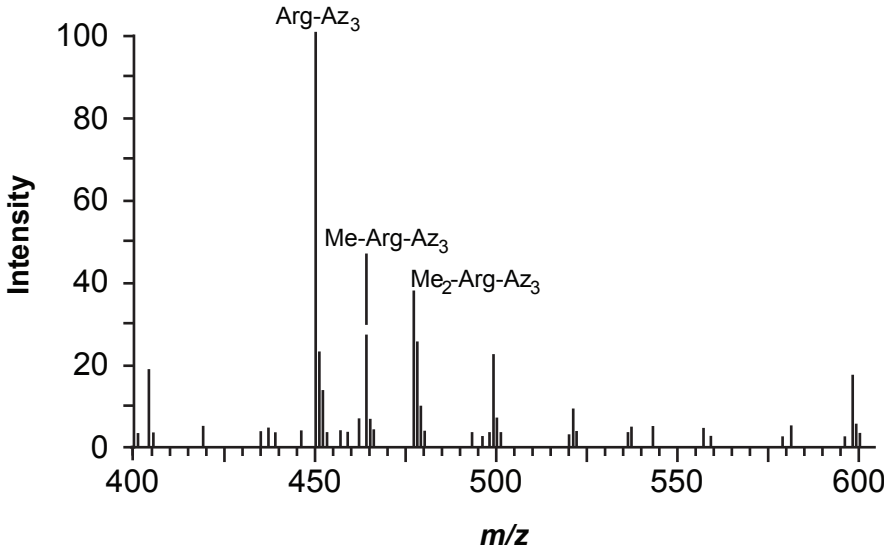

Figure 2.10 (A-C) Views showing that the capping region (colored in green) is polymorphic and changes from (A) a long loop in the BamL structure without substrate to (B) an α-helix in the BamL-SAH-Arg-Az_1 structure, and (C) a short helix-loop in the BamL-SAH-Arg-Az_3 structure. (D) The capping region is located in the poorly conserved *C*-terminus of BamL and is missing in methyltransferases from related biosynthetic clusters. Residues conserved among all sequences are shaded in black and those that are similar are shaded in light blue. The *C*-terminal extension is missing in CurL and BlinL and is designated by a series of periods.

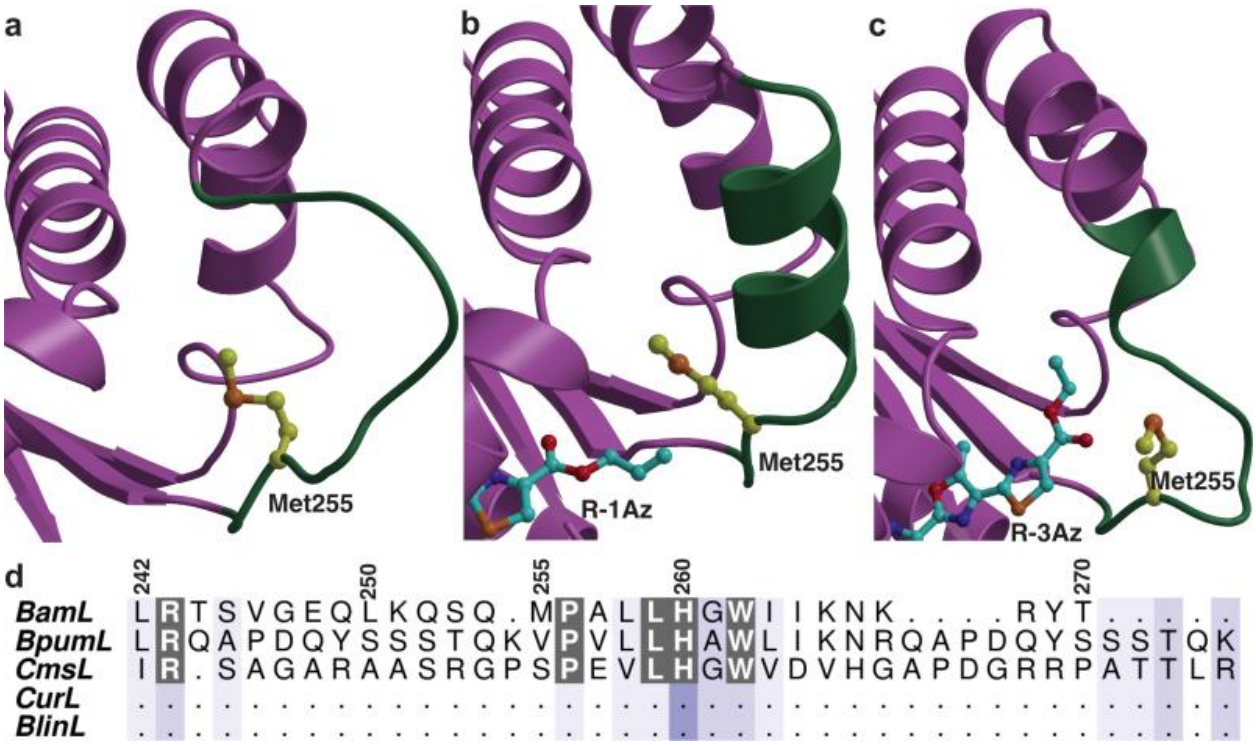

Figure 2.11 (A) Treatment with 24 μM PZN or Me_2-Arg-Az_5 is bactericidal against *B. anthracis* Sterne. However, Me_2-Arg-Az_5 but not PZN displays antibiotic activity against MRSA, as evidenced by cell density measurements after 12 h treatment (595 nm). Error bars, standard deviation. *, P<0.01 *vs* DMSO-treated *B. anthracis* st. Sterne. #, P<0.01 *vs* DMSO-treated MRSA. (B-D) Me_2-Arg-Az_5 displays antibiotic activity against *B. anthracis* but unlike PZN does not massively induce cell lysis of mid-exponential phase cells after 30 min. Scale bars, 5 μm. (B) Vehicle (DMSO)-treated *B. anthracis* vegetative cells. (C) *B. anthracis* treated with 4 μM PZN shows cell lysis. (D) *B. anthracis* remained mostly intact after treatment with 12 μM Me_2-Arg-Az_5.

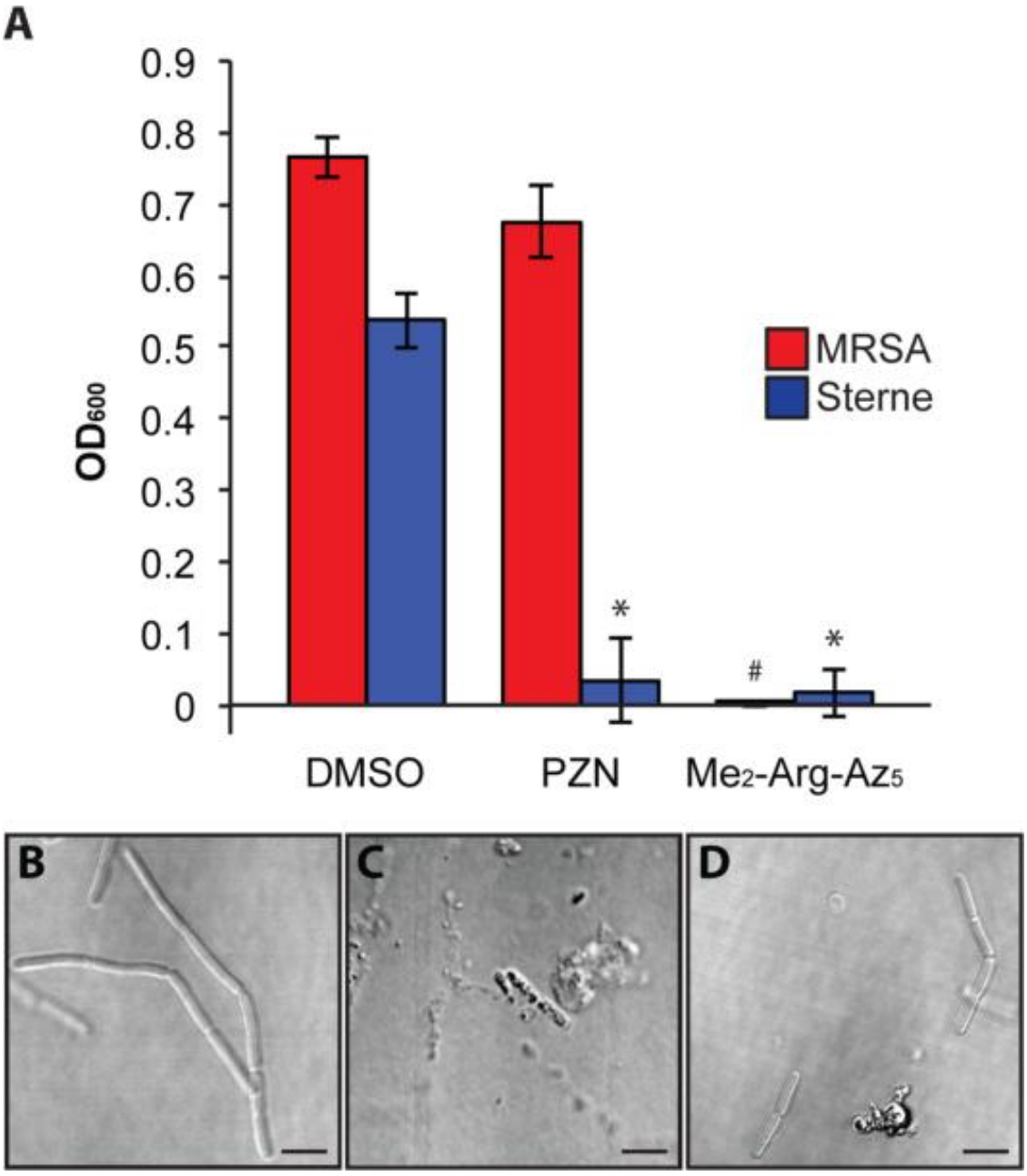

Figure 2.12 Relative purities (as determined by Coomassie-stained 10% SDS-PAGE) of wild-type and mutant BamL proteins used for experiments. Full-length maltose-binding protein (MBP)-tagged BamL and variants (76 kDa) were purified by Ni-NTA affinity chromatography and, following removal of the MBP tag by tobacco etch virus protease cleavage, further purified by size exclusion chromatography. Roughly 10 µg of protein was loaded in each lanes from 2 through 7. Lane 1: Molecular weight ladder, Lane 2: wild-type MBP-BamL, Lane 3: MBP- BamL-T38F, Lane 4: MBP-BamL-R42A, Lane 5: MBP-BamL-L132F, Lane 6: MBP-BamL- L162F, and Lane 7: MBP-BamL-Y182F.

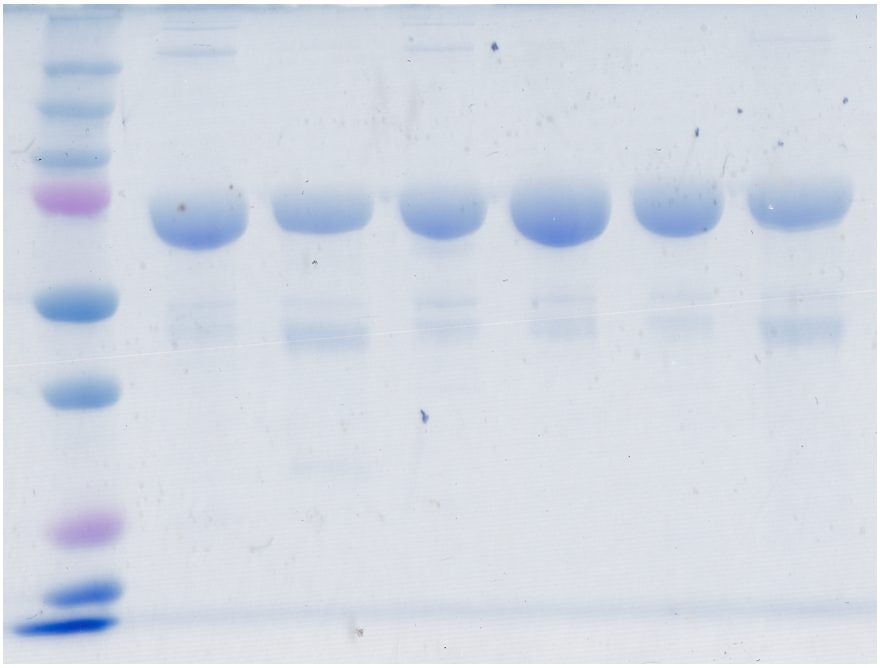

1 2 3 4 5 6 7

2.8 Tables

Table 2.1 Steady state kinetic parameters for BamL and BpumL against truncated PZN substrates.

BamL	K_M **(μM)**	k_{cat} **(10^{-2} s^{-1})**	k_{cat}/K_M **(M^{-1} s^{-1})**
Arg-Az_1	26.8 ± 3.3	9.3 ± 0.4	3.46×10^3
Arg-Az_3	18.3 ± 0.5	10.5 ± 0.1	5.75×10^3
Arg-Az_5	14.6 ± 2.0	11.0 ± 0.4	7.53×10^3
Arg-Az_3 (BpumL)	22.5 ± 2.3	14.4 ± 0.7	6.38×10^3

Table 2.2 Data collection, phasing, and refinement statistics.

	BamL		BpumL		
	Arg-Az$_1$	**Arg-Az$_3$**	**Arg-Az$_1$**	**Arg-Az$_3$**	**Arg-Az$_5$**
Data collection					
Space Group	$P2_1$	$P2_12_12_1$	$P2_12_12$	$P2_12_12$	$P2_12_12$
a, b, c (Å), β (°)	39.7, 71.4, 48.8, 107.5	48.8,96.5, 132.6	67.5, 78.6, 44.7	68.1, 78.8, 44.9	67.8, 78.8, 44.7
Resolution (Å)[a]	50-1.5 (1.6-1.5)	50-1.75 (1.78-1.75)	50-1.8 (1.83-1.8)	50-1.5 (1.6-1.5)	50-1.75 (1.78-1.75)
R_{sym} (%)[b]	6.0 (34.4)	11.1 (70.8)	7.4 (66.7)	5.4 (67.1)	7.5 (59.3)
I/σ(I)	15.6 (3.8)	17.0 (2.5)	23.3 (2.6)	23.2 (1.7)	27.0 (3.7)
Completeness (%)	96.1 (93.9)	100 (100)	99.7 (99.3)	96.6 (81.0)	100 (100)
Redundancy	4.7 (4.0)	6.9 (6.4)	6.6 (6.5)	5.6 (3.1)	8.0 (8.1)
Refinement					
Resolution (Å)	25.0-1.5	25.0-1.75	25.0-1.8	25.0-1.5	25.0-1.75
No. reflections	38,011	60,530	21,423	36,228	23,630
R_{work} / R_{free}[d] (%)	20.6/23.7	18.6/21.2	19.9/23.9	20.6/23.9	20.1/24.3
Number of atoms					
Protein	2133	4311	2071	2087	2080
(Poly)azole	20	70	26	37	44
SAH	26	52	26	26	26
Water	237	518	518	236	186
B-factors					
Protein	16.5	21.3	20.5	16.9	19.7
(Poly)azole	14.7	21.2	18.1	17.3	25.7
SAH	13.5	19.9	13.9	11.2	14.3
Water	25.9	31.3	29.9	29.1	30.9
R.m.s. deviations					
Bond lengths (Å)	0.006	0.007	0.006	0.006	0.006
Bond angles (°)	1.19	1.51	1.19	1.49	1.77

a. Highest resolution shell is shown in parentheses.
b. $R_{sym} = \Sigma |(I_i - \langle I_i \rangle | \Sigma I_i$ where I_i = intensity of the *i*th reflection and $\langle I_i \rangle$ = mean intensity.
c. Mean figure of merit (acentric and centric).
d. R-factor = $\Sigma(|F_{obs}|-k|F_{calc}|)/\Sigma |F_{obs}|$ and R-free is the R value for a test set of reflections consisting of a random 5% of the diffraction data not used in refinement.

Table 2.3 Steady state kinetic parameters for BamL variants against Arg-Az_3.

BamL	k_{cat}/K_M ($M^{-1}s^{-1}$)
Wild-type	57.5×10^2
T38F	3.3×10^2
R42A	4.7×10^2
L132F	3.5×10^2
L162F	1.2×10^2
Y182F	1.7×10^2

Table 2.4 Bioactivity of PZN truncations compared to PZN. Values reported as minimum inhibitory concentrations (μM).

Organism	Me_2-Arg-Az_1	Me_2-Arg-Az_3	Me_2-Arg-Az_5	PZN
Bacillus anthracis Sterne	>48	12	3	0.75-1.5
Bacillus megaterium 7A1	>48	12	3	>48
Bacillus subtilis 168	>48	24	6	>48
Enterococcus faecium U503	>48	>48	>48	>48
Listeria monocytogenes 4b F2365	>48	>48	>48	>48
Staphylococcus aureus NRS384	>48	>48	3	>48
Streptococcus pyogenes M1	>48	>48	>48	>48
Escherichia coli DH5a	>48	>48	>48	>48
Neisseria sicca ATCC 29256	>48	>48	>48	>48
Pseudomonas putida KT244	>48	>48	>48	>48

Table 2.5 Oligonucleotides (primers) used for cloning and site-directed mutagenesis of BamL. Primers ending with _f and _r correspond to the forward and reverse direction, respectively.

#	Primer Name	Primer Sequence (5' – 3')
1	BamL_f (cloning)	aaaaggatccatggaaattgaaacaattgtcagagagt
2	BamL_r (cloning)	aaaagcggccgctcacgtatacctttgttttttataatccaac
3	BpumL_f (cloning)	aagcagccgcatatgatacaagaaaaaatcaaagagcttgaa
4	BpumL_r (cloning)	ctagctcgagttagccagaatttttaataagccacgcatgta
5	T38F_f	gctttcggtatgatgagagggaattctcatccattagaagtatttca
6	T38F_r	tgaaatacttctaatggatgagaattccctctcatcataccgaaagc
7	R42A_f	gatgagagggaaacctcatccattgcaagtatttcaattgaaacatttctg
8	R42A_r	cagaaatgtttcaattgaaatacttgcaatggatgaggtttccctctcatc
9	L132F_f	gtgtctaagaagcaagacattatattcatacatttctgttttggactctttaagaatc
10	L132F_r	gattcttaaagagtccaaaacagaaatgtatgaatataatgtcttgcttcttagaca
11	L162F_f	agatcaatcatgtatctatattgtagacttcgacaggaacagtttgg
12	L162F_r	ccaaactgttcctgtcgaagtctacaatatagatacatgattgatct
13	Y182F_f	aatctcgtgaggaagaagccttttttaaaagatcaatatcgtgc
14	Y182F_r	gcacgatattgatcttttaaaaaggcttcttcctcacgagatt

2.9 References

1. Arnison, P. G.; Bibb, M. J.; Bierbaum, G.; Bowers, A. A.; Bugni, T. S.; Bulaj, G.; Camarero, J. A.; Campopiano, D. J.; Challis, G. L.; Clardy, J.; Cotter, P. D.; Craik, D. J.; Dawson, M.; Dittmann, E.; Donadio, S.; Dorrestein, P. C.; Entian, K. D.; Fischbach, M. A.; Garavelli, J. S.; Goransson, U.; Gruber, C. W.; Haft, D. H.; Hemscheidt, T. K.; Hertweck, C.; Hill, C.; Horswill, A. R.; Jaspars, M.; Kelly, W. L.; Klinman, J. P.; Kuipers, O. P.; Link, A. J.; Liu, W.; Marahiel, M. A.; Mitchell, D. A.; Moll, G. N.; Moore, B. S.; Muller, R.; Nair, S. K.; Nes, I. F.; Norris, G. E.; Olivera, B. M.; Onaka, H.; Patchett, M. L.; Piel, J.; Reaney, M. J.; Rebuffat, S.; Ross, R. P.; Sahl, H. G.; Schmidt, E. W.; Selsted, M. E.; Severinov, K.; Shen, B.; Sivonen, K.; Smith, L.; Stein, T.; Sussmuth, R. D.; Tagg, J. R.; Tang, G. L.; Truman, A. W.; Vederas, J. C.; Walsh, C. T.; Walton, J. D.; Wenzel, S. C.; Willey, J. M.; van der Donk, W. A., Ribosomally synthesized and post-translationally modified peptide natural products: overview and recommendations for a universal nomenclature. *Nat Prod Rep* **2013,** *30* (1), 108-160.
2. Melby, J. O.; Nard, N. J.; Mitchell, D. A., Thiazole/oxazole-modified microcins: complex natural products from ribosomal templates. *Curr Opin Chem Biol* **2011,** *15* (3), 369-378.
3. Kalyon, B.; Helaly, S. E.; Scholz, R.; Nachtigall, J.; Vater, J.; Borriss, R.; Sussmuth, R. D., Plantazolicin A and B: structure elucidation of ribosomally synthesized thiazole/oxazole peptides from *Bacillus amyloliquefaciens* FZB42. *Org Lett* **2011,** *13* (12), 2996-2999.
4. Scholz, R.; Molohon, K. J.; Nachtigall, J.; Vater, J.; Markley, A. L.; Sussmuth, R. D.; Mitchell, D. A.; Borriss, R., Plantazolicin, a novel microcin B17/streptolysin S-like natural product from *Bacillus amyloliquefaciens* FZB42. *J Bacteriol* **2011,** *193* (1), 215-224.

5. Li, Y. M.; Milne, J. C.; Madison, L. L.; Kolter, R.; Walsh, C. T., From peptide precursors to oxazole and thiazole-containing peptide antibiotics: Microcin B17 synthase. *Science* **1996,** *274* (5290), 1188-1193.
6. Molohon, K. J.; Melby, J. O.; Lee, J.; Evans, B. S.; Dunbar, K. L.; Bumpus, S. B.; Kelleher, N. L.; Mitchell, D. A., Structure determination and interception of biosynthetic intermediates for the plantazolicin class of highly discriminating antibiotics. *ACS Chem Biol* **2011,** *6* (12), 1307-1313.
7. McIntosh, J. A.; Schmidt, E. W., Marine molecular machines: heterocyclization in cyanobactin biosynthesis. *Chembiochem* **2010,** *11* (10), 1413-1421.
8. Milne, J. C.; Roy, R. S.; Eliot, A. C.; Kelleher, N. L.; Wokhlu, A.; Nickels, B.; Walsh, C. T., Cofactor requirements and reconstitution of microcin B17 synthetase: a multienzyme complex that catalyzes the formation of oxazoles and thiazoles in the antibiotic microcin B17. *Biochemistry* **1999,** *38* (15), 4768-4781.
9. Lee, J.; Hao, Y.; Blair, P. M.; Melby, J. O.; Agarwal, V.; Burkhart, B. J.; Nair, S. K.; Mitchell, D. A., Structural and functional insight into an unexpectedly selective N-methyltransferase involved in plantazolicin biosynthesis. *Proc Natl Acad Sci USA* **2013,** *110* (32), 12954-12959.
10. Spencer, R. C., *Bacillus anthracis*. *J Clin Pathol* **2003,** *56* (3), 182-187.
11. Kopycki, J. G.; Rauh, D.; Chumanevich, A. A.; Neumann, P.; Vogt, T.; Stubbs, M. T., Biochemical and structural analysis of substrate promiscuity in plant Mg2+-dependent O-methyltransferases. *J Mol Biol* **2008,** *378* (1), 154-164.
12. Lee, J. H.; Bae, B.; Kuemin, M.; Circello, B. T.; Metcalf, W. W.; Nair, S. K.; van der Donk, W. A., Characterization and structure of DhpI, a phosphonate O-methyltransferase involved in dehydrophos biosynthesis. *Proc Natl Acad Sci USA* **2010,** *107* (41), 17557-17562.
13. Zhang, C.; Albermann, C.; Fu, X.; Peters, N. R.; Chisholm, J. D.; Zhang, G.; Gilbert, E. J.; Wang, P. G.; Van Vranken, D. L.; Thorson, J. S., RebG- and RebM-catalyzed indolocarbazole diversification. *Chembiochem* **2006,** *7* (5), 795-804.
14. Piwowarska, N. A.; Banala, S.; Overkleeft, H. S.; Sussmuth, R. D., Arg-Thz is a minimal substrate for the N(a),N(a)-arginyl methyltransferase involved in the biosynthesis of plantazolicin. *Chem Commun* **2013,** *49* (91), 10703-10705.
15. Sharma, A.; Blair, P. M.; Mitchell, D. A., Synthesis of plantazolicin analogues enables dissection of ligand binding interactions of a highly selective methyltransferase. *Org Lett* **2013,** *15* (19), 5076-5079.
16. Choi-Rhee, E.; Cronan, J. E., A nucleosidase required for in vivo function of the S-adenosyl-L-methionine radical enzyme, biotin synthase. *Chem Biol* **2005,** *12* (5), 589-593.
17. Liscombe, D. K.; Louie, G. V.; Noel, J. P., Architectures, mechanisms and molecular evolution of natural product methyltransferases. *Nat Prod Rep* **2012,** *29* (10), 1238-1250.
18. Claesen, J.; Bibb, M. J., Biosynthesis and regulation of grisemycin, a new member of the linaridin family of ribosomally synthesized peptides produced by Streptomyces griseus IFO 13350. *J Bacteriol* **2011,** *193* (10), 2510-2516.
19. Zhang, Q.; van der Donk, W. A., Catalytic promiscuity of a bacterial alpha-N-methyltransferase. *FEBS Lett* **2012,** *586* (19), 3391-3397.
20. Deane, C. D.; Melby, J. O.; Molohon, K. J.; Susarrey, A. R.; Mitchell, D. A., Engineering unnatural variants of plantazolicin through codon reprogramming. *ACS Chem Biol* **2013,** *8* (9), 1998-2008.

21. Otwinowski, Z.; Borek, D.; Majewski, W.; Minor, W., Multiparametric scaling of diffraction intensities. *Acta Crystallogr A* **2003,** *59* (Pt 3), 228-234.
22. Kabsch, W., Processing of X-ray snapshots from crystals in random orientations. *Acta Crystallogr D Biol Crystallogr* **2014,** *70* (Pt 8), 2204-2216.
23. McCoy, A. J.; Grosse-Kunstleve, R. W.; Adams, P. D.; Winn, M. D.; Storoni, L. C.; Read, R. J., Phaser crystallographic software. *J Appl Crystallogr* **2007,** *40* (Pt 4), 658-674.
24. Adams, P. D.; Afonine, P. V.; Bunkoczi, G.; Chen, V. B.; Echols, N.; Headd, J. J.; Hung, L. W.; Jain, S.; Kapral, G. J.; Grosse Kunstleve, R. W.; McCoy, A. J.; Moriarty, N. W.; Oeffner, R. D.; Read, R. J.; Richardson, D. C.; Richardson, J. S.; Terwilliger, T. C.; Zwart, P. H., The Phenix software for automated determination of macromolecular structures. *Methods* **2011,** *55* (1), 94-106.
25. Emsley, P.; Cowtan, K., Coot: model-building tools for molecular graphics. *Acta Crystallogr D Biol Crystallogr* **2004,** *60* (Pt 12 Pt 1), 2126-2132.
26. Murshudov, G. N.; Skubak, P.; Lebedev, A. A.; Pannu, N. S.; Steiner, R. A.; Nicholls, R. A.; Winn, M. D.; Long, F.; Vagin, A. A., REFMAC5 for the refinement of macromolecular crystal structures. *Acta Crystallogr D Biol Crystallogr* **2011,** *67* (Pt 4), 355-367.
27. Laskowski, R. A.; Rullmannn, J. A.; MacArthur, M. W.; Kaptein, R.; Thornton, J. M., AQUA and PROCHECK-NMR: programs for checking the quality of protein structures solved by NMR. *J Biomol NMR* **1996,** *8* (4), 477-486.
28. Chen, V. B.; Arendall, W. B., 3rd; Headd, J. J.; Keedy, D. A.; Immormino, R. M.; Kapral, G. J.; Murray, L. W.; Richardson, J. S.; Richardson, D. C., MolProbity: all-atom structure validation for macromolecular crystallography. *Acta Crystallogr D Biol Crystallogr* **2010,** *66* (Pt 1), 12-21.

CHAPTER 3: PLANTAZOLICIN IS AN ULTRA-NARROW SPECTRUM ANTIBIOTIC THAT TARGETS THE *BACILLUS ANTHRACIS* MEMBRANE[2]

3.1 Abstract

Plantazolicin (PZN) is a ribosomally synthesized and post-translationally modified natural product from Bacillus methylotrophicus FZB42 and Bacillus pumilus. Extensive tailoring to 12 of the 14 amino acid residues in the mature natural product endows PZN with not only a rigid, polyheterocyclic structure, but also antibacterial activity. Here we report the remarkably discriminatory activity of PZN toward Bacillus anthracis, which rivals a previously described gamma (γ) phage lysis assay in distinguishing B. anthracis from other members of the Bacillus cereus group. We evaluate the underlying cause of this selective activity by measuring the RNA expression profile of PZN-treated B. anthracis, which revealed significant up-regulation of genes within the cell envelope stress response. PZN depolarizes the B. anthracis membrane like other cell envelope-acting compounds but uniquely localizes to distinct foci within the envelope. Selection and whole-genome sequencing of PZN-resistant mutants of B. anthracis implicate a relationship between the action of PZN and cardiolipin (CL) within the membrane. Exogenous CL increases the potency of PZN in wild type B. anthracis and promotes the incorporation of fluorescently tagged PZN in the cell envelope. We propose that PZN localizes to and exacerbates structurally compromised regions of the bacterial membrane, which ultimately results in cell lysis.

[2] Reprinted with permission from Molohon, K.J.*.; Blair, P.M.*; Park, S.; Doroghazi, J.R.; Maxson, T.; Hershfield, J.; Flatt, K.; Schroeder, N.; Ha, T.; Mitchell, D.A. "Plantazolicin is an ultra-narrow spectrum antibiotic that targets the *Bacillus anthracis* membrane." ACS Infect. Dis., 2:207-220 (2016). Copyright 2016 American Chemical Society. K.J.M. performed RNA-Seq, mutational studies, and spectrum of bioactivity assays; S.P. performed STORM; J.R.D. performed RNA-Seq analysis; T.M. created knockouts; J.H. performed BSL3 bioactivity assays; K.F. performed nematode killing assays.
*These authors contributed equally to this work.

3.2 Introduction

The current practice of employing broad-spectrum antibiotics to treat bacterial infections contributes to the rise of antibiotic resistance.[1] As a countermeasure, species-selective and narrow-spectrum antibacterial compounds are garnering increased attention in the medical community for their potential as therapeutics and/or diagnostics.[2-3] Plantazolicin (PZN) is a polyheterocyclic, linear compound of the ribosomally synthesized and post-translationally modified peptide (RiPP) natural product family with narrow-spectrum antibiotic activity (Figure 3.1).[4] More specifically, PZN is a member of the thiazole/oxazole-modified microcins (TOMMs), a recently grouped and rapidly expanding RiPP class with ~1500 identified gene clusters.[5-6] Previously, PZN was described as an antibiotic compound that inhibits Gram-positive organisms closely related to its producing organism, *Bacillus amyloliquefaciens* FZB42[4] (this organism has recently been taxonomically reclassified as *Bacillus velezensis* FZB42).[7] In 2011, by screening a small panel of microorganisms, we described PZN as having potent activity toward *Bacillus anthracis*, but not other Gram-positive pathogens.[8] Several additional PZN-like gene clusters have been identified in six distinct bacterial genera (from three phyla) through genome mining, but experimental data on antibiotic specificity has so far been limited to PZN.[4, 8] Although PZN has been the subject of total synthesis,[9-11] heterologous expression,[12] and enzymological studies,[13-15] insight into the mode of action (MOA) of PZN has not been reported in the eight years since the discovery of its biosynthetic gene cluster.[16]

B. anthracis, the causative agent of anthrax and a category A priority pathogen, is a Gram-positive bacterium and a member of the *B. cereus sensu lato* group, which includes *B. cereus*, *B. anthracis*, *B. thuringiensis*, and *B. mycoides*.[17] Microbiologists have debated whether these organisms should be considered as one species, given that some strains share >99% DNA sequence

identity. Despite being grouped with other *Bacillus* species, *B. anthracis* harbors a number of distinguishing features compared to other members of the *B. cereus* group. Fully virulent *B. anthracis* contains two conserved plasmids, pXO1 and pXO2, which harbor the genes responsible for producing the anthrax toxin and poly-D-glutamic acid capsule, respectively. However, homologous plasmids are also found in certain *B. cereus* strains.[18] Beyond characteristic plasmid content, *B. anthracis*, unlike other members of the *B. cereus* group, harbors a nonsense mutation in *plcR* (phospholipase C regulator), rendering *B. anthracis* nonmotile and nonhemolytic.[18] The unambiguous differentiation of *B. anthracis* from other nonpathogenic *B. cereus* species is critically important from a public health perspective, especially as it pertains to bioterrorism.

Other defining features of *B. anthracis* that may facilitate species selectivity are exterior to the cell wall. *B. anthracis* displays a two-dimensional protein lattice called the surface layer (S-layer). Decorated with surface-associated proteins in a *csaB* (cell surface attachment)-dependent manner,[19] the S-layer is noncovalently attached to the secondary cell wall polysaccharide (SCWP),[20] which is covalently tethered to the peptidoglycan. The *B. anthracis* SCWP is structurally unique[21] and serves as the binding site for gamma (γ) phage[22-23] and previously described *B. anthracis* typing antibodies.[24] γ phage produce a peptidoglycan hydrolase, PlyG, which specifically recognizes the terminal galactoses of the *B. anthracis* SCWP, allowing efficient digestion of the cell wall.[22] Similarly, typing methods using monoclonal antibodies to the SCWP also exploit differences in the terminal sugar unit. However, there exist atypical *B. anthracis* strains that would constitute false negatives in any diagnostic assay based on these methods.[24-25] Wip1, another *B. anthracis*-specific phage, is even more selective than γ phage, yet certain *B. cereus* strains remain sensitive.[26] Thus, the species specificity of PZN is intriguing not only from

a MOA standpoint but also as a rapid means to discriminate *B. anthracis* from other *B. cereus sensu lato* members.

Here we describe PZN as a remarkably selective small molecule antibiotic toward *B. anthracis*. The specificity of PZN was first examined by gene expression profiling, which yielded an expression signature distinct from broader spectrum antibiotics. We have identified and characterized a set of resistant mutants and evaluated their role in PZN resistance, which led us to further investigate the bacterial membrane as the most probable target of PZN. Using fluorescence-based approaches, we confirmed that PZN localizes to the cell envelope in a species-selective manner. PZN binding was associated with rapid and potent membrane depolarization. Taken together with the observation that PZN interacts synergistically with the negatively charged phospholipid, cardiolipin (CL), we propose that PZN localizes to and aggravates transient weaknesses present in the *B. anthracis* cell membrane.

3.3 Results

B. anthracis, the causative agent of anthrax, can often be mistaken for other members of the *B. cereus* group. As a bacterium with a history of use in bioterrorism, there is an urgent homeland security need for highly accurate and rapid identification of *B. anthracis*. We therefore set out to characterize and understand the selectivity of PZN.

3.3.1 Defining the species selectivity of PZN

PZN was originally described as a Gram-positive antibiotic, inhibiting the growth of *B. subtilis*, *B. cereus*, and *B. megaterium*.[4] It is important to note, however, that the spot-on-lawn assay employed to reach this conclusion used 1 mg of purified PZN per spot. We set out to obtain the minimum inhibitory concentration (MIC) of PZN by using a microbroth dilution assay. As expected, the

activity of PZN was revealed to be considerably more selective, in that antibacterial activity was detected toward only *B. anthracis* upon screening of a small panel of human pathogens.[8] We continued to define this unusually narrow spectrum of activity by screening a larger panel of strains with various degrees of genetic similarity (Table 3.1). PZN was found to be selective for vegetative *B. anthracis*, including fully virulent biosafety level 3 strains, with MICs between 1 and 16 μg/mL (0.75–12 μM). Endospores, the dormant phase of the *B. anthracis* life cycle, were resistant to PZN until germination was initiated (Table 3.2). By microbroth dilution, *B. subtilis* and *B. cereus* were not susceptible to PZN at concentrations up to 64 μg/mL, which contrasts with the previous spot-on-lawn assay.[4]

To further investigate the selectivity of PZN toward *B. anthracis*, we conducted a head-to-head comparison using the γ phage assay. Prior to modern genomic methods, γ phage sensitivity and other phenotype testing were popular methods for identifying *B. anthracis*.[25] Notwithstanding the reported 96% positive accuracy, non-*B. anthracis* strains that are sensitive to γ phage and true *B. anthracis* strains that are insensitive have been reported.[25, 27-28] We obtained a panel of atypical *B. cereus* strains that are sensitive to γ phage and tested them for PZN susceptibility (Table 3.3). *B. cereus* strains that generated a false positive in the γ phage assay were not susceptible to PZN.[26, 28-29]

To further define the attributes giving rise to the species selectivity of PZN, we procured various bacterial strains that address key differences between *B. anthracis* and *B. cereus*. *plcR*, encoding the phospholipase C regulator, is nonfunctional in *B. anthracis* but is intact in *B. cereus*.[18] Deletion of *plcR* in *B. cereus* did not increase its susceptibility to PZN (Table 3.1). Additionally, sortase-deficient strains of *B. anthracis*, which lack the ability to anchor various proteins to the cell wall, remain susceptible to PZN.[30] The activity of PZN was similarly not dependent on the

presence or composition of the *B. anthracis* S-layer, as strains deficient in S-layer assembly or decoration, namely those harboring mutations in *csaB*, *sap*, and *eag*, are equally susceptible to PZN.[19] We further confirmed that susceptibility to PZN is plasmid-independent given that a plasmid-deficient strain (LLNL A0517-1) and strains with both plasmids retained sensitivity (Table 3.1; Figure 3.2). Wip1 phage susceptibility and antibody typing have also been used to distinguish *B. cereus sensu lato* strains, but also have known exceptions to their specificity for *B. anthracis*.[24, 26] We obtained a "false-positive for *B. anthracis*" strain for each marker: *B. cereus* CDC32805 for Wip1 and *B. cereus* ATCC 7064 for antibody typing. We again observed no measurable PZN susceptibility for either strain (Table 3.1).

After extensive susceptibility testing, the only notable exception to the *B. anthracis* selectivity of PZN was *B. cereus* G9241 (MIC of 8 μg/mL). Strain G9241 encodes the genes for an anthrax-like toxin on its pBCXO1 plasmid, which is named for its homology to the *B. anthracis* pXO1 plasmid.[31] Because G9241 is encapsulated and toxigenic, it causes an anthrax-like disease but is undetectable in the γ phage assay.[27] Thus, from a pathogen detection perspective, the action of PZN toward G9241 could be considered fortuitous if it were to be further developed as a rapid diagnostic. Together, these data not only highlight the species discrimination of PZN but also rule out *plcR*-related effects, sortase-mediated proteins, the SCWP, the S-layer, and plasmid-borne entities as targets of PZN.

The spectrum of PZN activity calls into question whether bacteria are the naturally intended target. The canonical PZN-producing strain, *B. velezensis* FZB42 (formerly *amyloliquefaciens*), is a prolific producer of other natural products with antifungal and nematicidal activities.[7, 32] Liu et al. ascribed a nematicidal activity to PZN, derived from experiments showing that PZN-deficient FZB42 strains exhibit reduced nematicidal activity against *Caenorhabditis elegans*.[33] Because

these experiments employed crude cellular extracts, we evaluated purified PZN in a similar manner, embedding the compound in agar ("slow killing" assay) or providing PZN in a liquid suspension ("liquid fast killing" assay). PZN was found to be no more toxic to *C. elegans* than a vehicle control and is not nematicidal in its own right (Figure 3.3). Purified PZN was also not responsible for the antifungal activity of the native producer, leaving the ecological function of PZN unknown (Table 3.1).

After observing the specificity of PZN under one growth medium condition (Luria–Bertani broth, LB), we reassessed specificity against a smaller but representative panel of strains in two additional growth media (Mueller–Hinton and brain–heart infusion broths, Table 3.4). All tested strains of *B. anthracis* remained equally susceptible, but unexpectedly, some *Staphylococcus aureus* strains were susceptible to PZN under alternative growth media (MICs from 8 to 32 μg/mL). Only *S. aureus* showed media-dependent susceptibility to PZN; all other tested strains remained nonsusceptible to PZN.

3.3.2 Assessing potential macromolecules as the target of PZN

In an attempt to identify the molecular target(s) of PZN by affinity-based purification,[34] three PZN derivatives were prepared: N-terminal biotinylation, C-terminal biotinylation, and C-terminal modification functionalized with aziridinyl and alkynyl groups for photoaffinity capture (Figure 3.4). Only the C-terminal modifications retained bioactivity, albeit with ~16-fold reductions; therefore, these probes were utilized for affinity-based target identification. Despite numerous attempts, we were unable to identify interactions unique to PZN compared to the control (data not shown). Because affinity purification-based strategies to identify small molecule targets are most successful when the interaction is of high affinity to a protein,[35] we considered the possibility that PZN may interact with a nonprotein macromolecule. We thus monitored the formation of the cell

wall, fatty acids, and RNA (as well as protein) using radiolabeled, biosynthetic precursors in the presence of PZN. Similar to daptomycin and the nisin-like lanthipeptide Pep5, PZN extensively disrupted macromolecular biosynthesis (Figure 3.5).[36-37] Interestingly, and in contrast to vancomycin and daptomycin, PZN did not significantly block cell wall biosynthesis on the time scale of the experiment.

3.3.3 Gene expression signature of PZN

Sublethal antibiotic treatment stimulates rapid transcriptional responses in bacteria, and the induced/repressed genes may be indicative of MOA.[38] We thus performed RNA-Seq to evaluate the transcriptional response of *B. anthracis* following exposure to 0.25 μg/mL (0.25 × MIC) PZN for 10 min.[39] A total of 74 genes were differentially regulated, including 63 up-regulated and 11 down-regulated genes, with an adjusted false discovery rate (*q* value) of 0.01 (Figure 3.6; Table 3.5). The expression of a subset of these genes was validated by qRT-PCR (Table 3.6, Table 3.7). Fourteen of the up-regulated genes were transporter subunits, a common stress response upon antibiotic treatment.[40] Conversely, PZN treatment led to the down-regulation of genes associated with L-lactate metabolism, for which the implications remain unclear.

The most highly up-regulated *B. anthracis* genes upon PZN treatment were *bas1344* and*bas1345*, which encode a hypothetical protein and a predicted member of the PspA/IM30 family, respectively (Table 3.7). These genes are homologous to the *B. subtilis* genes *liaI* and *liaH* (lipid II cycle interfering antibiotics), which are involved in the cell envelope stress response. Induction of these genes upon antibiotic treatment is well documented in *B. subtilis*, specifically to antibiotics interacting with lipid II in some capacity (e.g., nisin, vancomycin, and bacitracin).[41] Induction of*liaI* and *liaH* is also seen in *B. subtilis* after daptomycin treatment, despite the lack of any known interaction between daptomycin and lipid II.[42] PZN

treatment also results in massive up-regulation of *bas5200* and *bas5201*, which are homologous to a *B. subtilis* thermosensor two-component system (TCS), *desRK*, that regulates the lipid desaturase, *des*.[43] Although *bas5200*and *bas5201* have yet to be experimentally interrogated, the response regulator and adjacent histidine kinase homologues are 62/89% and 38/71% similar/identical at the protein level to *B. subtilis*, respectively. BLAST-P searches using BAS5200 and BAS5201 as the query sequences retrieve DesK and DesR as the highest similarity hits in *B. subtilis*; the reverse BLAST-P search (*B. subtilis* DesK and DesR query sequences) likewise retrieves BAS5200 and BAS5201 has the top hits in *B. anthracis*. Pending experimental validation of BAS5200-1 as the bona fide *desRK*TCS in *B. anthracis*, PZN would be to our knowledge the first compound known to alter the expression of these regulators, which is further suggestive of a unique MOA.

Recently, we reported on the synthesis of a PZN derivative, Me_2-Arg-Az_5 (Figure 3.1).[15] Chemically, Me_2-Arg-Az_5 represents the N-terminal half of PZN, but the activity spectrum of Me_2-Arg-Az_5 is profoundly broader in LB and includes other *Bacillus* species as well as methicillin-resistant *S. aureus* (Table 3.8). Additionally, the later-described mutations in *bas4114* that conferred resistance to PZN did not confer resistance to other antibiotics or to Me_2-Arg-Az_5 (Tables 3.8 and 3.9). To investigate their differing spectra of activity, we recorded the gene expression profile of *B. anthracis* treated with Me_2-Arg-Az_5 under otherwise identical conditions (0.25 × MIC, 10 min) by RNA-Seq. The two compounds shared a minor portion of their expression profiles, but each profile was largely independent (Figure 3.7; Tables 3.10 and 3.11). For example, sublethal Me_2-Arg-Az_5 treatment also induced the *desRK* TCS, but expression of *liaIH* remained unchanged. Additionally, Me_2-Arg-Az_5 failed to induce *B. anthracis* lysis, in contrast to PZN (Figure 3.8). A possible explanation for the observed differences between PZN and Me_2-Arg-

Az_5 is that the C-terminal portion of the molecule is responsible for the species selectivity of the mature molecule and the N-terminal portion harbors the antibiotic activity, although this remains to be more extensively investigated. The expression profiles of PZN and Me_2-Arg-Az_5, together with strain susceptibility, suggest that PZN and Me_2-Arg-Az_5 pursue independent, but possibly related, targets. Thus, although Me_2-Arg-Az_5 is not useful as a mimic for the full-length natural product, it represents one strategy to broaden the antibiotic spectrum of PZN.

3.3.4 PZN depolarizes the *B. anthracis* membrane

The induction of *liaIH* and *desRK* by PZN suggests a potential relationship with components of the cell envelope. To determine if PZN treatment led to the loss of membrane potential, 3,3′-diethyloxacarbocyanine iodide ($DiOC_2(3)$) was used in a standard flow cytometry-based assay.[44] We observed a dose-dependent decrease in membrane potential upon treating *B. anthracis*with PZN, even at concentrations 100-fold below the MIC. These data further suggest that PZN exerts its action by disrupting the integrity of the cell membrane (Figure 3.9). Destabilization of the bacterial cell membrane is a common MOA for antibiotics; for example, both nisin and daptomycin are known to disrupt membrane potential in Gram-positive organisms.[45-47] By cotreating *B. anthracis* with either nisin or daptomycin and PZN, the resulting isobolograms elicited strong synergistic activity with PZN (Figure 3.9), suggesting independent but cooperative activities.[48]

3.3.5 Subcellular localization of PZN

With mounting evidence that PZN targets the cell membrane, we determined the subcellular localization of PZN by confocal microscopy. Antibiotics derivatized with fluorescent probes have previously been used to shed light on their MOAs.[49-50] Localization of PZN was established by employing a Cy5-labeled PZN derivative (PZN-Cy5) (Figure 3.1, Figure 3.10) that retained much

of its anti-*B. anthracis* activity (MIC of 4 μg/mL, 2 μM). PZN-Cy5 localized to distinct ~200 nm wide foci in *B. anthracis* Sterne (Figure 3.11). To establish if PZN-Cy5 behaved in a manner identical to that of unlabeled PZN, we carried out a competition assay using an excess of unlabeled PZN applied to*B. anthracis* Sterne followed by addition of PZN-Cy5. Due to the extensive cell lysis elicited by PZN, we employed a later-described, spontaneous PZN-resistant mutant (PR06) for the competition assay. Just as in *B. anthracis* Sterne, PZN-Cy5 localized to distinct foci in *B. anthracis*PR06, which is consistent with its susceptibility, albeit at higher concentrations of PZN (Figure 3.11). Importantly, PZN-Cy5 failed to label strain PR06 when an excess of unlabeled PZN was administered first, demonstrating that PZN and the PZN-Cy5 probe identically interact with *B. anthracis* (Figure 3.11). Due to the photoswitching properties of Cy5, we were able to further investigate PZN-Cy5 localization using stochastic optical reconstruction microscopy (STORM, Figure 3.12).[51] Using this super-resolution imaging technique, *B. anthracis* Sterne cells were again confirmed to accumulate PZN-Cy5 at the foci described above. These foci were clearly concentrated near the cellular surface, providing additional evidence that a component of the cell envelope is the target of PZN (Figure 3.13). *B. anthracis* cells contain 16 ± 2 foci per cell, each with a diameter of 181 ± 7 nm, as determined by analysis of 14 randomly chosen cells treated with PZN-Cy5 (Figure 3.13). The labeling pattern of PZN-Cy5 is strikingly different from that of BODIPY-vancomycin, which localizes strongly to bacterial septa where peptidoglycan synthesis is at a maximum.[52] If PZN were acting on the cell wall, sites of active peptidoglycan synthesis or the entire cell wall would be labeled with PZN-Cy5. The nonseptal, punctate labeling of PZN-Cy5 suggests that the target of PZN is neither nascent nor existing peptidoglycan, which is congruent with the observation that PZN did not block cell wall biosynthesis (Figure 3.5). PZN-Cy5 also does not appear to label nonsusceptible *Bacillus* species (Figure 3.14). Some modest labeling was

found with *B. cereus* G9241, which aligns with a somewhat elevated MIC for PZN (8 μg/mL). Combined with the evidence of PZN-Cy5 labeling PZN-resistant *B. anthracis* PR06 (Figure 3.11), these data suggest that PZN binding to the cell envelope is necessary, but insufficient, for bacterial killing.

3.3.6 Isolation and characterization of PZN-resistant mutants

An orthogonal strategy for obtaining antibiotic MOA information involves the selection and mapping of resistance-conferring polymorphisms.[53] The mutated gene(s) can be involved either directly in the MOA of the antibiotic or in a target-unrelated mechanism of immunity. We isolated PZN-resistant *B. anthracis* by growing the Sterne strain on agar plates containing PZN at 4 × MIC. The resistance frequency was determined to be 2.3×10^{-7}, and the resulting mutants exhibited MICs that were ≥32 μg/mL. Genomic DNA was isolated and sequenced for six independently selected PZN-resistant strains (PR01 through PR06) and the parent Sterne strain. Comparison of PR01 through PR06 to the parent revealed that all six polymorphisms were confined to a 50-nucleotide section of a single gene, *bas4114*, which is annotated as an AcrR transcriptional repressor (Table 3.12).[54] This particular AcrR protein is predicted to contain a single transmembrane domain near the C-terminus (Figure 3.15), which is precisely where the PZN resistance conferring mutations were found, all resulting in premature stop codons. Directly downstream of *bas4114* are two EmrE-type multidrug resistance efflux pumps, encoded as*bas4115–4116*. We hypothesized that as an AcrR-type transcriptional repressor, BAS4114 would negatively regulate *bas4115–4116* and that mutations near the C-terminus of BAS4114 would result in regulator mislocalization/dysfunction and derepression of the efflux pumps. This in turn would increase resistance to PZN. Multidrug resistant transporters have been shown to export membrane-associated antibiotics,[55-56] a concept that is consistent with our data supporting

the localization of PZN. One prediction is that BAS4115–6 actively efflux membrane-associated PZN, which lowers the steady-state membrane concentration of PZN. The MIC for PZN thus would increase with the increased expression of *bas4115–4116*. We employed RNA-Seq to compare the mRNA expression profiles of PR06 to the parent Sterne strain. This analysis revealed significant up-regulation of *bas4114–4116*, as well as an unknown gene immediately downstream, *bas4117* (Table 3.13). PR06 and the Sterne parent were equally susceptible to Me_2-Arg-Az_5 (Table 3.8), again underscoring differences between PZN and Me_2-Arg-Az_5. The susceptibility of PR06 to a panel of mechanistically diverse antibiotics, including daptomycin, was also assessed (Table 3.9). The mutation present in PR06 did not confer cross-resistance toward any other tested antibiotic. We then investigated if *bas4114–4117* were constitutively overexpressed in nonsusceptible *B. cereus* strains E33L and ATCC 4342, thereby conferring innate resistance to PZN. Using qRT-PCR, we could not identify constitutive overexpression of this locus in nonsusceptible *B. cereus*strains compared to *B. anthracis* (data not shown). This suggests that the *bas4114–4117* locus is not responsible for PZN resistance in nonsusceptible *B. cereus* strains. Frameshift mutations in the predicted transmembrane region of *bas4114* are clearly the favored route for generating PZN resistance in *B. anthracis*, as shown by the occurrence of multiple independent mutations within the same gene. To subvert this resistance mechanism, and to obtain more insightful information about the MOA of PZN, we deleted *bas4114–4117* from the parental strain by homologous recombination (Figure 3.16). *B. anthracis* Sterne Δ*bas4114–4117* thus became the new parental strain for isolating second-generation PZN-resistant mutants, as the removal of *bas4114–4117* rendered this strain as sensitive to PZN as wild type Sterne (1 μg/mL). This time, two routes were pursued for obtaining additional PZN-resistant strains. First, we selected spontaneous PZN-resistant mutants by challenging Δ*bas4114–4117* with 4 × MIC PZN.

Isolation of the spontaneous mutants resulted in a mutation frequency an order of magnitude lower than before (1.3×10^{-8}). Two independently selected, modestly resistant strains (PR07 and PR08) were subjected to whole-genome sequencing, revealing single missense mutations within *ftsE* (Table 3.14). In *Escherichia coli*, FtsE is an ATP-binding protein that associates with its cognate permease, FtsX, together comprising an ABC transporter that functions during cell wall elongation and septum formation.[57] The activity of FtsE/X in *B. subtilis* differs slightly, as it is responsible for initiating endospore formation via asymmetric septation.[58] Akin to *bas4114*, spontaneous mutations in *ftsE* alone cannot explain the species selectivity of PZN, as the amino acid sequence of *B. anthracis* FtsE is 100% identical to several nonsusceptible *B. cereus* strains. Other *B. cereus*strains, even the PZN-susceptible G9241 strain, are 98–99% identical to *B. anthracis* FtsE. Although there may be an indirect relationship between PZN and FtsE/X, our data support a MOA that does not involve a physical association with FtsE.

As a second strategy to obtain PZN-resistant mutants, we cultured *B. anthracis* Sterne Δ*bas4114–4117* in the presence of a sublethal concentration of PZN. The concentration of PZN was gradually increased with the number of passages.[59] We isolated genomic DNA from a first-passage strain (PR09-1, MIC 16 μg/mL) in addition to two independent fourth passage strains (PR09-4, PR10-4, MICs ≥ 64 μg/mL) for whole genome sequencing. PR09-1 contained a missense mutation in *bas1659*, which encodes a predicted CitB-like response regulator (Table 3.14). Downstream of *bas1659* are genes encoding a predicted histidine kinase (*bas1660*), ABC transporter subunits (*bas1661–1663*), and a cardiolipin (CL) synthase gene (*bas1664*). PR09-4 is a descendent of PR09-1, and as such, PR09-4 contained the same *bas1659* mutation as PR09-1 in addition to another missense mutation in *bas1662* (the permease domain of the locally encoded ABC transporter). PR10-4 contained a similar mutation series (*bas1663*, a second permease gene

for what is presumably a trimeric ABC transporter) but had an additional mutation in *bas1842*, which is implicated in petrobactin biosynthesis.[60] Upon further inspection, we found that deletion of the petrobactin biosynthetic gene cluster did not decrease susceptibility to PZN; therefore, the significance of this missense mutation remains unknown (Table 3.1).

3.3.7 Exogenous cardiolipin increases sensitivity to PZN

We hypothesized that the regulatory- and transport-related mutations upstream of the gene encoding CL synthase could alter CL concentrations and, thus, CL may be implicated in the MOA for PZN. We first examined the effect of exogenous CL on the interaction of PZN with the *B. anthracis* cell membrane. *B. anthracis* cells were treated with PZN-Cy5 (1 nM, 0.001 × MIC) in the presence and absence of exogenous CL (up to 100 μg/mL). PZN-Cy5 treated cells were then analyzed by flow cytometry. The extent of PZN-Cy5 binding to *B. anthracis* was significantly increased when cells were cotreated with CL (Figure 3.18). This result is in contrast to that of daptomycin, which acts on the bacterial membrane but exhibits an antagonistic relationship with CL in Enterococci.[61-62] As predicted, co-administration of CL did not increase the labeling efficiency of daptomycin-Cy5 on *B. anthracis* cells (Figure 3.1, Figure 3.17, and Figure 3.18).[61] Congruent with these data was the observation that CL potentiated the killing activity of PZN toward *B. anthracis*, but decreased daptomycin susceptibility 4-fold. Indeed, the strongly synergistic behavior with CL enhanced the potency of PZN upward of 16-fold, whereas CL alone had no antibiotic activity at the concentrations tested (Figure 3.18).

3.3.8 PZN Co-localizes with cardiolipin and regions of increased fluidity

The genetic and functional association with CL implicates the membrane as the most probable target for PZN. The lipid dye 10-*N*-nonyl acridine orange (NAO) approximates regions of the cell membrane enriched in CL.[63] In *B. subtilis* and *B. cereus*, NAO organizes into distinct foci primarily

at the septa and the poles (Figure 3.19),[64] but it appears that in *B. anthracis* Sterne, NAO labels distinct foci throughout the entirety of the cell membrane (Figures 3.19 and 3.20). CL has the potential to dramatically alter membrane architecture and may contribute to the susceptibility of *B. anthracis* through punctate localization throughout the cell. We therefore treated *B. anthracis* cells with PZN-Cy5 and NAO to investigate if PZN localized to CL-rich regions in the cell membrane. There existed a clear but imperfect co-localization of the two dyes, suggesting a possible interaction with CL in the bacterial membrane (Figure 3.20). Thus, *B. anthracis* appears to have a unique distribution of CL that facilitates an interaction with PZN and leads to cell death, whereas CL localization within other species may not facilitate the lytic activity of PZN. Additionally, 1,1′-didodecyl-3,3,3′,3′-tetramethylindocarbocyanine perchlorate, (DilC12(3)), is a dye reported to associate with regions of increased fluidity (RIF) within cell membranes of *B. subtilis* and may also be indicative of CL localization.[65] RIFs are transiently weakened regions within the bacterial membrane that affect lipid homeostasis and membrane fluidity. We observed co-localization of DilC12(3) and PZN-Cy5, consistent with PZN and CL co-associating with *B. anthracis* RIFs (Figure 3.20).

The proportion of CL in cell membranes has been reported to increase during growth in high-osmolarity medium, especially for *B. subtilis*.[66] We thus tested whether increasing the osmolarity of the *B. subtilis* medium (and thus the CL content) would induce susceptibility to PZN. When grown in standard LB supplemented with an additional 1.5 M NaCl (1.67 M final), PZN was weakly growth-suppressive toward *B. subtilis* (Table 3.15). By measuring CL from total lipid extractions, CL levels did increase compared to standard growth in LB (Table 3.15). However, exogenous CL alone did not induce PZN susceptibility in *B. subtilis* or *B. cereus* (data not shown). Members of *B. cereus sensu lato*, including *B. anthracis*, are not as osmotolerant as *B.*

subtilis;[67] the maximum salinity these strains can tolerate in LB is 0.67 M (standard LB supplemented with an additional 0.5 M NaCl). When grown under high osmotic stress, both wild type and PZN-resistant strains of*B. anthracis* display measurable susceptibility to PZN, although *B. cereus* strains remain resistant (Table 3.15). Unlike *B. subtilis*, CL content does not increase significantly when *B. anthracis* or *B. cereus* strains are grown in 0.5 M NaCl, suggesting that the observed susceptibilities may be due to the harsh growth conditions rather than CL content. Cell survival under conditions of increased osmolarity is dependent on membrane fluctuations with an increase in unsaturated fatty acid composition.[66] Increased CL levels are associated with high osmotic stress in *B. subtilis*, *E. coli*, *Lactococcus lactis*, and others.[66] Furthermore, excess CL within the membrane results in increased fluidity and lipid bilayer deformation, as observed when *B. subtilis* is grown in a high-osmolarity medium (Figure 3.21).[68] By increasing the osmolarity of the growth medium, we can induce a modest increase in the potency of PZN toward *B. anthracis* (Table 3.15). The resultant increase in CL, together with the activation of the *des* TCS, presumably shifts the lipid profile to a more fluid composition, which negatively affects membrane integrity. This phenotype is readily observed by confocal microscopy (Figure 3.21).[69] We hypothesize that PZN takes advantage of an already weakened *B. anthracis* membrane to elicit its selective antibacterial activity.

As stated previously, the stepwise-selected PZN-resistant strains accumulated mutations in genes upstream of one of five CL synthase genes (*cls*, *bas1664*). We analyzed the transcriptional response within the *bas1664* locus, including the upstream regulators/transporters, and observed a dramatic increase in the expression of several genes in PR09-1 and PR09-4, including *bas1664*itself and the nearby ABC transporter genes (*bas1661–1663*), but not the locally encoded response regulator and histidine kinase genes (*bas1659–1660*, Table 3.16). In stark

contrast, there was no differential expression of any tested gene in the PR10-4 strain. Although these results may seem contradictory, PR10-4 did acquire an additional mutation in a gene responsible for the production of the siderophore petrobactin (Table 3.14).[70] Given that it is well established that *B. subtilis* experiences iron limitation when grown under high osmotic stress,[71-72] it is possible that PR10-4 handles stress induced by PZN or high NaCl concentrations differently from PR09-1 and PR09-4. Furthermore, CL levels do not necessarily correlate to the number of *cls* transcripts (and there are multiple *cls* genes), which is suggestive of other regulatory mechanisms to avoid overproduction of CL.[73] With respect to PR09-1, PR09-4, and PR10-4, there is a complex relationship between CL content and PZN susceptibility. On the basis of our findings, we expect that in addition to CL, other membrane-associated biomolecules may also contribute to the ability of PZN to destabilize *B. anthracis* cell membranes.

3.4 Conclusion

Due to advances in genomics, *B. anthracis*, the causative agent of anthrax, can be distinguished from the other members of the *B. cereus sensu lato* group by whole genome sequencing, multilocus sequence typing, the presence of chromosomal lambdoid prophages, and the presence of a characteristic nonsense mutation in *plcR*.[18, 29] An alternative approach to *B. anthracis*identification now includes susceptibility to PZN, which is a natural product exhibiting potent and selective bactericidal activity for *B. anthracis* under standard laboratory conditions. Our data demonstrate that the species selectivity of PZN is even more discriminating than that of the reputedly selective γ phage.[25, 28-29, 74] Additionally, PZN on its own does not contribute to *B. methylotrophicus* FZB42 antifungal or nematicidal activity. *B. anthracis* is nearly identical to other members of the *B. cereus sensu lato* family and, remarkably, strains of *B. anthracis* selected to interrogate key genetic differences retain their respective susceptibility to PZN. Gene expression analysis, together with confocal and super-resolution microscopy, reveals that PZN operates by a different MOA than previously described cell envelope-targeting antibiotics. Thus, we present a model for PZN activity wherein PZN takes advantage of a locally weakened cell membrane, whether due to RIFs, CL-dependent membrane deformation, or some combination thereof. PZN accumulates to such membrane defects, resulting in membrane depolarization and lysis of *B. anthracis* in a species-specific manner. The activity of PZN suggests an immediate homeland security application, where it could be developed into a rapid *B. anthracis* detection test.

3.5 Methods

3.5.1 Strain and growth conditions

All strain references are displayed in Table 3.1. All strains were grown in LB broth unless otherwise described (10 g/L tryptone, 5 g/L yeast extract, 10 g/L (0.17 M) NaCl). Biosafety level 3 strains of *B. anthracis* were grown on Mueller–Hinton agar. *Neisseria* strains were grown in gonococcal medium base supplemented with Kellogg's I and II.[75] *Streptomyces* endospores were isolated on mannitol soybean flour agar (20 g/L mannitol, 20 g/L soybean flour, 1.5% agar) and used to determine PZN susceptibility in ISP2 (4 g/L yeast extract, 10 g/L malt extract, 4 g/L dextrose). Yeast strains were grown in YPD medium (10 g/L yeast extract, 20 g/L peptone, 20 g/L dextrose). *C. elegans* was cultured on nematode growth medium with *E. coli* OP50. Cultures were supplemented with 1.25 mM $CaCl_2$ when assaying daptomycin susceptibility. In cases when increased osmolarity was desired, the LB was supplemented with additional NaCl (final concentration of 1.67 M).

3.5.2 PZN production

Stationary phase cultures of RSpMarA2 (Δsfp, yczE, degU) (1) were grown in Luria-Bertani (LB) broth supplemented with 7 μg/mL kanamycin and 7 μg/mL chloramphenicol. Sterilized aluminum trays (12.75 × 9 in) were prepared with M9 agar medium supplemented with BME vitamin mix and ATCC trace mineral solution and the aforementioned antibiotics. Trays were inoculated with 1.5 mL stationary phase RSpMarA2 and incubated for 48 h at 37 °C. Bacterial lawns were loosened from the agar with a razor blade and resuspended in Tris-buffered saline (TBS) (150 mL/tray). The bacteria were then harvested via centrifugation (11,000 × g, 20 min, 4 ˚C). The supernatant was decanted and the cell pellets were stored at -20 °C until extraction.

3.5.3 PZN purification

PZN was extracted by resuspending the bacterial pellets in 150 mL MeOH/tray with intermittent vortexing for 15 min at 22 °C. The cells were then harvested by centrifugation as above. The supernatant was vacuum-filtered using Whatman filter paper, rotary evaporated, and subsequently lyophilized to dryness. The dried, crude PZN was resuspended in MeOH (1 mL/tray of extract) and centrifuged to remove insoluble debris (4,000 × g, 10 min, 4 ˚C). The supernatant was then injected onto a RediSep Rf High Performance 15.5 g HP C18 cartridge (Teledyne Isco) and purified by MPLC using a Combiflash Rf 200 system (25-100% MeOH/10 mM aqueous NH_4HCO_3 over 120 column volumes). The fractions containing PZN were pooled, rotary evaporated, and lyophilized to dryness, which yielded roughly 5 mg/tray. Purity was confirmed by analytical HPLC-ESI-MS (Agilent) inline with a BETASIL C18 column (Thermo, 250 mm × 4.6 mm, 5 µm particle size). On a 35 min gradient from 40-95% MeCN/10 mM aqueous NH_4HCO_3, the sample was monitored for absorption at 220 and 260 nm, all ions 400 – 2000 Da and the $[M+2H]^{2+}$ of PZN. After confirmation of purity, PZN was dissolved in DMSO at concentrations of 30-50 mg/mL and stored at -80 ˚C for later use.

3.5.4 Bacterial endospore preparation and susceptibility screening

B. anthracis Sterne 7702[2] endospores were prepared as described previously.[76] Briefly, *B. anthracis* Sterne 7702 cells were incubated overnight in LB at 37 °C. Difco Sporulation Media agar plates (8 g/L Nutrient Broth, 1 g/L KCl, 0.25 g/L MgSO4•7H_2O, and 17 g/L agar) was inoculated with 150 µL of the stationary phase culture and incubated at 30 °C for 5 d. Lawns were recovered by resuspension in sterile H2O and filtered using 3.1 and 1.2 µm filters to remove vegetative cells and aggregated endospores. Endospore filtrate was incubated at 65 °C for 1 h to remove any remaining vegetative cells. Endospores were harvested by centrifugation (8,000 × g,

25 min, 4 °C). After decanting the supernatant, the endospores were washed 3 times with 40 mL of H2O, harvesting by centrifugation. Endospores were stored at 4 °C in H2O and quantified by plating. Endospores were screened for PZN activity by incubating 1 × 109 endospores with PZN (0-16 μg/mL) in H2O for 20 h at 37 °C. Endospores were incubated at 65 °C for 1 h to destroy any remaining vegetative cells, followed by a 4 h recovery step at 4 ˚C, and then finally by serial dilution onto LB agar plates to assess germination. Plate counts represent the average of two trials.

3.5.5 PZN bioactivity

PZN and Me_2-Arg-Az_5 bioactivities were determined via microbroth dilution assay as described in the Clinical and Laboratory Standards Institute manual.[77] The optical density (OD_{600}) of a stationary phase culture was adjusted to 0.01 and added to a microtiter plate containing serially diluted PZN. Wells were visually inspected for turbidity, and the MIC was determined as the lowest compound concentration that incurred no growth after 16 h. MICs were determined in LB unless growth conditions required an alternative medium (see above). The *S. aureus* media-dependent PZN susceptibility was analyzed using LB, brain–heart infusion (BHI, Bacto), and Mueller–Hinton (BBL) broths. When indicated, CL was added to the medium at 100 μg/mL.

A *B. anthracis* growth curve was generated using Tecan Infinite M200 Pro. *B. anthracis* Sterne 7702 cultures were grown in LB to stationary phase at 37 °C. Cultures were diluted to OD_{600} of 0.05 with fresh LB and allowed to recover to an OD_{600} of 0.35. Cultures were aliquoted into 96-well plates containing PZN and incubated at 37 °C with orbital shaking. OD_{600} was measured every 2 min. Values were normalized to an initial OD_{600} of 0.35 and adjusted to a 1 cm path length. Error bars represent standard deviation of two independent experiments.

A growth curve in the presence of Me_2-Arg-Az_5 was generated as described above with the following differences: *B. anthracis* Sterne 7702 and cultures were grown in duplicate to OD_{600} 1.0

and aliquoted into 96-well plates. Wells were treated with 1:1 dilutions of Me_2-Arg-Az_5 at a maximum concentration of 12 μM. The plate was incubated at 37 °C with orbital shaking, and OD_{600} was measured every 2 min. Values were normalized to an initial OD_{600} of 1.0, adjusted to a 1 cm path length, and averaged at each time point.

3.5.6 Gamma (γ) phage sensitivity

γ phage are propagated as described previously[25] using *B. anthracis* Sterne 7702 cells on BHI agar plates, with no visible loss in infectivity. Phage infectivity was tested against a panel of *B. cereus* and *B. anthracis* strains using a serial dilution assay. Stationary phase cultures were adjusted to an OD_{600} of 0.1, and 100 μL was plated on BHI plates. Five microliters of phage stock (2.6×10^8 plaque-forming units/mL) was serially diluted (2-fold) and spotted onto the plates and allowed to dry. After incubation at 37 °C for 16 h, plates were removed and visually inspected for plaques.

3.5.7 RNA isolation and transcriptional profiling of PZN-treated Sterne cells

For the compound-treated samples, independent 3 mL cultures of *B. anthracis* Sterne 7702 cells were grown to an OD_{600} of 0.4, and 0.25 × MIC of PZN, 0.25 × MIC Me_2-Arg-Az_5,[15] or an equivalent volume of DMSO was added and allowed to incubate for 10 min at 37 °C. Together with resistant mutant PR06, RNA was isolated and prepared as described previously.[4] RNA-Seq libraries were created using the TruSeq Stranded RNA Sample Prep kit (Illumina, San Diego, CA, USA) after rRNA depletion using the RiboZero Bacteria kit (Epicenter, Madison, WI, USA). Sequencing was performed for 1 × 100 cycles on a HiSeq 2000 with version 3 Chemistry. Transcriptomic data were processed with the Rockhopper version 1.30 pipeline[78] using *B. anthracis* Sterne and *B. anthracis* Ames Ancestor plasmid pXO1 (NC_007322.2) as references. Default values (allowed mismatches 0.15, minimum seed length 0.33, minimum expression of

UTRs and ncRNAs 0.5) were used, with the exception that reverse complement reads were used for mapping. The RNA-Seq data discussed in this publication have been deposited in NCBI's Gene Expression Omnibus and are accessible through GEO Series accession no. GSE73343 (http://www.ncbi.nlm.nih.gov/geo/query/acc.cgi?acc=GSE73343).

3.5.8 Membrane depolarization

Three independent stationary phase cultures of *B. anthracis* Sterne 7702 were used to inoculate fresh LB and grown to OD_{600} of 0.5 at 37 °C with shaking. Aliquots (10 µL) were diluted to 1 mL in PBS containing 0.1 µM $DiOC_2(3)$ and compounds (DMSO, vehicle; 5 µM carbonyl cyanide *m*-chlorophenyl hydrazone (CCCP), 3.0 µM daptomycin, 0.5 µM PZN, 1.0 µM PZN). Cells were mixed at 21 °C for 30 min prior to analysis by flow cytometry (BD LSR II Flow Cytometry Analyzer). Voltages for fluorescein isothiocyanate (FITC) and propidium iodide (PI) fluorescence were set so that average counts per cell were between 10^3 and 10^4. Geometric means for fluorescence ratios were normalized to the control $DiOC_2(3)$ samples.

3.5.9 Confocal microscopy

In general, cells were prepared by inoculating 5 mL of LB with 200 µL of a stationary phase culture. After growing to an OD_{600} of 0.5 at 37 °C with shaking, 1 mL aliquots were centrifuged (3 min, 8000*g*), decanted, and resuspended in sterile PBS. Slides were prepared by mixing 1:1 (v/v) cell suspensions in PBS and liquefied low gelling temperature agarose (Sigma-Aldrich, 2% w/v in water). All microscopy images were obtained using a Zeiss LSM 700 confocal microscope with a 63×/1.4 Oil DIC objective and processed using Zen 2012 software. Laser intensity and gain were kept at a minimum and held constant for all experiments. Linear contrast was equally applied during image processing. To localize PZN, *B. anthracis* Sterne 7702 was treated in PBS with 0.2 µM PZN-Cy5 for 30 min at 22 °C. After washing in PBS (3 × 500 µL), cells were resuspended in

a final volume of 250 μL of PBS. Competition experiments were performed using PR06 (PZN-resistant) in PBS treated with DMSO (vehicle) or 1 μM PZN for 20 min at 22 °C before the addition of 0.05 μM PZN-Cy5. After 20 min at 21 °C, the cells were washed in PBS (3 × 500 μL) and resuspended in a final volume of 250 μL of PBS. Sterne underwent cotreatment in PBS with 0.2 μM PZN-Cy5 for 25 min before the addition of other fluorescent compounds. After 5 min of additional treatment, cells were washed in PBS (5 × 500 μL) and resuspended in a final volume of 250 μL of PBS. Concentrations used were as follows: NAO (Sigma-Aldrich), 1 μM; DilC12(3), 1 μM. For CL experiments, cells were treated with EtOH (vehicle), 10 μg/mL CL, or 100 μg/mL CL in addition to 0.2 μM PZN-Cy5 for 30 min. For high-osmolarity samples, cells were grown to stationary phase in standard LB and diluted into high-osmolarity medium (an additional 1.5 M NaCl was added to *B. subtilis* cultures; 0.50 M for *B. anthracis* and *B. cereus*).

3.5.10 Super-resolution microscopy (STORM)

Cells for 3D super-resolution microscopy were grown and treated with PZN-Cy5 as described for confocal microscopy. The cells were immobilized on a Nunc Lab-Tek 8-well chambered coverglass (Sigma-Aldrich) coated with 0.1% (w/v) poly-L-lysine (Sigma-Aldrich). After 10 min of incubation, unattached cells were removed by washing chambers with sterile PBS. Chambers were filled with 500 μL of imaging buffer (10 mM NaCl, 50 mM Tris-HCl (pH 8.5), 10% w/v glucose). Immediately prior to imaging, cysteamine (Sigma-Aldrich, 10 mM final concentration), catalase (EMD Millipore, 909 U/mL), and pyranose oxidase (Sigma-Aldrich, 4.44 U/mL) were added to the imaging buffer. 3D super-resolution microscopy was performed as described previously.[79-80] Briefly, samples were imaged using an Olympus IX-71 inverted microscope outfitted with a 100× NA 1.4 SaPo oil objective. Mechanical shutters (LS6T2, Unibliz) were used to alternatively excite the sample with a red laser (DL640-100-AL-O, Crystalaser) and reactivate

Cy5 with a violet laser (405 nm, 20 mW, Spectra Physics Excelsor). The lasers were expanded by 7.5×, reflected by a dichoroic mirror (Semrock FF408/504/581/667/762-Di01-25X36), and sent to the sample chamber with a focusing lens that also creates an incidental angle slightly smaller than the total internal reflection angle, reducing the background signal while allowing illumination of several hundred nanometers along the *z*-axis. The emission signal from the sample was passed through an emission filter (Semrock FF01-594/730-25) and two additional notch filters (Semrock NF01-568/647-25X5.0 and NF01-568U-25) and was imaged on an EMCCD camera (DV887ECS-BV, Andor Tech). A cylindrical lens (SCX-50.8-1000.0-UV-SLMF-520-820, CVI Melles Griot, 2 m focal length) in the emission beam path induced astigmatism for 3D detection.[51] ASI CRISP (Applied Scientific Instrumentation) and a piezo-objective (PI P-721.10) were used to compensate for vertical drift during data collection. The horizontal drift was corrected in the post data acquisition step by the analysis software utilizing the correlation function.[81] The data analysis software was provided by Xiaowei Zhuang[79] and modified for 3D imaging.

3.5.11 2D projection analysis

2D projection analysis was used to determine spatial localization of PZN on *B. anthracis* Sterne 7702 cells. A total of 11 cells imaged by super-resolution microscopy were aligned lengthwise along the y-axis, and then sectioned to remove poles and septa. Cells were projected onto the XZ plane and divided into units of 30 × 30 nm^2. Within each unit, spot density was determined and color-mapped. The probability of finding a dye molecule at distance R from the y-axis was calculated for radial windows with a 20 nm bin size and normalized to the area of the radial window.

3.5.12 PZN-Cy5 cluster analysis

A density-based clustering analysis algorithm, DBSCAN,[8] was used as previously reported[9, 10] to analyze super-resolution images of PZN-Cy5-treated *B. anthracis* Sterne 7702. Briefly, spots in super-resolution images of 14 cells were grouped into clusters based on spatial density. The required *Npts* and *Eps* parameters were set to 19 and 40 nm, respectively, and used to identify core points in high density spots. Parameter values empirically set such that core points within a cluster were within *Eps* distance of each other and surrounded by at least *Npts* points. Cluster borders were defined by points located with *Eps* distance to any core point. Cluster size was calculated as twice the average distance between the cluster center and every point in the cluster.

3.5.13 Selection of spontaneous PZN-resistant mutants

Spontaneous PZN-resistant mutants were generated by plating 2×10^8 *B. anthracis* Sterne 7702 cells grown to stationary phase onto a PZN plate containing 4 × MIC PZN. Surviving colonies were tested for sustained PZN resistance via microbroth dilution as described above. Resistant mutants PR01, PR02, PR05, and PR06 were subjected to genomic DNA isolation as follows: 3 × 10 mL cultures of each strain were grown to stationary phase, harvested, and resuspended in 400 µL of water. Cells were lysed with 50 µL of 10% SDS and 5 µL of 20 mg/mL RNase solution at 22 °C for 5 min. DNA was isolated via 25:24:1 phenol/chloroform/isoamyl alcohol extraction, followed by addition of 24:1 chloroform/isoamyl alcohol. DNA precipitation via cold isopropyl alcohol and a subsequent 70% ethyl alcohol wash resulted in purified genomic DNA.

After genetic deletion of *bas4114–4117*, a second round of spontaneously resistant mutants to PZN was selected and isolated as above. Serial-passage mutants were isolated as previously described,[59] starting with three independent cultures of an OD_{600} of 0.1 *B. anthracis* Sterne 7702 Δ*bas4114–4117* in 0.25 µg/mL (0.25 × MIC) PZN LB. Cultures that grew were diluted to an

OD_{600} of 0.1 and subjected to increased concentrations of PZN until cultures were resistant to 64 μg/mL. Cultures were serially passaged onto PZN-free medium to confirm mutant stability. Genomic DNA was isolated as described above. All mutants derived from the Δ*bas4114–4117* deletion strain were sequenced as described and assembled via CLC Genomics Workbench, and SNP analysis was performed with Mauve version 2.3.1.

3.5.14 Whole genome sequencing and assembly

Genomic libraries for resequencing were prepared using the TruSeq DNaseq Sample Prep Kit (Illumina). Sequencing was performed on a HiSeq 2000 with version 3 Chemistry for 1 × 100 cycles. SNP and DIP discovery was performed with two different methods. Regarding PR02, PR05, and PR06, CLC Genomics Workbench SNP and DIP discovery pipelines were employed using with the publicly available *B. anthracis* str. Sterne genome NC_005945.1 as a reference. PR01 required de novo assembly with IDBA UD version 1.0.9, followed by whole genome alignment and SNP discovery using Mauve version 2.3.1. Resistant mutants PR03 and PR04 were selected separately and underwent Sanger sequencing after PCR amplification of *bas4114*and sequencing with the *Bam*HI-BAS4114-f primer (Table 3.6). The WGS data discussed in this publication have been deposited in NCBI's GenBank and are accessible via BioProject accession no. PRJNA295544. Within this BioProject are individual accession numbers for each *B. anthracis*strain (taxId: 1392) for which whole genome sequencing was performed: CP012720, PR01; CP012721, PR02; CP012722, PR05; CP012723, PR06; CP012724, PR07; CP012725, PR08; CP012726, PR09–1; CP012727, PR09–4; CP012728, PR10–4; CP012730, Parent1 (for PR01 through PR06); CP012729, Parent2 (for PR07 through PR10-4).

3.5.15 Effect of cardiolipin on fluorescence intensity

Three independent stationary phase cultures of *B. anthracis* Sterne 7702 were used to inoculate fresh LB (200 µL into 5 mL of LB), and the new cultures were grown to OD_{600} of 0.5 at 37 °C with shaking. Samples were prepared by diluting 10 µL aliquots of culture to 1 mL in PBS containing 1 nM PZN-Cy5 and vehicle (EtOH), 10 µg/mL CL (Sigma-Aldrich), or 100 µg/mL CL. After mixing at 22 °C for 30 min, cells were analyzed by flow cytometry as described above for differences in PZN-Cy5 fluorescence intensity. Geometric means were normalized to the control samples.

3.5.16 Cardiolipin quantification from total lipid extracts

Cultures of *B. anthracis* Sterne 7702, *B. anthracis* Δ*bas4114–4117*, *B. anthracis* PR09-4, *B. anthracis* PR10-4, *B. subtilis* 168, *E. faecium* U503, and *S. aureus* USA300 (three independent 10 mL cultures for each strain) were grown for 20 h at 37 °C. LB containing an additional 1.5 M NaCl was inoculated with 200 µL aliquots of stationary phase cultures of *B. subtilis* 168 or 0.5 M NaCl for *B. anthracis* and *B. cereus* (three independent 10 mL cultures for each strain) and grown for 40 h at 37 °C. The cells were harvested by centrifugation (4000*g*, 10 min, 4 °C) and resuspended in 5 mL of 2:1 $CHCl_3$/MeOH and 1.25 mL of PBS and then extracted for 1 h at 22 °C. The supernatant was removed after centrifugation (4000*g*, 10 min, 4 °C), and layers were washed with 1 mL of $CHCl_3$ and 1 mL of PBS. The organic layer was removed and dried by speed vacuum. The crude lipids were redissolved in 200 µL of $CHCl_3$ and transferred to microfuge tubes and then dried again. The lipids were then dissolved in 20 µL of $CHCl_3$, spotted (2 µL) onto Merck Silica Gel 60 F_{254} analytical TLC plates, and separated using 80:20:5 $CHCl_3$/MeOH/AcOH. Pure CL was used as a standard. The plates were imaged using a Bio-Rad ChemiDoc XRS+. ImageJ was used to subtract background and measure spot density to determine percent CL out of total lipid content.

3.5.17 *C. elegans* nematicidal assays

Wild-type N2 *Caenorhabditis elegans* were cultured on *Escherichia coli* OP50 using standard techniques.[32] Eggs were isolated from gravid hermaphrodites using standard bleaching protocols[82] and incubated for 18 h at 20 °C to obtain synchronized L1 larvae. Cultures were then transferred to new nematode growth media (NGM) plates seeded with OP50 E. coli and incubated for 48 h at 25 °C. Resulting L4 larvae were used for assays adapted from Liu et al.[33] S3 Slow killing assays were performed using 12-well culture dishes with wells containing 1 mL NGM agar amended with 64 µg/mL PZN dissolved in DMSO or an equivalent volume (2 µL) of DMSO alone. One half of the slow killing assay wells were also seeded with 10 µL of OP50 E. coli. Subsequently, 40-60 L4 hermaphrodites were transferred to each well, incubated at 25 °C and assessed every 24 h for 3 d. Each treatment was performed with two biological replicates, each having three technical replicates. Liquid fast killing assays were also performed using 12-well cell culture dishes with wells containing 1 mL M9 buffer combined with 64 µg/mL PZN dissolved in DMSO or DMSO alone. 40-60 L4 larvae were transferred into each well and incubated at 25 °C for 24 h. Fast killing assays were replicated similarly to the slow killing assay (two biological, three technical replicates). For the duplicate assay, an additional control of M9 buffer was included. In both fast and slow killing assays, animals were scored according to criteria shown in Liu et al. Mortality rates were also calculated using identical ratios.

3.5.18 cDNA construction and qRT-PCR analysis

cDNA was generated using the published protocol from the Promega Improm-II system, replacing the reverse transcriptase with Invitrogen m-MLV reverse transcriptase. qRT-PCR was performed with iTaq universal SYBR Green Supermix and following manufacturer's instructions using a

Roche Lightcycler 480 System. Fold changes upon PZN treatment were calculated as described previously.[8]

3.5.19 Compound preparation

Me_2-Arg-Az_5

Me_2-Arg-Az_5 was synthesized as previously described.[14]

PZN-Cy5

PZN (500 µg, 3.74×10^{-7} mol) in 20 µL dimethylformamide (DMF) was mixed with 5 µL N,N'-diisopropylethylamine (DIPEA), 10 µL of a 190 mM solution of 1-hydroxybenzotriazole (HOBt) in DMF, and 10 µL of a 190 mM solution of 1-ethyl-3-(3-dimethylaminopropyl) carbodiimide (EDC) in DMF for 15 min at 21 °C. Then 29.3 µL of a 10 µg/µL solution of Cy5 amine (Lumiprobe) in DMF was added. The reaction was protected from light and stirred at 22 °C for 24 h. The sample was dried by speed vacuum, redissolved in 5% MeOH, and purified on a Sep-Pak C18 cartridge (Waters) on a gradient from 0 – 100% MeOH. Fractions containing PZN-Cy5, as determined by matrix-assisted, laser desorption/ionization time-of-flight (MALDI-TOF) mass spectrometry (MALDI-TOF-MS), were combined and their purity assessed by analytical HPLC (Thermo BetaSil C18 column [250 mm × 4.6 mm], 40 – 95% MeOH). Concentration was determined using the extinction coefficient of Cy5 in DMSO (ε_{646} = 250 L cm^{-1} $mmol^{-1}$).

Daptomycin-Cy5

A 1 mg/mL solution of daptomycin in DMSO was prepared and 33 µL was mixed with 2 µL of 10 mM Cy5 NHS ester (Lumiprobe) and stirred at 22 °C, protected from light, for 4 h. Labeled compound was purified by reverse-phase chromatography on a Perkin Elmer Flexar HPLC outfitted with a Thermo Scientific BetaSil C18 column (250 mm × 4.6 mm I.D., 5 µm particle size) using 10 mM NH_4HCO_3 as the aqueous phase on a 45 min gradient from 25 – 95% MeCN at

a flow rate of 1 mL/min. Absorbance monitoring at 647 nm was used to identify the fraction containing daptomycin-Cy5, which was confirmed by MALDI-TOF mass spectrometry. Purity was determined by a second analytical HPLC run using the same solvents on a 30 min gradient from 40 – 95% MeOH. Concentration was determined using the extinction coefficient of Cy5 in DMSO.

Biotin-PZN (N-terminal label)

A 100 mM solution of EZ-link N-hydroxysuccinimide (NHS) Biotin (Thermo Scientific) in 80% MeCN, 10 mM 3-(N-morpholino)propanesulfonic acid (pH 8.0) was prepared. DesmethylPZN (200 μg, 1.53×10^{-7} mol) was dissolved in 24 μL of the same buffer and treated with 6 μL EZ-link NHS biotin solution for 4 h at 22 °C. The solvent was removed by speed vacuum and the sample was dissolved in MeOH for purification by HPLC (BetaSil C18 column, 250 mm × 4.6 mm, 1 mL/min, 50 – 95% MeOH over 60 min, 10 mM NH_4HCO_3 aqueous phase, S4 monitored at 254 nm). Fractions containing purified biotin-PZN, as determined by MALDI-TOFMS, were combined, dried, and redissolved in DMSO. *B. anthracis* Sterne 7702 susceptibility was determined to be >32 μg/mL using a standard microbroth dilution assay.

PZN-Biotin (C-terminal label)

PZN (500 μg, 3.74×10^{-7} mol) was dissolved in 10 μL DMF and 1 μL DIPEA was added to the sample. A solution of 2.0 mM EDC and 2.0 mM HOBt in DMF was prepared and 2 μL was added to the PZN. After 5 min stirring, 1.0 mg biotin cadaverine was added to the reaction and allowed to proceed at 22 °C for 30 h. The reaction was dried by speed vacuum, redissolved in MeOH, and purified by HPLC (BetaSil C18 column, 250 mm × 4.6 mm, 1 mL/min, 50 – 95% MeOH over 60 min, 10 mM NH_4HCO_3 aqueous phase, monitored at 254 nm). Fractions containing purified PZN-biotin, as determined by MALDI-TOF-MS, were combined, dried, and redissolved in DMSO. *B.*

anthracis Sterne 7702 susceptibility was determined to be 32 μg/mL by a standard microbroth dilution assay.

PZN-diazirine-alkyne

PZN (6.68 mg, 5.0×10^{-6} mol) was dissolved in 75 μL DMF and 1.4 μL Et3N was added with stirring. The sample was cooled in an ice bath to 0 ˚C. HOBt (0.95 mg, 0.007 mmol) and EDC (1.1 mg, 0.007 mmol) were dissolved in 100 μL DMF and added to the PZN. 2- (2-azidoethyl)-2-(but-3-ynyl)-1,3-dioxolane (0.96 mg, 0.007 mmol)[83] was dissolved in 200 μL DMF and 24 μL was added after 10 min at 0 ˚C with stirring, protected from light. The reaction was allowed to warm to 22 ˚C and proceeded for 24 h. The solvent was removed by speed vacuum and the sample was redissolved in MeOH. The sample was purified by HPLC (BetaSil C18 column, 250 mm × 4.6 mm, 1 mL/min, 50 – 95% MeOH over 60 min, 10 mM NH_4HCO_3 aqueous phase, monitored at 254 nm). Fractions containing purified PZN-diazirine-alkyne, as determined by MALDI-TOF-MS, were combined, dried, and redissolved in DMSO. *B. anthracis* Sterne 7702 susceptibility was determined to be 32 μg/mL using a standard microbroth dilution assay.

3.5.20 Structural characterization of PZN derivatives

Purified samples were dried by speed vacuum and dissolved in 50% MeCN supplemented with 1% (v/v) acetic acid. The diluted samples were directly infused using an Advion Nanomate 100 to an LTQ-FTMS/MS (ThermoFisher) operating at 11 T. The MS was calibrated weekly using calibration mixture following the manufacturer's instructions, and tuned daily with Pierce LTQ Velos ESI Positive Ion Calibration Solution (ThermoFisher). Spectra were collected in profile mode with a resolution of 100,000. The singly charged ions were targeted for CID using an isolation width of 5 m/z, a normalized collision energy of 35, an activation q value of 0.4, and an activation time of 30 ms. Data analysis was performed using Thermo Xcalibur software.

3.5.21 Affinity purification using PZN-Biotin

LB (200 mL) was inoculated with 10 mL stationary phase *B. anthracis* Sterne 7702. The culture was grown with shaking at 37 °C to OD600 of 0.5. Samples were divided into 100 mL aliquots, harvested by centrifugation, and individually resuspended in 1.5 mL lysis buffer (50 mM Tris, 500 mM NaCl, 2.5% v/v glycerol, 0.1% v/v Triton X-100, pH 7.5) with 500 mU mutanolysin. After equilibrating for 30 min at 22 °C, the cells were disrupted by sonication (4 × 30 s, 50% amplitude) and harvested by centrifugation (17,000 × g, 10 min). The insoluble fractions were resuspended in 1.5 mL 3-[(3-cholamidopropyl)dimethylammonio]-1-propanesulfonate (CHAPS) buffer (50 mM Tris-HCl, 150 mM NaCl, 1% w/v CHAPS, pH 7.5) and disrupted by sonication (10 s, 50% amplitude). One sample was treated with 1.0×10^{-7} mol PZN-biotin and the other was treated with vehicle (DMSO). The samples were treated for 30 min at 22 °C before the addition of 100 µL streptavidin-agarose resin suspension (pre-equilibrated with Tris buffer, 50 mM Tris-HCl, 150 mM NaCl, pH 7.5). After mixing for 3 h at 22 °C, samples were applied to Bio-Rad spin columns and the flow through was collected. The resin was washed (5 × 4 mL Tris buffer). The resin was then resuspended in 200 µL 1% SDS in PBS and incubated at 95 ˚C for 10 min. After cooling, the S5 eluent was collected and analyzed by SDS-PAGE for the presence of unique bands in the sample containing PZN-biotin. Unique bands, as visualized by Coomassie and silver stain, were not found compared to the vehicle-treated sample (data not shown). Samples were also analyzed by Western blot using the following procedure: proteins were transferred by electroblot to a polyvinylidene fluoride (PVDF) transfer membrane (EMD Millipore). The membrane was blocked overnight at 4 °C in TBS containing 0.1% (v/v) Tween-20 (TBS/T), treated for 1 h at 4 °C with 1:3,000 dilution of streptavidin-horseradish peroxidase (HRP) in TBS/T, and then washed (2 × 30 s then 5 × 5 min) with TBS/T. After washing once in PBS (1 × 30 s), the membrane was treated

with 1:1 hydrogen peroxide solution:luminol solution (Bio-Rad) for chemiluminescent imaging on HyBlot CL autoradiography film (Denville Scientific) using a Futura 2000K Film Processor.

3.5.22 Photoaffinity purification using PZN-diazirine-alkyne

The procedure used for photoaffinity purification studies was similar to that of affinity purification experiments, except that the samples were incubated with PZN-diazirine-alkyne or vehicle (DMSO) for 4 h at 4 °C, protected from light. The cells were then exposed to UV (4 W, 365 nm) for 15 min at 22 °C to induce crosslinking. The samples were pelleted and resuspended in PBS containing 1 mM CuSO4, 128 μM tris(3-hydroxypropyltriazolylmethyl)amine, 1.2 mM sodium ascorbate, and 50 μM biotin-azide for 1 h at 22 °C. The cells were then harvested by centrifugation (4,000 × g, 2 min, 22 ˚C), the supernatant was decanted, and the cells resuspended in PBS supplemented with 200 U/mL mutanolysin. After digestion proceeded for 1 h at 37 °C, cells were sonicated as previously described. The insoluble fraction was separated by centrifugation and resuspended as previously described. Clarified lysates and insoluble fractions were all enriched with streptavidin-agarose resin as previously described, and eluents were compared by SDSPAGE followed by Western blot and mass spectrometric analysis.

3.5.23 Macromolecular synthesis assay

Radiolabel incorporation into cellular macromolecules was carried out as previously described.[36] Briefly, identical *B. anthracis* Sterne 7702 cultures were grown to an OD600 of 0.6 in LB and diluted to a final OD600 of 0.3. Radiolabelled precursor was to 0.1 μCi, and compound (either PZN or control) was added to 1 ×, or 2 × the minimum inhibitory concentration (MIC). Samples were taken at 1 h post-PZN addition. OD600 at each time point was determined using identically treated cultures lacking radioactive precursor compound. The macromolecules of the cultures treated with radiation were precipitated using trichloroacetic acid on glass filter disks and washed

with 10% and 5% trichloroacetic acid and ethanol successively. The filters were placed in scintillation vials with Ultima Gold scintillation cocktail. Radioactive counts were determined using a liquid scintillation analyzer (PerkinElmer Tri-Carb 2910 TR). The macromolecules, radiolabelled precursors, and their corresponding control antibiotics were as follows: cell wall: [1,6- 3 H (N)] N-acetyl-D-glucosamine (ARC, ART 0142), vancomycin control protein: [U- 14C] L-amino acid mixture (MP, 1014750), chloramphenicol control RNA: [14C(U)] uridine (ARC, ARC 0154), rifampicin control fatty acid: acetic acid [1- 14C] sodium salt (ARC, ARC 0101A), triclosan control.

3.5.24 Genetic deletion of *bas4114-bas4117*

Markerless genetic deletions were created in *B. anthracis* Sterne 7702 as described previously.[4] The 500 base pairs upstream of *bas4114* and 500 base pairs downstream of *bas4117* were Gibson cloned into the homologous recombination vector pBKJ236 (New England Biolabs) using the BamHI and NotI restriction sites. The pBKJ236 constructs were transformed into the *E. coli dam-/dcm-* strain SCS110. Stationary phase cultures of pBKJ236-transformed SCS110 grown in LB with 500 μg/mL erythromycin were used for conjugation along with stationary phase cultures of the conjugation helper strain *E. coli* SS1827 grown in LB with 200 μg/mL ampicillin and *B. anthracis* Sterne 7702 grown in brain-heart infusion (BHI) broth. From the stationary phase cultures, 400 μL were removed and washed by two rounds of centrifugation and resuspension in 500 μL of LB to remove residual antibiotic. The pellets were ultimately resuspended in 200 μL of LB, then mixed thoroughly in equal volumes, and 150 μL of the mixture was inoculated onto a BHI agar plate without spreading. The inoculum was allowed to dry and the plate was incubated at 22 °C for 24 h. The entire culture was then carefully removed from the plate, resuspended in 200 μL of LB, and spotted onto a BHI agar plate containing 5 μg/mL erythromycin and 60 U/mL

polymyxin B (BHIep). The culture was allowed to dry and then subsequently replated and incubated at 22 °C until single colonies of *B. anthracis* Sterne 7702 were visible (~48 h). A single colony was used to inoculate a 2 mL culture of BHI-containing 5 μg/mL erythromycin, and the culture was incubated with shaking at 22 °C overnight. The saturated culture was used to inoculate a fresh culture of BHI containing 5 μg/mL erythromycin at a 1:1000 dilution. This culture was incubated at 37 °C with shaking until saturation (~8 h), then 150 μL of the culture was spotted onto a BHIep plate and allowed to dry. The spot was streaked for single colonies and the plate was incubated at 37 °C overnight. A single colony was picked and used to make competent cells as previously described.[84] Briefly, a colony was used to inoculate a 1 mL culture of LB containing 0.1% glucose (LBG). The culture was incubated at 37 °C without shaking for 10 min, and then used to inoculate 25 mL of LBG in a 250 mL sealable Erlenmeyer flask. The culture was incubated with shaking at 100 rpm at 37 °C until it reached an OD_{600} of 0.20, at which point it was transferred to a 50 mL conical tube and pelleted at 4000 × *g* at 4 °C for 10 min. The spent media was discarded and the pellet was washed with ice cold electroporation buffer (EB; 10% *w/v* sucrose, 15% *v/v* glycerol, 2 mM potassium phosphate, pH 7.8) twice. The cells were resuspended in 400 μL of cold EB, transferred to a 0.4 cm gap electroporation cuvette (USA Scientific), and incubated on ice for 10 min. A plasmid encoding the I-SceI restriction enzyme, pSS4332,[85] was added as 10 μL of a 500 ng/μL stock and the cells were pulsed one time at 2.5 kV, 25 μF, 200 Ω (mean time constant of 4.4 ms). The cells were then placed on ice for 10 min before being diluted with 600 μL LBG. The cells were recovered at 37 °C for 2 h and then plated on LBG agar plates containing 25 μg/mL kanamycin. Colonies were pooled and passaged repeatedly on BHI agar plates containing 25 μg/mL kanamycin until erythromycin sensitive colonies could be isolated. Sensitive colonies with the desired genes deleted were determined by PCR amplification with the cloning primers and

were then repeatedly streaked on antibiotic free BHI agar plates until kanamycin sensitive colonies were isolated. Gene deletion was confirmed by PCR amplification with gene specific primers (Figure 3.13) and the strains were confirmed to be sensitive to both kanamycin and erythromycin by plating on the appropriate antibiotic containing BHI agar plates.

3.6 Figures

Figure 3.1 Chemical structures of PZN (A), Me_2-Arg-Az_5 (B), Biotin-PZN (C), PZN-Biotin (D), PZN-photoaffinity probe (E), PZN-Cy5 (F), daptomycin (Dap)-Cy5 (G), NAO, 10-N-nonyl acridine orange (H), and DilC12(3) perchlorate (I).

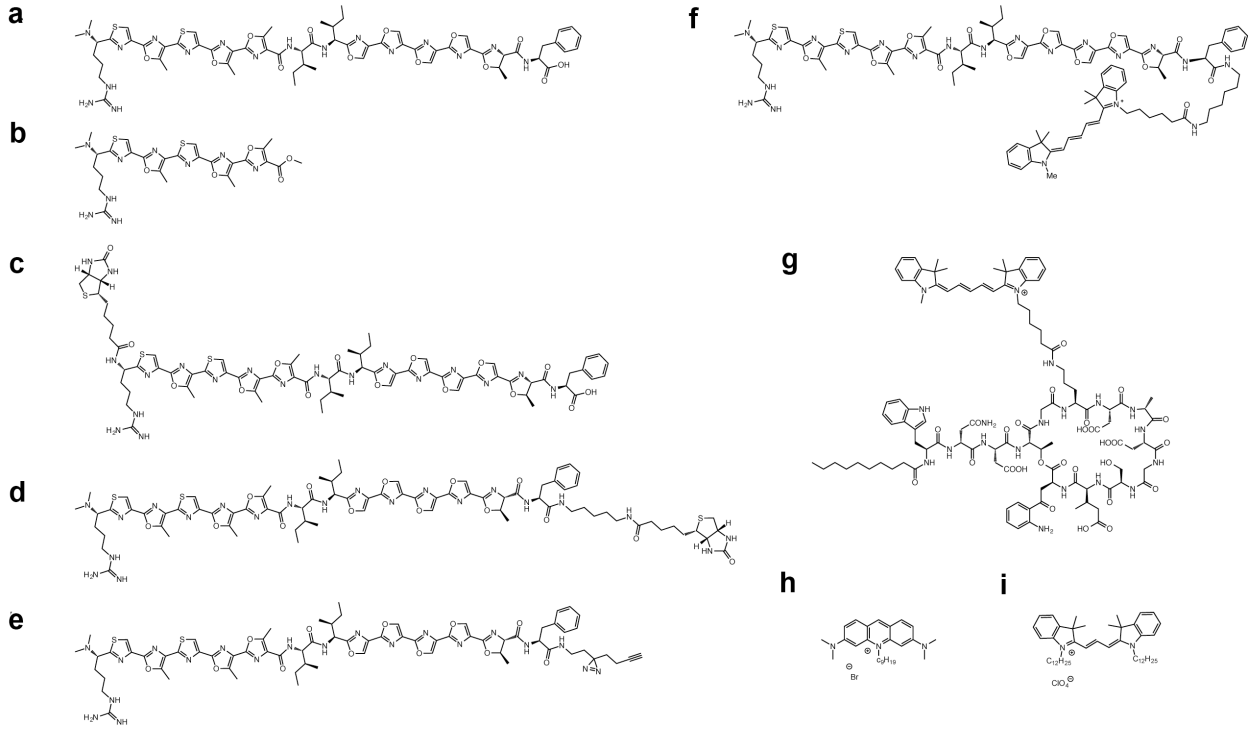

Figure 3.2 Confirmation of plasmid loss in *B. anthracis* 34F2 LLNL A0517-1. (Top) PCR of a conserved chromosomal gene, *bas4114*. (Bottom) pXO1 encoded gene *lef* is not present in A0517-1 or the select *B. cereus* strains.

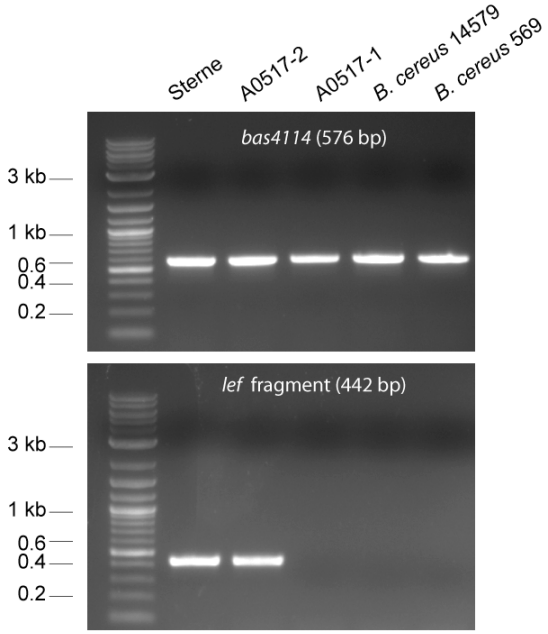

Figure 3.3 Purified PZN is not toxic to *Caenorhabditis elegans* using three different survival assays. (A) The liquid fast killing assay monitors survival for 24 h in minimal broth medium. Solid agar slow killing assays analyzes survival for 72 h without (B) and with *E. coli* (C). Animals were treated with 64 µg/mL PZN and analyzed by live/dead screening over the course of the experiments. P-values were generated using the Log-rank (Mantel-Cox) test. NC, no compound.

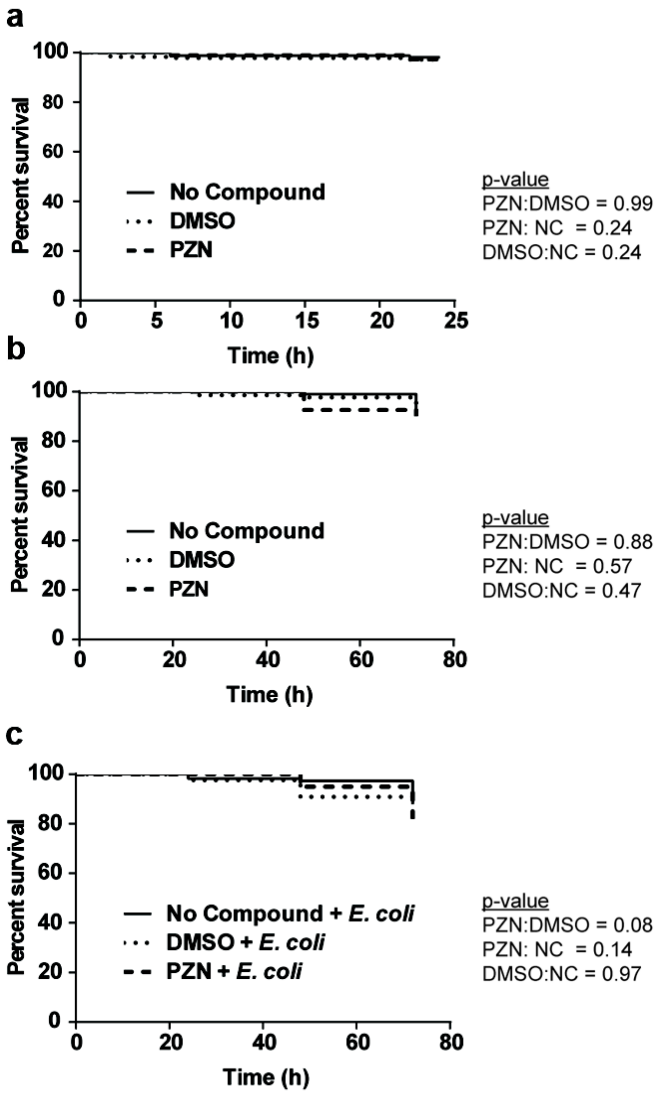

Figure 3.4 Mass spectrometry-based structural characterization of PZN derivatives used in affinity purification. (A) Structure, exact mass, and MS/MS fragmentation determined from the collision-induced dissociation (CID) spectrum (B) of the singly charged *N*-biotinylated PZN ion acquired by LTQ-FT-MS/MS. (C) Structure, exact mass, and MS/MS fragmentation determined from the CID spectrum (D) of the singly charged *C*-terminally biotinylated PZN ion. (E) Structure, exact mass, and MS/MS fragmentation determined from the CID spectrum (F) of the singly charged and MS-induced N_2-cleaved PZN-diazirine-alkyne ion.

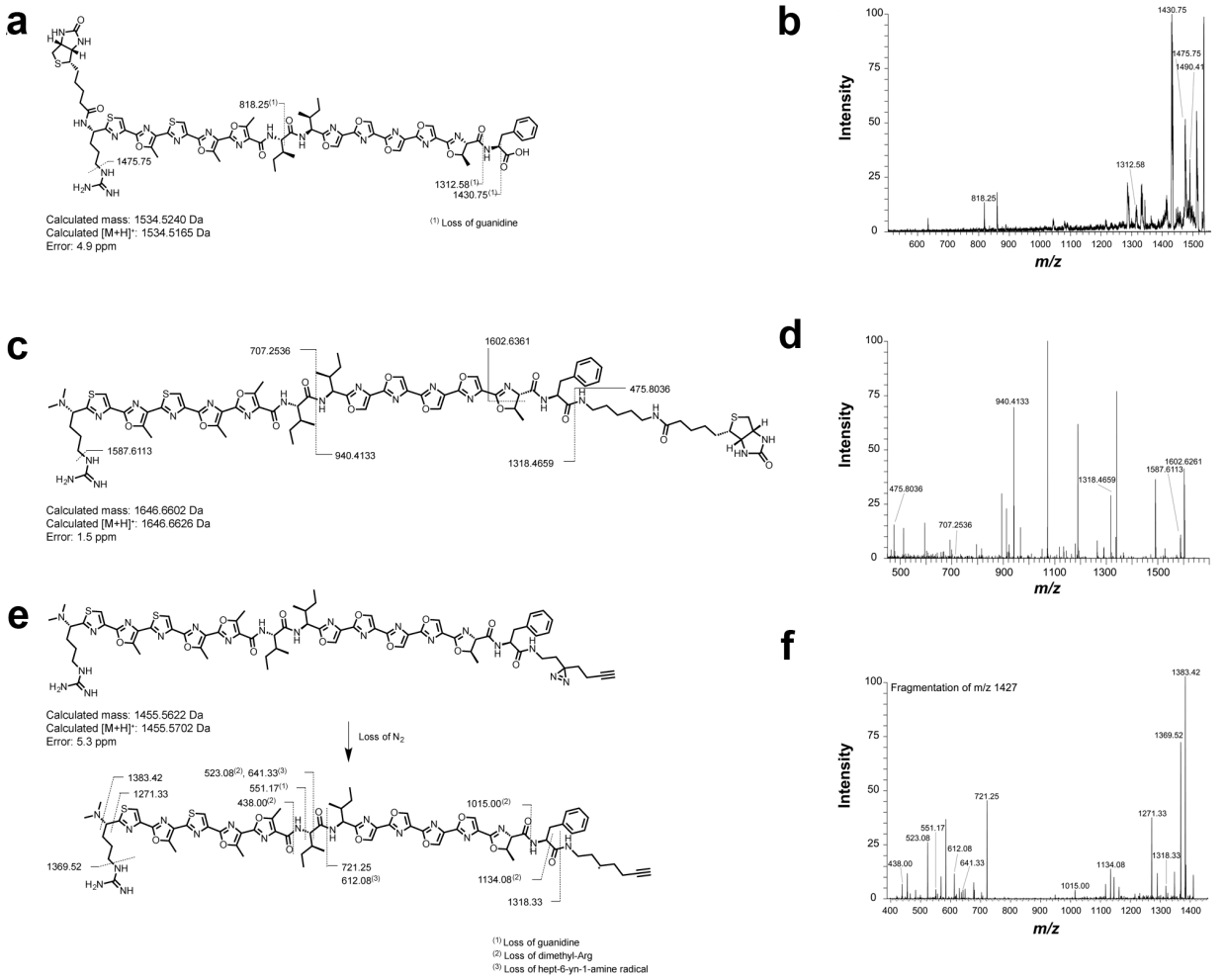

Figure 3.5 PZN treatment results in the inhibition of three out of four analyzed macromolecular pathways. *B. anthracis* cells were treated with 1 × or 2 × MIC PZN and the appropriate radiolabelled precursor to the macromolecule of interest. After incubation for 1 h, macromolecules were precipitated and the extent of radiolabel incorporated was measured for protein (A), fatty acid (B), RNA (C), or peptidoglycan (D) was measured. Each experiment included samples treated with a control compound that is known to affect a particular pathway (protein: Chl, chloramphenicol; fatty acid: Tri, triclosan; RNA: Rif, rifampicin; peptidoglycan: Dap, daptomycin, Van, vancomycin) All compounds were added at 1 × or 2 × MIC, except rifampicin, which required significantly lower concentrations to observe incorporation at 1 h. Percent incorporation was determined by comparing radioactive incorporation between cells containing compound vs. vehicle. Error is reported as standard deviation with $n \geq 3$. * indicates $p < 0.05$ while ** indicates $p < 0.01$ compared to vehicle control.

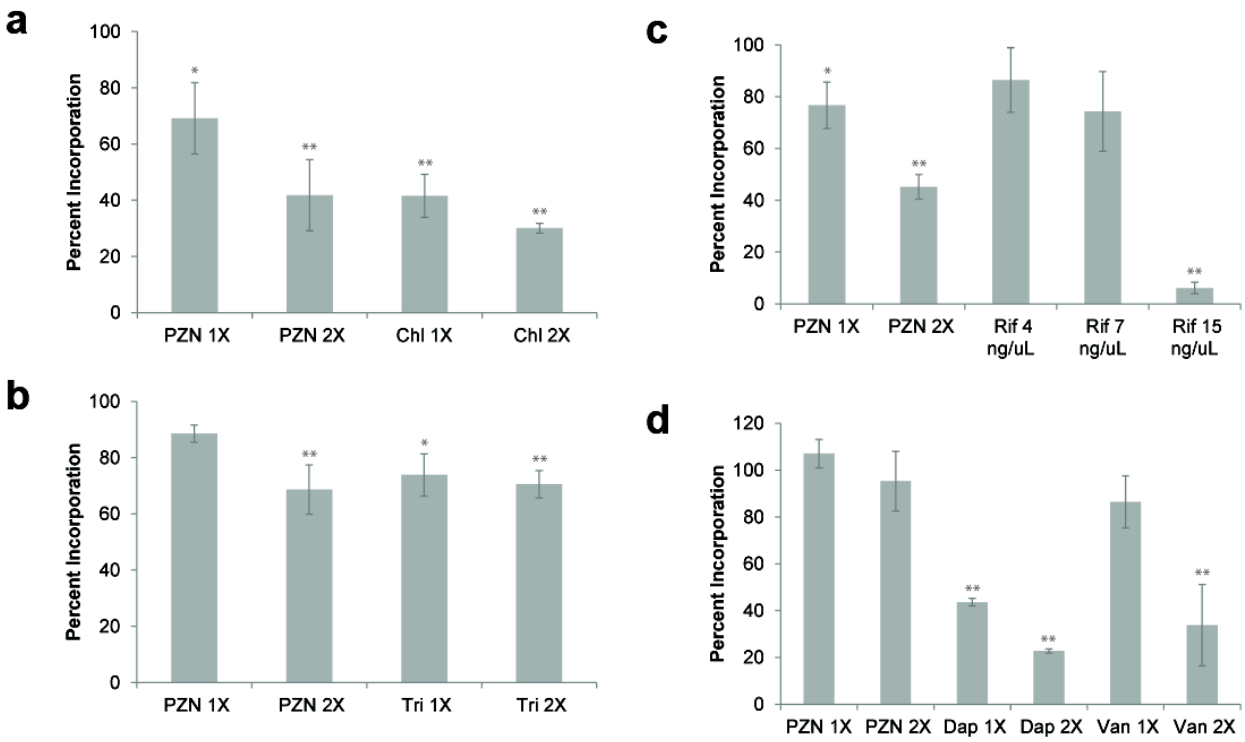

Figure 3.6 *B. anthracis* gene expression profile when treated with PZN. A volcano plot represents the set of differentially regulated genes in response to a 10 min treatment of PZN at 0.25 × MIC. Red (up-regulated) and green (down-regulated) points are genes with significantly altered expression in response to PZN treatment, whereas black genes did not meet the *q* value (<0.01) threshold. Genes with *q* value = 0 were given an arbitrary value of 1×10^{-105} for graphing purposes. Abbreviations: #, hypothetical; *, transporter, ^, transcriptional regulator; *bdbD*, *B. subtilis* hypothetical homologue, *lldP-1*, L-lactate permease; *ldh2/3*, L-lactate dehydrogenase; *cydA-2*, cytochrome *d* ubiquinol oxidase; *mmgD*, citrate synthase 3; *hutHIU*, histidine utilization genes; *gerN*, germination genes; *gerN*, germination protein; *kamA*, L-lysine 2,3-aminomutase; §, remaining up-regulated genes. All differentially expressed genes are further described in Table 3.5.

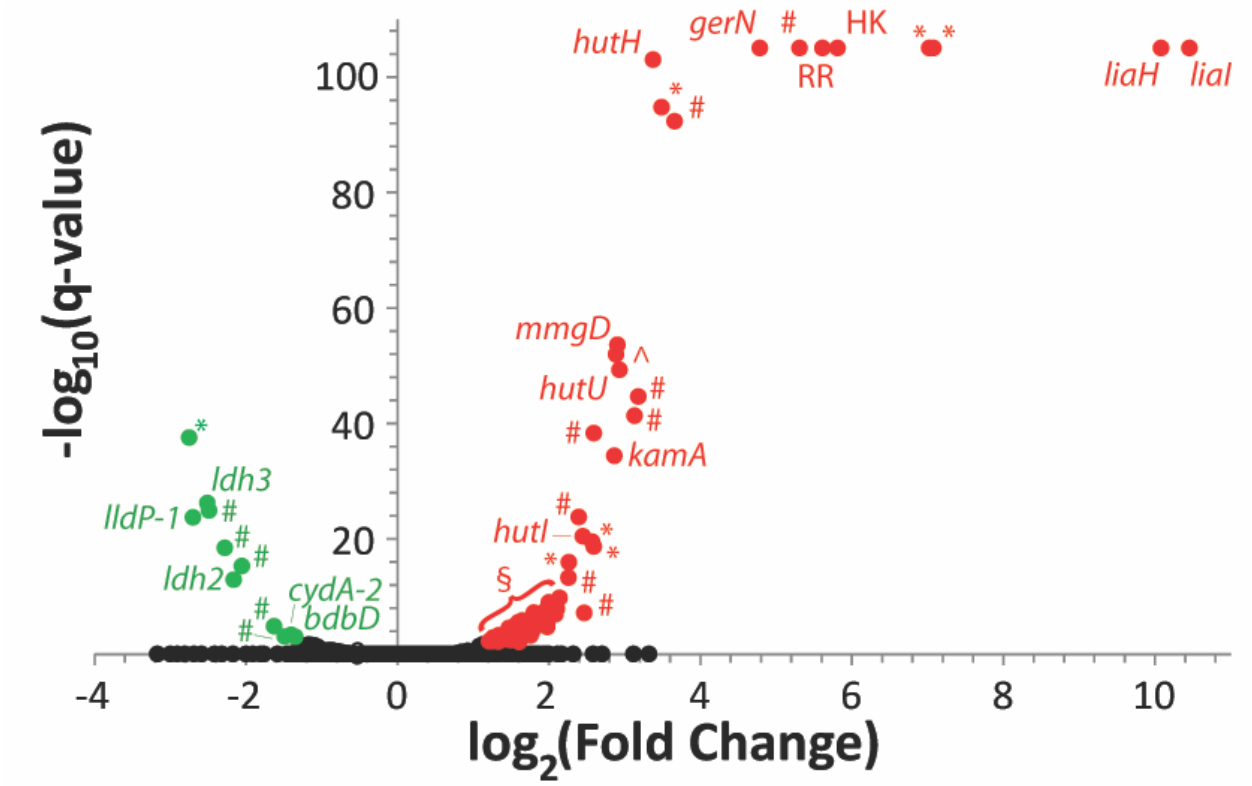

Figure 3.7 The *B. anthracis* gene expression profile with Me_2-Arg-Az_5 differs from PZN treatment. (A) A volcano plot represents the set of differentially regulated genes (red, upregulated; green, downregulated) in response to treatment with 0.25 × MIC of Me_2-Arg-Az_5. Black points indicate genes that did not meet the q-value (< 0.01) threshold. Genes where the q-value = 0 were given an arbitrary value of E-155 for graphing purposes. Abbreviations: # hypothetical; * transporter; ^ transcriptional regulator; atpI, ATP synthase protein I; hmp, nitric oxide dioxygenase; lldP-1, L-lactate permease; ldh2/3, L-lactate dehydrogenase; sugE-1, EmrE protein (cationic drug membrane transporter); RR, response regulator; HK, histidine kinase; § remaining upregulated. All genes are summarized in Table 3.11. (B) Venn diagram demonstrating the commonality of the PZN and Me_2-Arg-Az_5 expression profiles. The compilation of common genes is located in Table 3.10.

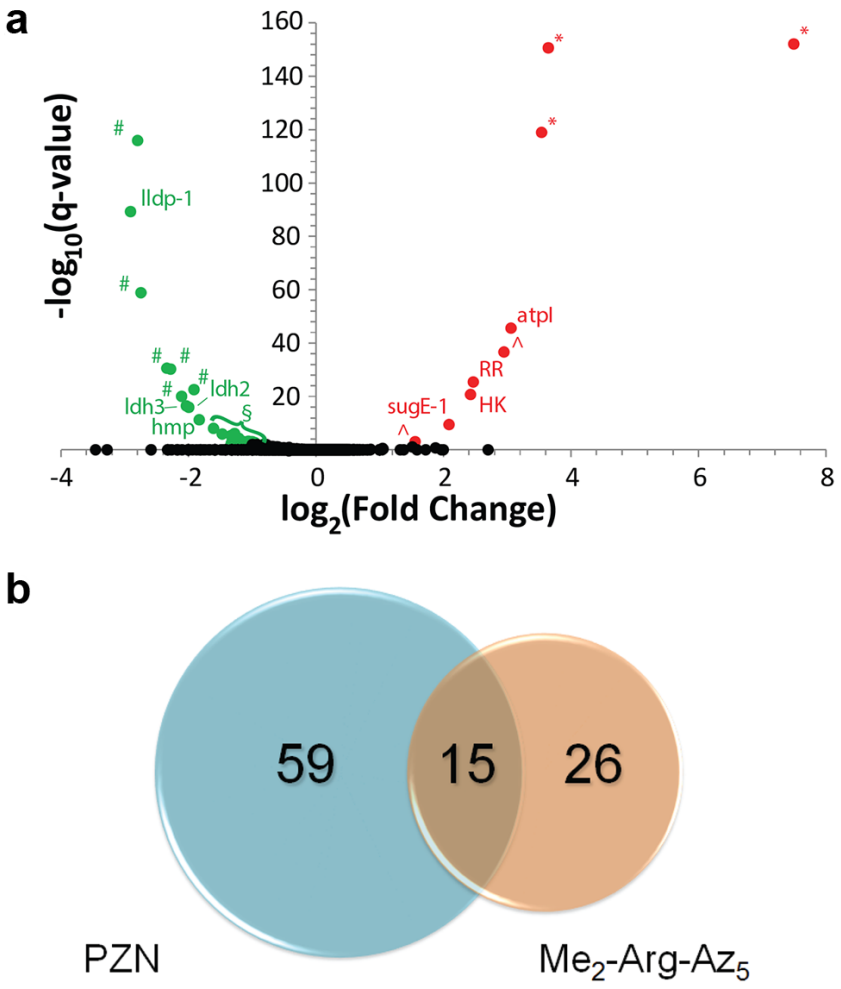

Figure 3.8 Growth curves of PZN and Me_2-Arg-Az_5 reveal different phenotypes. (A) *B. anthracis* cells treated with PZN undergo rapid decrease in optical density with concentrations above the minimum inhibitory concentration (MIC, determined from microbroth dilution assays). Time points were collected every two minutes and adjusted to a 1-cm path length. Error is reported as standard deviation with n = 3. (B) *B. anthracis* treated with Me_2-Arg-Az_5. Reduction in optical density is observed briefly at 4 × MIC. Both growth curves were measured in duplicate and normalized to OD_{600} 0.35 (A) and 1.0 (B) at t = 0.

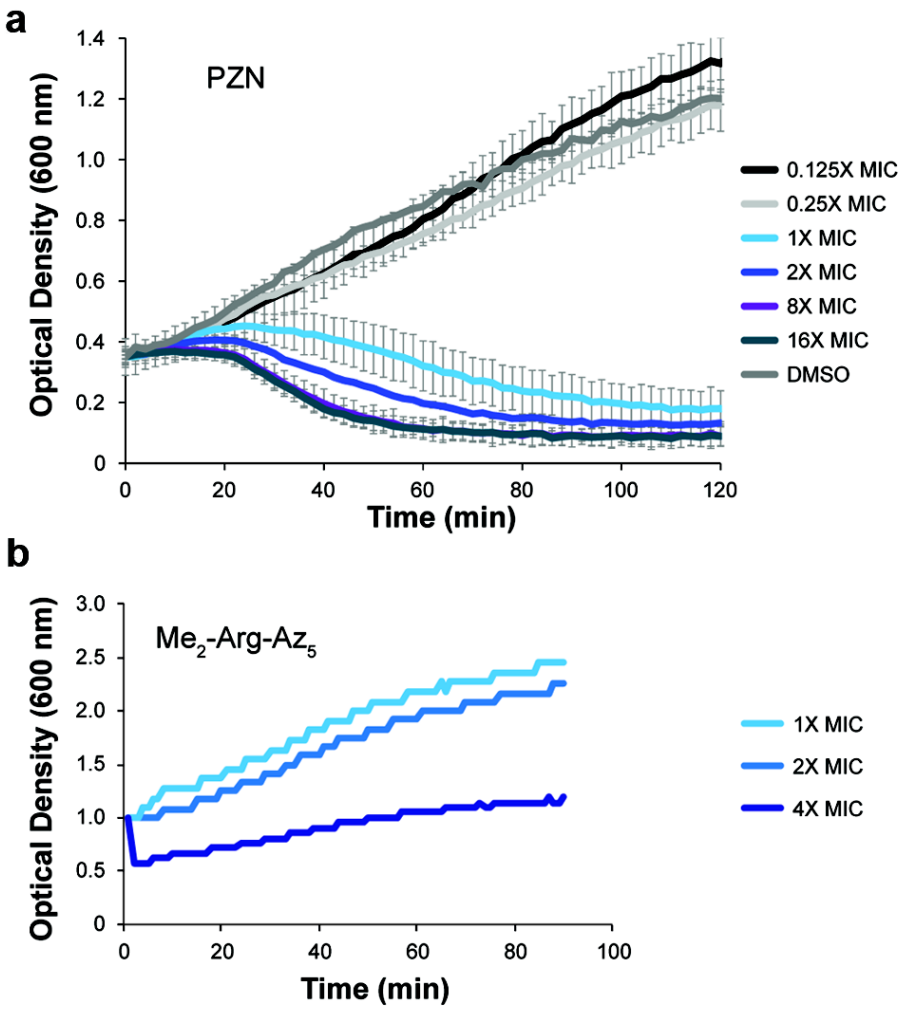

Figure 3.9 PZN depolarizes the *B. anthracis* membrane and acts synergistically with cell envelope-acting antibiotics. (A) Detection of membrane potential in *B. anthracis*. Red/green ratios were calculated using mean fluorescence intensities of cells treated for 30 min at room temperature with 0.1 μM $DiOC_2(3)$ and the vehicle of DMSO (negative control), 0.1 μM $DiOC_2(3)$ and 5.0 μM CCCP (positive control), 0.1 μM $DiOC_2(3)$ and 0.5 μM PZN, and 0.1 μM $DiOC_2(3)$ and 1.0 μM PZN. Data were normalized to the positive control sample of $DiOC_2(3)$ and vehicle (DMSO). Error is given as standard deviation with n = 3. P values are given relative to the DMSO control with ∗ indicating <0.0005 and ** indicating <0.0001. Abbreviations: Dap, daptomycin; $DiOC_2(3)$, 3,3'-diethyloxacarbocyanine iodide; CCCP, carbonyl cyanide *m*-chlorophenyl hydrazine. (B) Isobolograms of the minimum inhibitory concentrations (μg/mL) of PZN with nisin (top) and daptomycin (bottom). Interactions taking place below the dotted line with a fractional inhibitory concentration index below 0.5 represent synergistic behavior.

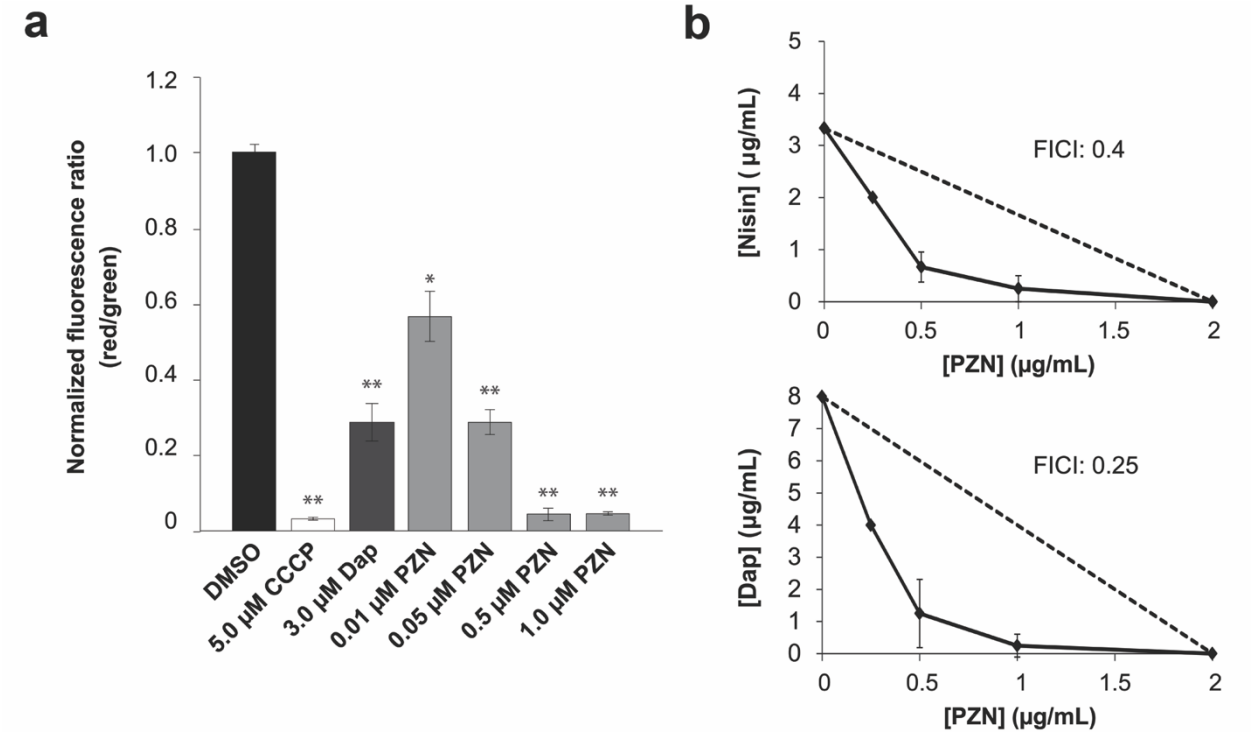

Figure 3.10 Mass spectrometry characterization of PZN-Cy5. (A) Mass spectrum of the $[M+H]^{2+}$ species by LTQ-FT-MS, which was used to calculate exact mass. (B) CID spectrum of the singly charged ion acquired by LTQ-FT-MS. Labeled peaks correspond to identified fragments of PZN-Cy5, shown on the structure in panel (C).

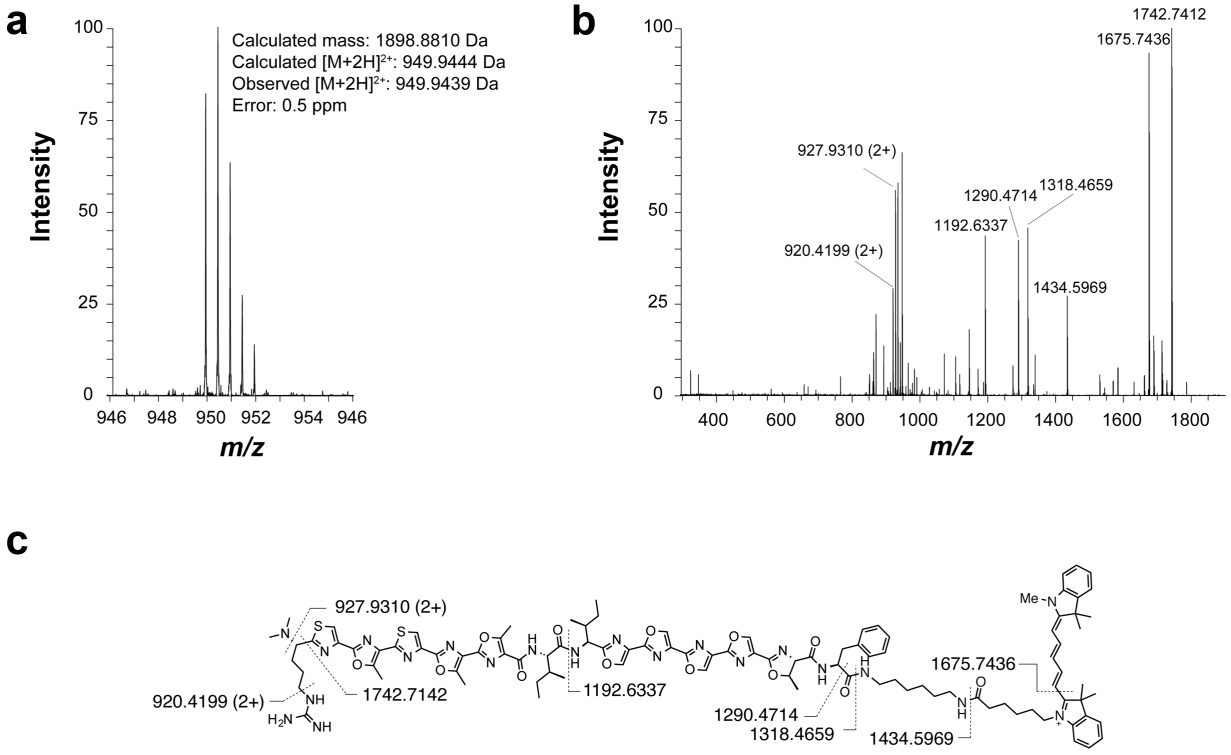

Figure 3.11 PZN-Cy5 localizes to distinct foci on *B. anthracis*. (A) Representative fluorescence microscopy images are shown for the Cy5, DIC, and merged channels of *B. anthracis* Sterne treated with 0.1 μM PZN-Cy5 (0.05 × MIC) for 30 min. Competition experiments in a PZN-resistant *B. anthracis* strain (PR06, *vide infra*) show (B) robust labeling with 0.05 μM PZN-Cy5 in the absence of unlabeled PZN and (C) significantly decreased labeling when cells are pretreated with 1 μM PZN (0.016 × MIC, resistant strain PR06) for 20 min. Scale bars = 2 μm.

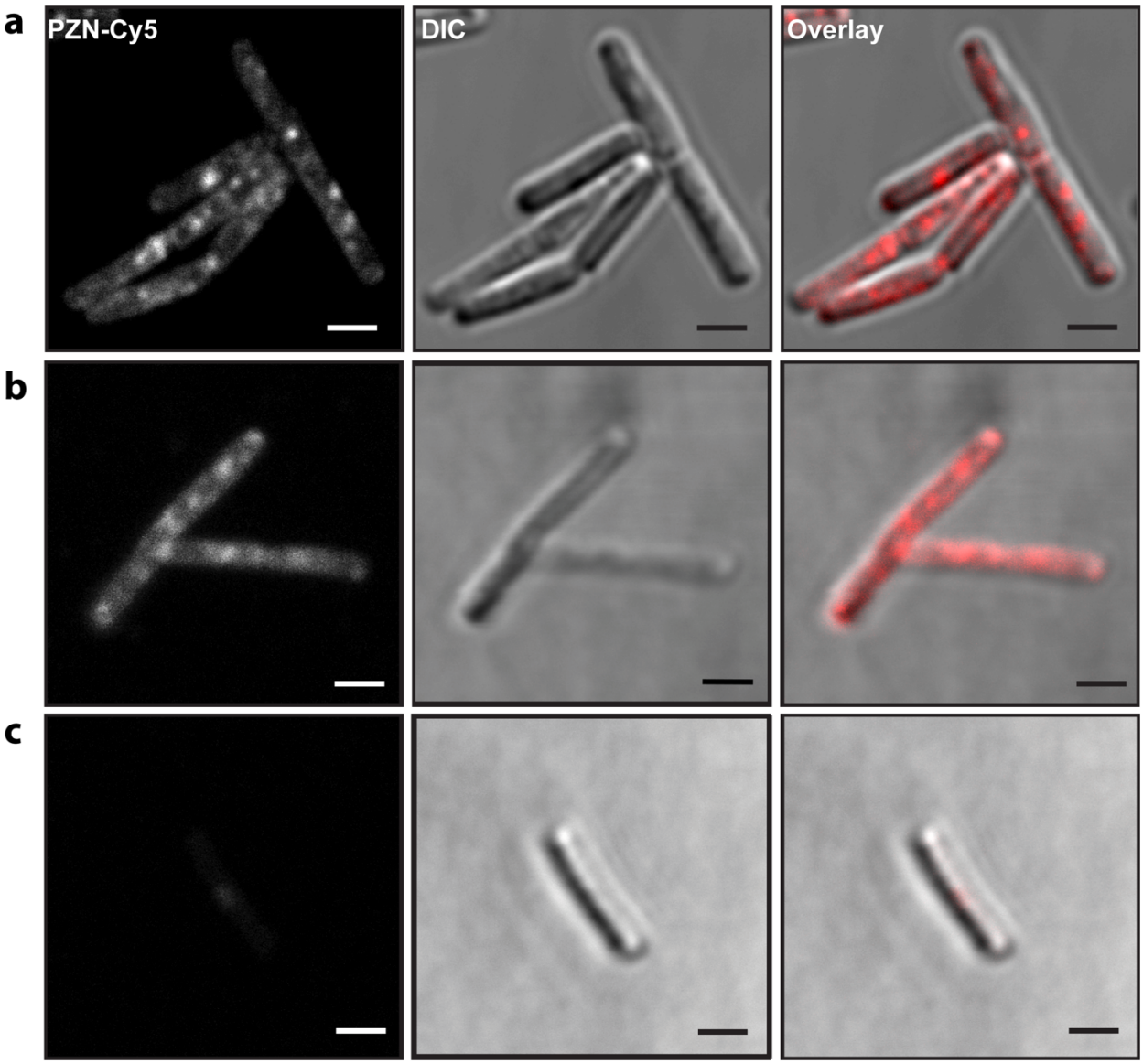

Figure 3.12 STORM images of PZN-Cy5-labeled *B. anthracis*. (A) 3-D super-resolution images of 12 representative *B. anthracis* cells treated with PZNCy5. (B) Two representative cells rotated about the z-axis show distinct, nonseptal localization of PZN-Cy5. Green, blue, and yellow circles mark three individual foci in each rotated view. Scale bars = 1 μm.

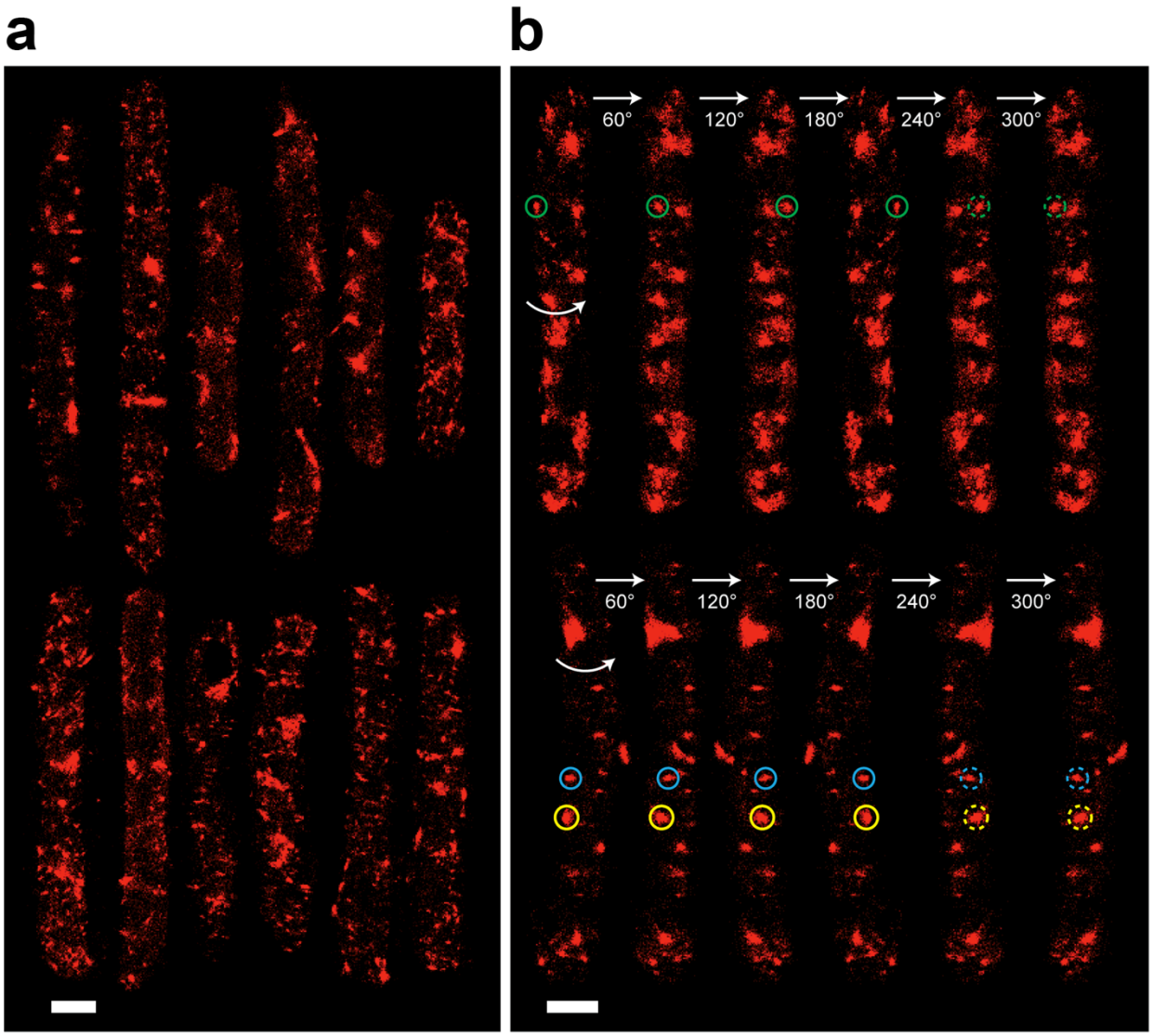

Figure 3.13 Density-based clustering analysis of *B. anthracis* treated with PZN-Cy5 and imaged by super-resolution microscopy. (A) Representation of cell alignment used in subsequent analyses. (B) PZN-Cy5 color density map of a representative cell projected onto the XZ plane. (C) Probability density of PZN-Cy5 increases as distance from the center of the cell (R) increases, reaching a maximum at the cell membrane. (D) Cluster analysis of two representative *B. anthracis* cells (top) shows identified clusters (bottom) used in subsequent size calculations.

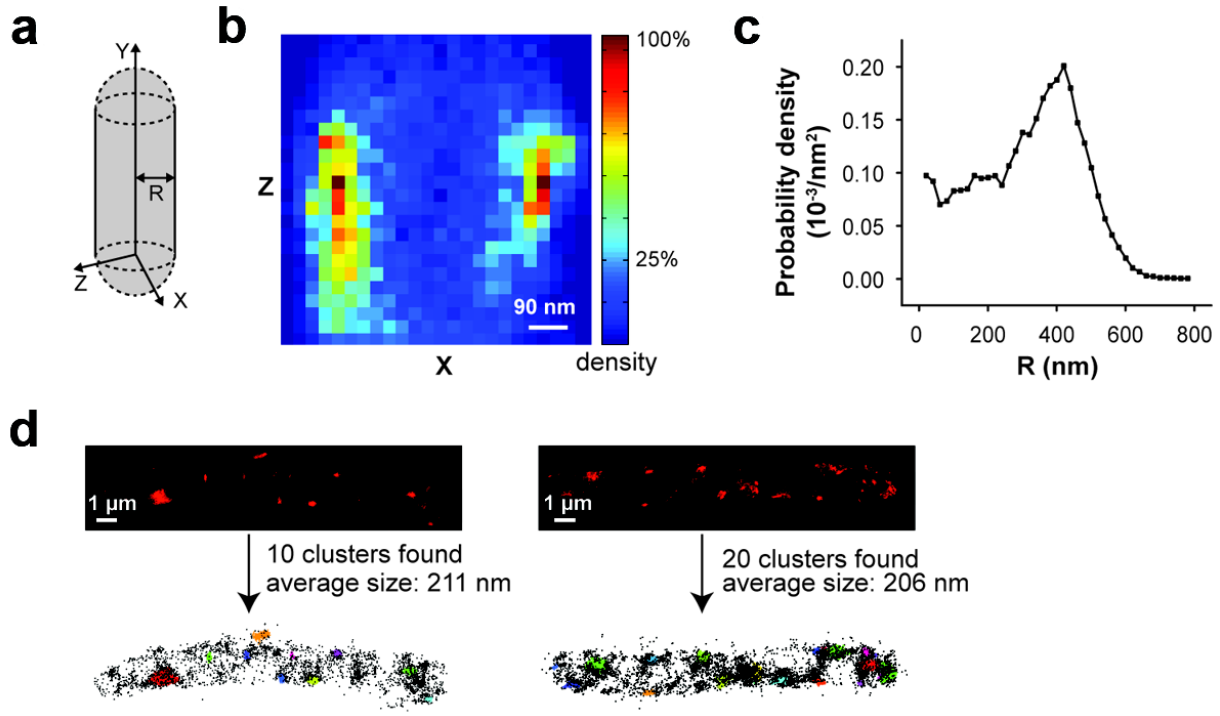

Figure 3.14 Fluorescence microscopy images of *B. subtilis*, *B. cereus* E33L, *B. cereus* 4342 and *B. cereus* G9241 strains treated with PZN-Cy5 under conditions used for observation of PZN-Cy5 labeling of wild type *B. anthracis* Sterne 7702. Modest labeling is observed with G9241, which is PZN-susceptible.

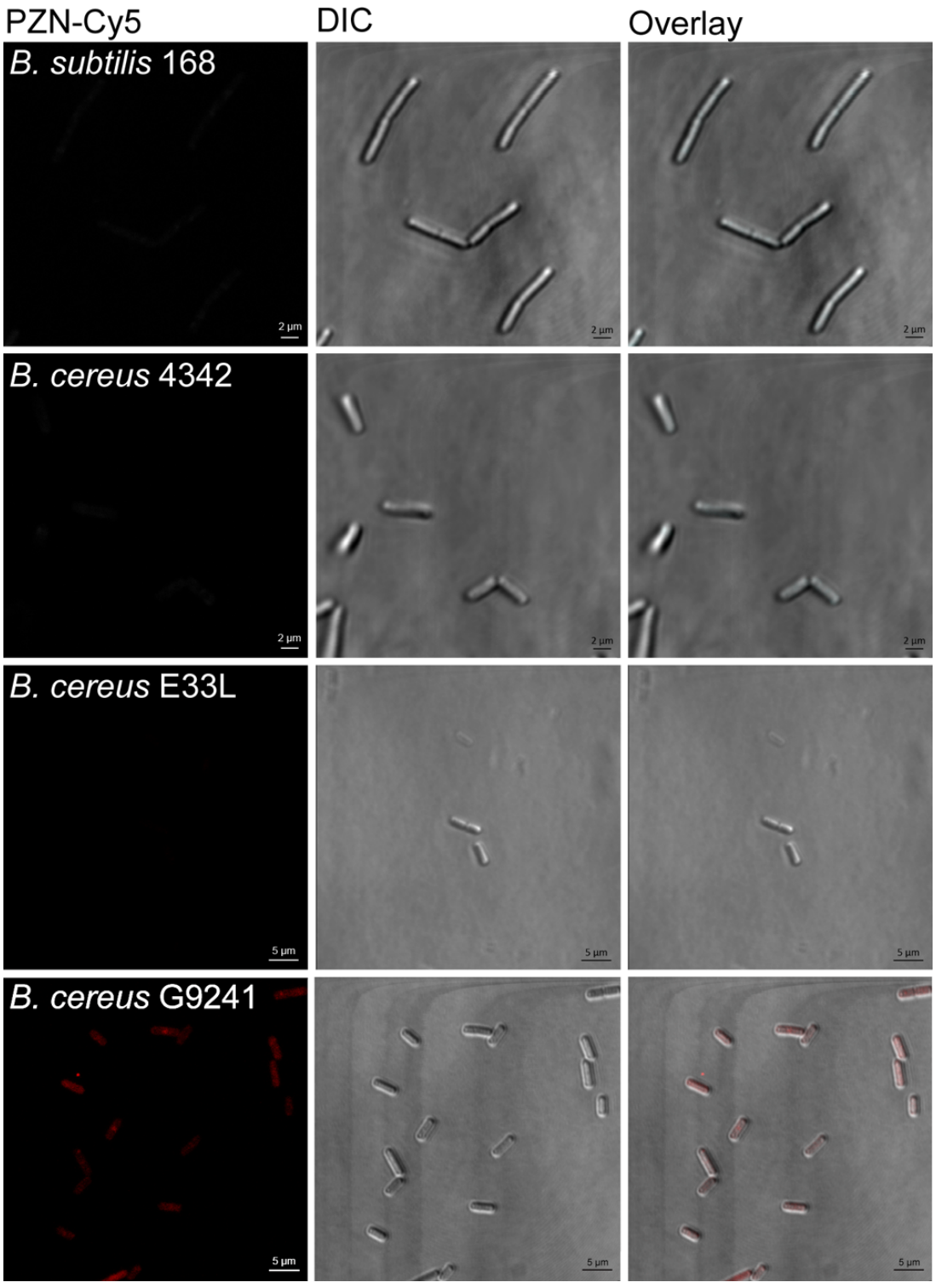

Figure 3.15 Hydropathy plot of BAS4114 reveals a single transmembrane helix. (A) The amino acid sequence of BAS4114 was analyzed using SPOCTOPUS, which predicted a transmembrane domain from residues 151-171. (B) Primary sequence of BAS4114, color-coded as in panel A.

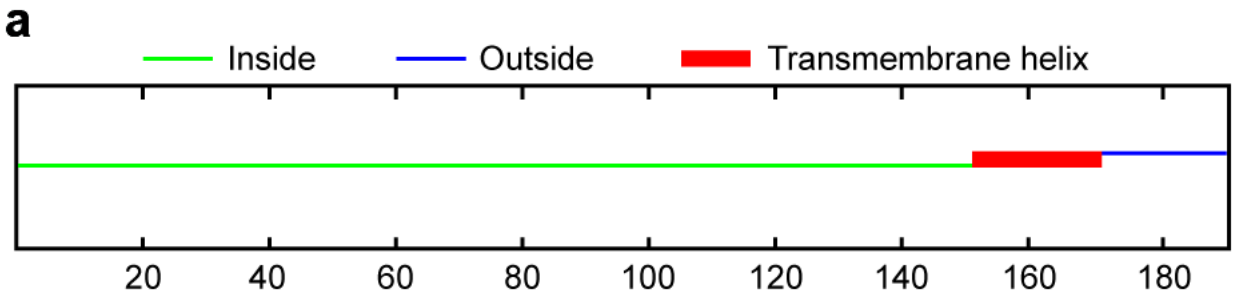

b

```
        10         20         30         40         50         60
MTANRIKAVA LSHFARYGYE GTSLANIAQE VGIKKPSIYA HFKGKEELYF ICLESALQKD

        70         80         90        100        110        120
LQSFTDDIEN FSNSSTEELL LQLLKGYAKR FGESEESMFW LRTSYFPPDA FREQIIEKAN

       130        140        150        160        170        180
AHIENVGKLL FPIFKQANEK SELHNIEVKD ALEAFLCLLD GLMVELLFAG LNRFETRLNA

       190
SWQVFWRGLS N
```

Figure 3.16 Confirmation of *bas4114-4117* deletion in *B. anthracis* Sterne. Gene specific primers were used to confirm their absence in *B. anthracis* Sterne 7702 Δ*bas4114-4117*. WT: *B. anthracis* Sterne 7702. KO: *B. anthracis* Sterne 7702 Δ*bas4114-4117*.

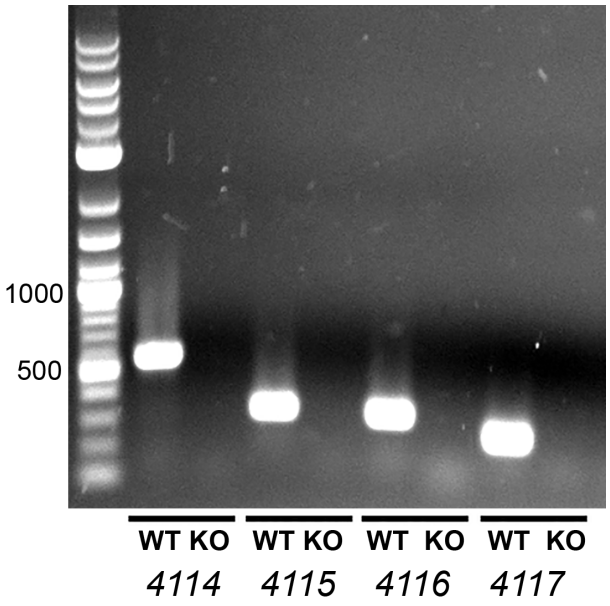

Figure 3.17 Mass spectrometry characterization of daptomycin-Cy5. (A) Mass spectrum of the $[M+2H]^{2+}$ species by LTQ-FT-MS, which was used to calculate exact mass. (B) CID spectrum of the doubly charged ion acquired by LTQ-FT-MS. Labeled peaks correspond to identified fragments of daptomycin-Cy5, which are structurally overlaid (C).

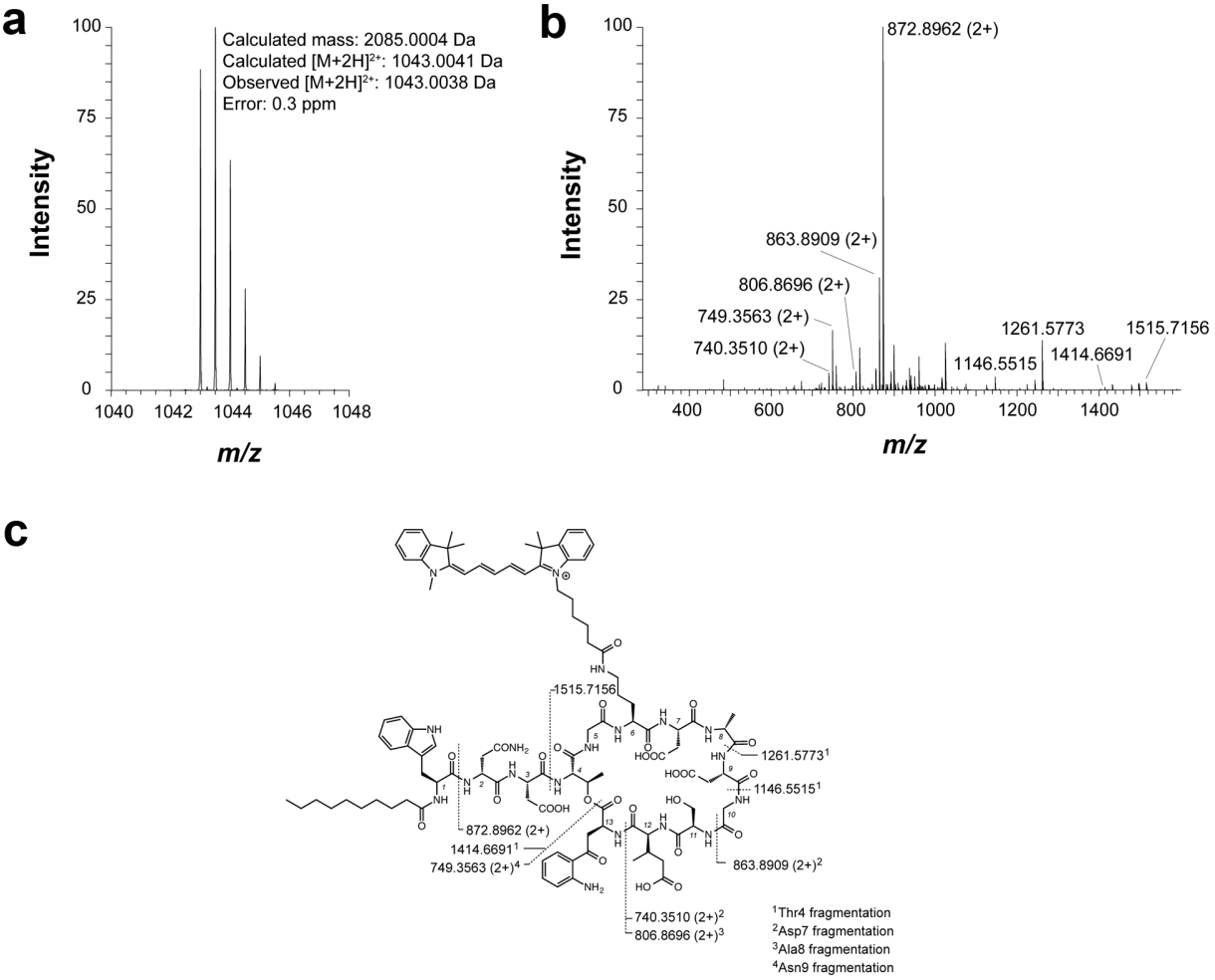

Figure 3.18 Cardiolipin increases PZN-Cy5 interaction with bacterial cells. (A) Mean fluorescence intensities of *B. anthracis* cell populations treated with daptomycin-Cy5 or PZN-Cy5 in the presence or absence of exogenous cardiolipin (CL) were determined by flow cytometry and normalized to cells treated with only the Cy5-labeled compound and vehicle. Error is reported as standard deviation with n = 3. The PZNCy5 P values are given relative to the 0 μg/mL control with ∗ indicating 0.01. (B) Isobologram of the minimum inhibitory concentrations (μg/mL) of PZN and CL. The Y-intercept was arbitrarily assigned for CL, which in the absence of PZN was not toxic to *B. anthracis* at concentrations up to 200 μg/mL. Interactions taking place below the dotted line with a fractional inhibitory concentration index (FICI) < 0.5 represent synergistic behavior.

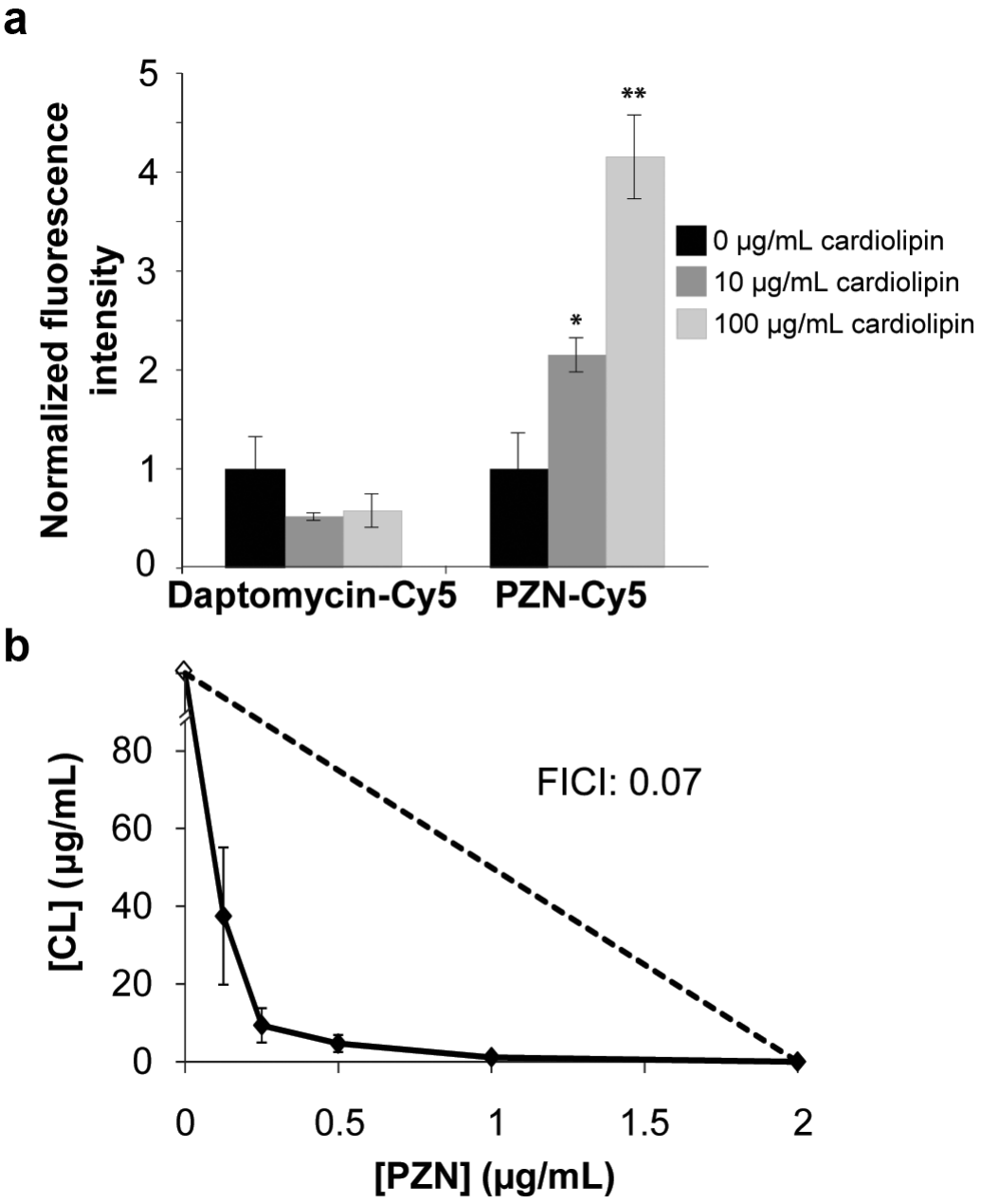

Figure 3.19 Fluorescence microscopy images of nonyl acridine orange (NAO, top) and 1,1'-Didodecyl-3,3,3',3'-tetramethylindocarbocyanine perchlorate (DilC12(3), bottom) localization in *B. anthracis*, *B. cereus*, and *B. subtilis* strains, showing approximate cellular distributions of cardiolipin[64] and regions of increased fluidity[65], respectively. Scale bars, 5 μm.

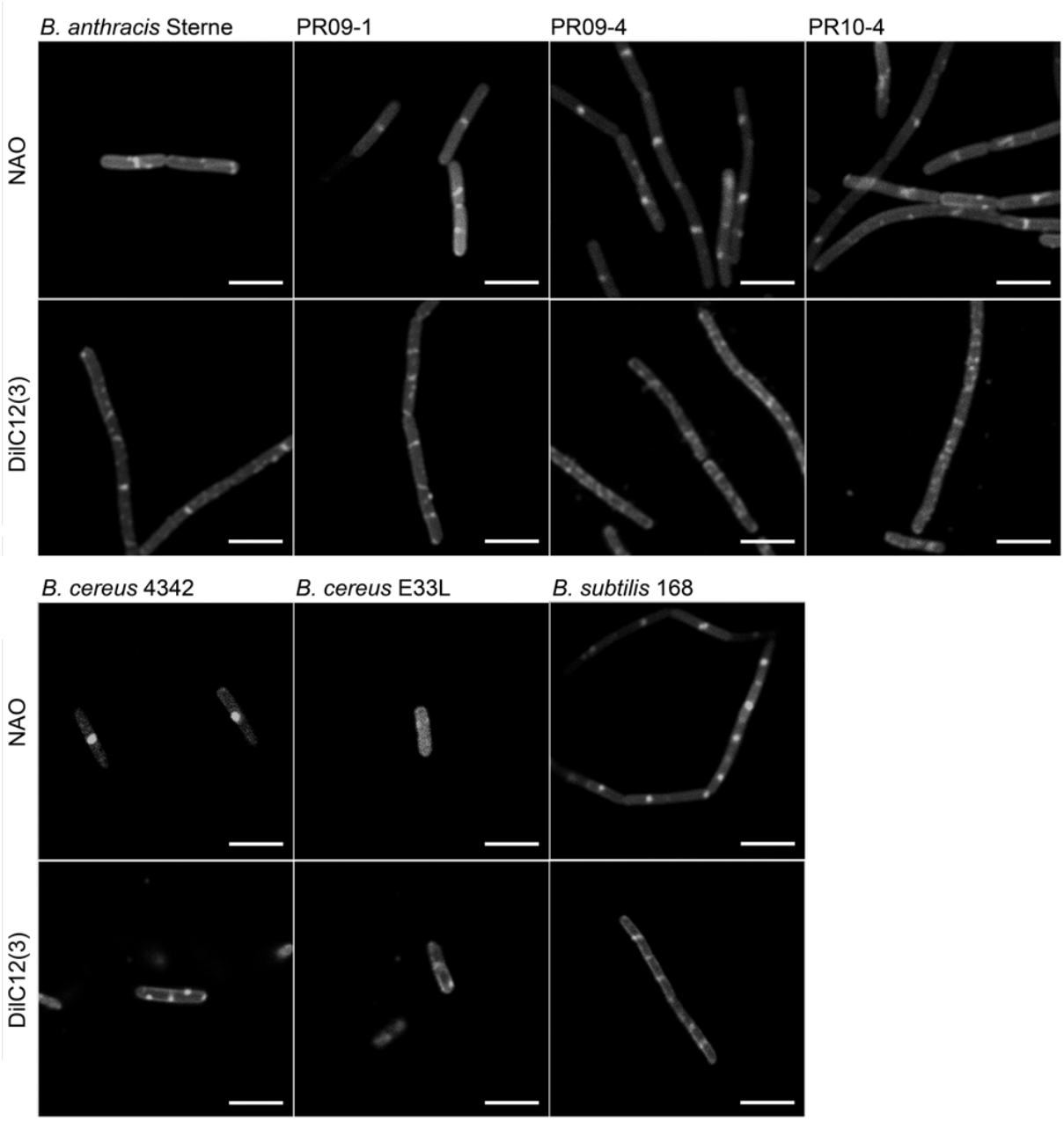

Figure 3.20 PZN co-localizes with CL- and RIF-specific dyes. (A) From left to right, the channels for NAO, Cy5, DIC, and a merged image are shown to illustrate the false-color co-localization (magenta) of NAO (blue) and PZN (red). (B) The same as panel a but with DilC12(3) replacing NAO. Scale bars = 2 µm.

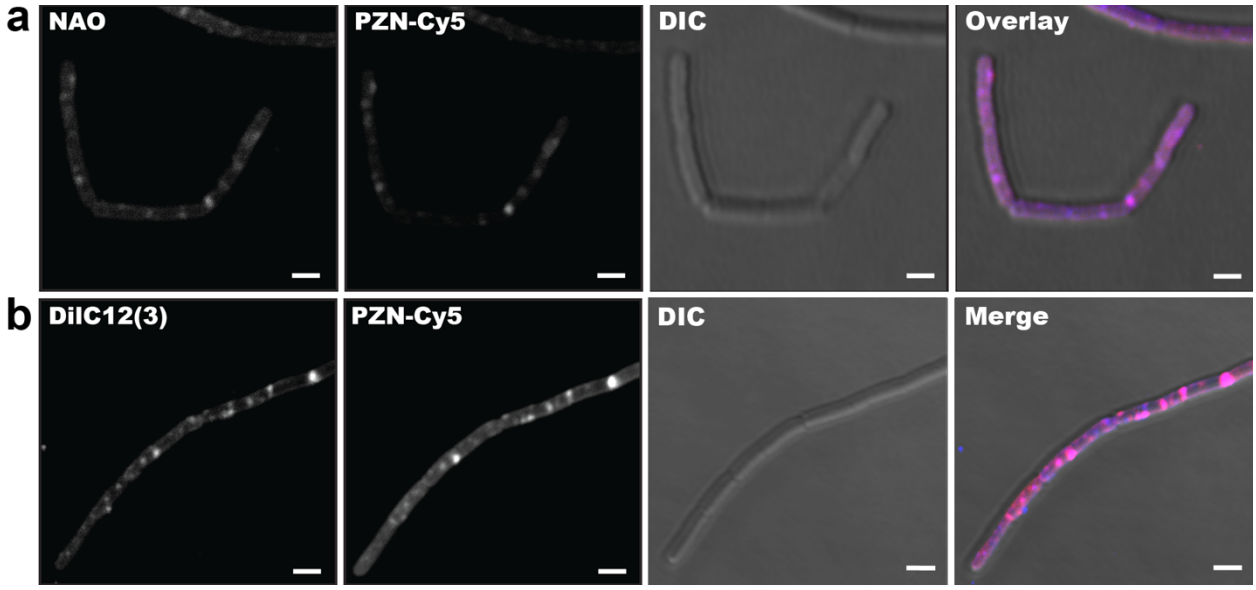

Figure 3.21 Fluorescence microscopy, DIC, and overlay images of *B. anthracis* Sterne 7702 cells grown in a higher osmolarity medium (0.52 M NaCl) and treated with PZN-Cy5 (top) or NAO (bottom). Scale bars, 5 µm.

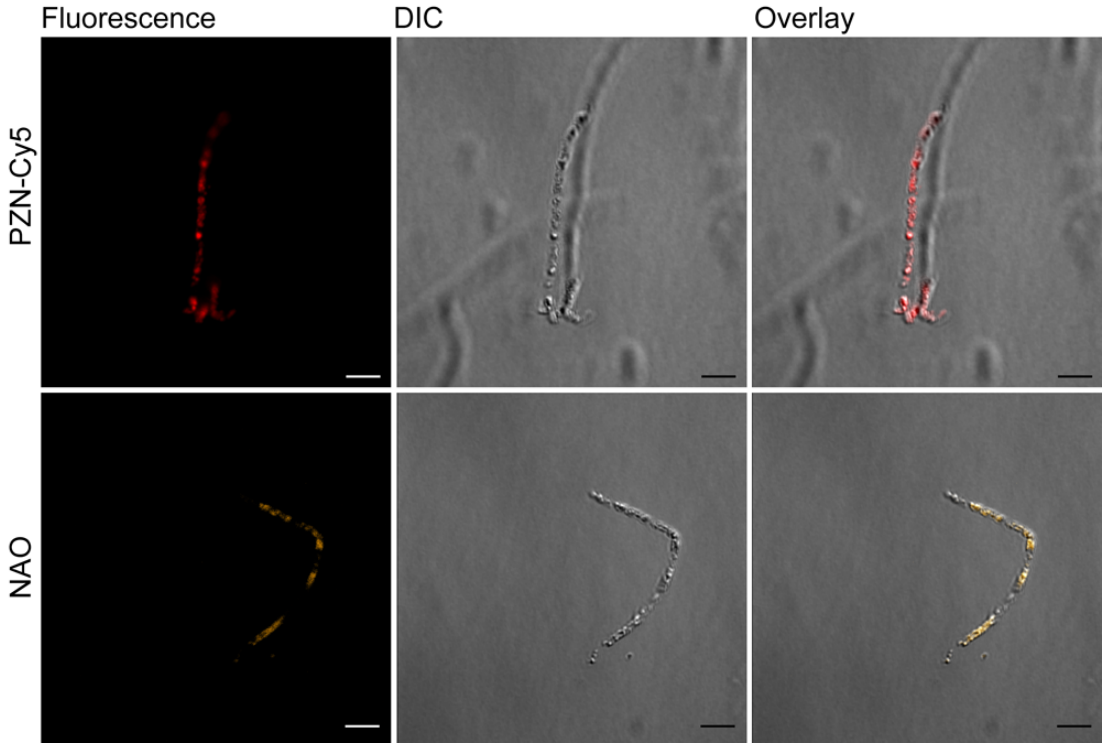

3.7 Tables

Table 3.1 The antimicrobial spectrum of plantazolicin (PZN).

Strain	MIC (μg/mL)	MIC (μM)	Source
***B. cereus* group**			
B. anthracis Sterne 34F2	1	0.75	S. Blanke (UIUC[b])
B. anthracis Sterne 7702	1	0.75	USDA[b]
B. anthracis Sterne 7702 *Δbas4114-4117*	1	0.75	This study
B. anthracis Sterne 7SBON30	1	0.75	[30]
B. anthracis Sterne 7SBON40	1	0.75	[30]
B. anthracis Sterne 7SDG30	1	0.75	[30]
B. anthracis Sterne 7SBTR30	1	0.75	[30]
B. anthracis Sterne 7SBONTO	1	0.75	[30]
B. anthracis Sterne 7SBTRTO	1	0.75	[30]
B. anthracis Sterne 7SBTO30	1	0.75	[30]
B. anthracis BSL3 strains	2 – 16	1.5 – 12	USAMRIID
B. anthracis CDC 684	2	1.5	USAMRIID
B. anthracis Sterne 34F2 A0517-1	1	0.75	BEI
B. anthracis Sterne 34F2 A0517-2	2	1.5	BEI
B. anthracis Sterne 34F2 Δ*blsO*	1	0.75	[86]
B. anthracis Sterne 34F2 Δ*csaB*	1	0.75	[20]
B. anthracis Sterne 34F2 Δ*sap*	1	0.75	[52]
B. anthracis Sterne 34F2 Δ*eag*	1	0.75	[52]
B. anthracis Sterne 34F2 Δanthrose	1	0.75	C. Turnbough (U. Alabama Birmingham)
B. anthracis Sterne 34F2 Δ*bclA*	1	0.75	[87]
B. anthracis Sterne BA850 (Δpetrobactin)	1	0.75	[88]
B. anthracis Sterne BA781	1	0.75	BEI
B. anthracis Weybridge	1	0.75	BEI
B. cereus 14579	>64	>48	USDA
B. cereus 541 (Δ*plcR*)	>64	>48	[89]
B. cereus ATCC 7064	>64	>48	ATCC[b]
B. cereus ATCC 13472	>64	>48	BGSC
B. *cereus* BAG4x2-1	>64	>48	BEI
B. *cereus* E33L	>64	>48	BEI
B. cereus G9241	8	6	BEI
B. cereus GP7	>64	>48	BGSC[b]

Table 3.1 (cont.)

B. cereus Rock3-44	64	48	NMRS[b]
B. *cereus* VD014	>64	>48	BEI
B. *cereus* VD115	>64	>48	BEI
B. mycoides 96/3308	>64	>48	BGSC
B. samanii C1	>64	>48	BEI
B. thuringiensis Konkukian 97-27	>64	>48	BEI
B. thuringiensis israelensis ATCC 35646	>64	>48	BEI
B. thuringiensis subsp. *thuringiensis*	>64	>48	BGSC
Atypical gamma phage sensitivity			
B. cereus ATCC 4342	>64	>48	BEI
B. cereus CDC 32805	>64	>48	[27]
B. cereus 2002013145	>64	>48	CDC[b]
B. cereus 2002013146	>64	>48	CDC
B. cereus 2002013100	>64	>48	CDC
B. cereus 2000031002	>64	>48	CDC
Non *B. cereus* group			
B. amyloliquefaciens FZB42	>64	>48	BGSC
B. amyloliquefaciens B-14393T	>64	>48	BGSC
B. megaterium 899	32	24	BGSC
B. pumilus SAFR-032	>64	>48	BGSC
B. subtilis			
AKP4 (Δ*des*)	>64	>48	D. de Mendoza (U. Nacional de Rosario)
AKP21 (Δ*desRK*)	>64	>48	D. de Mendoza (U. Nacional de Rosario)
BSU-LIKE1 (Δ*liaIH*)	>64	>48	BGSC
HB0042	>64	>48	Personal Collection
HB0934 (Δ*liaGFSR*)	>64	>48	J. Helmann (Cornell)
HB5126 (Δ*liaIH*)	>64	>48	J. Helmann (Cornell)
str. 168	>64	>48	J. Wells (USCF[b])
Brevibacillus formosus SS 86-3	>64	>48	BGSC
Brevibacillus laterosporus ATCC 9141	>64	>48	BGSC
Neisseria meningititis serotype C	>64	>48	[75]
Neisseria sicca	>64	>48	ATCC
Staphylococcus aureus			
12608	>64	>48	P. Hergenrother (UIUC)
29213	64	48	P. Hergenrother (UIUC)

Table 3.1 (cont.)

S. aureus 33591	64	48	P. Hergenrother (UIUC)
Staphylooccus aureus USA300	>64	>48	P. Hergenrother (UIUC)
Streptomyces coelicolor	>64	>48	USDA
Streptomyces lividans	>64	>48	USDA
Eukaryotic organisms			
Caenorhabditis elegans N2	>64	>48	CGC[b]
Saccharomyces cerevisiae	>64	>48	H. Zhao (UIUC)
Talaromyces stipitatus	>64	>48	H. Zhao (UIUC)

[a] Minimum inhibitory concentrations (MICs) were measured by microbroth dilution in LB (n ≥ 3 replicates)
[b] Abbreviations: UIUC, University of Illinois at Urbana-Champaign; USDA, United States Department of Agriculture; USAMRIID, United States Army Medical Research Institute of Infectious Diseases; BEI, Biodefense and Emerging Infections Research Resources Repository; ATCC, American Type Culture Collection; BGSC, Bacillus Genetic Stock Center; NMRS, Navel Medical Research Center; CDC, Center for Disease Control and Prevention; UCSF, University of California San Francisco; CGC, Caenorhabditis Genetics Center
[c] Susceptibility was assessed at 21 °C, 37 °C, and 42 °C; Susceptibility to PZN was unchanged by temperature Strains whose entries are highlighted in yellow were also tested for gamma phage susceptibility

Table 3.2 PZN is not antibacterial against *B. anthracis* endospores.

[PZN] (μg/mL)	**CFU/mL[a]**
Vehicle (DMSO)	$9.8 \pm 2.0 \times 10^5$
0.5	$4.3 \pm 0.3 \times 10^5$
1	$8.3 \pm 1.0 \times 10^5$
2	$6.8 \pm 0.6 \times 10^5$
4	$3.4 \pm 1.1 \times 10^5$
8	$6.5 \pm 0.1 \times 10^5$
16	$3.5 \pm 1.4 \times 10^5$

[a]Colony forming units per mL of endospore suspension

Table 3.3 γ phage sensitivity and PZN susceptibility of *Bacillus* strains.

Strain	γ Phage Sensitivity	PZN MIC[a]	Source
B. anthracis Sterne 7702	+++[b]	1	USDA
B. anthracis Sterne 34F2 A0517-1[c]	+++	2	BEI
B. cereus 2002013145	+++	>64	CDC[d]
B. cereus 2002013146	+++	>64	CDC[d]
B. cereus 2002013100	++	>64	CDC[d]
B. cereus 2000031002	+++	>64	CDC[d]
B. cereus ATCC 4342	+	>64	ATCC
B. cereus ATCC 7064	+	>64	ATCC
B. cereus CDC 32805	+	>64	ref
B. cereus G9241	-	8	BEI
B. megaterium 899	-	32	BGSC
B. mycoides 96/3308	-	>64	BGSC

[a]MIC (Minimum inhibitory concentation) as determined by microbroth dilution, measured in μg/mL.

[b]"+" indicate the level of phage sensitivity, with "+++" representing the most sensitive and "-" representing no sensitivity

[c]LLNL A0517 was obtained from BEI Resources as a mixture of two colony types. A0517_1 was confirmed to be devoid of pXO1 (Figure 3.2)

[d]Strains identified by Multilocus sequence typing analysis[29]

Table 3.4 MICs of representative strains demonstrating PZN activity in various rich media.

	MIC (μg/mL)		
Strain	**LB[a]**	**MH**	**BHI**
Bacillus anthracis Sterne	1	1	1
Bacillus cereus CDC32805	>64	>64	>64
Bacillus cereus ATCC 4242	>64	>64	>64
Bacillus Al Hakam	>64	>64	>64
Bacillus amyloliquefaciens FZB42	>64	>64	>64
Bacillus subtilis strain 168	>64	>64	>64
Enterococcus faecium U503	>64	>64	>64
Listeria monocytogenes 4b	>64	>64	>64
Staphylococcus aureus ATCC 12608	>64	16	32
Staphylococcus aureus ATCC 29213	64	8	16
Staphylococcus aureus ATCC 33591	64	8	16
Staphylococcus aureus USA300	>64	>64	>64

[a]Luria-Bertani (LB), Mueller-Hinton (MH), Brain Heart Infusion (BHI)

Table 3.5 RNA-Seq analysis of all differentially expressed *B. anthracis* Sterne 7702 genes after PZN treatment.

Locus Tag	Gene	Description	Fold Change	q-value
BAS1222	*ywcJ*[a]	formate/nitrite transporter family protein	-7	3.19E-38
BAS0577	*lldp-1*	L-lactate permease	-7	2.14E-24
BAS4869	*ldh3*	L-lactate dehydrogenase	-6	6.40E-27
BAS0169		hypothetical protein	-6	1.30E-25
BAS4146		hypothetical protein	-5	3.66E-19
BAS4762	*ldh2*	L-lactate dehydrogenase	-4	1.19E-13
BAS1089	*yjzC*[a]	hypothetical protein	-4	5.38E-16
BAS1615	*yfmQ*[a]	hypothetical protein	-3	1.49E-05
BAS3917		hypothetical protein	-3	9.12E-04
BAS4690	*cydA-2*	cytochrome d ubiquinol oxidase subunit I	-3	4.40E-04
BAS0513	*bdbD*	hypothetical protein	-3	1.00E-03
BAS1942	*sdpI*[a]	hypothetical protein	2	5.98E-03
BAS3405		ahpC/TSA family protein	2	6.00E-03
BAS2363		hypothetical protein	2	1.27E-03
BAS2776	*yetG*[a]	hypothetical protein	2	9.17E-04
BAS1163		hypothetical protein	3	2.06E-03
BAS0730	*yfhC*[a]	nitroreductase family protein	3	6.85E-03
BAS4453		hypothetical protein	3	4.90E-04
BAS2568		TetR family transcriptional regulator	3	1.43E-03
BAS2566	*kynB*	hypothetical protein	3	2.83E-03
BAS0683	*yqgI*[a]	phosphate ABC transporter permease	3	7.44E-04
BAS4452		hypothetical protein	3	2.81E-05
BAS2565	*kynA*	tryptophan 2,3-dioxygenase family protein	3	3.85E-03
BAS3439	*hutG*[a]	formimidoylglutamase	3	1.17E-03
BAS3871		hypothetical protein	3	1.35E-05
BAS0214	*lagB*	invasion protein LagB	3	2.21E-04
BAS1691	*fabH2*	3-oxoacyl-ACP synthase	3	6.35E-04
BAS4502	*ytpI*[a]	hypothetical protein	3	2.71E-06
BAS1573		hypothetical protein	3	8.18E-03
BAS0849		hypothetical protein	3	1.49E-06
BAS1346	*liaF*[a]	hypothetical protein	3	1.77E-04
BAS0525	*yuaG*[a]	hypothetical protein	3	6.06E-04
BAS0610	*rocE*[a]	amino acid ABC transporter permease	3	1.77E-04

Table 3.5 (cont.)

BAS4777	*sodC*	superoxide dismutase, Cu-Zn	3	6.63E-08
BAS0524	*yuaF*[a]	hypothetical protein	4	2.77E-07
BAS0848	*yhaR*[a]	enoyl-CoA hydratase	4	1.25E-07
BAS4173	*pstC*	phosphate ABC transporter permease	4	9.53E-06
BAS4172	*pstA*	phosphate ABC transporter permease	4	2.15E-07
BAS4171	*pstB*	phosphate transporter ATP-binding protein	4	7.63E-07
BAS1307	*ilvE1*	branched-chain amino acid aminotransferase	4	1.40E-08
BAS4560	*acsA*	acetyl-CoA synthetase	4	5.09E-06
BAS3772	*ylbP*[a]	hypothetical protein	4	2.05E-05
BAS0464	*rocR-1*	arginine utilization regulatory protein RocR	4	1.01E-09
BAS4877	*fadN*[a]	3-hydroxyacyl-CoA dehydrogenase	4	1.18E-09
BAS0624	*dppC*[a]	oligopeptide ABC transporter permease	4	7.90E-08
BAS4174	*phoX*	phosphate ABC transporter substrate-binding protein	4	1.87E-08
BAS5194	*fadF*[a]	ferredoxin, 4Fe-4S	4	1.32E-07
BAS1894	*dppE*[a]	oligopeptide ABC transporter substrate-binding protein	4	1.46E-08
BAS1070		hypothetical protein	4	1.73E-10
BAS4778		hypothetical protein	5	5.76E-14
BAS0681	*pstS*[a]	phosphate ABC transporter substrate-binding protein	5	1.12E-16
BAS4512		hypothetical protein	5	1.76E-24
BAS3440	*hutI*	imidazolonepropionase	5	3.49E-21
BAS2288		hypothetical protein	6	7.47E-08
BAS0625	*appB, oppB*[a]	oligopeptide ABC transporter permease	6	3.26E-20
BAS2146	*yokU*[a]	hypothetical protein	6	5.30E-39
BAS0626	*appF, oppF*[a]	oligopeptide ABC transporter ATP-binding protein	6	2.29E-19
BAS2145	*kamA*	L-lysine 2,3-aminomutase	7	4.12E-35
BAS3024		arsR family transcriptional regulator	7	1.17E-52
BAS2188	*mmgD*	citrate synthase 3	8	2.67E-54
BAS3441	*hutU*	urocanate hydratase	8	5.49E-50
BAS2649		hypothetical protein	9	5.16E-42
BAS2650		hypothetical protein	9	2.30E-45
BAS3442	*hutH*	histidine ammonia-lyase	10	9.17E-104
BAS0627	*appD, oppD*[a]	ABC transporter nucleotide-binding protein	11	1.62E-95
BAS2287	*yaaN*[a]	hypothetical protein	13	4.38E-93
BAS1521	*gerN*	germination protein gerN	28	0

Table 3.5 (cont.)

BAS3456		hypothetical protein	40	0
BAS5200	*yvfU, desR*[a]	DNA-binding response regulator	49	0
BAS5201	*yvfT, desK*[a]	sensor histidine kinase	56	0
BAS5202	*yvfS*[a]	ABC transporter permease	130	0
BAS5203	*yvfR*[a]	ABC transporter ATP-binding protein	135	0
BAS1345	*liaH*[a]	PspA/IM30 family protein	1084	0
BAS1344	*liaI*[a]	membrane protein	1407	0

[a]Genes are annotated by sequence homology to the corresponding *Bacillus subtilis* gene
The q-value is an adjusted p-value, taking in to account the false discovery rate

Table 3.6 Primers used in this study.

Confirmation of LLNL A0517_1 pXO1 plasmid loss	
pXO1_0172 lef RT-r	GATGCGAAAGTAGTGCCAAAGA
pXO1_0172 lef RT-r	CCACAGCATGTCCAAATTCG
Confirmation of spontaneous mutants	
BamHI-BAS4114-f	AAAAGGATCCATGACAGCAAACCGCATTAAAG
NotI-BAS4114-r	AAAAGCGGCCGCTCAGTTTGAAAGGCCTCGC
Generation and Confirmation of the BAS4114-BAS4117 deletion strain	
G236Tet-up-vec-f	TGGAGCTCCACCGCGGTGGCAGGCGTTTGCTGATACAC
G236Tet-up-down-r	TAAAAAAGGACAGTTTCATCCCCTACCTACC
G236Tet-down-up-f	GGGGATGAAACTGTCCTTTTTTATATTCATTCAGAC
G236Tet-down-vec-r	TCGACCTGCAGCCAAGGACGCATCTGTCTTTGTTTCAGTG
TetR-f	GCAAACCGCATTAAAGCTGTAGC
TetR-r	CAGTTTGAAAGGCCTCGCC
SugE4115-f	GGCATGGATTTATGTAATCTTAGCTGG
SugE4115-r	GCCTCCTTCGCTTCTTTTTCTTC
SugE4116-f	GGCTTGGGTATTTTTAATTCTAGCTGG
SugE4116-r	CTTAATAGTTTTAAGCCAACAGCGCC
BAS4117-f	GTGGAAAGAAAAAGGGAAGCAACTG
BAS4117-r	GTTCAGAAGAACTGTCCTTTTTAAATAACTTATTCC
RT-qPCR	
Banth 16S qRT-f	CGGAATTATTGGGCGTAAAG
Banth 16S qRT-r	TCTCCCAGTTTCCAATGACC
BAS0577 lldp-1 qRT-f	TGGTTCACTATTCGCACCAC
BAS0577 lldp-1 qRT-r	TTTGCTATTGTGCCACCAAC
BAS0627 appD qRT-f	ACGAATTATCTGGCGGAATG
BAS0627 appD qRT-r	AGCCGTTGTTGGCTCATC
BAS1344 liaI qRT-f	GGAGCAGGAGTTGTGTACTGG
BAS1344 liaI qRT-r	GATGGACAAGCCGATTAAACC
BAS1345 liaH qRT-f	ATCAAAGCAAGCGCTTATCG
BAS1345 liaH qRT-r	TTCTAATCGAGTTACTTGCCCTTC
BAS1521 gerN qRT-f	ACGAATGACTGGATTTGATGC
BAS1521 gerN qRT-r	GAAAGTCCTGTTCCTGCAATG
BAS1659 CitB RR qRT-f	AACGACGTTCGATGATGATG
BAS1659 CitB RR qRT-r	TTATCGCATCACGAATACGC
BAS1660 Sensor HK qRT-f	TGAAAGCATTCGGATTACATTG
BAS1660 Sensor HK qRT-r	TCATGCTTACTGGCAAATTCC
BAS1661 ABC trans qRT-f	TGCGAAGATGAATATTGGTGTC
BAS1661 ABC trans qRT-r	ACCCGTACAGTCCAGCAAAG
BAS1662 ABC trans qRT-f	CGGTTGTAATGACGACGATG
BAS1662 ABC trans qRT-r	TAGGCGCAGCAATAAGGTG
BAS1663 ABC trans qRT-f	TATGGGAATGTAGGGCAAGG

Table 3.6 (cont.)

BAS1663 ABC trans qRT-r	AGAAATTTCACCGTATCATTTGC
BAS1664 minor cls ClsB qRT-f	TGGCACAACAAACTTTACTTCG
BAS1664 minor cls ClsB qRT-r	AACGCCTTATTAACTTGCCCTAC
BAS1842 asbE qRT-f	GGGTATTTGCTTTCTGGTCTTG
BAS1842 asbE qRT-r	TTTCACGGAAGTATGCAAAGG
BAS1843 asbF qRT-f	CAGATCCAGTTGACAGCTTCC
BAS1843 asbF qRT-r	CGGTTCGAACACATGTAAATAATC
BAS3439 hutG qRT-f	TAACGGGCTTTGCAAACAG
BAS3439 hutG qRT-r	CATTTGACGGACCACCATC
BAS3440 hutI qRT-f	TGACCCGCATACTCATCTTG
BAS3440 hutI qRT-r	AAGAATACCTCCGCCTTGTTC
BAS3441 hutU qRT-f	ATTTGTTGGCTTGGTTACGG
BAS3441 hutU qRT-r	CACGACCGATAACGATTGG
BAS3442 hutH qRT-f	TGCGATGGTTGCTCTTACAG
BAS3442 hutH qRT-r	AAAGAACTCCTTGCGCTGTC
BAS4762 ldh2 qRT-f	AATCGTTCGCGGTATTATGG
BAS4762 ldh2 qRT-r	TGGTAGACCAGATTCTTTCCAAG
BAS4869 ldh3 qRT-f	AATCATGAACGTGCAGTTGG
BAS4869 ldh3 qRT-r	TTGCAGTCTTCATAGCTTCCTG
BAS5033 ftsX qRT-f	CGGAAAGACGTTTGAGTTATTTG
BAS5033 ftsX qRT-r	TCGCAATTGTTGCTGTATCTG
BAS5034 ABC ftsE qRT-f	TCTTGAAGATCGTGCAGACG
BAS5034 ABC ftsE qRT-r	ATCGGCAATTACGACTTTCG
BAS5200 desR qRT-f	TTGAAGTAATTGGGCAAGCTG
BAS5200 desR qRT-r	TCTAACCCGCTTTGAATTGG
BAS5201 desK qRT-f	GCAGTGACGAATGTTGTAAAGC
BAS5201 desK qRT-r	CCAATTCCGTTATCTTCTACCG
BAS5288 TetR reg qRT-f	AAGATGAGGAATTGCTTGTTACG
BAS5288 TetR reg qRT-r	CTTGTATAACCGGAATCCTTGG
BAS5289 transporter qRT-f	CGGAGCTCTTGTTGCCTTAC
BAS5289 transporter qRT-r	AAGCACGATTGCGTTTGTTAC

Table 3.7 RNA-Seq and qRT-PCR analysis of PZN-treated *B. anthracis* Sterne 7702.

			Fold Change	
Locus Tag	**Gene**	**Description**	**RNA-Seq**	**qRT-PCR**
BAS0577	*lldp-1*	L-lactate permease	-7	-7 ± 2[a]
BAS4869	*ldh3*	L-lactate dehydrogenase	-6	-24 ± 14
BAS4762	*ldh2*	L-lactate dehydrogenase	-4	-3 ± 1
BAS3439	*hutG*	formimidoylglutamase	3	3 ± 1
BAS3440	*hutI*	imidazolonepropionase	5	4 ± 0
BAS3441	*hutU*	urocanate hydratase	8	3 ± 0
BAS3442	*hutH*	histidine ammonia-lyase	10	5 ± 2
BAS0627	*appD, oppD*	ABC transporter nucleotide-binding protein	11	6 ± 3
BAS1521	*gerN*	germination protein	28	14 ± 9
BAS5200	*yvfU, desR*[b]	DNA-binding response regulator	49	37 ± 30
BAS5201	*yvfT, desK*[b]	sensor histidine kinase	56	94 ± 36
BAS1345	*liaH*[b]	PspA/IM30 family protein	1084	138 ± 10
BAS1344	*liaI*[b]	membrane protein	1407	352 ± 191

[a] Error is defined as one standard deviation, n ≥ 3

[b] Genes are derived from sequence homology to the given *B. subtilis* gene

Table 3.8 Susceptibility of select bacteria towards Me_2-Arg-Az_5 reveals a broader spectrum of activity relative to PZN.

Strain	**MIC[a] (μg/mL)**	**MIC[a] (μM)**
Bacillus anthracis Sterne 7702	2.2	3
Bacillus anthracis PR06	2.2	3
Bacillus anthracis A0517-1	2.2	3
Bacillus cereus ATCC 4342	4.4	6
Bacillus megaterium 899	2.2	3
Bacillus subtilis 168	4.4	6
Escherichia coli DH5a	>35	>48
Enterococcus faecium U503	35	48
Listeria monocytogenes 4b	>35	>48
Neisseria sicca ATCC 29256	>35	>48
Staphylococcus aureus USA300	2.2	3
Streptococcus pyogenes M1	35	48
Pseudomonas putida	>35	>48

[a] Minimum inhibitory concentrations (MICs) were determined by microbroth dilution assay and are reported in μg/mL and μM (the molecular weight of Me_2-Arg-Az_5 is ~half of PZN).

Table 3.9 Antibiotic susceptibility of *B. anthracis* Sterne and PR06.

Compound	*B. anthracis* Sterne[a]	*B. anthracis* PR06[b]
Plantazolicin	1	64
Tetracycline	0.125	0.125
Vancomycin	1	1
Triclosan	1	1
Nisin	2	2
Kanamycin	4	4
Cerulenin	4	8
Spectinomycin	8	4
Chloramphenicol	8	4
Daptomycin	8	8
Ethidium Bromide[c]	16	16

[a] MICs were measured by microbroth dilution (LB) in 2-fold increments and are reported as μg/mL
[b] Strain PR06 derives from Sterne and contains a frameshift mutation leading to a premature stop codon in *bas4114* (see Table 3.11)
[c] Ethidium bromide was included in this assay owing to previous reports that EmrE/SugE-type efflux pumps confers resistance to quaternary ammonium compounds and ethidium[90]

Table 3.10 Differentially expressed genes that are common to both PZN and Me_2-Arg-Az_5 treatment.

			Fold Change[a]	
Locus Tag	**Gene**	**Description**	**PZN**	**Me_2-Arg-Az_5**
BAS0169		hypothetical protein	-6	-4
BAS0513	*bdbD*	hypothetical protein	-3	-2
BAS0577	*lldp-1*	L-lactate permease	-7	-7
BAS1089		hypothetical protein	-4	-4
BAS1222	*ywcJ*[b]	formate/nitrite transporter family protein	-7	-7
BAS1615		hypothetical protein	-3	-3
BAS3917		hypothetical protein	-3	-2
BAS4146		hypothetical protein	-5	-5
BAS4690	*cydA-2*	cytochrome d ubiquinol oxidase subunit I	-3	-2
BAS4762	*ldh2*	L-lactate dehydrogenase	-4	-4
BAS4869	*ldh3*	L-lactate dehydrogenase	-6	-4
BAS5200	*ycfU,desR*[b]	DNA-binding response regulator	49	6
BAS5201	*yvfT, desK*[b]	sensor histidine kinase	56	5
BAS5202	*yvfS*[b]	ABC transporter permease	130	13
BAS5203	*yvfR*[b]	ABC transporter ATP-binding protein	135	12

[a] Fold change compared to wild type *B. anthracis* Sterne using RNA-Seq
[b] Genes are annotated by sequence homology to the corresponding *Bacillus subtilis* gene

Table 3.11 RNA-Seq analysis of all differentially expressed *B. anthracis* genes after Me_2-Arg-Az_5 treatment.

Locus Tag	Gene	Description	Fold Change	qValue[b]
BAS0577	*lldp-1*	L-lactate permease	-7	5.95E-90
BAS1222	*ywcJ*[a]	formate/nitrite transporter family protein	-7	1.30E-59
BAS4134		hypothetical protein	-7	1.61E-116
BAS4146		hypothetical protein	-5	6.09E-31
BAS4711		hypothetical protein	-5	3.53E-31
BAS0169		hypothetical protein	-4	9.57E-21
BAS1089	*yjzC*[a]	hypothetical protein	-4	2.76E-23
BAS1357	*hmp*	nitric oxide dioxygenase	-4	6.57E-12
BAS4762	*ldh2*	L-lactate dehydrogenase	-4	1.24E-16
BAS4869	*ldh3*	L-lactate dehydrogenase	-4	3.46E-17
BAS1023		hypothetical protein	-3	3.80E-06
BAS1349		hypothetical protein	-3	1.12E-08
BAS1615	*yfmQ*[a]	hypothetical protein	-3	1.28E-06
BAS4990	*cggR*	gapA transcriptional regulator CggR	-3	0.004179
BAS0070	*pabC*	4-amino-4-deoxychorismate lyase	-2	0.003344
BAS0513	*bdbD*	hypothetical protein	-2	8.87E-04
BAS0547	*maeN*[a]	citrate cation symporter family protein	-2	0.002003
BAS0566	*rapD, rapI*[a]	transcriptional regulator	-2	0.004179
BAS0631	*rbsR*	ribose operon repressor	-2	6.17E-05
BAS1024		hypothetical protein	-2	8.87E-04
BAS1185		hypothetical protein	-2	0.007387
BAS1273		ABC transporter permease	-2	8.71E-05
BAS1666	*gltT*[a]	proton/sodium-glutamate symport protein	-2	5.37E-04
BAS2706		hypothetical protein	-2	0.003549
BAS2707		ABC transporter ATP-binding protein	-2	8.05E-04
BAS3173		transcriptional regulator	-2	8.18E-07
BAS3917		hypothetical protein	-2	8.14E-04
BAS4414		succinate dehydrogenase, cytochrome b558 subunit	-2	0.003007
BAS4690	*cydA-2*	cytochrome d ubiquinol oxidase subunit I	-2	0.004179
BAS4922	*nupC*[a]	NupC family nucleoside transporter	-2	0.004085
BAS5002	*whiA*	hypothetical protein	-2	0.007026
BAS5316	*yycI*[a]	YycI protin	-2	7.74E-04
BAS0982	*fadR, yvdT*[a]	TetR family transcriptional regulator	3	8.50E-04
BAS4115	*sugE-1*	sugE protein	4	4.42E-10
BAS5201	*yvfT, desK*[a]	sensor histidine kinase	5	2.03E-21
BAS5200	*yvfU, desR*[a]	DNA-binding response regulator	6	4.21E-26
BAS0375	*yuxN, yfiR*[a]	TetR family transcriptional regulator	8	2.92E-37
BAS0902	*atpI*[a]	ATP synthase protein I	8	2.99E-46

Table 3.11 (cont.)

BAS5203	*yvfR*[a]	ABC transporter ATP-binding protein	12	1.66E-119
BAS5202	*yvfS*[a]	ABC transporter permease	13	2.82E-151
BAS0376	*ykuC, yfiS*[a]	major facilitator family transporter protein	181	0

[a] Genes are annotated by sequence homology to the corresponding *Bacillus subtilis* gene
[b] The q-value is an adjusted p-value, taking in to account the false discovery rate

Table 3.12 Spontaneous PZN-resistance mutations appear exclusively in *B. anthracis* Sterne *bas4114*, a predicted AcrR family transcriptional regulator gene.

Strain[c]	**Mutation**	**Consequence**[a]
Sterne	Wild type	D**ALEAFLCLLDGLMVELLFAGL**NRFETRLNASWQVFWRGLSN
PR01	457G→T	DAL*
PR02	492^T	DALEAFLCLLDGLMV*
PR03	495^AG	DALEAFLCLLDGLMVESYYSQV*
PR04	504^C	DALEAFLCLLDGLMVELLFRRFKSL*
PR05	506^GC	DALEAFLCLLDGLMVELLFAQV*
PR06	507^ATTCGCA	DALEAFLCLLDGLMVELLFAIRRFKSL*

[a] Amino acids 150-191 of BAS4114. Bold residues represent the predicted transmembrane region, as defined by Spoctopus (Figure 3.16)[25]
Asterisks (*) represent the location of a premature stop codon due to a nonsense mutation
[c] MICs for all PZN-resistant mutants here (PR01-06) are ≥ 32 μg/mL PZN, compared to 1 μg/mL for the wild type

Table 3.13 Expression change of *bas4114-4117* in strain PR06 (PZN-resistant mutant).

Gene	Annotation	Fold change[a]
BAS4114	*acrR* family transcriptional regulator	34
BAS4115	*emrE* drug efflux pump	152
BAS4116	*emrE* drug efflux pump	47
BAS4117	hypothetical protein	62

[a] Fold change compared to wild type *B. anthracis* Sterne using RNA-Seq

Table 3.14 PZN-Resistant Mutants of B. anthracis Sterne *Δbas4114−4117*.

Strain	Mutation	Annotation	Consequence	MIC[a]
PR07	*bas5034: A425G*	cell division ABC transporter, FtsE	E142G	8
PR08	*bas5034: G270T*	cell division ABC transporter, FtsE	L90F	32
PR09-1	*bas1659: G190C*	CitB RRb /luxR family	V64L	16
PR09-4	*bas1659: G190C*	CitB RRb /luxR family	V64L	>64
	bas1662: A638G	ABC transporter permease	H213R	
PR10-4	*bas1659: C248T*	CitB RRb /luxR family	T83M	64
	bas1663: C1127T	ABC transporter permease	A376V	
	bas1842: A43G	petrobactin biosynthesis, AsbE	S15G	

[a] MICs were determined by microbroth dilution assay, measured in μg/mL.
[b] Response regulator.

Table 3.15 Effect of *B. anthracis* Sterne mutations and growth conditions on PZN susceptibility and cardiolipin content of bacterial membranes.

Strain	MIC[a]	[NaCl][b]	% CL[c]
B. anthracis Sterne 7702	1	0.17	8.8 ± 4.0
B. anthracis Sterne 7702	0.25	0.67	12.2 ± 3.4
B. anthracis Sterne 7702 Δ*bas4114-4117*	1	0.17	11.5 ± 1.3
B. anthracis PR09-4	>64	0.17	14.3 ± 1.7
B. anthracis PR09-4	32	0.67	16.3 ± 0.9
B. anthracis PR10-4	64	0.17	10.7 ± 2.3
B. anthracis PR10-4	16	0.67	11.0 ± 4.3
B. subtilis 168	>128	0.17	16.7 ± 0.7
B. subtilis 168	32	1.67	24.1 ± 0.9*
B. cereus E33L	>64	0.17	11.2 ± 2.0
B. cereus E33L	>64	0.67	18.7 ± 2.0*
B. cereus ATCC 4342	>64	0.17	20.6 ± 5.1
B. cereus ATCC 4342	>64	0.67	21.6 ± 2.6

[a] Minimum inhibitory concentrations (MIC) for PZN were determined by the microbroth dilution method and are reported as μg/mL
[b] The NaCl concentration of the media is given in M (0.17 M is the standard for LB)
[c] The percentage of cardiolipin (CL) within the total lipid fraction was determined by a TLC-based densitometric assay. Error is given as standard deviation with n = 3. Asterisks indicate $P<0.05$ relative to the same strain grown in LB with 0.17 M NaCl. PZN was absent from CL quantification experiments

Table 3.16 qRT-PCR of *cls* locus in step-wise evolved PZN-resistant mutants.

		Fold change[a]		
Gene	Annotation	PR09-1[b]	PR09-4[c]	PR10-4[d]
bas1659	Response regulator	NS	NS	NS[e]
bas1660	Histidine kinase	NS	NS	NS
bas1661	ABC transporter (ATPase)	21 ± 7	43 ± 20	NS
bas1662	ABC transporter (permease)	23 ± 13	NS	NS
bas1663	ABC transporter (permease)	24 ± 9	39 ± 24	NS
bas1664	Cardiolipin synthase	39 ± 7	77 ± 19	NS
bas1842	Petrobactin biosynthesis	-	-	NS
bas1843	Petrobactin biosynthesis	-	-	NS

[a] Error is given as standard deviation with n ≥ 3 biological replicates
[b] PR09-1 contains a missense mutation in *bas1659*
[c] PR09-4 contains missense mutations in *bas1659* and *bas1662*
[d] PR10-4 contains missense mutations in *bas1659*, *bas1663*, and *bas1842*
[e] $p < 0.05$; NS: Not significant

3.8 References

1. de Man, P.; Verhoeven, B. A.; Verbrugh, H. A.; Vos, M. C.; van den Anker, J. N., An antibiotic policy to prevent emergence of resistant bacilli. *Lancet* **2000,** *355* (9208), 973-978.
2. Wilson, D. N.; Harms, J. M.; Nierhaus, K. H.; Schlunzen, F.; Fucini, P., Species-specific antibiotic-ribosome interactions: implications for drug development. *Biol Chem* **2005,** *386* (12), 1239-1252.
3. Payne, D. J., Desperately seeking new antibiotics. *Science* **2008,** *321* (5896), 1644-1645.
4. Scholz, R.; Molohon, K. J.; Nachtigall, J.; Vater, J.; Markley, A. L.; Sussmuth, R. D.; Mitchell, D. A.; Borriss, R., Plantazolicin, a novel microcin B17/streptolysin S-like natural product from *Bacillus amyloliquefaciens* FZB42. *J Bacteriol* **2011,** *193* (1), 215-224.
5. Arnison, P. G.; Bibb, M. J.; Bierbaum, G.; Bowers, A. A.; Bugni, T. S.; Bulaj, G.; Camarero, J. A.; Campopiano, D. J.; Challis, G. L.; Clardy, J.; Cotter, P. D.; Craik, D. J.; Dawson, M.; Dittmann, E.; Donadio, S.; Dorrestein, P. C.; Entian, K. D.; Fischbach, M. A.; Garavelli, J. S.; Goransson, U.; Gruber, C. W.; Haft, D. H.; Hemscheidt, T. K.; Hertweck, C.; Hill, C.; Horswill, A. R.; Jaspars, M.; Kelly, W. L.; Klinman, J. P.; Kuipers, O. P.; Link, A. J.; Liu, W.; Marahiel, M. A.; Mitchell, D. A.; Moll, G. N.; Moore, B. S.; Muller, R.; Nair, S. K.; Nes, I. F.; Norris, G. E.; Olivera, B. M.; Onaka, H.; Patchett, M. L.; Piel, J.; Reaney, M. J.; Rebuffat, S.; Ross, R. P.; Sahl, H. G.; Schmidt, E. W.; Selsted, M. E.; Severinov, K.; Shen, B.; Sivonen, K.; Smith, L.; Stein, T.; Sussmuth, R. D.; Tagg, J. R.; Tang, G. L.; Truman, A. W.; Vederas, J. C.; Walsh, C. T.; Walton, J. D.; Wenzel, S. C.; Willey, J. M.; van der Donk, W. A., Ribosomally synthesized and post-translationally modified peptide natural products: overview and recommendations for a universal nomenclature. *Nat Prod Rep* **2013,** *30* (1), 108-160.
6. Cox, C. L.; Doroghazi, J. R.; Mitchell, D. A., The genomic landscape of ribosomal peptides containing thiazole and oxazole heterocycles. *BMC Genomics* **2015,** *16* (1), 778.
7. Dunlap, C. A.; Kim, S. J.; Kwon, S. W.; Rooney, A. P., Phylogenomic analysis shows that *Bacillus amyloliquefaciens* subsp. *plantarum* is a later heterotypic synonym of *Bacillus methylotrophicus*. *Int J Syst Evol Microbiol* **2015,** *65* (7), 2104-2109.
8. Molohon, K. J.; Melby, J. O.; Lee, J.; Evans, B. S.; Dunbar, K. L.; Bumpus, S. B.; Kelleher, N. L.; Mitchell, D. A., Structure determination and interception of biosynthetic intermediates for the plantazolicin class of highly discriminating antibiotics. *ACS Chem Biol* **2011,** *6* (12), 1307-1313.
9. Banala, S.; Ensle, P.; Sussmuth, R. D., Total synthesis of the ribosomally synthesized linear azole-containing peptide plantazolicin A from *Bacillus amyloliquefaciens*. *Angew Chem Int Ed Engl* **2013,** *52* (36), 9518-9523.
10. Wilson, Z. E.; Fenner, S.; Ley, S. V., Total syntheses of linear polythiazole/oxazole plantazolicin A and its biosynthetic precursor plantazolicin B. *Angew Chem Int Ed Engl* **2015,** *54* (4), 1284-1288.
11. Wada, H.; Williams, H. E. L.; Moody, C. J., Total Synthesis of the Posttranslationally Modified Polyazole Peptide Antibiotic Plantazolicin A. *Angewandte Chemie International Edition* **2015,** *54* (50), 15147-15151.
12. Deane, C. D.; Melby, J. O.; Molohon, K. J.; Susarrey, A. R.; Mitchell, D. A., Engineering unnatural variants of plantazolicin through codon reprogramming. *ACS Chem Biol* **2013,** *8* (9), 1998-2008.
13. Lee, J.; Hao, Y.; Blair, P. M.; Melby, J. O.; Agarwal, V.; Burkhart, B. J.; Nair, S. K.; Mitchell, D. A., Structural and functional insight into an unexpectedly selective N-

methyltransferase involved in plantazolicin biosynthesis. *Proc Natl Acad Sci USA* **2013,** *110* (32), 12954-12959.
14. Sharma, A.; Blair, P. M.; Mitchell, D. A., Synthesis of plantazolicin analogues enables dissection of ligand binding interactions of a highly selective methyltransferase. *Org Lett* **2013,** *15* (19), 5076-5079.
15. Hao, Y.; Blair, P. M.; Sharma, A.; Mitchell, D. A.; Nair, S. K., Insights into methyltransferase specificity and bioactivity of derivatives of the antibiotic plantazolicin. *ACS Chem Biol* **2015,** *10* (5), 1209-1216.
16. Lee, S. W.; Mitchell, D. A.; Markley, A. L.; Hensler, M. E.; Gonzalez, D.; Wohlrab, A.; Dorrestein, P. C.; Nizet, V.; Dixon, J. E., Discovery of a widely distributed toxin biosynthetic gene cluster. *Proc Natl Acad Sci USA* **2008,** *105* (15), 5879-5884.
17. Rasko, D. A.; Altherr, M. R.; Han, C. S.; Ravel, J., Genomics of the *Bacillus cereus* group of organisms. *FEMS Microbiol Rev* **2005,** *29* (2), 303-329.
18. Kolsto, A. B.; Tourasse, N. J.; Okstad, O. A., What sets *Bacillus anthracis* apart from other *Bacillus* species? *Annu Rev Microbiol* **2009,** *63*, 451-476.
19. Mesnage, S.; Fontaine, T.; Mignot, T.; Delepierre, M.; Mock, M.; Fouet, A., Bacterial SLH domain proteins are non-covalently anchored to the cell surface via a conserved mechanism involving wall polysaccharide pyruvylation. *EMBO J* **2000,** *19* (17), 4473-4484.
20. Kern, J.; Ryan, C.; Faull, K.; Schneewind, O., *Bacillus anthracis* surface-layer proteins assemble by binding to the secondary cell wall polysaccharide in a manner that requires *csaB* and *tagO*. *J Mol Biol* **2010,** *401* (5), 757-775.
21. Weidenmaier, C.; Peschel, A., Teichoic acids and related cell-wall glycopolymers in Gram-positive physiology and host interactions. *Nat Rev Microbiol* **2008,** *6* (4), 276-287.
22. Ganguly, J.; Low, L. Y.; Kamal, N.; Saile, E.; Forsberg, L. S.; Gutierrez-Sanchez, G.; Hoffmaster, A. R.; Liddington, R.; Quinn, C. P.; Carlson, R. W.; Kannenberg, E. L., The secondary cell wall polysaccharide of *Bacillus anthracis* provides the specific binding ligand for the C-terminal cell wall-binding domain of two phage endolysins, PlyL and PlyG. *Glycobiology* **2013,** *23* (7), 820-832.
23. Schuch, R.; Pelzek, A. J.; Raz, A.; Euler, C. W.; Ryan, P. A.; Winer, B. Y.; Farnsworth, A.; Bhaskaran, S. S.; Stebbins, C. E.; Xu, Y.; Clifford, A.; Bearss, D. J.; Vankayalapati, H.; Goldberg, A. R.; Fischetti, V. A., Use of a bacteriophage lysin to identify a novel target for antimicrobial development. *PLoS ONE* **2013,** *8* (4), e60754.
24. Ezzell, J. W.; Abshire, T. G.; Little, S. F.; Lidgerding, B. C.; Brown, C., Identification of *Bacillus anthracis* by using monoclonal antibody to cell wall galactose-*N*-acetylglucosamine polysaccharide. *J Clin Microbiol* **1990,** *28* (2), 223-231.
25. Abshire, T. G.; Brown, J. E.; Ezzell, J. W., Production and validation of the use of gamma phage for identification of *Bacillus anthracis*. *J Clin Microbiol* **2005,** *43* (9), 4780-4788.
26. Kan, S.; Fornelos, N.; Schuch, R.; Fischetti, V. A., Identification of a ligand on the Wip1 bacteriophage highly specific for a receptor on *Bacillus anthracis*. *J Bacteriol* **2013,** *195* (19), 4355-4364.
27. Hoffmaster, A. R.; Hill, K. K.; Gee, J. E.; Marston, C. K.; De, B. K.; Popovic, T.; Sue, D.; Wilkins, P. P.; Avashia, S. B.; Drumgoole, R.; Helma, C. H.; Ticknor, L. O.; Okinaka, R. T.; Jackson, P. J., Characterization of *Bacillus cereus* isolates associated with fatal pneumonias: strains are closely related to *Bacillus anthracis* and harbor *B. anthracis* virulence genes. *J Clin Microbiol* **2006,** *44* (9), 3352-3360.

28. Schuch, R.; Fischetti, V. A., Detailed genomic analysis of the beta and gamma phages infecting *Bacillus anthracis*: implications for evolution of environmental fitness and antibiotic resistance. *J Bacteriol* **2006,** *188* (8), 3037-3051.
29. Marston, C. K.; Gee, J. E.; Popovic, T.; Hoffmaster, A. R., Molecular approaches to identify and differentiate *Bacillus anthracis* from phenotypically similar *Bacillus* species isolates. *BMC Microbiol* **2006,** *6*, 22.
30. Davison, S.; Couture-Tosi, E.; Candela, T.; Mock, M.; Fouet, A., Identification of the *Bacillus anthracis* gamma phage receptor. *J Bacteriol* **2005,** *187* (19), 6742-6749.
31. Hoffmaster, A. R.; Ravel, J.; Rasko, D. A.; Chapman, G. D.; Chute, M. D.; Marston, C. K.; De, B. K.; Sacchi, C. T.; Fitzgerald, C.; Mayer, L. W.; Maiden, M. C.; Priest, F. G.; Barker, M.; Jiang, L.; Cer, R. Z.; Rilstone, J.; Peterson, S. N.; Weyant, R. S.; Galloway, D. R.; Read, T. D.; Popovic, T.; Fraser, C. M., Identification of anthrax toxin genes in a *Bacillus cereus* associated with an illness resembling inhalation anthrax. *Proc Natl Acad Sci USA* **2004,** *101* (22), 8449-8454.
32. Burkett-Cadena, M.; Kokalis-Burelle, N.; Lawrence, K. S.; van Santen, E.; Kloepper, J. W., Suppressiveness of root-knot nematodes mediated by rhizobacteria. *Biol Control* **2008,** *47* (1), 55-59.
33. Liu, Z.; Budiharjo, A.; Wang, P.; Shi, H.; Fang, J.; Borriss, R.; Zhang, K.; Huang, X., The highly modified microcin peptide plantazolicin is associated with nematicidal activity of *Bacillus amyloliquefaciens* FZB42. *Appl Microbiol Biotechnol* **2013,** *97* (23), 10081-10090.
34. Ziegler, S.; Pries, V.; Hedberg, C.; Waldmann, H., Target identification for small bioactive molecules: Finding the needle in the haystack. *Angew Chem Int Ed Engl* **2013,** *52* (10), 2744-2792.
35. Burdine, L.; Kodadek, T., Target identification in chemical genetics: the (often) missing link. *Chem Biol* **2004,** *11* (5), 593-597.
36. Hobbs, J. K.; Miller, K.; O'Neill, A. J.; Chopra, I., Consequences of daptomycin-mediated membrane damage in *Staphylococcus aureus*. *J Antimicrob Chemother* **2008,** *62* (5), 1003-1008.
37. Sahl, H. G.; Brandis, H., Mode of action of the staphylococcin-like peptide Pep 5 and culture conditions effecting its activity. *Zentralbl Bakteriol Mikrobiol Hyg A* **1982,** *252* (2), 166-175.
38. Brazas, M. D.; Hancock, R. E., Using microarray gene signatures to elucidate mechanisms of antibiotic action and resistance. *Drug Discov Today* **2005,** *10* (18), 1245-1252.
39. Shaw, K. J.; Morrow, B. J., Transcriptional profiling and drug discovery. *Curr Opin Pharmacol* **2003,** *3* (5), 508-512.
40. Li, X. Z.; Nikaido, H., Efflux-mediated drug resistance in bacteria: an update. *Drugs* **2009,** *69* (12), 1555-1623.
41. Jordan, S.; Hutchings, M. I.; Mascher, T., Cell envelope stress response in Gram-positive bacteria. *FEMS Microbiol Rev* **2008,** *32* (1), 107-146.
42. Wecke, T.; Zuhlke, D.; Mader, U.; Jordan, S.; Voigt, B.; Pelzer, S.; Labischinski, H.; Homuth, G.; Hecker, M.; Mascher, T., Daptomycin versus Friulimicin B: in-depth profiling of *Bacillus subtilis* cell envelope stress responses. *Antimicrob Agents Chemother* **2009,** *53* (4), 1619-1623.
43. Martin, M.; de Mendoza, D., Regulation of *Bacillus subtilis* DesK thermosensor by lipids. *Biochem J* **2013,** *451* (2), 269-275.
44. Novo, D.; Perlmutter, N. G.; Hunt, R. H.; Shapiro, H. M., Accurate flow cytometric membrane potential measurement in bacteria using diethyloxacarbocyanine and a ratiometric technique. *Cytometry* **1999,** *35* (1), 55-63.

45. Ruhr, E.; Sahl, H. G., Mode of action of the peptide antibiotic nisin and influence on the membrane potential of whole cells and on cytoplasmic and artificial membrane vesicles. *Antimicrob Agents Chemother* **1985,** *27* (5), 841-845.
46. Silverman, J. A.; Perlmutter, N. G.; Shapiro, H. M., Correlation of daptomycin bactericidal activity and membrane depolarization in *Staphylococcus aureus*. *Antimicrob Agents Chemother* **2003,** *47* (8), 2538-2544.
47. Epand, R. M.; Walker, C.; Epand, R. F.; Magarvey, N. A., Molecular mechanisms of membrane targeting antibiotics. *Biochim Biophys Acta* **2016,** *1858* (5), 980-987.
48. Berenbaum, M. C., What is synergy? *Pharmacol Rev* **1989,** *41* (2), 93-141.
49. Tiyanont, K.; Doan, T.; Lazarus, M. B.; Fang, X.; Rudner, D. Z.; Walker, S., Imaging peptidoglycan biosynthesis in *Bacillus subtilis* with fluorescent antibiotics. *Proc Natl Acad Sci USA* **2006,** *103* (29), 11033-11038.
50. Bindman, N. A.; van der Donk, W. A., A general method for fluorescent labeling of the N-termini of lanthipeptides and its application to visualize their cellular localization. *J Am Chem Soc* **2013,** *135* (28), 10362-10371.
51. Huang, B.; Wang, W.; Bates, M.; Zhuang, X., Three-dimensional super-resolution imaging by stochastic optical reconstruction microscopy. *Science* **2008,** *319* (5864), 810-813.
52. Nguyen-Mau, S. M.; Oh, S. Y.; Kern, V. J.; Missiakas, D. M.; Schneewind, O., Secretion genes as determinants of *Bacillus anthracis* chain length. *J Bacteriol* **2012,** *194* (15), 3841-3850.
53. Silver, L. L., Challenges of antibacterial discovery. *Clin Microbiol Rev* **2011,** *24* (1), 71-109.
54. Deng, W.; Li, C.; Xie, J., The underling mechanism of bacterial TetR/AcrR family transcriptional repressors. *Cell Signal* **2013,** *25* (7), 1608-1613.
55. Poelarends, G. J.; Mazurkiewicz, P.; Konings, W. N., Multidrug transporters and antibiotic resistance in Lactococcus lactis. *Biochim Biophys Acta* **2002,** *1555* (1-3), 1-7.
56. Collins, B.; Curtis, N.; Cotter, P. D.; Hill, C.; Ross, R. P., The ABC transporter AnrAB contributes to the innate resistance of *Listeria monocytogenes* to nisin, bacitracin, and various beta-lactam antibiotics. *Antimicrob Agents Chemother* **2010,** *54* (10), 4416-4423.
57. Yang, D. C.; Peters, N. T.; Parzych, K. R.; Uehara, T.; Markovski, M.; Bernhardt, T. G., An ATP-binding cassette transporter-like complex governs cell-wall hydrolysis at the bacterial cytokinetic ring. *Proc Natl Acad Sci USA* **2011,** *108* (45), E1052-E1060.
58. Garti-Levi, S.; Hazan, R.; Kain, J.; Fujita, M.; Ben-Yehuda, S., The FtsEX ABC transporter directs cellular differentiation in *Bacillus subtilis*. *Mol Microbiol* **2008,** *69* (4), 1018-1028.
59. Friedman, L.; Alder, J. D.; Silverman, J. A., Genetic changes that correlate with reduced susceptibility to daptomycin in *Staphylococcus aureus*. *Antimicrob Agents Chemother* **2006,** *50* (6), 2137-2145.
60. Lee, J. Y.; Janes, B. K.; Passalacqua, K. D.; Pfleger, B. F.; Bergman, N. H.; Liu, H.; Hakansson, K.; Somu, R. V.; Aldrich, C. C.; Cendrowski, S.; Hanna, P. C.; Sherman, D. H., Biosynthetic analysis of the petrobactin siderophore pathway from *Bacillus anthracis*. *J Bacteriol* **2007,** *189* (5), 1698-1710.
61. Zhang, T.; Muraih, J. K.; Tishbi, N.; Herskowitz, J.; Victor, R. L.; Silverman, J.; Uwumarenogie, S.; Taylor, S. D.; Palmer, M.; Mintzer, E., Cardiolipin prevents membrane translocation and permeabilization by daptomycin. *J Biol Chem* **2014,** *289* (17), 11584-11591.
62. Palmer, K. L.; Daniel, A.; Hardy, C.; Silverman, J.; Gilmore, M. S., Genetic basis for daptomycin resistance in Enterococci. *Antimicrob Agents Chemother* **2011,** *55* (7), 3345-3356.

63. Mileykovskaya, E.; Dowhan, W., Visualization of phospholipid domains in *Escherichia coli* by using the cardiolipin-specific fluorescent dye 10-N-nonyl acridine orange. *J Bacteriol* **2000,** *182* (4), 1172-1175.
64. Mileykovskaya, E.; Dowhan, W., Cardiolipin membrane domains in prokaryotes and eukaryotes. *Biochim Biophys Acta* **2009,** *1788* (10), 2084-2091.
65. Strahl, H.; Burmann, F.; Hamoen, L. W., The actin homologue MreB organizes the bacterial cell membrane. *Nat Commun* **2014,** *5*, 3442.
66. Romantsov, T.; Guan, Z.; Wood, J. M., Cardiolipin and the osmotic stress responses of bacteria. *Biochim Biophys Acta* **2009,** *1788* (10), 2092-2100.
67. Peters, A. C.; Thomas, L.; Wimpenny, J. W., Effects of salt concentration on bacterial growth on plates with gradients of pH and temperature. *FEMS Microbiol Lett* **1991,** *61* (2-3), 309-314.
68. Unsay, J. D.; Cosentino, K.; Subburaj, Y.; Garcia-Saez, A. J., Cardiolipin effects on membrane structure and dynamics. *Langmuir* **2013,** *29* (51), 15878-15887.
69. Aguilar, P. S.; Cronan, J. E., Jr.; de Mendoza, D., A *Bacillus subtilis* gene induced by cold shock encodes a membrane phospholipid desaturase. *J Bacteriol* **1998,** *180* (8), 2194-2200.
70. Hotta, K.; Kim, C. Y.; Fox, D. T.; Koppisch, A. T., Siderophore-mediated iron acquisition in *Bacillus anthracis* and related strains. *Microbiology* **2010,** *156* (Pt 7), 1918-1925.
71. Steil, L.; Hoffmann, T.; Budde, I.; Volker, U.; Bremer, E., Genome-wide transcriptional profiling analysis of adaptation of *Bacillus subtilis* to high salinity. *J Bacteriol* **2003,** *185* (21), 6358-6370.
72. Hoffmann, T.; Schutz, A.; Brosius, M.; Volker, A.; Volker, U.; Bremer, E., High-salinity-induced iron limitation in *Bacillus subtilis*. *J Bacteriol* **2002,** *184* (3), 718-727.
73. Ohta, A.; Obara, T.; Asami, Y.; Shibuya, I., Molecular cloning of the cls gene responsible for cardiolipin synthesis in *Escherichia coli* and phenotypic consequences of its amplification. *J Bacteriol* **1985,** *163* (2), 506-514.
74. Kan, S.; Fornelos, N.; Schuch, R.; Fischetti, V. A., Identification of a ligand on the Wip1 bacteriophage highly specific for a receptor on *B. anthracis*. *J Bacteriol* **2013**.
75. Kellogg, D. S., Jr.; Peacock, W. L., Jr.; Deacon, W. E.; Brown, L.; Pirkle, D. I., *Neisseria gonorrhoeae*. I. Virulence genetically linked to clonal variation. *J Bacteriol* **1963,** *85*, 1274-1279.
76. Harrold, Z. R.; Hertel, M. R.; Gorman-Lewis, D., Optimizing *Bacillus subtilis* spore isolation and quantifying spore harvest purity. *J Microbiol Methods* **2011,** *87* (3), 325-329.
77. Clinical and Laboratory Standards Institute. In *Methods for Dilution Antimicrobial Susceptibility Tests for Bacteria that Grow Aerobically—Seventh Edition: Approved Standard*, CLSI: Wayne, PA, USA, 2006.
78. McClure, R.; Balasubramanian, D.; Sun, Y.; Bobrovskyy, M.; Sumby, P.; Genco, C. A.; Vanderpool, C. K.; Tjaden, B., Computational analysis of bacterial RNA-Seq data. *Nucleic Acids Res* **2013,** *41* (14), e140.
79. Rust, M. J.; Bates, M.; Zhuang, X., Sub-diffraction-limit imaging by stochastic optical reconstruction microscopy (STORM). *Nat Methods* **2006,** *3* (10), 793-795.
80. Fei, J.; Singh, D.; Zhang, Q.; Park, S.; Balasubramanian, D.; Golding, I.; Vanderpool, C. K.; Ha, T., RNA biochemistry. Determination of in vivo target search kinetics of regulatory noncoding RNA. *Science* **2015,** *347* (6228), 1371-1374.
81. Bates, M.; Huang, B.; Dempsey, G. T.; Zhuang, X., Multicolor super-resolution imaging with photo-switchable fluorescent probes. *Science* **2007,** *317* (5845), 1749-1753.

82. Porta-de-la-Riva, M.; Fontrodona, L.; Villanueva, A.; Cerón, J., Basic Caenorhabditis elegans Methods: Synchronization and Observation. *J Vis Exp* **2012,** (64).
83. Li, Z.; Hao, P.; Li, L.; Tan, C. Y. J.; Cheng, X.; Chen, G. Y. J.; Sze, S. K.; Shen, H.-M.; Yao, S. Q., Design and synthesis of minimalist terminal alkyne-containing diazirine photo-crosslinkers and their incorporation into kinase inhibitors for cell- and tissue-based proteome profiling. *Angew Chem Int Ed Engl* **2013,** *52* (33), 8551-8556.
84. Koumoutsi, A.; Chen, X. H.; Henne, A.; Liesegang, H.; Hitzeroth, G.; Franke, P.; Vater, J.; Borriss, R., Structural and functional characterization of gene clusters directing nonribosomal synthesis of bioactive cyclic lipopeptides in *Bacillus amyloliquefaciens* strain FZB42. *J Bacteriol* **2004,** *186* (4), 1084-1096.
85. Plaut, R. D.; Stibitz, S., Improvements to a markerless allelic exchange system for *Bacillus anthracis*. *PLoS ONE* **2015,** *10* (12), e0142758.
86. Anderson, V. J.; Kern, J. W.; McCool, J. W.; Schneewind, O.; Missiakas, D., The SLH-domain protein BslO is a determinant of *Bacillus anthracis* chain length. *Mol Microbiol* **2011,** *81* (1), 192-205.
87. Tan, L.; Turnbough, C. L., Jr., Sequence motifs and proteolytic cleavage of the collagen-like glycoprotein BclA required for its attachment to the exosporium of *Bacillus anthracis*. *J Bacteriol* **2010,** *192* (5), 1259-1268.
88. Carlson, P. E., Jr.; Dixon, S. D.; Janes, B. K.; Carr, K. A.; Nusca, T. D.; Anderson, E. C.; Keene, S. E.; Sherman, D. H.; Hanna, P. C., Genetic analysis of petrobactin transport in *Bacillus anthracis*. *Mol Microbiol* **2010,** *75* (4), 900-909.
89. Pomerantsev, A. P.; Kalnin, K. V.; Osorio, M.; Leppla, S. H., Phosphatidylcholine-specific phospholipase C and sphingomyelinase activities in bacteria of the *Bacillus cereus* group. *Infect Immun* **2003,** *71* (11), 6591-6606.
90. He, G. X.; Zhang, C.; Crow, R. R.; Thorpe, C.; Chen, H.; Kumar, S.; Tsuchiya, T.; Varela, M. F., SugE, a new member of the SMR family of transporters, contributes to antimicrobial resistance in *Enterobacter cloacae*. *Antimicrob Agents Chemother* **2011,** *55* (8), 3954-3957.

CHAPTER 4: REACTIVITY-BASED SCREENING FOR CITRULLINE-CONTAINING NATURAL PRODUCTS REVEALS A FAMILY OF BACTERIAL PEPTIDYL ARGININE DEIMINASES[3]

4.1 Abstract

Efforts to discover natural products with antibiotic activity traditionally relied on bioassay-guided techniques, but such screens were biased toward the most highly produced compounds and missed less abundant but potentially useful compounds. The genomic revolution has provided great insight into the vast amount of chemical space covered by natural products, and new methods are needed to aid in the discovery and isolation of these compounds. A genome-mining tool recently enabled extensive bioinformatic characterization of the lasso peptide family of ribosomally synthesized and post-translationally modified peptide natural products (RiPPs), and subsequent isolation revealed a class of lasso peptides with an unpredicted citrulline modification. Herein we describe the use of reactivity-based screening of bacterial extracts to discriminate between arginine- and citrulline-containing lasso peptides. This classification enabled the identification of a distally-encoded protein with putative peptidyl arginine deiminase (PAD) activity. Heterologous expression and *in vitro* enzymatic assays were used to demonstrate the activity of the first bacterial PAD of its kind. The family of PADs were then surveyed bioinformatically for deeper understanding of its genomic context and potential role in posttranslational modification of RiPPs. These data reveal the importance of validating natural product structural prediction software as well as demonstrate the prevalence of citrulline modifications in bacterial natural products.

[3] Manuscript in preparation.

4.2 Introduction

Natural products of bacterial origin have historically been a fruitful source for antibiotics, but the traditional method of antibiotic discovery, bioassay-guided isolation, is limited to high-abundance natural products and leads to high rates of rediscovery.[1] However, the genomic revolution has shown that bacteria have the capacity to produce many more natural products than previously predicted.[2] Structural prediction programs, relying on analysis of proteins within these biosynthetic gene clusters (BGCs), suggest that these natural products cover a broad swath of chemical space, and many of these compounds could have great potential as therapeutic agents.[2-3] Additionally, by connecting genes to molecules, improvements to genome-mining and structure prediction programs can be made. New strategies for identifying, isolating, and characterizing the products of these gene clusters are needed.

Reactivity-based screening (RBS) is a recently-developed technique for the rapid discovery of natural products bearing specific functional groups in organic extracts of cultured bacteria (Figure 4.1). The basis of RBS is the chemoselective labeling of a reactive functional group on natural products in in order to rapidly detect if molecules with that functional group are present in the sample. The strategy relies on comparing mass spectra of unreacted and reacted cellular extracts, searching for differences in the spectra that correspond to the mass of the probe, which is selective for the functional group of interest. RBS enabled the discovery and subsequent characterization of the thiopeptide cyclothiazomycin C,[4] the nonribosomal peptide (NRP) deimino-antipain,[5] the hybrid NRP-PKS tirandalydigin,[6] and the hygrobafilomycin JBIR-100,[7] to name a few. RBS is a valuable tool for validating bioinformatics-guided natural product identification, enabling a more rapid screen for the production of predicted compounds. Additionally, RBS is useful for rapid dereplication of already-characterized natural products,[4]

detection of low-abundance species using a sensitive ionization technique, and the facile use of more sophisticated probes that enhance detection due to unique isotope patterns of labeled compounds or selective enrichment through affinity purification.[5, 8-9]

We have previously reported on RBS probes for dehydrated amino acids, aldehydes, and ketones. These reactive functional groups are ubiquitous in ribosomally synthesized and post-translationally modified peptide natural products (RiPPs) as well as other natural products. We sought to characterize a more rare functional group in the context of bacterial natural products. The modification of arginine to citrulline is an enzyme-dependent deimination of the primary guanidinium group on the arginine side chain (Figure 4.2). Although this is a modest chemical transformation, isoelectric point of the guanidinium side chain of arginine is 10.76 but drops to 6.1 upon deimination. The loss of a positive charge at neutral pH can dramatically alter the structure and function of the substrate, and is thought to lead to the misfolding of myelin basic protein, filaggrin and trichohyalin, leading to rheumatoid arthritis.[10] Deimination of proteins has been implicated in other human disease states as well, such as Alzheimer's disease and cancer.[11]

To our knowledge, only one bacterial PAD has thus far been characterized, and in the context of virulence. The PAD from *Porphyromonas gingivalis* is a conserved enzyme in the family of periodontal pathogens.[12] As an essential virulence factor, the *P. gingivalis* PAD is responsible for deimination of human fibrinogen, leading to gingivitis and increasing the risk of rheumatoid arthritis.[13] The *P. gingivalis* PAD is omnipresent in the oral pathogen, but is absent in even closely related nonpathogenic species.[12] Extracellular arginine has been implicated in development of biofilm formation, with enzymes dedicated not only to deimination but also proteolysis of C-terminal arginine residues.[14] Unlike the human PAD, the *P. gingivalis* enzyme is not calcium-dependent and, in addition to accepting a variety of peptide and protein substrates, is

able to convert free arginine to citrulline.[15] Such substrate promiscuity is likely the result of a critical dependance on extracellular concentrations of arginine for *P. gingivalis* virulence. An arginine deiminase (ADI) secreted from *Streptococcus intermedius*, a commensal oral bacterium. *S. intermedius* inhibits *P. gingivalis* biofilm formation through decreasing the concentration of extracellular arginine. In arginine-starved conditions, the *P. gingivalis* fimbriae genes *fimA* and *mfa1,* which are virulence determinants necessary for biofilm formation, are dramatically downregulated.[16]

In contrast, little is known about the biosynthesis of citrulline in natural products. Few primary ureido-containing natural products have been identified. Currently, only 61 entries (excluding plant-derived molecules) in the Dictionary of Natural Products contain primary ureido groups, and many have not been matched to biosynthetic gene clusters (Figure 4.3). The majority are nonribosomal peptide (NRP) natural products such as enduracidin and azotobactin, in which the citrulline is thought to be directly installed into the nascent peptide,[17-18] but, to our knowledge, no PAD has been identified for RiPPs. By identifying natural products with this modification, we can gain a broader understanding of the importance of deimination and identify the citrullinating enzyme. However, detection of this modification is challenging due to the small mass change (NH→O, +0.98 Da) associated with the post-translational modification, a mass which is easily overlooked or assumed to be an isotope peak or with the deamidation of the substrate.[19] Therefore, citrulline-modified natural products are a prime candidate for characterization using RBS.

Herein, we describe the expansion of RBS as a biological tool to aid in the discovery of the enzyme responsible for peptidyl arginine deimination in bacteria. Repurposeing the work of Thompson,[20-21] the specific labeling of citrulline over arginine with a phenylglyoxal probe is rapidly achieved at low pH. We employed this reaction to confirm the presence of citrulline in a

subset of lasso peptides, and use the positive hits to conduct a bioinformatic screen to identify putative PADs. We compared the PAD enzymes from *Streptomyces glaucescens* and *Streptomyces albulus*, two confirmed producers of citrulline-containing lasso peptides, and found significant differences from the *P. gingivalis* PAD. We heterologously expressed the *S. albulus* and *S. glaucescens* PAD enzymes *in vitro* and tested for arginine deimination of lasso peptide precursors, and demonstrate for the first time the activity of a RiPP arginine deiminase. Finally, we conducted a bioinformatic survey of bacterial PADs to reveal their taxonomic breadth and the diversity of genomic contexts in which the PADs are encoded.

4.3 Results

In the course of characterizing lasso peptides as a proof-of-concept for a new natural product discovery and mass prediction program, a new family of lasso peptides was defined.[22] Lasso peptides have a very highly conserved lasso cyclase and highly conserved precursor peptide sequences. However, a subset of lasso peptides with a remarkably conserved precursor peptide (Figure 4.4) contain an additional modification: an enzymatic arginine deimination resulting in a citrulline-containing mature natural product (Figure 4.2). Additional posttranslational modifications to lasso peptides beyond isopeptide bond formation have been demonstrated, such as in the case of the phosphorylated lasso peptide paeninodin.[23] Despite conservation of the arginine residue directly C-terminal to the isopeptide bond (Figure 4.4), not all citrulassins contain the modified amino acid. High-resolution MS/MS confirmed that of the nine citrulassin producers screened, seven exported a lasso peptide that contained citrulline.[22]

Heterologous expression of the citrulassin A gene cluster from *S. albulus* along with 11 open reading frames (ORFs) upstream and 17 ORFs downstream of the citrulassin BGC resulted

in *des*-citrulassin A (i.e. arginine, rather than citrulline, was present in the natural product, Figure 4.5). This suggested that either (*a*) a distally encoded PAD was responsible, or (*b*) a PAD that was locally encoded was is nonfunctional in *Streptomyces lividans*.[22] However, none of the genes near the citrulassin BGC are homologous to any known PAD (Figure 4.5 and Table 4.2). We thus set out to characterize additional members of the citrulassin family as citrulline- or arginine-containing lasso peptides in order to determine the prevalence of the posttranslational modification and to guide the search the PAD responsible for the citrulline-containing variants.

4.3.1 Glyoxal probe validation for RBS

We selected a citrulline-specific reaction in order to more easily identify primary ureido-containing citrulassins by MALDI-TOF-MS. Thompson and coworkers have previously used phenylglyoxal probes at low pH to selectively label citrulline over arginine in eukaryotic cellular extracts (Figure 4.2).[20-21] At low pH, guanidino groups are protonated and thus inaccessible to reaction with glyoxal, but the neutral ureido group will react rapidly, resulting in robust labeling at 30 min and nearly complete conversion in 60 min at 37 ˚C in the example of histone H3 and using 10 molar excess probe.[20] The reaction has been further elaborated to more easily identify labeled species in complex samples with the use of 3-bromophenylgloyxal, which provides a distinct isotopic pattern and whose UV-absorbing properties impart increased signal intensity.[24] The glyoxal labeling reaction, while not suitable for acid-labile natural products, facilitates discovery of primary ureido-containing natural products from bacterial extracts, and can easily be modified to enrich for labeled compounds using a biotin-conjugated glyoxal probe.[20] As predicted, the free amino acid L-citrulline was robustly labeled unlike L-arginine under similar conditions (Figure 4.6). To test the reaction for selectivity on natural products, purified citrulassin A from *Streptomyces albulus* B-3066 and purified des-citrulassin A (heterologously expressed in *S.*

lividans[22]) were treated with 5 molar equivalents of 3-bromophenylglyoxyl for 30 min at 37 ˚C in 75% MeCN with 20% (*w/v*) trichloroacetic acid. Under these conditions, citrulassin A was robustly labeled while no observable product was observed for des-citrulassin A (Figures 4.7 and 4.8). The non-ribosomal peptide antipain, a protease inhibitor, was resistant to the probe, unlike deimino-antipain, a recently-identified citrulline-containing analog of antipain also from *S. albulus* B-3066 (Figure 4.9).[5] Next, we harvested *S. albulus* B-3066 cultured for 7 days at 30 ˚C on ATCC172 media, extracted exported compounds from the cells with MeCN, and tested the probe in the crude extract diluted to contain 20% (*w/v*) trichloroacetic acid. The lasso peptide was in very low abundance in the crude extract, but along with the ~1:1 abundance of ^{79}Br:^{81}Br, substantial label-assisted signal enhancement enabled identification of labeled citrulassin A (Figure 4.7). Thus, pramary ureido-containing natural products are an ideal target for RBS, and the glyoxal probe is an effective labeling strategy for aiding in the discovery of ureido-functionalized natural products.

4.3.2 RBS of predicted citrulassin producers

Next, we sought to identify which members of the citrulassin family of lasso peptides were post-translationally modified with a PAD (Figure 4.2). Previous screening of extracts suggested that not all citrulassins contained a citrulline,[22] but because of the small mass difference between guanidino-containing and ureido-containing products, we elected to test for the presence of citrulline using the 3-bromophenylglyoxal probe. We thus obtained a selection of 80 strains from the Agriculture Research Service (ARS) Culture Collection and, after a 7 d cultivation at 30 ˚C, the bacteria were harvested and metabolites were extracted from the cell surface using MeCN over a 24 h time period at 22 ˚C. Reactions were performed directly on crude organic-extracted cell surface extracts, desalted, and analyzed by MALDI-TOF-MS for the presence of primary ureido groups in the 1500 – 2200 Da mass range. Not all organisms produced an identifiable citrulassin

under the growth conditions tested, and extracts of bacteria cultured on ATCC172 media were generally most likely to contain detectable levels of natural products in the mass range of interest. Those that did produce a predicted citrulassin were screened for the mass of the labeled citrulassin (Figure 4.10). Twenty-six strains were confirmed to produce the predicted citrulassin, and of those, nineteen were validated with the 3-bromophenylglyoxal probe to contain citrulline.

4.3.3 Comparative genomics to identify peptidyl arginine deiminases

In order to determine the enzyme responsible for deimination of the citrulassins, we performed comparative genomics using the Joint Genome Institute Integrated Microbial Genomes and Microbiome Samples Phylogenetic Profiler for Single Genes (https://img.jgi.doe.gov). With the subset of citrulline-producing species whose genomes were available in the program, we performed partial phylogenetic profiling to compare the genomes of citrulassin producers and des-citrulassin producers using *S. glaucescens* GLA.O as the genome against which other species were initially compared. None of the homologs unique to the citrulline producers were identified as PADs, but the isochorismatase is in the genomic neighborhood of a hypothetical PAD from PF03068 in *S. glaucescens* GLA.O (Figure 4.11, Table 4.3). By performing an iterative BLAST-P search using the *S. glaucescens* putative PAD, we confirmed that the strains that strains producing arginine-containing citrulassins lacked a homolog to the *S. glaucescens* PAD. We thus set out to bioinformatically characterize the bacterial PAD.

4.3.4 Comparison with other characterized PADs

While the bacterial PAD is classified within in the same Pfam as eukaryotic PADs (PF03068), the sequence identity is only 20 - 28% between each of the six families of *Homo sapiens* PADs and the PAD from *S. glaucescens* (Table 4.5). Unlike members of PF03068, the *P. gingivalis* PAD is not calcium-dependent and does share a conserved active site with *S. albulus*, *S. glaucescens*, and

H. sapiens. In contrast, the *S. glaucescens* and *S. albulus* PADs have 70% identity and an even higher degree of similarity. In spite of the low sequence identity, an alignment of *S. glaucescens* PAD with the *H. sapiens* PAD4 shows conservation of active site residues (Figure 4.12). The *H. sapiens* PADs are calcium-dependent enzymes with a conserved catalytic Cys645 and stabilizing triad of Asp350-His471-Asp473.[25]

The *P. gingivalis* PAD, a member of Pfam PF04371, is responsible for deimination of human fibrinogen and is essential for *P. gingivalis* pathogenesis.[12, 26] This enzyme is highly conserved in all sequenced strains of *P. gingivalis* (Figure 4.13), but has no homolog in *S. glaucescens* or other confirmed citrulassin producers. The *P. gingivalis* PAD has only 18% identity to the *S. glaucescens* PAD, which also has low identity to the *S. intermedius* PAD involved in inhibiting *P. gingivalis* biofilm formation (Table 4.4). The low degree of identity is also reflected in a lack of alignment in the active site residues, and furthermore suggests that the *S. albulus* and *S. glaucescens* PADs accept different substrates than the *P. gingivalis* PAD despite a similar enzymatic activity.

4.3.5 Genetic context of the bacterial PAD

The *S. glaucescens* hypothetical protein, putatively named a PAD and part of the Pfam PF03068, was used to generate a dataset of 224 unique bacterial PADs using an iterative BLAST-P query against all bacterial genomes in the nonredundant database in GenBank.[27] Protein accession numbers were compiled and sequentially analyzed with RODEO,[22] and then used to generate a sequence similarity network (SSN) in order to illustrate taxonomic relationships and phylogenetic distribution (Figure 4.14).[28] Diverse phyla (*Actinobacteria*, *Cyanobacteria*, *Firmicutes*, *Proteobacteria*, and *Sphingobacteria*) are represented, but the PF03068 PAD is not widespread in bacteria. In contrast, members of PF04371, of which the *P. gingivalis* enzyme is a member, are pervasive across prokaryotes and especially prevalent in *Actinobacteria* and *Firmicutes*, of which

P. gingivalis is a member (Figure 4.13). Instead, many PADs closely related to the *S. glaucescens* enzyme are found within *Actinobacteria* and in particular the genus *Streptomyces*, but are not pervasive within any one genus. Importantly, none of the RBS-confirmed des-citrulassin producers are predicted to contain a PAD.

There is no indication of horizontal gene transfer (HGT), as proteins clustered with other PADs from species within the same phylum (Figure 4.14). Additionally, the %GC content is nearly identical to the overall organism %GC.[29] (Figure 4.15). These data indicate the bacterial PAD is not widespread due to HGT, although we cannot rule out the possibility that the gene was acquired by organisms having similar GC content. Intriguingly, two outliers contain lasso peptide BGCs, but the *Leptolyngbya* BGC does not encode a citrulassin precursor. *Streptomyces* sp. NRRL F-5140, contains a citrulassin BGC and the product was detected from bacteria grown on ATCC172 (Figure 4.16), indicating an active enzyme. Species with similar GC content in the PAD nucleotide sequence are from *Cyanobacteria*, which may suggest that *Streptomyces* sp. NRRL F-5140 acquired the gene from a member of this phylum.

The co-occurrence analysis of genes (± 8 ORFs) shows an abundance of genes related to transport and transcriptional regulation (Table 4.3). However, the PADs do not appear to be contained within defined BGCs. Using genome neighborhood network analysis, we compared ORFs between PADs that clustered together based on sequence similarity (Figure 4.16). Even PADs with a high degree of similarity appear in diverse genome neighborhoods, which do not bear resemblance to RiPP biosynthetic gene clusters. Thus, the PAD likely exerts its activity on a distally encoded substrate.

4.3.6 *In vitro* reconstitution of the *Streptomyces* PAD

The *S. albulus* B-3066 PAD is a predicted cytosolic protein, unlike the exported *Streptococcus intermedius* enzyme, with no transmembrane regions.[16, 30] We therefore sought to reconstitute the enzymatic activity and test the citrulassin A precursor peptide (CitA) as a substrate for the bacterial PAD *in vitro*. CitA was cloned from *S. albulus* B-3066 (producer of citrulassin A) and *S. glaucescens* B-2900 (producer of citrulassin E) and overexpressed in *E. coli* with an N-terminal, tobacco etch virus (TEV)-cleavable maltose-binding protein (MBP) tag (Figure 4.18). The hypothetical PADs (Accession numbers: *S. albulus*, WP_064069846.1; *S. glaucescens*, AIR96488.1) were also cloned and overexpressed in the pET28 vector.

The purified enzymes were tested for activity using an enzyme-linked immunosorbent assay.[31] While the assay does not allow for localization of the newly formed citrulline residue(s), it is independent of mass spectrometry techniques which are not highly accurate for such large peptides (MBP-CitA has a mass of about 50 kDa). PAD activity was tested both in the presence and absence of 5 μM TEV, as flocculent precipitate was observed when the MBP tags were cleaved *in situ*. MBP-CitA was treated with purified PAD, reactions were quenched with an equivalent volume of 50% TCA and immediately subjected to probe labeling with a biotin-conjugated glyoxal (Figure 4.18). As a control, MBP-tagged CitA was subjected to identical conditions without the addition of enzyme. After 1 h at 37 ˚C, the probe reactions were quenched with a saturated solution of citrulline. Proteins were resolubilized with urea, separated by SDS-PAGE and electroblotted. PAD activity, indicated by biotin-glyoxal labeling and secondary interaction with Streptavidin-HRP conjugate, was visualized by enhanced chemiluminsecence (ECL).[20] Slight nonspecific labeling of the arginine-containing control peptide was observed (Figure 4.18), but notable signal enhancement occurred in samples treated with MBP-PAD. Robust labeling is indicative of PAD

activity, although the location of the citrulline within the peptide remains to be determined and is an ongoing area of investigation. However, MBP does not appear to be the substrate, as cleavage of the peptide *in situ* results in a loss of luminescence associated at the mass of MBP (Figure 4.18). Notably, the PAD shows low specificity for the native substrate, as the PAD from *S. albulus* was able to process CitA from *S. glaucescens* in addition to the Arg-containing substrates MBP-BamA, MBP-TbtA A19R, and MBP-TbtA A25R (data not shown). This suggests that citrulassin library generation is possible, and that the PAD could be used to install citrullines on the precursor peptides of other classes of RiPPs.

4.4 Conclusion

In this study, we employed a citrulline-specific probe to selectively label and subsequently identify citrulline-containing natural products from bacterial extracts. This technique, called reactivity-based screening (RBS),[4-5, 7] has been previously used to discover and characterize natural products modified with aldehydes, ketones, and Michael acceptors, but was expanded to allow for identification of the bacterial enzyme responsible for the posttranslational deimination of primary guanidino groups. The new family of bacterial PADs appear in diverse genomic contexts rather than within RiPP biosynthetic gene clusters. Through heterologous expression and *in vitro* enzyme assays, it was determined that the PAD does act as a peptidyl arginine deiminase, although its specificity for specific arginine residues within a peptide remains to be determined. Further work will establish rules for enzyme selectivity through extensive MS analysis and additional enzymatic assays on alternative arginine-containing RiPP precursor peptides.

4.5 Methods

4.5.1 General materials and methods

Reagents for molecular biology experiments were purchased from New England BioLabs (Ipswich, MA), Thermo Fisher Scientific (Waltham, MA), and Gold Biotechnology Inc. (St. Louis, MO). Chemicals were purchased from Sigma-Aldrich (St. Louis, MO) and New England BioLabs. Plasmid maintenance and protein overexpression were carried out using *Escherichia coli* DH5α and BL21 (DE3) strains, respectively.

4.5.2 Bacterial growth and extraction

Unless otherwise noted, *Streptomyces* strains were streaked from frozen 50% glycerol backstocks onto ATCC 172 plates (15 g/L agar, 10 g/L glucose, 20 g/L soluble starch, 5 g/L yeast extract, 5 g/L N-Z Amine Type A, 1 g/L $CaCO_3$, autoclaved). Single colonies from plates were used to inoculate 5 mL liquid ATCC 172 cultures. Plates and liquid cultures were incubated at 30 ˚C for 7 days prior to use. Cells were harvested from plates using a sterile razor blade and transferred to sterile 15 mL conicals containing 1 – 5 mL MeCN. Compounds were extracted from cells for 16 h at 22 ˚C with moderate agitation prior to centrifugation (4,000 × *g*, 10 min) and decanting into 20 mL scintillation vials. Extracts were used immediately or dried by speed vacuum and stored at -20 ˚C and redissolved in MeCN prior to use.

4.5.3 Citrulassin A isolation and purification

Citrulassin A was extracted from *S. albulus* B-3066 and purified by high performance liquid chromatography as described previously.[22]

4.5.4 Citrulline labeling reaction

In general, reactions were carried out in freshly prepared 20% trichloroacetic acid (TCA) with 50 – 75% aq. MeCN. Bromophenylglyoxal hydrate was prepared as a stock solution (10 mM in

DMSO). Purified compounds were dissolved at a concentration of 10 μM before the addition of bromophenylglyoxal hydrate to a concentration of 10 μM. After 30 min at 37 ˚C, reactions were quenched by the addition of an equivalent volume of saturated L-citrulline in slightly acidified water. Samples were dried by speed vacuum, redissolved in water, and desalted prior to analysis. Reactions on crude cellular extracts were performed by diluting 10 μL of cell extract (in MeCN) with 10 μL of 40% TCA in 50% aq. MeCN and treating with 1 μL of the bromophenylglyoxal hydrate stock solution.

4.5.5 Molecular biology techniques

Oligonucleotides were purchased from Integrated DNA Technologies Inc. (Coralville, IA). The gene encoding CitA was amplified from *S. glaucescens* B-2900 and the genes encoding the PAD from *S. albulus* B-3066 and *S. glaucescens* B-2900 were amplified from genomic DNA using the primers listed in Table 4.1. The DNA was purified using a QIAprep Miniprep Kit (Qiagen). The purified DNA was digested with BamHI-HF and XhoI-HF, and then purified by gel extraction on a 1% (*w/v*) agarose gel using a QIAQuick gel extraction kit (Qiagen). The pET28 vector, encoding an N-terminal MBP tag with at TEV proteolysis site, and an Arg_3 motif in the case of the CitA precursor, was likewise digested and purified. digested with BamHI-HF and XhoI-HF and purified using a QIAQuick gel extraction kit (Qiagen). Ligation reactions with T4 DNA Ligase (NEB) were used to transform chemically competent *E. coli* DH5α cells. The cells were plated onto Luria-Bertani (LB) agar plates supplemented with 50 μg/mL kanamycin and grown at 37 ˚C. Resulting colonies were propagated in LB broth (50 μg/mL kanamycin) for 16 h at 37 ˚C prior to plasmid isolation using a QIAprep Spin Miniprep Kit. The constructs were sequenced using MBP forward primer and T7 reverse primer at ACGT Inc. (Wheeling, IL) (Table 4.1).

The co-expression of the citrulassin gene cluster and the PAD was achieved by cloning into a pCDFDuet vector. The backbone was amplified using the primers listed in Table 4.1 and the PAD and gene cluster were amplified from genomic DNA. The inserts and backbone were purified using gel extraction as described above. Stepwise insertion of the gene cluster and then the PAD was accomplished with Gibson one-step isothermal DNA assembly.[32] The resulting constructs (10 μL) were used to transform *E. coli*, propagated, and sequenced as described above.

4.5.6 Expression and purification of MBP-PAD and MBP-CitA

Chemically competent *E. coli* BL21 (DE3) cells (50 μL) were transformed with 100 ng purified pET28 plasmid constructs using heat shock, and cells were plated onto LB agar plates containing 50 μg/mL kanamycin. After growing for 12 h at 37 ˚C, single colonies were used to inoculate 5 mL LB cultures (50 μg/mL each kanamycin and chloramphenicol) and grown for 16 h at 37 ˚C. The 5 mL cultures were used to inoculate 500 mL cultures of Terrific Broth (TB) media (24 g/L yeast extract, 12 g/L tryptone, 0.4% (*v/v*) glycerol, 17 mM KH_2PO_4, 72 mM K_2HPO_4), supplemented with kanamycin and chloramphenicol, and grown to a final OD_{600} of 0.6 – 0.8. Protein overexpression was induced by dropping the temperature of the cultures to 16 ˚C for 16 h and supplementing with 0.4 mM isopropyl β-D-1-thiogalactopyranoside (IPTG). Cells were harvested by centrifugation (4,000 × *g*, 10 min, 4 ˚C), washed with phosphate-buffered saline (PBS, 137 mM NaCl, 2.7 mM KCl, 10 mM Na_2HPO_4, 1.8 mM KH_2PO_4, pH 7.6) and centrifuged a second time. Cell pellets were stored at -20 ˚C for 8 h before use.

Purification using amylose resin was carried out as described previously.[33] Briefly, cell pellets were thawed on ice and resuspended in lysis buffer (50 mM Tris-HCl pH 7.5, 150 mM NaCl, 2.5% (*v/v*) glycerol, 0.1% Triton X-100, 4 mg/mL lysozyme, 2 μM leupeptin, 2 μM benzamidine, 2 μM E64, 2 μM PMSF). After 15 min at 4 ˚C, cells were homogenized by sonication

(3 × 40 s, 10 min apart) and the insoluble fraction was separated by centrifugation (20,000 × *g*, 60 min, 4 ˚C).

4.5.7 *In vitro* PAD activity testing

100 μM MBP-CitA was treated with MBP-PAD (10 μM) in reaction buffer (50 mM HEPES [pH 7.6], 50 mM NaCl, 10 mM CaCl2, 2 mM DTT) for 1 h at 37 ˚C or for various lengths of time at 22 ˚C. Control reactions were set up with an equivalent volume of protein storage buffer in place of MBP-PAD. Reactions were quenched with the addition of an equivalent volume of 50% TCA and immediately reacted with phenylglyoxal-biotin (final concentration 50 μM) for 1 h at 37 ˚C. The reaction was quenched with a solution saturated citrulline.

Proteins were resuspended by neutralizing the solution and adding 2 volumes of 1 M urea. For Western blot detection of PAD activity, 5-10 μg of MBP-CitA was separated on 12% SDS-PAGE and transferred by immunoblot (Towbin buffer [25 mM Tris, 192 mM glycine, 20% MeOH], 45 V, 2 h, 4 ˚C) to Immobilon-P membrane (EMD Millipore). The membrane was blocked with 5% bovine serum albumin in TBS-T (100 mM Tris [pH 7.6], 100 mM NaCl, 0.1% Tween-20) for 2 h at 22 ˚C prior to treatment with streptavidin-horseradish peroxidase conjugate (0.5 μL, 1:20,000) in TBS-T for 60 min at 22 ˚C. The membrane was washed with TBS-T (5 mL; 3 × 30 s and 3 × 5 min) before visualization using Pierce ECL Western Blotting Substrate and imaging using the Chemiluminsecence HR setting on a Bio-Rad ChemiDoc.

4.5.8 Phenylglyoxal-biotin preparation

The phenylglyoxal-biotin probe was prepared from azidophenyglyxoal (1 mM) and biotin-PEG4-alkyne (1 mM) in 50% DMSO with 10 mM $CuSO_4$, 1 mM tris(3-hydroxypropyltriazolylmethyl)amine (THPTA), and 10 mM $C_6H_7NaO_6$. The reaction was stirred at 37 ˚C for 1 h and added without further purification to *in vitro* PAD reactions.

4.5.9 Partial phylogenetic profiling

Differences in genomes of citrulassin producers and des-citrulassin producers were determined using the Joint Genome Institute Integrated Microbial Genomes and Microbiome Samples (JGI IMG/M) (https://img.jgi.doe.gov).[34] The *S. glaucescens* GLA.O genome was intersected for homologs in citrulassin producer species *S. albulus, S. griseus, S. orientalis,* and *A. orientalis*. The single genes analysis was processed by subtracting genes with homologs in *S. avermitilis*, *S. auratus,* and *S. natalensis.*

4.5.10 Sequence similarity network (SSN) generation

SSNs were generated using EFI-EST (http://efi.igb.illinois.edu/efi-est/).[28] The network was generated using an alignment score cutoff of e^{-150} as a clustering threshold. The network was visualized using the Organic layout within Cytoscape v. 3.4.0[35] and Adobe Illustrator.

4.5.11 Genome neighborhood network (GNN) generation

GNNs were generated using EFI-GNT (http://efi.igb.illinois.edu/efi-gnt/index.php). The program currently accepts only SSNs generated from Pfam or BLAST searches, not user-generated SSNs, so the *S. glaucescens* PAD was used in a BLAST search for homologous enzymes. The resulting SSN (with an alignment score cutoff of e-^{150} was uploaded to EFI-GNT. Neighborhood size was set to 10 and lower limit for co-occurrence was set to 20%. Only bacterial species were included in the subsequent GNN analysis (n = 79).

4.5.12 Analysis of GC content

The %GC of nucleotide sequences for a representative set of bacterial peptidyl arginine deiminases (n = 160) were calculated and plotted against NCBI Taxonomy records of the organism %GC content. The best-fit line was drawn using linear regression and had a slope of 0.98 with an R^2 of

0.98. Outliers with a greater than 5% deviation from the best-fit line (n = 4) were highlighted. Program script was written by Parth Patel.

4.5.13 Sequence logo generation

The precursor peptides of the 55 characterized citrulassins found using BLAST and RODEO[22] were aligned using MUSCLE v.3.8.31[36] prior to sequence logo generation using WebLogo 2.8.2 (http://weblogo.berkeley.edu/).[37]

4.5.14 Percent identity matrix and sequence alignment

The following accession numbers were used: *Homo sapiens*, NP_036519.2; *P. gingivalis*, WP_01245737.1; *S. intermedius*, AFV46229.1; *S. albulus*, WP_064069846.1; *S. glaucescens*, AIR96488.1. FASTA sequences were analyzed using EMBL-EFI Multiple Sequence Comparison by Log-Expectation (MUSCLE) (www.ebi.ac.uk/Tools/msa/muscle).

4.5.15 MALDI mass spectrometry

Cell extracts were screened using matrix-assisted laser desorption/ionization time-of-flight mass spectrometry (MALDI-TOF MS). After desalting samples, 1 µL aliquots were co-spotted with 1 µL 50% aq. MeCN (0.1% formic acid) saturated with α-Cyano-4-hydroxycinnamic acid(CHCA).

4.5.16 High resolution mass spectrometry

Purified and desalted compounds were dissolved in 75% MeCN with 1% AcOH and subjected to centrifugation (17,000 × g, 5 min). Samples were infused onto a ThermoFisher Orbitrap Fusion ESI-MS using an Advion TriVersa NanoMate. The MS was calibrated weekly using calibration mixture, following manufacturer instructions, and tuned daily with Pierce LTQ Velos ESI Positive Ion Calibration Solution (ThermoFisher). Spectra were collected in profile mode with a resolution of 100,000. Ions were selected for fragmentation in the Ultra-High-Field Orbitrap Mass Analyzer using an isolation width of 2 *m/z*, normalized collision energies of 20-35, an activation q value of

0.4, and an activation time of 30 ms. Data analysis was performed using Thermo Xcalibur software.

4.6 Acknowledgments

Dr. Tucker Maxson provided deimino-antipain and the heterologous expression system for des-citrulassin A. Parth Patel provided the script for %GC analysis. Graham A. Hudson aided in cloning of the citrulassin precursor peptides and peptidyl arginine deiminases.

4.7 Figures

Figure 4.1 Strategy for reactivity-based screening (RBS). The gene of interest is used to mine bacterial genomes for biosynthetic gene clusters. Prioritized strains are cultured, harvested, and extracted with organic solvents. Reactions with the RBS probe are performed in the extract and analyzed by MALDI-TOF-MS for new peaks compared to the unlabeled extract that are associated with the mass of the probe. Labeled species are selected for further purification and characterization.

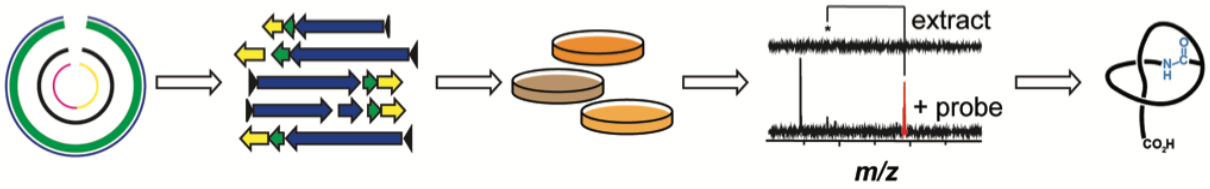

Figure 4.2 PAD enzyme activity and reactivity-based screening strategy for identification of citrulline-containing natural products. (A) Proposed mechanism for enzyme-dependent arginine deimination. (B) Phenylgloxal probes, such as 3-bromophenylglyoxal (**1**) selectively react with citrulline at low pH.

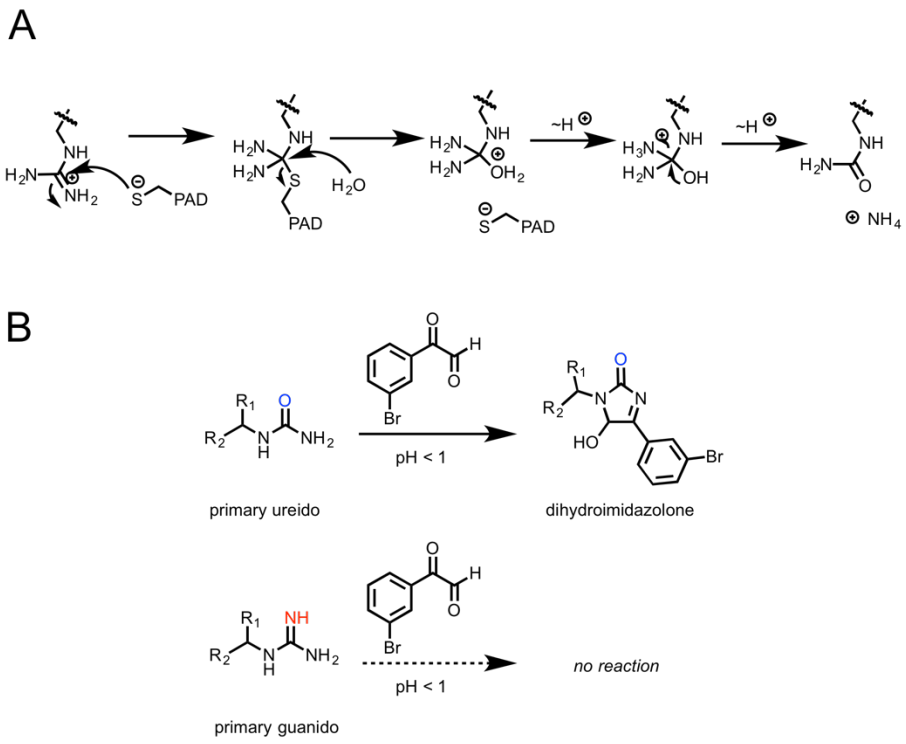

Figure 4.3 Representative structures of primary ureido-containing natural products, generally divided into categories based on biosynthetic pathways. The citrulassins, represented by citrulassin A (**2**), are currently the ownly known RiPPs containing citrulline.

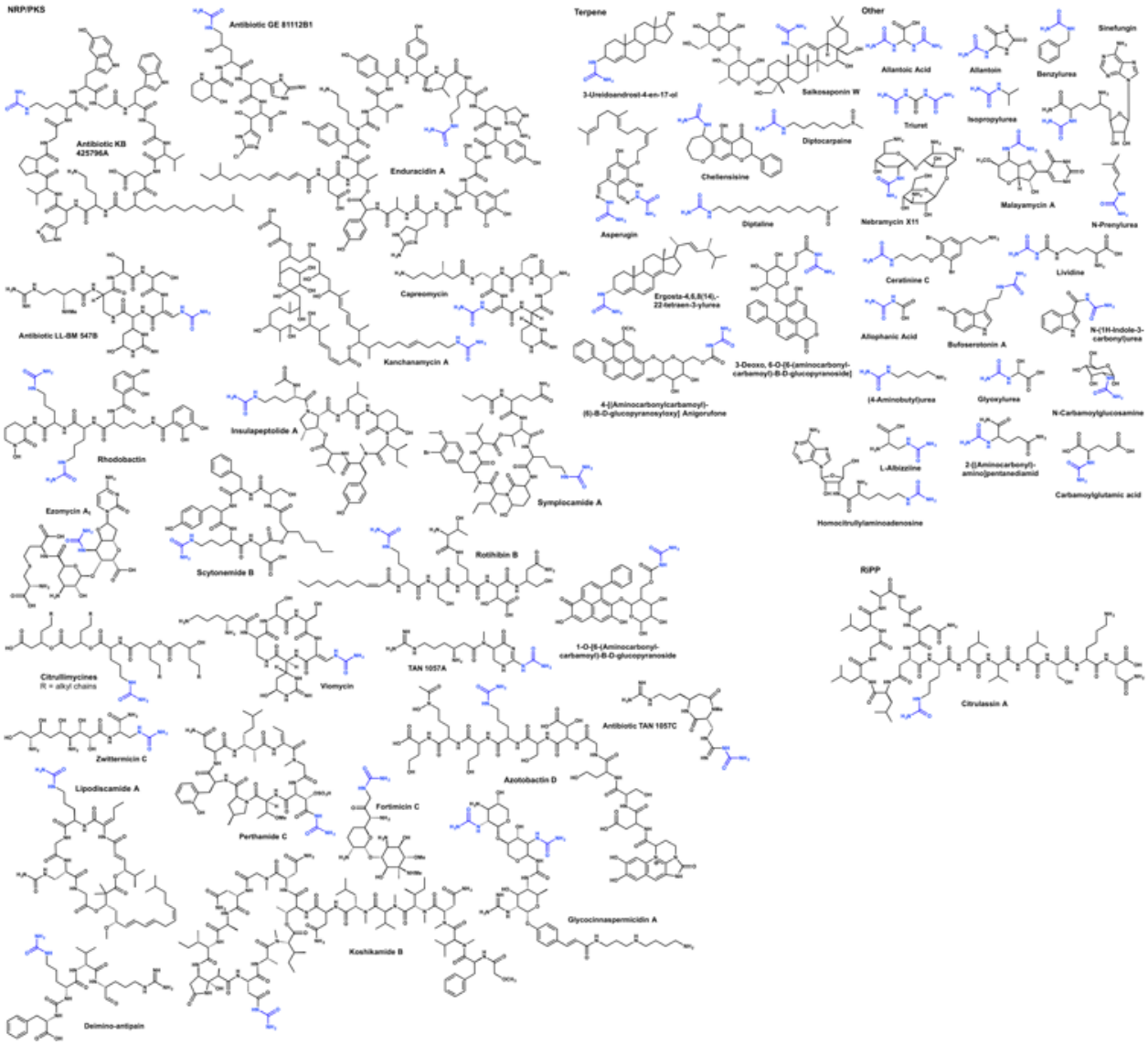

Figure 4.4 Multiple sequence alignment (http://weblogo.berkeley.edu/logo.cgi) of the 55 bioinformatically-discovered citrulassin precursor peptides shows remarkable sequence homology, especially in the core peptide region. Isopeptide bond formation between the side chain aspartic acid and N-terminus of the core peptide is indicated with a black bar. Arginine residue which is post-translationally modified to citrulline is indicated with an asterisk.

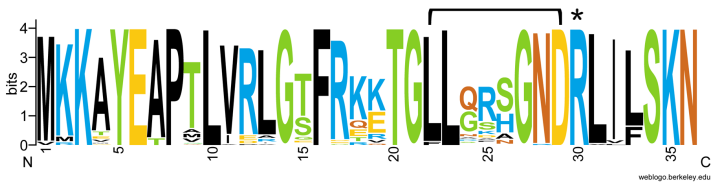

Figure 4.5 Genomic context of the citrulassin A biosynthetic gene cluster cloned from *Streptomyces albulus* B-3066 and structural characterization of the heterologously expressed lasso peptide. (A) None of the genes within the neighborhood of the citrulassin A cluster, which were heterologously expressed in *S. lividans*, have homology to known peptidyl arginine deiminases. (B) High resolution mass of des-citrulassin A (**3**), extracted from *S. lividans*. (C) Collision-induced dissociation (CID) spectrum of des-citrulassin A with b- and y-ions indicated in blue and orange, respectively. (D) Bubble diagram of des-citrulassin A marked with b- and y-ions from (C). (E) Mass list of fragment ions from (C) used to confirm the presence of arginine in *des*-citrulassin A. Figure adapted from Tietz & Schwalen, *et al* (2016).[22]

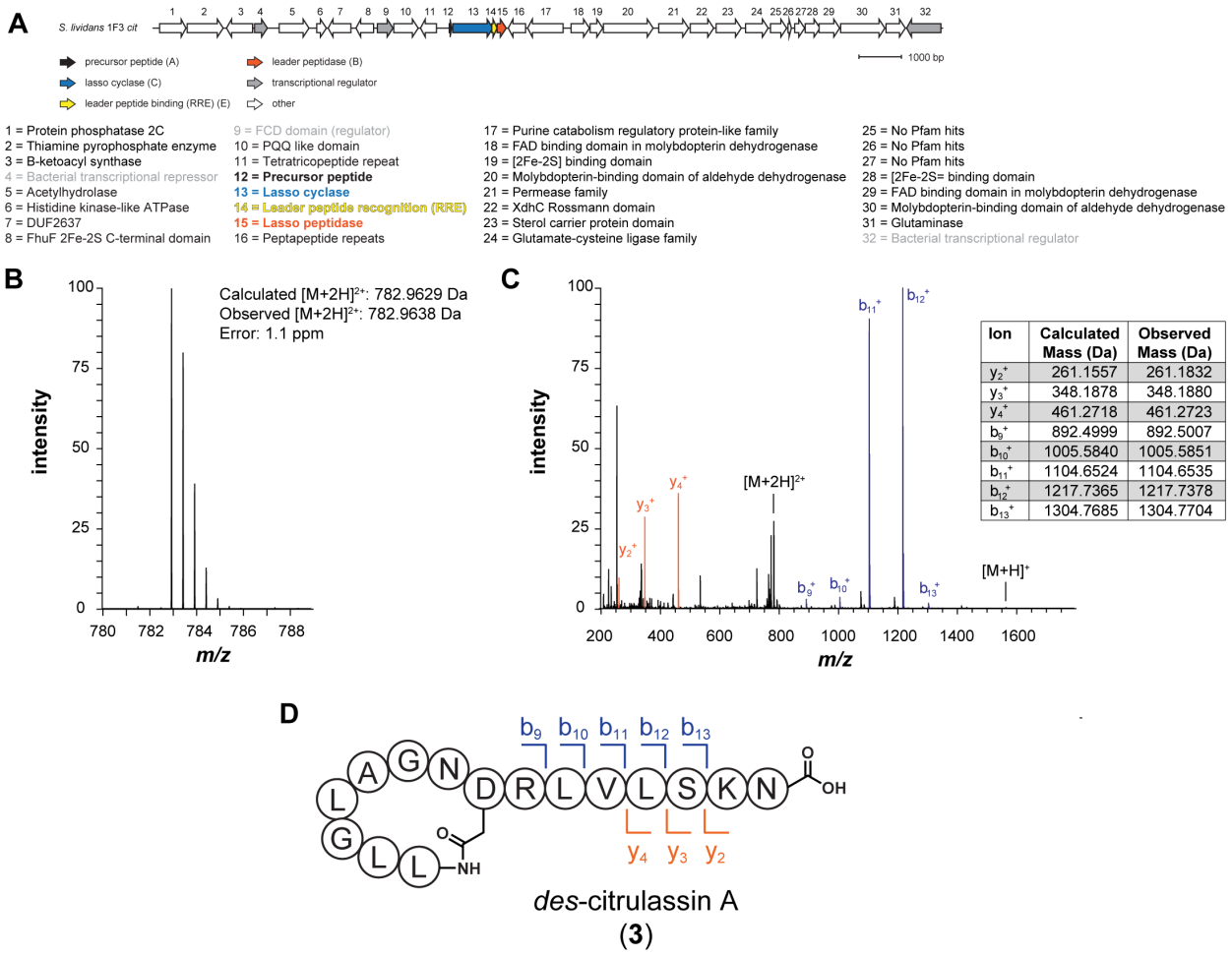

Figure 4.6 3-Bromophenylglyoxal in 20% (*w/v*) trichloroacetic acid does not react with (A) the free amino acid arginine but will label (B) citrulline under identical conditions. Reactions were analyzed by ESI-MS.

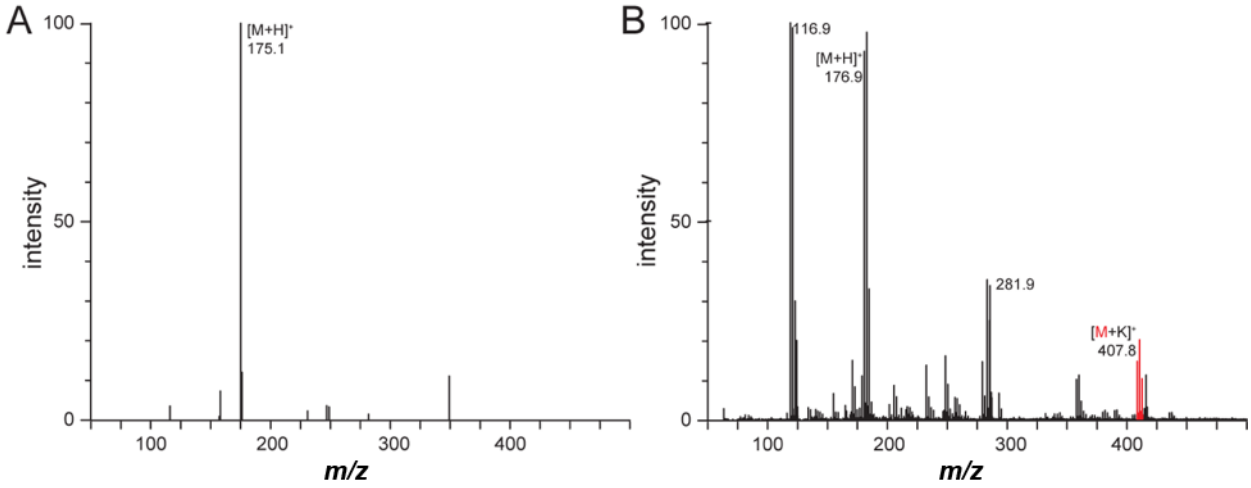

Figure 4.7 Confirmation of glyoxal reaction selectivity and robustness. (A) MALDI-TOF-MS of of purified citrulassin A (unreacted, top) reacted with 3-bromophenylglyoxal (bottom). (B) MALDI-TOF-MS of heterologously expressed and purified *des*-citrulassinA (unreacted, top) and reacted under identical conditions as citrulassin A (bottom). (C) MALDI-TOF-MS of *Streptomyces albulus* B-3066 (citrulassin A producer) extract, either unreacted (top) or reacted with probe (bottom). The labeled peak is expanded (inset) to show the altered labeling pattern resulting from the bromine-containing probe.

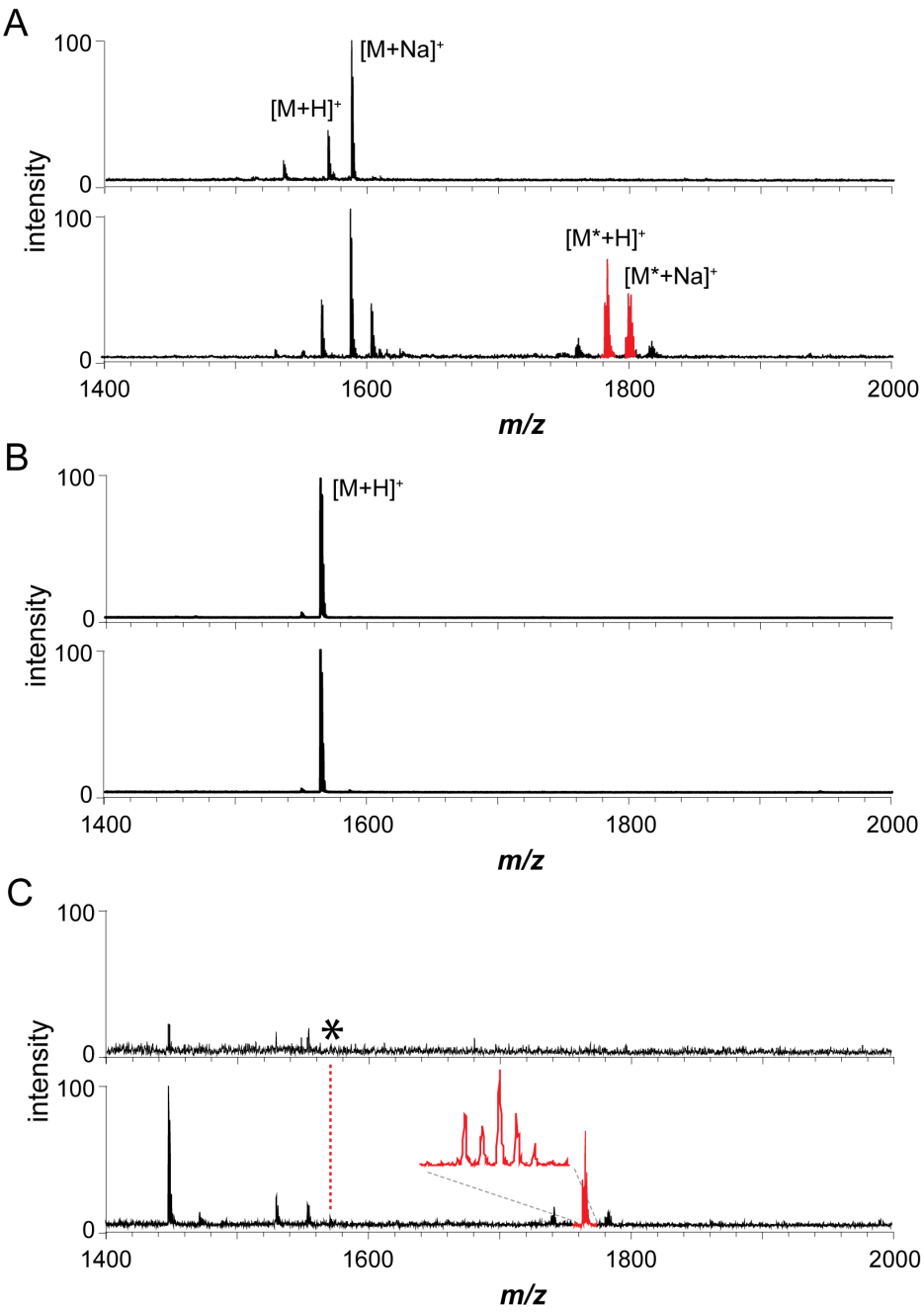

Figure 4.8 Structural characterization of 3-bromophenylglyoxal labeled citrulassin A. (A) High resolution mass spectrum of the $[M+2H]^{2+}$ of labeled citrulassin A. (B) CID spectrum of the $[M+2H]^{2+}$ ion. Labeled peaks correspond to identified b- and y- ions, identified in the table. (C) Schematized bubble diagram of labeled citrulassin A used to confirm the location of the probe.

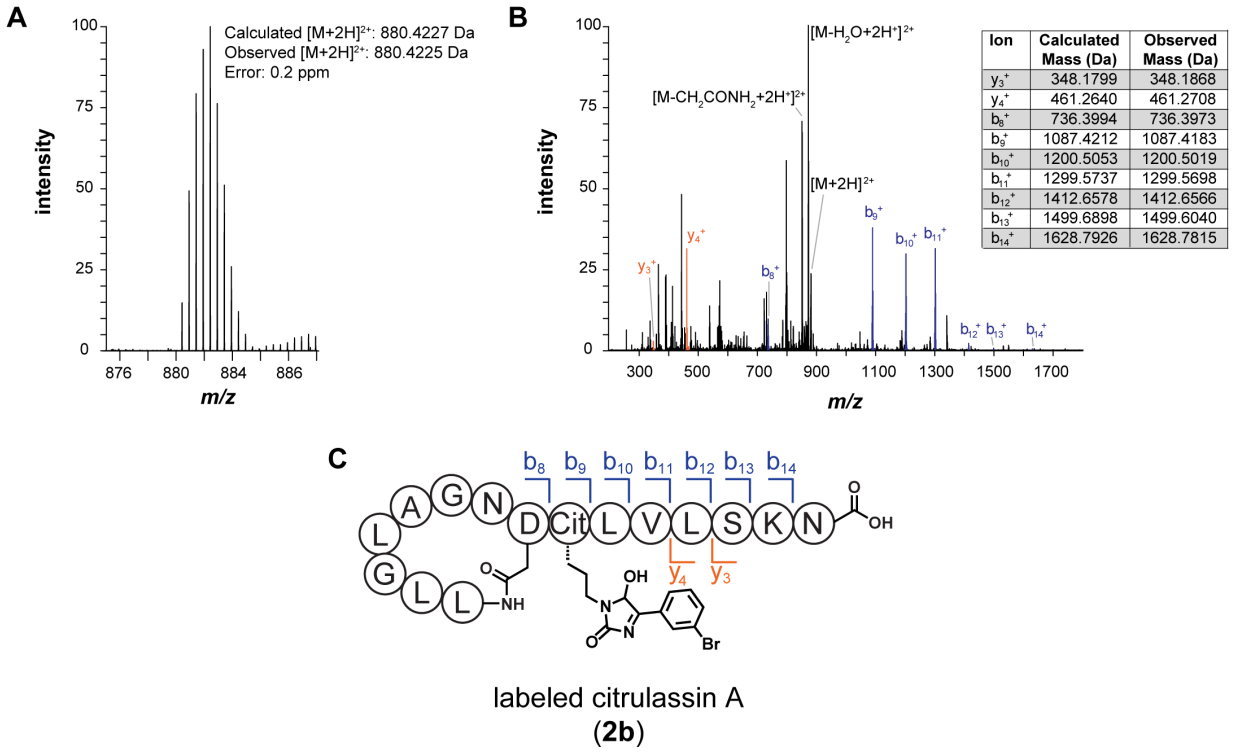

Ion	Calculated Mass (Da)	Observed Mass (Da)
y_3^+	348.1799	348.1868
y_4^+	461.2640	461.2708
b_8^+	736.3994	736.3973
b_9^+	1087.4212	1087.4183
b_{10}^+	1200.5053	1200.5019
b_{11}^+	1299.5737	1299.5698
b_{12}^+	1412.6578	1412.6566
b_{13}^+	1499.6898	1499.6040
b_{14}^+	1628.7926	1628.7815

Figure 4.9 3-Bromophenylglyoxal robustly labels natural products containing citrulline such as (A) deimino-antipain (**5a**), but will not react with (B) arginine-containing antipain (**6**) under identical conditions.

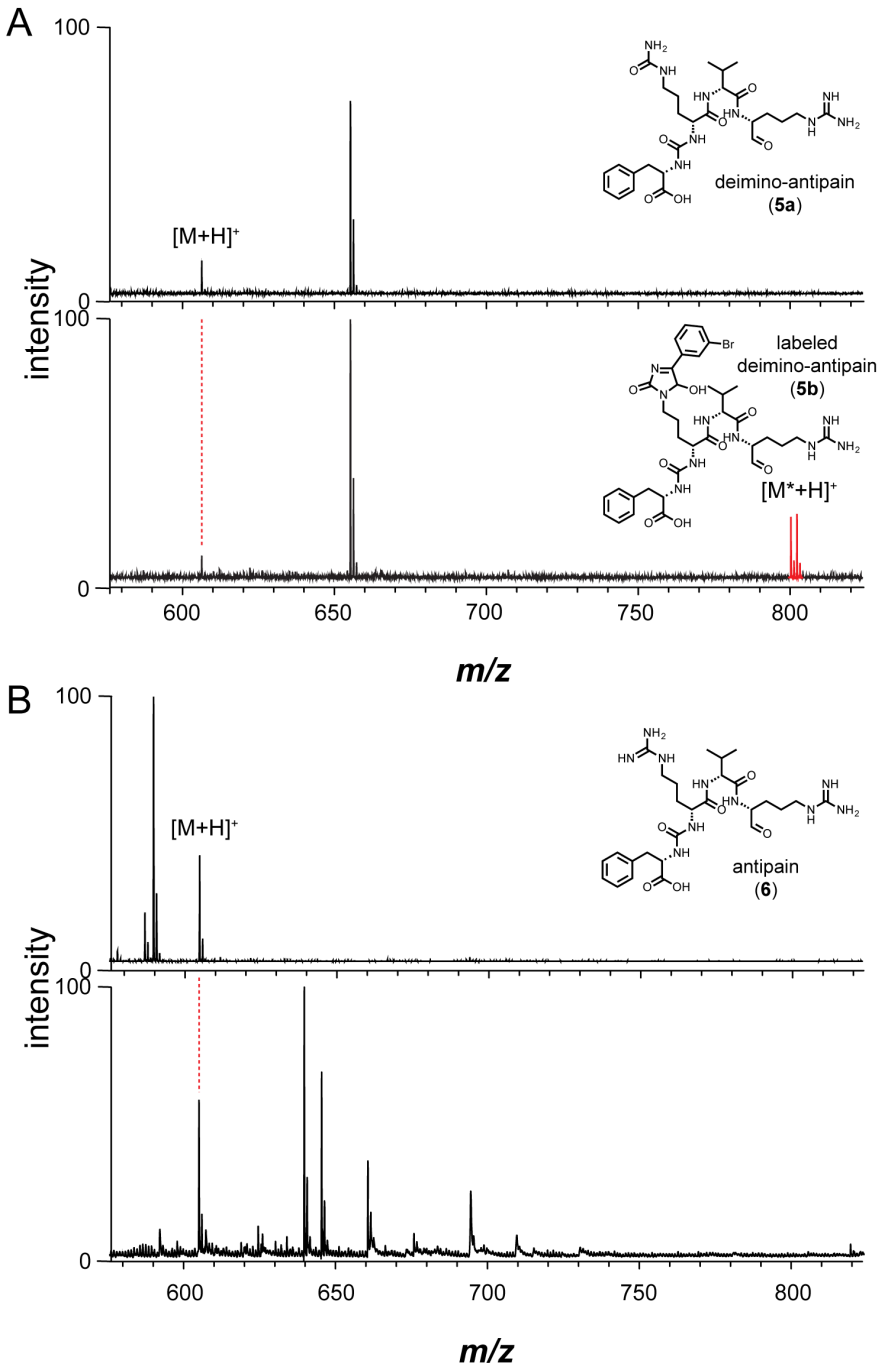

Figure 4.10 Representative spectra from the screening of citrulassin producers with the bromophenylglyoxal probe. Labeled products are highlighted in red, with the corresponding citrulline shown in the amino acid sequence. Unmodified arginine residues in the des-citrulassin samples are in bold. Extracts from (A) *S. aurantiacus* B-2806, (B) *S. katrae* NRRL B-16271, (C) *S. glaucescens* B-2900, (D) *S. avermitilis* B-16169, (E) *S. sp.* NRRL S-1813, (F) *S. natalensis* B-5314, (G) *S. mutabilis* ISP-5169, (H) *S. alboniger* B-1820, (I) *S. auratus* 8097, and (J) *A. orientalis* B-5485.

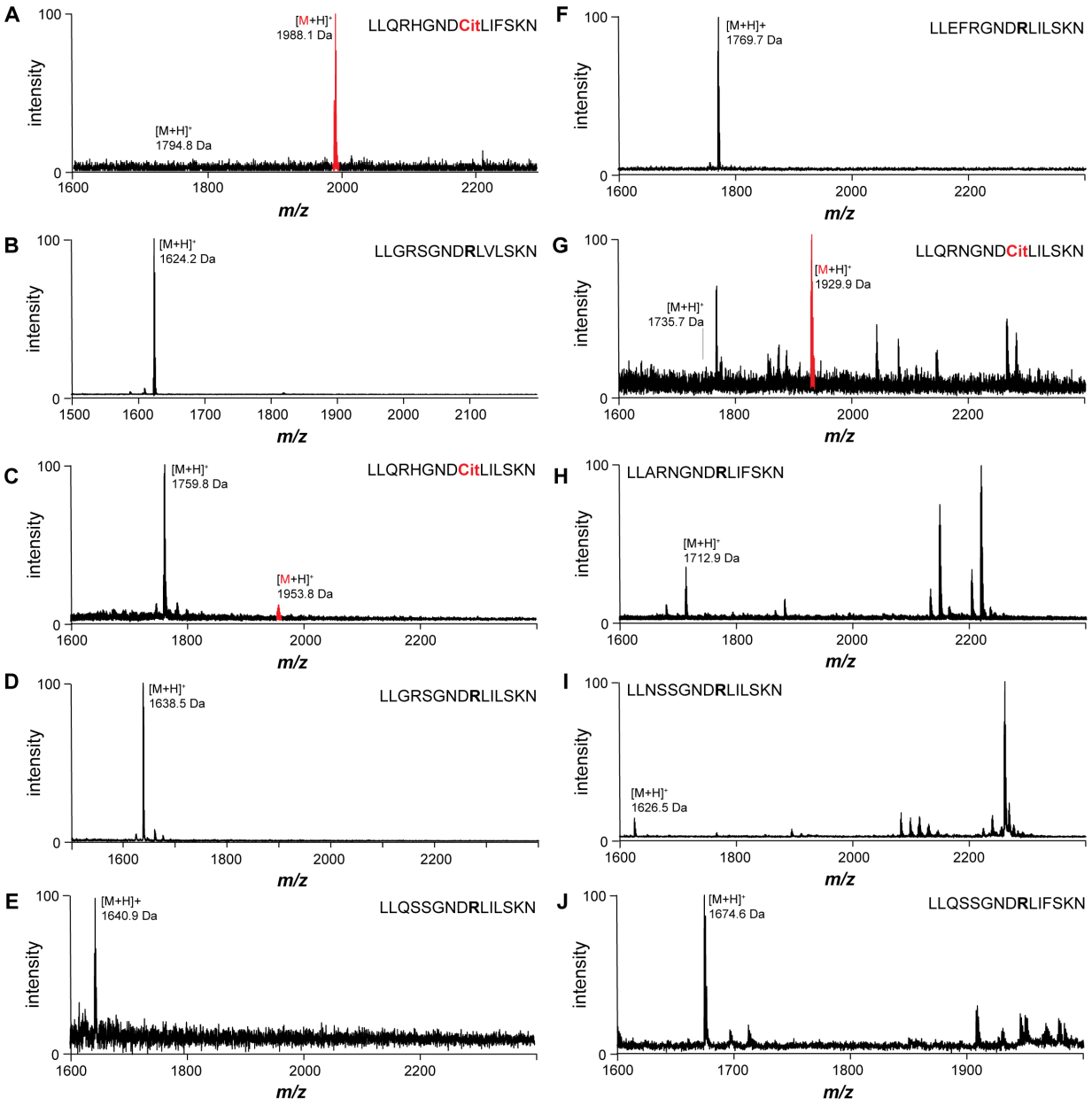

Figure 4.11 Genomic context of the *Streptomyces glaucescens* PAD. Arrows indicate open reading frames (ORFs) and length of arrow corresponds to gene length. Blue arrow, PAD; gray arrow, isochorismatase hit from comparative genomics. DUF, domain of unknown function.

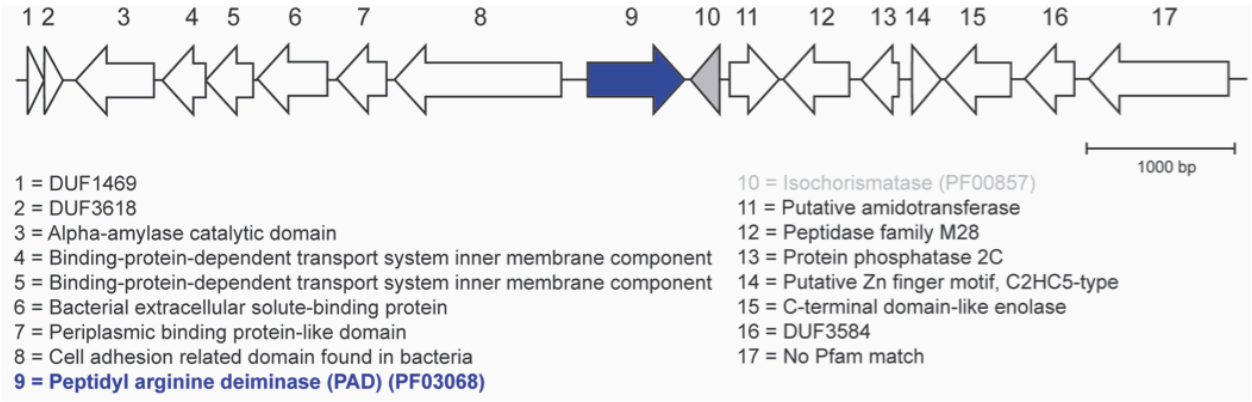

Figure 4.12 Protein sequence alignment of the *Homo sapiens* (NP_036519.2), *Streptomyces glaucescens* (AIR96488.1), and *Streptomyces albulus* (WP_064069846.1) PADs. *, conserved residues; :, strongly similar residues; ., weakly similar residues. Highlighted residues are designated as the active site residues in the *H. sapiens* PAD. Alignment algorithm used was MUSCLE with default settings.

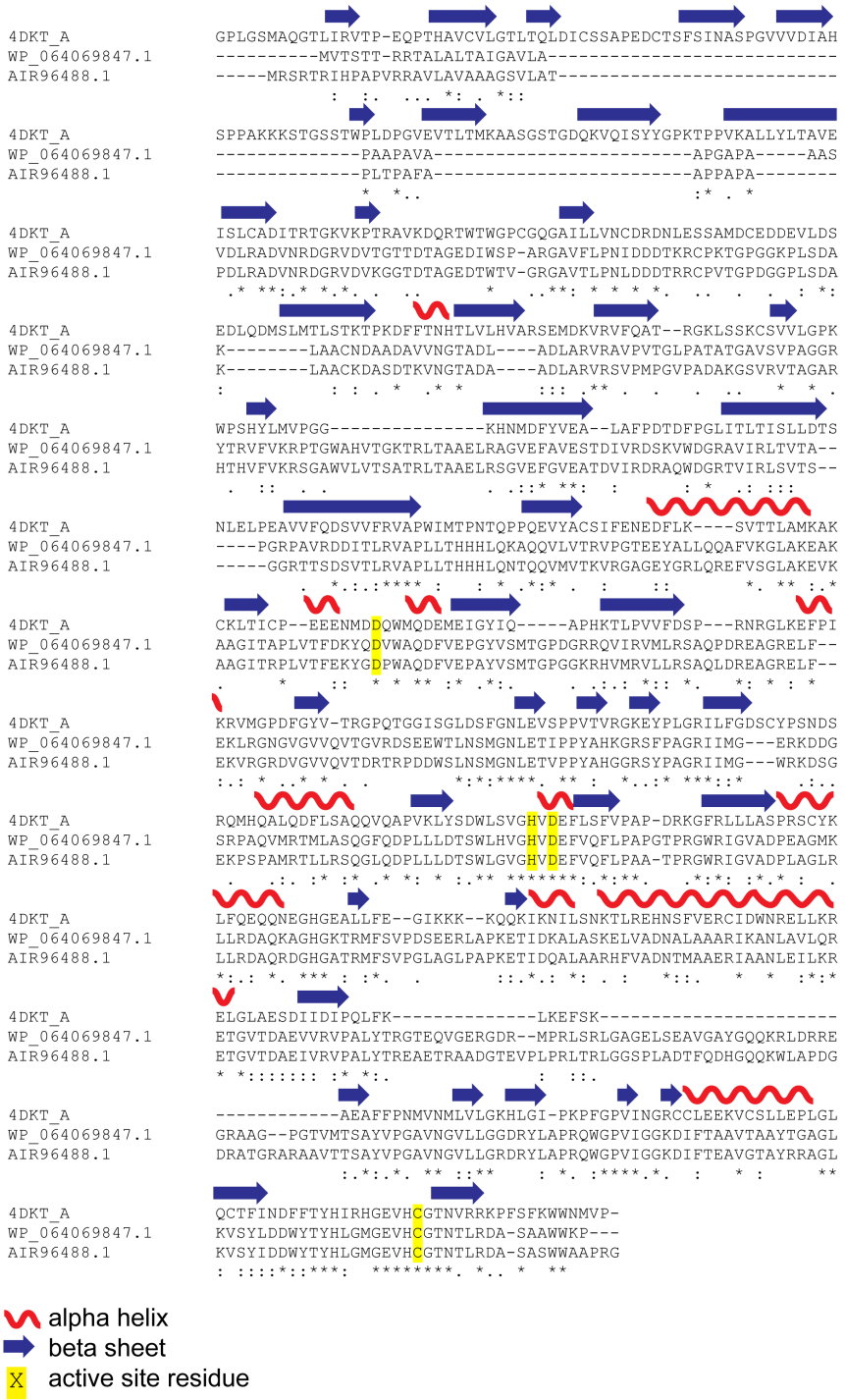

Figure 4.13 Sequence similarity network[28] of the *Porphyromonas gingivalis* PAD. Each node represents a unique PPAD protein, and lines are drawn between nodes if the proteins share a BLAST e-value of < e^{-150}. Nodes are colored by phylum, and *P. gingivalis* strains are further colored to show sequence conservation within the pathogen family. Network was created using the Enzyme Function Initiative – Enzyme Similarity Tool (EFI-EST). Image was generated using Cytoscape.[38]

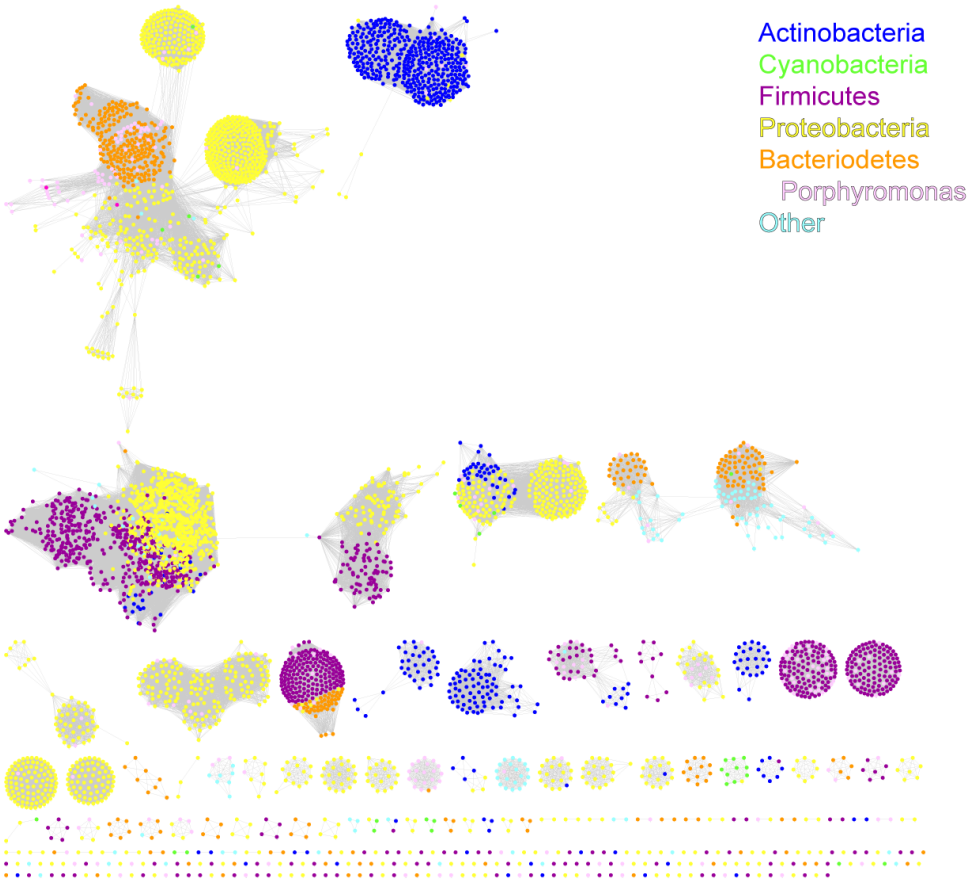

Figure 4.14 Sequence similarity network[28] of the bacterial protein arginine deiminase. Each node represents a unique PAD protein, and lines are drawn between nodes if the proteins share a BLAST e-value of at least e^{-150}. Nodes are colored by phylum. Uncharacterized genomes are grouped in the Other category. Clusters are labeled if the majority of nodes are from a single genus. Network was created using EFI-EST and image was generated using Cytoscape.[38]

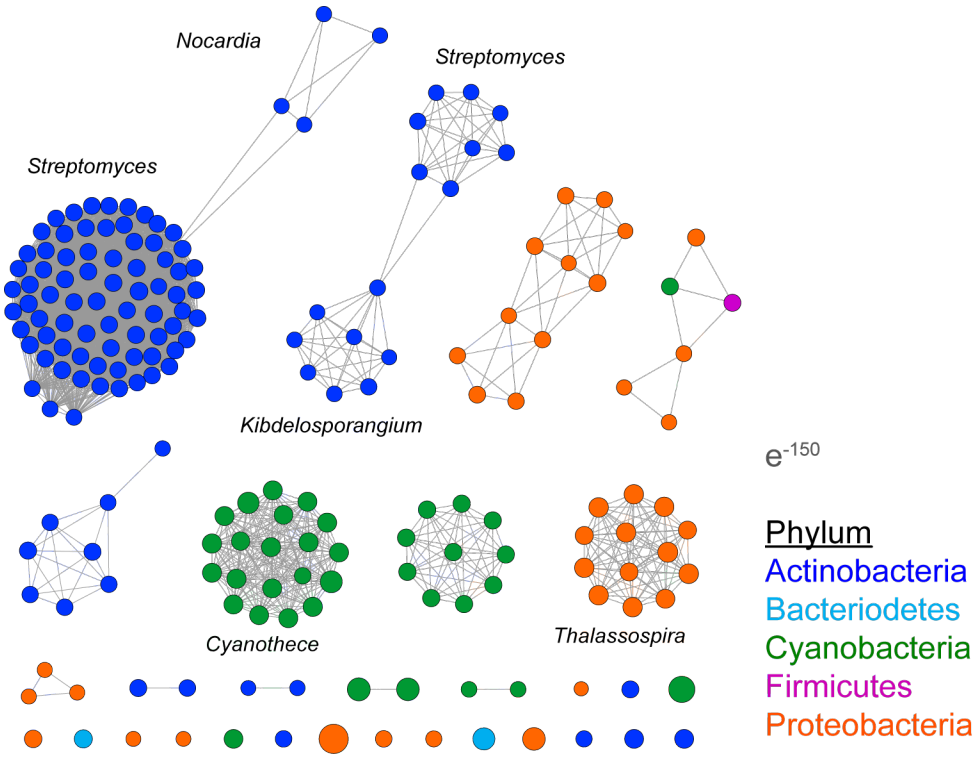

Figure 4.15 %GC content analysis for inference of horizontal gene transfer. Linear regression was calculated (slope = 0.98) and outliers (>5%) are indicated in blue.

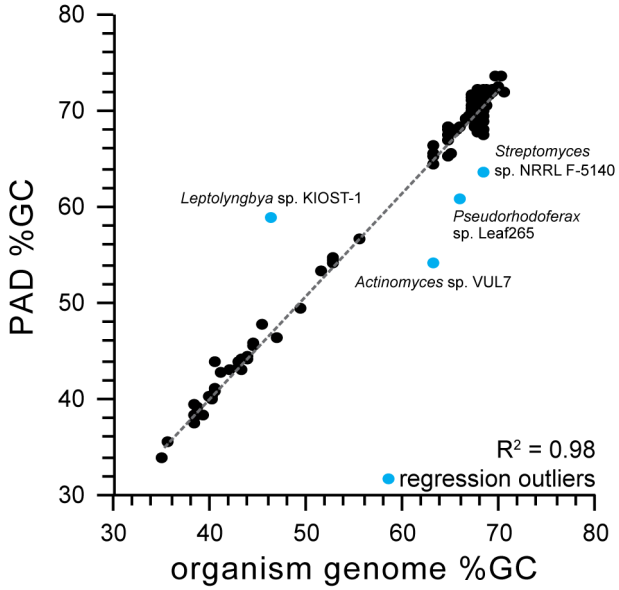

Figure 4.16 *Streptomyces* sp. NRRL F-5140, which has a lower %GC content in its PAD than in the entire genome, produces a citrulline-containing lasso peptide. High-resolution MS is consistent with the modification, and the natural product is labeled within bacterial extracts (not shown).

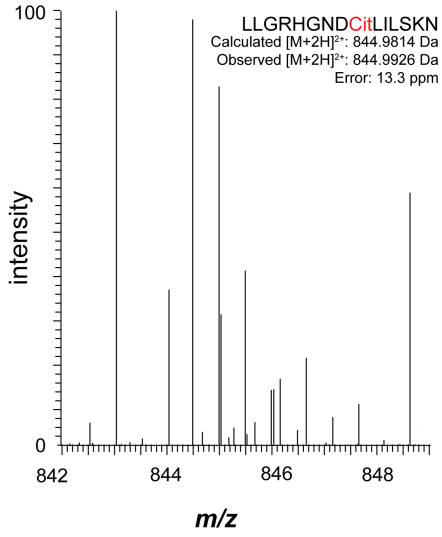

Figure 4.17 Cytoscape genome neighborhood network (GNN)[28] of co-occurring genes with the bacterial protein arginine deiminase. (A) Subset of PADs from the SSN from Figure 4.6 that were used in the EFI-GNT analysis, arranged as previously shown. As before, each cluster represents a

unique PAD protein, and lines are drawn between nodes if the proteins share a BLAST e-value of at least e^{-150}. Clusters are labeled if the majority of nodes are from a single genus. (B) GNN of the clusters from (A) with the clusters from (A) represented as the central hubs and Pfams with a co-occurrence ≥20% shown as nodes. Size correlates to co-occurrence value. N-value is the number of PADs included in the co-occurrence analysis for each cluster.

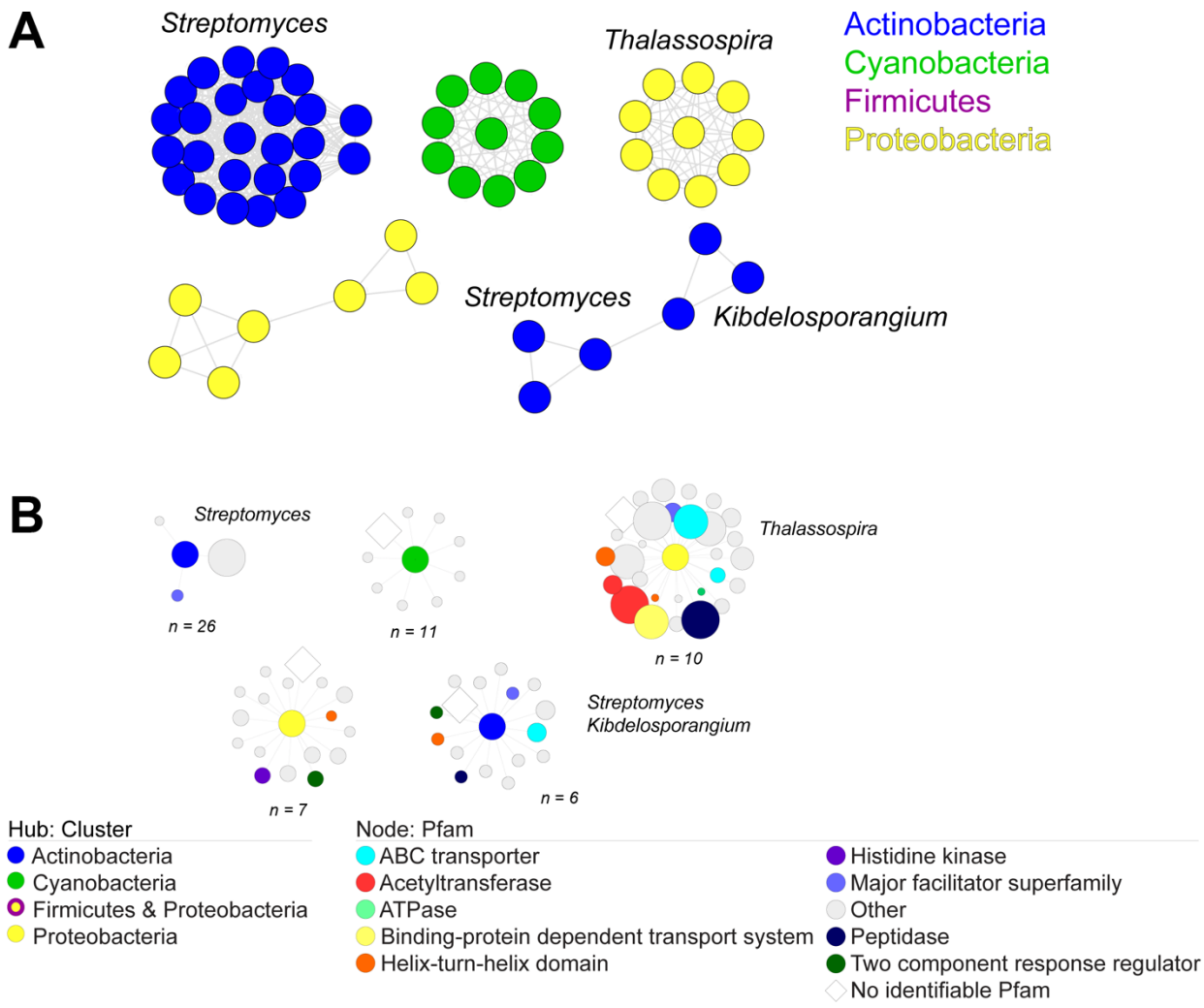

Figure 4.18 Chemiluminescence immunoassay demonstrating PAD activity. (A) SDS-PAGE of purified MBP-CitA (10 µg). (B) SDS-PAGE of purified MBP-PAD from *S. albulus* and *S. glaucescens*. (C) MBP- MBP-CitA (50 µM) was treated with MBP-PAD (0.1 µM) prior to reaction with APG-Biotin and subsequent imaging with Streptavidin-HRP. Grey lines indicate molecular weight standards. Cleavage of MBP-CitA results in a loss of luminescence, indicating PAD activity is on the CitA precursor.

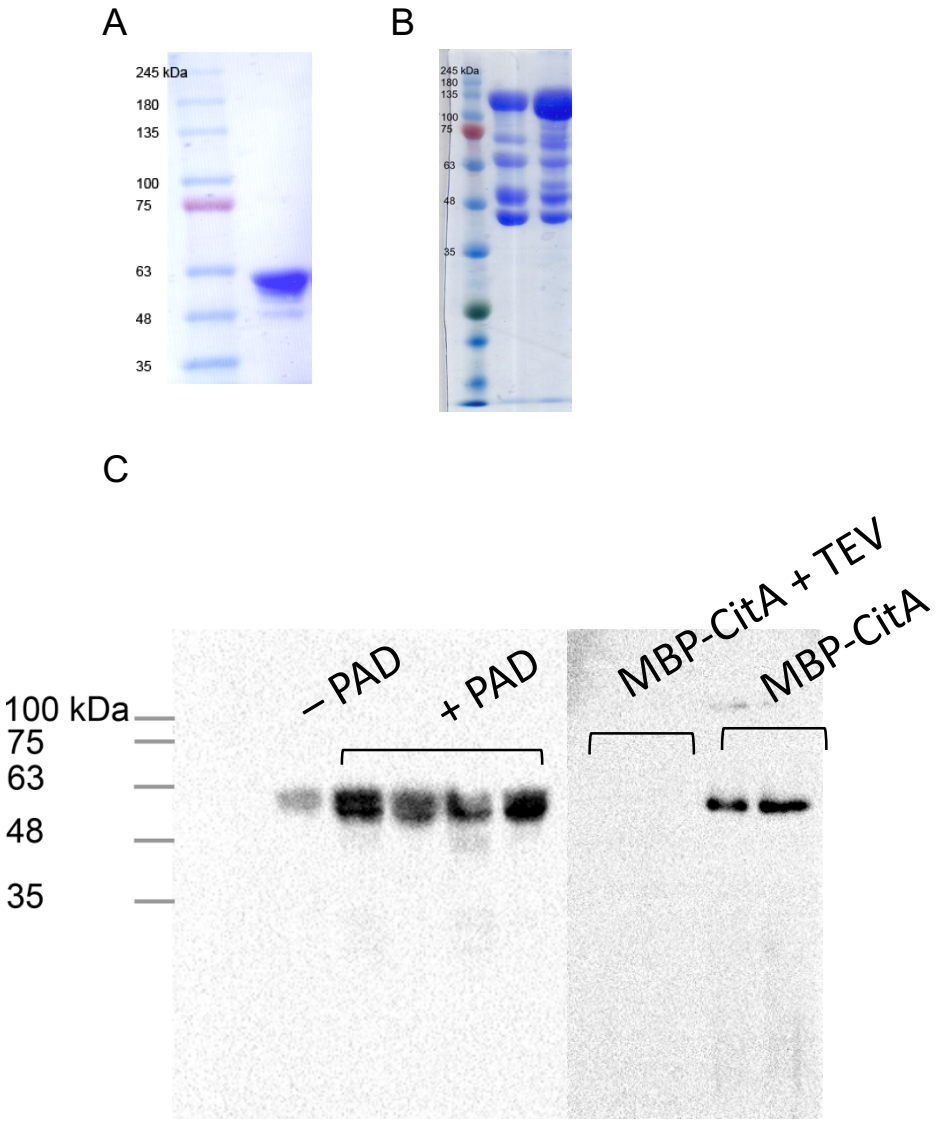

Figure 4.19 Synthesis of the biotin-glyoxal probe (**9**) used for immunoassays of PAD activity.

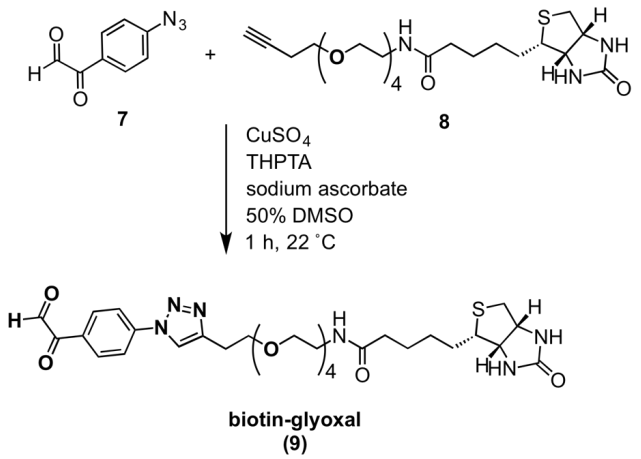

4.8 Tables

Table 4.1 Primers used in this study.

Primer Name	Oligonucleotide sequence
MBP F (sequencing)	GAGGAAGAGTTGGCGAAAGATCCACGTA
T7 F (sequencing)	TAATACGACTCACTATAGGG
T7 R (sequencing)	GCTAGTTATTGCTCAGCGG
PAD F (sequencing)	CGCGGACGTGAACCGC
PAD R (sequencing)	GCACCTCGCCCATGCC
Salb PAD F	AAAGGATCCGTGGTTACGAGCACCACGAGACGAACAGC
Salb PAD R	TTTCTCGAGTCATACGGCTTCCACCACGCGGCG
Salb CitA F	AAAGGATCCATGAAGAAGGCCTACGAGGCGCCGACG
Salb CitA R	TTTCTCGAGTCAGTTCTTGCTGAGGACGAGACGGTCGTTGC
Sglau PAD F	AAAGGATCCATGGTGCGCTCACGTACGCGCATACACC
Sglau PAD R	TTTCTCGAGTCAGCCCCTGGGTGCGGCCC
Sglau CitA F	AAAGGATCCATGAAGAAGGCGTACGAGGCCCCGACG
Sglau CitA R	TTTCTCGAGTCAGTTCTTGCTGAGGATCAGACGGTCGTTGCC
Salb_cluster ins F	ATAATTTTGTTTAACTTTAATAAGGAGATATACCATGAAGCACCATCAGCCCTGCTCAAC
Salb_cluster ins R	GTTGAGCAGGGCTGATGGTGCTTCATGGTATATCTCCTTATTAAAGTTAAACAAAATTAT
Salb_cluster BB F	CCAGCGGTTCTTCATGGTGGACTGAGGCAGCAGCCATCACCATCATCACCACAGCCAGG
Salb_cluster BB R	CCTGGCTGTGGTGATGATGGTGATGGCTGCTGCCTCAGTCCACCATGAAGAACCGCTGG
Salb PAD ins F	TATTAGTTAAGTATAAGAAGGAGATATACATATGGTGGTTACGAGCACCACGAGACGAAC
Salb PAD ins R	GTTCGTCTCGTGGTGCTCGTAACCACCATATGTATATCTCCTTCTTATACTTAACTAATA
Salb PAD BB F	GCCGCGTGGTGGAAGCCGTAGTGGATATCGGCCGGCCACGCGATCGCTGACGTCGGTACC
Salb PAD BB R	GGTACCGACGTCAGCGATCGCGTGGCCGGCCGATATCCACTACGGCTTCCACCACGCGGC

Abbreviations: F, forward primer; R, Reverse primer; Salb, *S. albulus* B-3066; Sglau, *S. glaucescens* B-2900; ins, insert; BB, backbone

Table 4.2 Genomic context of the citrulassin gene cluster, represented with an ORF diagram in Figure 4.5. A co-occurrence analysis of ORFs upstream and downstream of the 55 unique citrulassin gene clusters shows no PAD.

Pfam	Count	Occurrence (%)	Pfam Name	Pfam Description
PF00733	56	102	Asn_synthase	Asparagine synthase
PF00005	53	96	ABC_tran	ABC transporter
PF05402	52	95	PqqD	Coenzyme PQQ synthesis protein D (PqqD)
PF00664	51	93	ABC_membrane	ABC transporter transmembrane region
PF13471	51	93	Transglut_core3	Transglutaminase-like superfamily
PF08544	18	33	GHMP_kinases_C	GHMP kinases C terminal
PF00440	12	22	TetR_N	Bacterial regulatory proteins, tetR family
PF00528	12	22	BPD_transp_1	Binding-protein-dependent transport system inner membrane component
PF12802	9	16	MarR_2	MarR family
PF02540	8	15	NAD_synthase	NAD synthase
PF00009	6	11	GTP_EFTU	Elongation factor Tu GTP binding domain
PF00561	6	11	Abhydrolase_1	alpha/beta hydrolase fold
PF00583	6	11	Acetyltransf_1	Acetyltransferase (GNAT) family
PF03466	6	11	LysR_substrate	LysR substrate binding protein
PF12697	6	11	Abhydrolase_6	Alpha/beta hydrolase family
PF00106	5	9	adh_short	short chain dehydrogenase
PF01590	5	9	GAF	GAF domain

Table 4.3 Joint Genome Institute–Integrated Microbial Genomes and Microbiome Samples Phylogenetic Profiler results for homologous genes present in citrulassin producers but not in des-citrulassin producers. The nicotinamidase immediately adjacent to the *S. glaucescens* PAD is italicized.

Gene ID	Locus Tag	Gene Name	Length (AA)	% Identity
2630312895	Ga0069422_121095	Ribosomal protein S18 acetylase RimI	168	59.8
2630313800	Ga0069422_122005	Ferredoxin-NADP reductase	351	88.4
2630315137	Ga0069422_123344	Alkaline phosphatase	462	72.2
2630315277	Ga0069422_123484	Pimeloyl-ACP methyl ester carboxylesterase	287	80.5
2630315346	Ga0069422_123553	AraC-type DNA-binding protein	139	65.2
2630315364	*Ga0069422_123571*	*Nicotinamidase-related amidase*	*196*	*73.8*
2630315441	Ga0069422_123648	F420-dependent oxidoreductase, G6PDH family	323	61.1
2630317310	Ga0069422_125526	Signal transduction histidine kinase	401	61.1
2630317737	Ga0069422_125955	Acetyl-CoA N-acetyltransferase	247	65.7

Table 4.4 Co-occurrence analysis shows bacterial PADs are not located in a common genomic context. Co-occurrence was calculated for +/- 8 ORFs from the PAD.

Pfam	Counts	Co-occurrence (%)	Pfam Name	Pfam description
PF03068	223	100	PAD	Protein-arginine deiminase
No Pfam match	173	77		
PF00005	56	25	ABC_tran	ABC Transporter
PF13304	46	21	AAA_21	APTases associated with diverse cellular activities
PF07690	45	20	MFS_1	Major facilitator superfamily
PF00072	43	19	Response_Reg	Response regulator receiver domain
PF00440	39	17	TetR_N	TetR regulatory protein
PF00583	33	15	Acetyltransf_1	Acetyltransferase (GNAT) family
PF00196	32	14	Ger_E	LuxR-type DNA-binding HTH domain
PF07730	28	13	HisKA_3	Histidine kinase
PF02518	28	13	HATPase_c	Histidine kinase-, DNA gyrase B-, and HSP90-like ATPase
PF12802	24	11	MarR_2	MarR family
PF13673	23	10	Acetyltransf_10	Acetyltransferase (GNAT) family
PF07719	23	10	TPR_2	Tetratricopeptide repeat
PF00528	22	10	BPD_Transp_1	Binding-protein-dependent transport system, inner membrane component
PF12833	22	10	HTH_18	Helix-turn-helix domain

Table 4.5 Identity matrix of the bacterial PAD enzymes previously determined in *P. gingivalis* has no homology to the *S. albulus S. glaucescens* PADs, which are in the same Pfam as the *H. sapiens* PADs. Identity and similarity matrix was generated using EMBL-EBI Multiple Sequence comparison by Log-Expectation (MUSCLE).

	PF03068 ***H. sapiens***	PF03068 ***S. albulus***	PF03068 ***S. glaucescens***	PF04371 ***P. gingivalis***
H. sapiens	100	21	22	9
S. albulus	35	100	69	10
S. glaucescens	34	76	100	9
P. gingivalis	17	21	20	100

% identity
% similarity

4.9 References

1. Baltz, R. H., Marcel Faber Roundtable: is our antibiotic pipeline unproductive because of starvation, constipation or lack of inspiration? *J Ind Microbiol Biotechnol* **2006,** *33* (7), 507-513.
2. Bentley, S. D.; Chater, K. F.; Cerdeno-Tarraga, A. M.; Challis, G. L.; Thomson, N. R.; James, K. D.; Harris, D. E.; Quail, M. A.; Kieser, H.; Harper, D.; Bateman, A.; Brown, S.; Chandra, G.; Chen, C. W.; Collins, M.; Cronin, A.; Fraser, A.; Goble, A.; Hidalgo, J.; Hornsby, T.; Howarth, S.; Huang, C. H.; Kieser, T.; Larke, L.; Murphy, L.; Oliver, K.; O'Neil, S.; Rabbinowitsch, E.; Rajandream, M. A.; Rutherford, K.; Rutter, S.; Seeger, K.; Saunders, D.; Sharp, S.; Squares, R.;

Squares, S.; Taylor, K.; Warren, T.; Wietzorrek, A.; Woodward, J.; Barrell, B. G.; Parkhill, J.; Hopwood, D. A., Complete genome sequence of the model actinomycete Streptomyces coelicolor A3(2). *Nature* **2002,** *417* (6885), 141-147.
3. Cimermancic, P.; Medema, M. H.; Claesen, J.; Kurita, K.; Wieland Brown, L. C.; Mavrommatis, K.; Pati, A.; Godfrey, P. A.; Koehrsen, M.; Clardy, J.; Birren, B. W.; Takano, E.; Sali, A.; Linington, R. G.; Fischbach, M. A., Insights into secondary metabolism from a global analysis of prokaryotic biosynthetic gene clusters. *Cell* **2014,** *158* (2), 412-421.
4. Cox, C. L.; Doroghazi, J. R.; Mitchell, D. A., The genomic landscape of ribosomal peptides containing thiazole and oxazole heterocycles. *BMC Genomics* **2015,** *16* (1), 778.
5. Maxson, T. T., J.I.; Hudson, G.A.; Mitchell, D.A., Targeting aldehydes and ketones for reactivity-based natural product discovery. **2016**, In revision.
6. Castro-Falcon, G.; Hahn, D.; Reimer, D.; Hughes, C. C., Thiol Probes To Detect Electrophilic Natural Products Based on Their Mechanism of Action. *ACS Chem Biol* **2016,** *11* (8), 2328-2336.
7. Molloy, E. M.; Tietz, J. I.; Blair, P. M.; Mitchell, D. A., Biological characterization of the hygrobafilomycin antibiotic JBIR-100 and bioinformatic insights into the hygrolide family of natural products. *Bioorg Med Chem* **2016**, In Press, doi:10.1016/j.bmc.2016.1005.1021.
8. Palaniappan, K. K.; Pitcher, A. A.; Smart, B. P.; Spiciarich, D. R.; Iavarone, A. T.; Bertozzi, C. R., Isotopic signature transfer and mass pattern prediction (IsoStamp): An enabling technique for chemically-directed proteomics. *ACS Chem Biol* **2011,** *6* (8), 829-836.
9. Capehart, S. L.; Carlson, E. E., Mass spectrometry-based assay for the rapid detection of thiol-containing natural products. *Chemical Communications* **2016**.
10. van Venrooij, W. J.; Pruijn, G. J., Citrullination: a small change for a protein with great consequences for rheumatoid arthritis. *Arthritis Res* **2000,** *2* (4), 249-251.
11. Vossenaar, E. R.; Zendman, A. J.; van Venrooij, W. J.; Pruijn, G. J., PAD, a growing family of citrullinating enzymes: genes, features and involvement in disease. *Bioessays* **2003,** *25* (11), 1106-1118.
12. Gabarrini, G.; de Smit, M.; Westra, J.; Brouwer, E.; Vissink, A.; Zhou, K.; A. Rossen, J. W.; Stobernack, T.; van Dijl, J. M.; Jan van Winkelhoff, A., The peptidylarginine deiminase gene is a conserved feature of Porphyromonas gingivalis. *Scientific Reports* **2015,** *5*, 13936.
13. Nielen, M. M.; van Schaardenburg, D.; Reesink, H. W.; van de Stadt, R. J.; van der Horst-Bruinsma, I. E.; de Koning, M. H.; Habibuw, M. R.; Vandenbroucke, J. P.; Dijkmans, B. A., Specific autoantibodies precede the symptoms of rheumatoid arthritis: a study of serial measurements in blood donors. *Arthritis Rheum* **2004,** *50* (2), 380-386.
14. Masuda, K.; Yoshioka, M.; Hinode, D.; Nakamura, R., Purification and Characterization of Arginine Carboxypeptidase Produced by Porphyromonas gingivalis. *Infection and Immunity* **2002,** *70* (4), 1807-1815.
15. Abdullah, S. N.; Farmer, E. A.; Spargo, L.; Logan, R.; Gully, N., Porphyromonas gingivalis peptidylarginine deiminase substrate specificity. *Anaerobe* **2013,** *23*, 102-108.
16. Cugini, C.; Stephens, D. N.; Nguyen, D.; Kantarci, A.; Davey, M. E., Arginine deiminase inhibits Porphyromonas gingivalis surface attachment. *Microbiology* **2013,** *159* (Pt 2), 275-285.
17. Yin, X.; Zabriskie, T. M., The enduracidin biosynthetic gene cluster from Streptomyces fungicidicus. *Microbiology* **2006,** *152* (Pt 10), 2969-2983.
18. Demange, P.; Bateman, A.; Dell, A.; Abdallah, M. A., Structure of azotobactin D, a siderophore of Azotobacter vinelandii strain D (CCM 289). *Biochemistry* **1988,** *27* (8), 2745-2752.

19. Clancy, K. W.; Weerapana, E.; Thompson, P. R., Detection and identification of protein citrullination in complex biological systems. *Curr Opin Chem Biol* **2016,** *30*, 1-6.
20. Lewallen, D. M.; Bicker, K. L.; Subramanian, V.; Clancy, K. W.; Slade, D. J.; Martell, J.; Dreyton, C. J.; Sokolove, J.; Weerapana, E.; Thompson, P. R., Chemical Proteomic Platform To Identify Citrullinated Proteins. *ACS Chem Biol* **2015,** *10* (11), 2520-2528.
21. Bicker, K. L.; Subramanian, V.; Chumanevich, A. A.; Hofseth, L. J.; Thompson, P. R., Seeing Citrulline: Development of a phenylglyoxal-based probe to visualize protein citrullination. *J Am Chem Soc* **2012,** *134* (41), 17015-17018.
22. Tietz, J. I. S., C.J.; Patel, P.S.; Maxson, T.; Blair, P.M.; Tai, H.-C.; Zakai, U.I.; Mitchell, D.A., A new genome mining tool redefines the lasso peptide biosynthetic landscape. **2016**, In revision.
23. Zhu, S.; Hegemann, J. D.; Fage, C. D.; Zimmermann, M.; Xie, X.; Linne, U.; Marahiel, M. A., Insights into the unique phosphorylation of the lasso peptide paeninodin. *J Biol Chem* **2016,** *291* (26), 13662-13678.
24. Choi, M.; Song, J. S.; Kim, H. J.; Cha, S.; Lee, E. Y., Matrix-assisted laser desorption ionization-time of flight mass spectrometry identification of peptide citrullination site using Br signature. *Anal Biochem* **2013,** *437* (1), 62-67.
25. Ke, Z.; Zhou, Y.; Hu, P.; Wang, S.; Xie, D.; Zhang, Y., Active site cysteine is protonated in the PAD4 Michaelis complex: evidence from Born-Oppenheimer ab initio QM/MM molecular dynamics simulations. *J Phys Chem B* **2009,** *113* (38), 12750-12758.
26. Wegner, N.; Wait, R.; Sroka, A.; Eick, S.; Nguyen, K.-A.; Lundberg, K.; Kinloch, A.; Culshaw, S.; Potempa, J.; Venables, P. J., Peptidylarginine deiminase from Porphyromonas gingivalis citrullinates human fibrinogen and α-enolase: Implications for autoimmunity in rheumatoid arthritis. *Arthritis and rheumatism* **2010,** *62* (9), 2662-2672.
27. Altschul, S. F.; Gish, W.; Miller, W.; Myers, E. W.; Lipman, D. J., Basic local alignment search tool. *J Mol Biol* **1990,** *215* (3), 403-410.
28. Gerlt, J. A.; Bouvier, J. T.; Davidson, D. B.; Imker, H. J.; Sadkhin, B.; Slater, D. R.; Whalen, K. L., Enzyme Function Initiative-Enzyme Similarity Tool (EFI-EST): A web tool for generating protein sequence similarity networks. *Biochim Biophys Acta* **2015,** *1854* (8), 1019-1037.
29. Lawrence, J. G.; Hartl, D. L., Inference of Horizontal Genetic Transfer from Molecular Data: An Approach Using the Bootstrap. *Genetics* **1992,** *131* (3), 753-760.
30. Viklund, H.; Bernsel, A.; Skwark, M.; Elofsson, A., SPOCTOPUS: a combined predictor of signal peptides and membrane protein topology. *Bioinformatics* **2008,** *24* (24), 2928-2929.
31. Engvall, E.; Perlmann, P., Enzyme-linked immunosorbent assay (ELISA). Quantitative assay of immunoglobulin G. *Immunochemistry* **1971,** *8* (9), 871-874.
32. Gibson, D. G.; Young, L.; Chuang, R. Y.; Venter, J. C.; Hutchison, C. A., 3rd; Smith, H. O., Enzymatic assembly of DNA molecules up to several hundred kilobases. *Nat Methods* **2009,** *6* (5), 343-345.
33. Lee, J.; Hao, Y.; Blair, P. M.; Melby, J. O.; Agarwal, V.; Burkhart, B. J.; Nair, S. K.; Mitchell, D. A., Structural and functional insight into an unexpectedly selective N-methyltransferase involved in plantazolicin biosynthesis. *Proc Natl Acad Sci U S A* **2013,** *110* (32), 12954-12959.
34. Markowitz, V. M.; Korzeniewski, F.; Palaniappan, K.; Szeto, E.; Werner, G.; Padki, A.; Zhao, X.; Dubchak, I.; Hugenholtz, P.; Anderson, I.; Lykidis, A.; Mavromatis, K.; Ivanova, N.;

Kyrpides, N. C., The integrated microbial genomes (IMG) system. *Nucleic Acids Research* **2006,** *34* (suppl 1), D344-D348.
35. Su, G.; Morris, J. H.; Demchak, B.; Bader, G. D., Biological network exploration with Cytoscape 3. *Curr Protoc Bioinformatics* **2014,** *47*, 8 13 11-24.
36. Edgar, R. C., MUSCLE: multiple sequence alignment with high accuracy and high throughput. *Nucleic Acids Res.* **2004,** *32* (5), 1792-1797.
37. Crooks, G. E.; Hon, G.; Chandonia, J. M.; Brenner, S. E., WebLogo: a sequence logo generator. *Genome Res* **2004,** *14* (6), 1188-1190.
38. Lopes, C. T.; Franz, M.; Kazi, F.; Donaldson, S. L.; Morris, Q.; Bader, G. D., Cytoscape Web: an interactive web-based network browser. *Bioinformatics* **2010,** *26* (18), 2347-2348.

APPENDIX A: PDF REPRINTS OF OTHER COAUTHORED PUBLICATIONS

A.1 Structural and functional insight into an unexpectedly selective *N*-methyltransferase involved in plantazolicin biosynthesis

Reprinted with permission from Lee, J.*; Hao, Y.I; Blair, P.M.; Melby, J.O.; Agarwal, V.; Burkhart, B.J.; Nair, S.K.; Mitchell, D.A. Structural and functional insight into an unexpectedly selective *N*-methyltransferase involved in plantazolicin biosynthesis. *Proc. Natl. Acad. Sci.* **2013**, *110*, 12954-12959.

The document may be found in the supplemental file named **A.1 Structural and functional insight into an unexpectedly selective N-methyltransferase involved in plantazolicin biosynthesis.pdf**.

In addition to contributing to the writing and editing of the manuscript, I aided in site-directed mutagenesis, overexpression, and purification of BamL mutants. I performed the experiments to determine relative conversion ratios of desmethylplantazolicin (desmethyl-PZN) to plantazolicin (PZN). I discovered the Y182F mutant that could be used to monoalkylate desmethyl-PZN. I synthesized and purified ethyl-SAM and performed all enzymatic reactions and follow-up experiments to characterize the products of the reaction.

A.2 Synthesis of plantazolicin analogues enables dissection of ligand binding interactions of a highly selective methyltransferase

Reprinted with permission from Sharma A.; Blair, P.M.; Mitchell, D.A. Synthesis of plantazolicin analogues enables dissection of ligand binding interactions of highly selective methyltransferase. *Org. Lett.* **2013**, *15*, 5076-5079.

The document may be found in the supplemental file named **A.2 Synthesis of plantazolicin analogues enables dissection of ligand binding interactions of a highly selective methyltransferase.pdf**.

I evaluated the synthetic compounds as substrates for the methyltransferase, which I expressed and purified. I performed isothermal titration calorimetry binding experiments to determine how well the analogues bound to the protein.

A.3 Structure, bioactivity, and resistance mechanism of streptomonomicin, an unusual lasso peptide from an understudied halophilic Actinomycete

Reprinted with permission from Metelev, M.; Tietz, J.I.; Melby, J.O.; Blair, P.M.; Zhu, L.; Livnat, I.; Severinov, K.; Mitchell, D.A. Structure, bioactivity, and resistance mechanism of streptomonomicin, an unusual lasso peptide from an understudied halophilic Actinomycete. *Chem. Biol.*. **2015**, *22*, 241-250.

The document may be found in the supplemental file named **A.3 Structure, bioactivity, and resistance mechanism of streptomonomicin, an unusual lasso peptide from an understudied halophilic Actinomycete.pdf**.

I aided in collection of mass spectrometry data for streptomonomicin. I prepared samples for confocal microscopy, took the images, and evaluated the growth phenotypes.

A.4 Biological characterization of the hygrobafilomycin antibiotic JBIR-100 and bioinformatic insights into the hygrolide family of natural products

Reprinted with permission from Molloy, E.M.; Tietz, J.I.; Blair, P.M.; Mitchell, D.A. Biological characterization of the hygrobafilomycin antibiotic JBIR-100 and bioinformatics insights into the hygrolide family of natural products. *Bioorg. Med Chem.* **2016**, doi: 10.1016/j.bmc.2016.05.021.

The document may be found in the supplemental file named **A.4 Biological characterization of the hygrobafilomycin antibiotic JBIR-100 and bioinformatic insights into the hygrolide family of natural products.pdf**.

For this manuscript, I collected the data for FT-MS/MS analysis and analyzed all mass spectrometry data. I assisted in preparation of samples for microscopy, took all confocal and fluorescence microscopy images, and analyzed the data. I conducted the membrane depolarization assay. I determined the kinetics of growth for the JBIR-100 resistant mutant strains compared to wild-type *B. subtilis*. I performed the PCR to confirm mutations in the JBIR-100 resistant strains, determined through microbroth dilution assays the cross-resistance of the mutants to other antibiotics, and performed qRTPCR (not included in the final publication).

A.5 *In vitro* biosynthesis and substrate tolerance of the plantazolicin family of natural products

Reprinted with permission from Deane, C.D.; Burkhart, B.J.; Blair, P.M.; Tietz, J.I.; Lin, A.; Mitchell, D.A. *In vitro* biosynthesis and substrate tolerance of the plantazolicin. *A.C.S. Chem. Biol.* **2016**, *11*, 2232-2243.

The document may be found in the supplemental file named **A.5 *In vitro* biosynthesis and substrate tolerance of the plantazolicin family of natural products.pdf**.

I performed the mass spectrometry for all of the compounds, determining the structures of the enzymatically treated peptides. This was essential for determining the cyclized residues and thus the pattern of enzymatic processing.

A.6 A new genome mining tool redefines the lasso peptide biosynthetic landscape

Reprinted with permission from Tietz, J.I.*; Schwalen, C.J.*; Patel, P.S.; Maxson, T.M.; Blair, P.M.; Tai, H.-C.; Zakai, U.I.; Mitchell, D.A. A new genome mining tool redefines the lasso peptide biosynthetic landscape. **2016.** *Nature Chem Biol.* Accepted.

The document may be found in the supplemental file named **A.6 A new genome mining tool redefines the lasso peptide biosynthetic landscape.pdf**.

I performed the mass spectrometry for the lasso peptides and was involved in determining the post citrulline post-translational modification of citrulassin A. I assisted in determining the threading of the lasso peptides through analysis of carboxypeptidase-treated samples.